

6-28-2022

Development of Electrochemical Aptamer-based Sensors for Sensitive and Specific Detection of Small-molecule Targets

Yingzhu Liu
yliu111@fiu.edu

Follow this and additional works at: <https://digitalcommons.fiu.edu/etd>

 Part of the [Analytical Chemistry Commons](#), and the [Biochemistry Commons](#)

Recommended Citation

Liu, Yingzhu, "Development of Electrochemical Aptamer-based Sensors for Sensitive and Specific Detection of Small-molecule Targets" (2022). *FIU Electronic Theses and Dissertations*. 5016.
<https://digitalcommons.fiu.edu/etd/5016>

This work is brought to you for free and open access by the University Graduate School at FIU Digital Commons. It has been accepted for inclusion in FIU Electronic Theses and Dissertations by an authorized administrator of FIU Digital Commons. For more information, please contact dcc@fiu.edu.

FLORIDA INTERNATIONAL UNIVERSITY

Miami, Florida

DEVELOPMENT OF ELECTROCHEMICAL APTAMER-BASED SENSORS FOR
SENSITIVE AND SPECIFIC DETECTION OF SMALL-MOLECULE TARGETS

A dissertation submitted in partial fulfillment of

the requirements for the degree of

DOCTOR OF PHILOSOPHY

in

CHEMISTRY

by

Yingzhu Liu

2022

To: Dean Michael R. Heithaus
College of Arts, Sciences and Education

This dissertation, written by Yingzhu Liu, and entitled Development of Electrochemical Aptamer-Based Sensors for Sensitive and Specific Detection of Small-Molecule Targets, having been approved in respect to style and intellectual content, is referred to you for judgment.

We have read this dissertation and recommend that it be approved.

Wenzhi Li

Xiaotang Wang

Yuk-Ching Tse-Dinh

Bruce McCord

Yi Xiao, Major Professor

Date of Defense: June 28, 2022

The dissertation of Yingzhu Liu is approved.

Dean Michael R. Heithaus
College of Arts, Sciences and Education

Andrés G. Gil
Vice President for Research and Economic Development
and Dean of the University Graduate School

Florida International University, 2022

© Copyright 2022 by Yingzhu Liu

All rights reserved.

DEDICATION

I dedicate this work to my parents Minghua Liu and Jun Xiao,
my grandparents Yingao Xiao and Ailan Wang, and my husband Dr. Biwei Deng,
for their support with my deepest love.

ACKNOWLEDGMENTS

During my Ph.D. study, many people have offered their generous support and genuine advice to me, and I am deeply grateful for all of them. Without the warm and ample help from these kind and knowledgeable people, this dissertation could not be possible. Moreover, I will carve my deepest gratitude at the bottom of my heart, and I am forever in debt to these beautiful people and this outstanding university.

First and foremost, I want to give my most sincere thanks to my Ph.D. advisor, Dr. Yi Xiao. The first day I entered her lab in the Department of Chemistry, she offered me full support without any conditions. Thanks to her, I gained, bit by bit, the skills and pieces of knowledge that eventually constitute my Ph.D. research. She inspired me with her career and motto as a successful woman scientist. I have learned many from her, such as responsibility, independence, honesty and fairness, high standards, and caring for others. I also have become brave and confident to face challenges and solve problems in difficult situations because she is always there to help me, support me, and provide me with useful guidance and advice. I am so lucky that I chose Dr. Xiao's lab as a home for my Ph.D. years and that Dr. Xiao accepted me as her student. I owe all my achievements to Dr. Xiao.

I am most grateful to my committee members, Dr. Xiaotang Wang and Dr. Yuk-Ching Tse-Dinh, for their support and guidance in my research and helped me build up a foundation in the biochemistry field as my biochemistry course instructors. Dr. Bruce McCord always provided me with thoughtful advice for my projects in the forensic chemistry field and meaningful guidance in the organic chemistry field. Dr. Wenzhi Li helped me a lot with my physics research, especially with his deep understanding of optical

and electrochemical instruments. They have been supportive of me for the past years and offered me their kind advice.

I also want to thank all my lab mates that helped me through my Ph.D. research life. Particularly, I would like to thank Dr. Haixiang Yu, Obtin Alkhamis, Juan Canoura, Jordan Moliver, and Xintong Liu for their direct contribution to my dissertation research. Without their help, this dissertation would not be in its current shape.

I want to thank the funding support from the National Institutes of Health - National Institute on Drug Abuse, the National Institute of Justice, and the National Science Foundation. Without this funding, I could not complete my dissertation research. I also want to thank FIU, the Graduate & Professional Student Committee, and the College of Arts, Sciences & Education for the travel award to support my attendance at the conferences.

I want to thank all the staff who helped me along the way in the Department of Chemistry and other administrative departments at FIU, and their help has been vital to me so that my study and research can go smoothly.

Last but not least, I am deeply grateful to my parents. They love me with all their hearts no matter where I am. They watched me grow and travel worldwide, provided me with unconditional support, and shared my joy and tears. I also want to thank my husband, Dr. Biwei Deng, for his love, understanding, and unlimited support. Every achievement in my life, I owe to them.

ABSTRACT OF THE DISSERTATION

DEVELOPMENT OF ELECTROCHEMICAL APTAMER-BASED SENSORS FOR SENSITIVE AND SPECIFIC DETECTION OF SMALL-MOLECULE TARGETS

by

Yingzhu Liu

Florida International University, 2022

Miami, Florida

Professor Yi Xiao, Major Professor

Electrochemical aptamer-based (E-AB) sensors have been applied for diverse applications such as forensic science, pharmaceutical diagnostics, food safety, environmental monitoring, and personal medical care due to their rapid, accurate, and specific detection of analytes in complex samples. However, limited sensitivity and a lack of portable devices for point-of-care applications have greatly hindered the maturation of E-AB sensors from proof-of-concept designs to commercial systems. This dissertation describes several novel strategies to improve the sensitivities of E-AB sensors and fabricate portable paper-based devices to remedy these problems. We first detail the development of a novel approach to utilize a defined mixture of two bioreceptors that exhibit different binding profiles to tune the sensitivity and extend the dynamic range of E-AB sensors for the detection and analysis of drug families. We successfully measure 12 synthetic cathinones, a family of dangerous illicit designer drugs, with high cross-reactivity while minimizing the influence of 17 interferents. We then further enhance the sensitivity of E-AB sensors from the microscale level by developing a generalizable target-assisted

immobilization strategy to control the spatial morphology of aptamers modified onto the electrode surface and thereby achieve maximum signal output. We immobilize the aptamers in a bound and folded state to ensure that the modified aptamers have sufficient space for efficient target-induced folding and signal transduction. This approach greatly improves E-AB sensor sensitivity and signal-to-noise ratio (SNR) compared to sensors fabricated by conventional methods. Finally, building on the optimal E-AB sensor design developed in my first two projects, we focus on developing portable paper-based electrochemical devices to convert these E-AB sensors from benchtop-based platforms to on-site applications. Specifically, we utilize filter paper to fabricate multiplexed aptamer-modified paper electrochemical devices (mPEDs) via ambient vacuum filtration. The fabrication process is simple, low-cost, and environmentally friendly. Moreover, the resulting postage stamp-sized paper-based devices are portable, enabling accurate and specific multianalyte detection in a microliter of a single biological sample within seconds. We believe our paper-based devices have the potential to enable sensitive and precise on-site detection for multiple analytes.

TABLE OF CONTENT

CHAPTER	PAGE
1: Introduction.....	1
1.1. Overview	1
1.2. Motivation and goals	2
1.3. Scope of the dissertation	4
2: Background and Literature Review	6
2.1. Aptamer-based sensors for small-molecule detection.....	6
2.1.1. Aptamer-based optical biosensors	7
2.1.2. Aptamer-based field-effect transistor (FET)	9
2.1.3. Electrochemical aptamer-based (E-AB) sensors	11
2.2. Advanced strategies to enhance E-AB sensor performance.....	12
2.2.1. Improving sensitivity via sensor probe design	12
2.2.1.1. Aptamer truncation to enhance sensor performance.....	12
2.2.1.2. Tuning sensor performance via multiprobe modification.....	14
2.2.2. Improving sensitivity via new sensing strategies	15
2.2.3. Effect of surface monolayer on sensing performance	17
2.2.4. Effect of measurement parameters on sensing performance	22
2.2.5. Effect of redox reporters on sensor performance	24
2.2.6. Effects of electrode morphology on sensor performance	25
2.3. Other electrode types developed for in vitro applications.....	28
2.4. E-AB sensors for in vivo detection	30
2.5. Small-molecule targets used in this work	34
2.5.1. Synthetic cathinones	34
2.5.2. Cocaine	34
2.5.3. Adenosine	35
2.5.4. Acetyl fentanyl	36
3: Tuning Biosensor Cross-Reactivity Using Aptamer Mixtures	37
3.1. Introduction	37
3.2. Experimental section	39
3.2.1. Materials	39
3.2.2. Cy7 dye-displacement assay.....	41
3.2.3. Exonuclease digestion of aptamers	42
3.2.4. Circular dichroism (CD).....	43
3.2.5. Isothermal titration calorimetry (ITC) experiments	43
3.2.6. Electrochemical aptamer-based sensor fabrication and detection.....	45
3.2.7. Mathematical prediction of signal gain using a mixture of two aptamers	46
3.3. Result and discussion	47
3.3.1. Determination the binding profiles of SCA1.1 and SCA2.1 using the Cy7 dye-displacement assay	47
3.3.2. Employing defined mixtures of aptamers to control the cross-reactivity of biosensors.....	53

3.3.3. Identification of structure-switching aptamers for the E-AB sensors	56
3.3.4. Fabrication of dual-aptamer-based electrochemical sensors	60
3.4. Conclusion.....	75
4: Immobilization Strategies for Enhancing Sensitivity of Electrochemical Aptamer	
-Based Sensors	78
4.1. Introduction	78
4.2. Experimental section	81
4.2.1. Materials	81
4.2.2. Fabrication of E-AB sensors.	82
4.2.3. Electrochemical measurements	83
4.2.4. Aptamer affinity measurement via isothermal titration calorimetry (ITC)	83
4.3. Results and discussion.....	85
4.3.1. Rationale for enhancing E-AB sensor performance by controlling micro	
-scale probe spacing	85
4.3.2. Effects of target-assisted aptamer immobilization on E-AB sensor	
performance.....	86
4.3.3. Confirmation of the generalizability of target-assisted aptamer	
immobilization.....	91
4.3.4. Relationship between the concentration of aptamer-target complex used for	
electrode modification and E-AB sensor performance	92
4.3.5. Dependency of E-AB sensor performance on the ionic strength of the	
immobilization buffer	95
4.3.6. Effect of the type of buffering system used for aptamer immobilization on	
E-AB sensor performance	98
4.3.7. Target-assisted immobilization is effective independent of aptamer	
sequence, structure, and affinity	99
4.3.8. Effect of buffer pH used for aptamer immobilization on E-AB sensor	
performance	107
4.4. Conclusion.....	111
5: Aptamer-Integrated Multi-Analyte Detecting Paper Electrochemical Device	113
5.1. Introduction	113
5.2. Experimental section	115
5.2.1. Materials	115
5.2.2. Synthesis of metal nanoparticles	117
5.2.3. Isothermal titration calorimetry (ITC).....	118
5.2.4. Fabrication of multiplex paper electrochemical devices (mPEDs)	118
5.2.5. Fabrication of aptamer-modified mPEDs.....	119
5.2.6. Fabrication of polydimethylsiloxane (PDMS) chamber	120
5.2.7. Electrochemical measurements	121
5.2.8. Aptamer digestion experiments	121
5.3. Results and discussion.....	122
5.3.1. Design and fabrication of the mPED.....	122
5.3.2. Evaluation of mPED electrochemical performance	124

5.3.3. Fabrication and testing of aptamer-modified mPEDs for small-molecule detection	125
5.3.4. Multi-target detection in biological samples	130
5.3.5. Incorporation of a sample confinement zone into a triple-modified mPED .	144
5.4. Conclusion.....	145
6: Summary and Future Work.....	148
6.1. Summary	148
6.2. Future work	150
REFERENCES	152
VITA.....	168

LIST OF TABLES

TABLE	PAGE
CHAPTER 3	
3-1. Sequence ID and DNA sequences used in Chapter 3.....	40
3-2. Aptamer, ligand, and ligand concentration used for ITC experiments and determined K_{DS}	44
CHAPTER 4	
4-1. ITC parameters and conditions used in this work and the calculated K_{DS}	84
CHAPTER 5	
5-1. Recoveries from spike-and-recovery experiments with ternary mixture detection in buffer, 50% urine, and 50% saliva.....	137
5-2. Recoveries obtained from spike-and-recovery experiments with a ternary mixture in 50% saliva using a PDMS-confined triple-modified mPED.....	139

LIST OF FIGURES

FIGURE	PAGE
CHAPTER 2	
2-1. Aptamer-based sensors for small-molecule target detection.	10
2-2. Overview of E-AB sensor design and fabrication.	12
2-3. Overview of exonuclease-based assay for generating structure-switching aptamers.	13
2-4. Probe-based strategies for improving the sensitivity of E-AB sensors.	18
2-5. Chemical structures of different synthetic cathinones used in this work.	35
2-6. Chemical structure of small molecule targets.	35
CHAPTER 3	
3-1. Target-binding spectra of SCA1.1, SCA2.1, and their mixtures in a Cy7- displacement assay.	48
3-2. Cy7-displacement assay for MDPV detection.	49
3-3. Characterization of the target-binding affinity of SCA1.1 using ITC.	49
3-4. Chemical structures of different synthetic cathinones and interferents used in this work.	50
3-5. Results of Cy7-displacement assays performed with SCA2.1 or SCA1.1 alone.	51
3-6. Target cross-reactivity and specificity of the Cy7-displacement dual-aptamer assay	52
3-7. Relationship between fraction of aptamer and signal gain for the Cy7- displacement assay.	53
3-8. Cy7-based displacement assays using SCA2.1, SCA1.1, and a mixture of both aptamers to detect different mixtures of synthetic cathinones.	54
3-9. PAGE analysis of Exo III digestion of SCA1.1 and SCA2.1.	57
3-10. PAGE analysis of SCA1.1 and SCA2.1 digestion with a mixture of Exo III and Exo I.	58
3-11. PAGE analysis of exonuclease digestions and the structures of the digestion products.	59
3-12. PAGE analysis of SCA1.1-40 and SCA2.1-40 digestion with Exo I.	60
3-13. Circular dichroism (CD) spectra of SCA1.1-40 and SCA2.1-40.	61
3-14. Characterization of the target-binding affinity of SCA2.1-40 using ITC.	61
3-15. Characterization of the target-binding affinity of SCA1.1-40 using ITC.	62
3-16. Characterization of the target-binding affinity of SCA2.1-34 using ITC.	62
3-17. Characterization of the target-binding affinity of SCA1.1-34 using ITC.	63
3-18. SCA2.1/1.1 and SCA2.1-34/1.1-34 mixture performance in the Cy7- displacement assay.	63
3-19. Results of Cy7-displacement assays performed with SCA2.1-34, SCA1.1-34 or the mixture of both aptamers.	64

3-20. Cross-reactivity of SCA2.1/1.1 and SCA2.1-34/1.1-34 mixture performance in the Cy7-displacement assay.	65
3-21. Performance of an E-AB sensor modified with SCA2.1-34-MB alone.	66
3-22. Performance of an E-AB sensor modified with SCA1.1-34-MB alone.	67
3-23. Characterization of the interferent-binding affinity of SCA1.1-34 using ITC.	68
3-24. Comparison of surface coverages of aptamer-modified electrodes.	69
3-25. Dual-aptamer-based E-AB sensor.	70
3-26. Experimental and predicted cross-reactivity of E-AB sensor fabricated with aptamer mixture for synthetic cathinones and interferents.	70
3-27. Square-wave voltammograms produced by various synthetic cathinones.	71
3-28. Square-wave voltammograms produced by various interferents.	72
3-29. Square-wave voltammetry spectra for binary mixtures.	73
3-30. Signal gain and cross-reactivity for binary mixtures.	74
3-31. Cross-reactivity of aptamer mixture of SCA2.1-34 and SCA1.1-34 in the Cy7-displacement assay and an E-AB sensor.	74

CHAPTER 4

4-1. Characterization of the affinity of ADE-25 for adenosine using isothermal titration calorimetry (ITC).	87
4-2. Adenosine detection with electrodes modified with ADE-25-MB using the conventional immobilization approach.	88
4-3. Simulated binding curve for ADE-25 based on its affinity for adenosine in high-salt PBS.	89
4-4. Surface coverage of electrodes fabricated with ADE-25-MB via different methods.	89
4-5. E-AB sensor performance using electrodes modified with ADE-25-MB either alone or bound to adenosine.	90
4-6. Performance of electrodes fabricated with COC-32-MB via target-assisted immobilization or conventional means in high-salt PBS.	92
4-7. Characterization of the affinity of COC-32 for cocaine using ITC.	93
4-8. Surface coverage of electrodes modified with COC-32-MB and cocaine in high-salt PBS.	94
4-9. Simulated binding curve for COC-32 based on its affinity for cocaine in high-salt PBS.	94
4-10. E-AB sensor performance using electrodes modified with COC-32-MB via target-assisted immobilization.	95
4-11. Performance of electrodes fabricated with COC-32-MB via conventional means in different buffers.	97
4-12. Simulated binding curve for COC-32 based on the affinity for cocaine in low-salt PBS.	97
4-13. Surface coverage of electrodes modified with COC-32-MB with different methods.	98
4-14. E-AB sensor performance using electrodes modified with target-bound COC-32-MB.	100

4-15. Performance of electrodes fabricated with COC-32-MB via target-assisted immobilization in different buffers.	100
4-16. Sensitivity and LOD for cocaine detection in 50% saliva with different electrodes.	101
4-17. Simulated binding curve for SC-34 based on affinity for MDPV in low-salt Tris buffer.....	101
4-18. Electrodes fabricated using SC-34-MB via target-assisted aptamer immobilization with various concentrations of MDPV.	102
4-19. Detection of MDPV in 50% urine using electrodes fabricated via different methods.	102
4-20. E-AB sensor performance using electrodes fabricated with SC-34-MB.....	103
4-21. Characterization of the affinity of SC-34 for MDPV using ITC.	104
4-22. Simulated binding curve for SC-34 based on affinity for MDPV in high-salt PBS	104
4-23. Performance of electrodes fabricated with SC-34-MB via target-assisted immobilization in different buffers.	105
4-24. Performance of electrodes fabricated with SC-34-MB via different methods.	105
4-25. ITC characterization of SC-34 affinity for MDPV in high-salt Tris buffer.	108
4-26. E-AB sensor performance in various pH buffers.	108
4-27. Surface coverage of electrodes fabricated with SC-34-MB in various pH buffers	109
4-28. Performance of electrodes fabricated with SC-34-MB via different methods.	110
4-29. Characterization of the pH-dependence of SC-34 affinity for MDPV using ITC.	111

CHAPTER 5

5-1. Scheme for the fabrication of mPEDs using ambient vacuum filtration.....	123
5-2. Determination of the surface area and electrochemical performance of mPEDs....	125
5-3. Determination of electron transfer rates of different working electrodes.	126
5-4. Surface area measurements of the working electrodes for four different mPEDs were tested.	126
5-5. Determination of the binding affinity of COC-apt to cocaine using isothermal titration calorimetry (ITC).	127
5-6. Detection of cocaine using a COC-32-modified mPED.....	128
5-7. Determination of the binding affinity via ITC.....	129
5-8. Detection of acetyl fentanyl using a mPED modified with AF-32.....	130
5-9. Detection of MDPV using a mPED modified with MDPV-34.	131
5-10. Detection of adenosine using a mPED modified with ADE-25.	132
5-11. Stability of ADE-25 modified mPEDs.	133
5-12. Characterization of the specificity of different aptamers using the exonuclease-based binding assay.....	134
5-13. Simultaneous detection of multiple small-molecule analytes using triple-modified mPEDs.....	134
5-14. SWV response of the triple-modified mPED to ternary mixtures.....	135

5-15. Simultaneous detection of multiple small-molecule analytes with triple-modified mPEDs.....	136
5-16. Detection of different targets in 50% urine using single-aptamer-modified mPEDs.....	138
5-17. Detection of various targets in 50% saliva using a single-aptamer-modified mPEDs.....	139
5-18. SWV response of each working electrode of a triple-modified mPED in 50% urine.....	140
5-19. SWV response of each working electrode of a triple-modified mPED in 50% saliva.....	141
5-20. Fabrication of an aptamer-modified mPED with a PDMS sample-containment chamber.....	142
5-21. SWV response of each working electrode of a PDMS-confined triple-modified mPED in 50% saliva.....	143

LIST OF ABBREVIATIONS

ACRONYMS

ACV	Alternating current voltammetry
apt	Aptamer
bp	Base pair
CD	Circular dichroism
cDNA	Complementary DNA
CE	Counter electrode
Ctrl	Control
CV	Cyclic Voltammetry
DPV	Differential pulse voltammetry
E	Potential
e.g.	Exempli gratia
E-AB sensor	Electrochemical aptamer-based sensor
E_{pa}	Anodic peak potential
E_{pc}	Cathodic peak potential
FET	Field-effect transistors
HPLC	High performance liquid chromatography
I	Current
i.e.	Id est
ITC	Isothermal titration calorimetry
KDM	Kinetic differential measurement

LOD	Limit of detection
mPED	Multiplex paper electrochemical device
NA	Not applicable
PAGE	Polyacrylamide gel electrophoresis
PCR	Polymerase chain reaction
PDMS	Polydimethylsiloxane
PED	Paper electrochemical device
pH	Potential of hydrogen
RE	Reference electrode
SAM	Self-assembled monolayer
SELEX	Systematic evolution of ligands by exponential enrichment
SNR	Signal-to-noise ratio
SWV	Square wave voltammetry
vs.	Versus
w/	With
w/o	Without
WE	Working electrode

CHEMICALS AND MATERIALS

3-FMC	3-Fluoromethcathinone
4-FMC	4-Fluoromethcathinone
4-MMC	4-Methylmethcathinone

ADE	Adenosine
ADP	Adenosine diphosphate
AF	Acetyl fentanyl
AgNP	Silver nanoparticle
AMP	Adenosine monophosphate
ATP	Adenosine triphosphate
AuNP	Gold nanoparticle
BSA	Bovine serine albumin
COC	Cocaine
Cy7	Diethylthiatricarbocyanine
DMSO	Dimethyl sulfoxide
DNA	Deoxyribonucleic acid
DTT	Dithiothreitol
EDTA	Ethylenediaminetetraacetic acid
Exo I	Exonuclease I
Exo III	Exonuclease III
G	Guanine
MB	Methylene blue
MCH	6-Mercapto-1-hexanol
MDMA	3,4-Methylenedioxymethamphetamine
MDPV	3,4-Methylenedioxypropionerone
NGAL	Neutrophil gelatinase-associated lipocalin

PBS	Phosphate buffered saline
PEG	Polyethylene glycol
PET	Polyterephthalate
PSE	Pseudoephedrine
PVP	Polyvinyl pyrrolidone
rATP	Adenosine ribonucleotide triphosphate
RNA	Ribonucleic acid
SC	Synthetic cathinone
SH	Thiol
SWCNT	Single-walled carbon nanotube
Tris	Tris(hydroxymethyl)aminomethane
α -PVP	Alpha-pyrrolidinopentiophenone

UNITS AND PROPERTIES

\$	US dollar
%	Percent
°C	Degrees Celsius
μ A	Microampere
cm	Centimeter
hr or h	Hour
$K_{1/2}$	Ligand concentration producing half occupation in Hill equation
K_D	Dissociation constant

M	Molar
mg	Milligram
min	Minute
mL	Milliliter
mm	Millimeter
mM	Millimolar
ms	Millisecond
mV	Milliovolt
MΩ	Milliohm
N	Binding stoichiometries
nL	Nanoliter
nm	Nanometer
nM	Nanomolar
nt	Nucleotide
s or sec	Second
U	Activity unit
V	Volt
w/v	Weight/volume
w/w	Weight/weight
λ	Wavelength
μg	Microgram
μL	Microliter

μm Micrometer

μM Micromolar

CHAPTER 1: Introduction

1.1. Overview

Aptamer-based sensors have been widely used for varying applications, including forensic detection of illicit drugs, pharmaceutical diagnostics, food safety, environmental monitoring, and personal medical care. Aptamers are single-stranded deoxyribonucleic acid (DNA) or ribonucleic acid (RNA) oligonucleotides that recognize specific targets such as small molecules, proteins, or cells. Aptamers are isolated *in vitro* via a technique known as Systematic Evolution of Ligands by Exponential Enrichment (SELEX). Compared to antibodies, aptamers exhibit many advantages: low cost (typically 10-fold lower than antibodies),¹ fast development time (2–6 weeks for aptamers versus 6–18 months for antibodies),² high stability with long shelf life (years for aptamers versus months for antibodies),² controllable binding properties, and the potential to generate reagents against a far broader range of targets. So far, hundreds of small-molecule-binding aptamers have been isolated, and these could offer a powerful tool for biosensing purposes. One promising class of biosensors is the electrochemical aptamer-based (E-AB) sensor; these are based on the target-induced conformational change of a redox-tagged aptamer coupled to the surface of a gold electrode. E-AB sensors provide a suitable platform for achieving sensitive and specific detection of targets in complex samples within seconds. More importantly, E-AB sensors have the potential to be used as portable devices for on-site drug detection or at-home testing.

However, E-AB sensors face a major challenge with regard to sensitivity, especially when applied to biofluid samples. Multiple strategies have been developed to improve E-

AB sensors' sensitivities, such as utilizing split aptamers or enzyme-assisted assays to reduce the background signal, using complementary DNA strand displacement to enhance the signal gains, or amplifying signals via enzyme-assisted target recycling. However, these strategies also suffer important drawbacks, requiring careful and thoughtful experimental design. Furthermore, it is critical to fabricate electrode formats that can enable the accurate and specific detection of E-AB sensors in on-site scenarios. Commercially-available gold rod electrodes are costly and not portable, which makes them ill-suited for on-site monitoring. Therefore, new strategies for improving the sensitivity of E-AB sensors and fabricating portable sensor devices could accelerate the real-world application of E-AB sensors.

1.2. Motivation and goals

My dissertation focuses on developing sensitive and specific E-AB sensors and paper-based devices for detecting small molecules in real-world applications. We implemented three innovative approaches: 1) developing dual-aptamer-based E-AB sensors for specific detection of families of drugs; 2) establishing a target-assisted immobilization strategy to enhance the sensitivity and improve the SNR of E-AB sensor detection in biofluid matrices; and 3) fabricating multiplexed aptamer-modified paper electrochemical devices (mPEDs) for simultaneous detection of multiple analytes in a single sample within seconds.

I initially focused on detecting a designer drug family in seized substances (see Chapter 3), as it is more efficient to measure analyte families simultaneously than to detect individual targets multiple times. However, finding a proper bioreceptor that can recognize all compounds in a given chemical family while retaining minimal response against non-

target interferents is very difficult. To overcome this challenge, we developed a novel method that utilizes binary mixtures of aptamers at optimized ratios to fabricate aptamer-based sensors for the detection of synthetic cathinones, a family of designer drugs. We first performed a Cy7 dye-displacement assay using two aptamers with distinct binding properties to determine their optimal molar ratio. Then we fabricated dual-aptamer-based E-AB sensors and achieved sensitive detection of 12 drug targets while maintaining minimal response towards 17 interferents in the samples. We believe our strategy should be generalizable to other biosensors for tuning their cross-reactivity and specificity by using mixtures of different aptamers at an optimized ratio.

In my second project, we developed an innovative target-assisted immobilization strategy to fabricate E-AB sensors with sufficient spacing between the immobilized aptamers on the electrode surface to achieve optimal signal transduction and high signal-to-noise ratio (see Chapter 4). Specifically, we incubated electrodes with aptamer-target complexes instead of aptamers alone, such that the aptamers maintain a folded state during immobilization. We also found that modifying at lower ionic strength conditions (20 mM NaCl and 0.5 mM MgCl₂ versus 1 M NaCl and 1 mM MgCl₂) can effectively reduce aptamer bundling on the electrode surface. Using this strategy, we fabricated sensitive E-AB sensors that produce two-fold lower limits of detection (LOD) in biological samples and two-fold higher signal gains than sensors modified by conventional methods. This strategy should be generalizable as a strategy for improving the sensitivity of E-AB sensors fabricated with any arbitrary small-molecule-binding aptamer, regardless of their sequences and secondary structures.

In my final project, we focused on fabricating multiplexed aptamer-modified PEDs (see Chapter 5). We transferred the optimized E-AB sensors developed in my first two projects onto postage stamp-sized paper devices to simultaneously detect multiple analytes in a microliter sample volume within seconds. We utilized ambient vacuum filtration to deposit carbon nanotubes and gold or silver nanoparticles in layers on designed areas of a filter paper substrate. Three specific small-molecule-binding aptamers were then immobilized onto three different working electrodes. We achieved sensitive and accurate measurements in saliva and urine for all three small-molecule analytes: acetyl fentanyl, 3,4-methylenedioxypyrovalerone (MDPV), and adenosine. Our paper-based devices are easy to fabricate without batch-to-batch variations, and low-cost (< \$2), and therefore have considerable promise for the on-site detection of various small-molecule targets.

1.3. Scope of the dissertation

Chapter 2 provides a general overview of electroanalytical chemistry, aptamers, aptamer-based sensors, E-AB sensors, strategies for enhancing the sensitivity of E-AB sensors, different types of electrodes, *in vivo* detection with E-AB sensors, and the small-molecule targets used in work. Chapter 3 demonstrates the colorimetric dye-displacement assay and the fabrication of dual-aptamer E-AB sensors that employing a mixture of two aptamers with various binding properties to detect illicit drugs from the synthetic cathinone family. Chapter 4 describes the development of a target-assisted immobilization strategy to enhance sensitivity and signal gain in both buffer and biofluid sample matrices. Chapter 5 presents the fabrication of mPEDs for simultaneous detection of multiple analytes in a

single microliter volume of biosample within seconds. Chapter 6 summarizes my work for the dissertation and proposes directions for future work.

2.1. Aptamer-based sensors for small-molecule detection

Aptamers have increasingly attracted attention for biosensor applications due to their advantages over antibodies.^{1,2} Aptamers are short single-stranded DNA or RNA oligonucleotides that can specifically and strongly bind to various targets, such as small molecules, cells, and proteins.^{3,4} Aptamers can be generated *in vitro* through a technique termed SELEX (Systematic Evolution of Ligands by Exponential Enrichment).^{3,4} Usually, the SELEX process starts by incubating the target with an oligonucleotide library pool containing massive numbers (10^{15} ~ 10^{16}) of random sequences. The target-bound sequences are then isolated and amplified using the polymerase chain reaction (PCR). The PCR product is used as an initial library for the subsequent isolation round. The entire process is then repeated until target-binding sequences dominate the pool. Finally, the aptamer pool is subjected to analysis via Sanger sequencing⁵ or high-throughput sequencing⁵.

Aptamers have several advantages compared to antibodies that make them a very promising choice as bioreceptors for use in analytical and diagnostic applications: (1) aptamers can be isolated to bind to almost any category of target, including metal ions, proteins, small molecules, and cells, while the generation of antibody suffers from target limitations;⁵ (2) unlike antibodies, aptamers can be readily engineered so that they not only function as an affinity element, but can also serve as signal reporters;⁶ (3) whereas antibodies are produced through *in vivo* immunization of animals, which requires a long generation time and high cost, aptamer generation is a faster (2–6 weeks for aptamers

versus 6–18 months for antibodies) and cheaper (typically 10-fold lower than antibodies) *in vitro* process;⁷ (4) aptamers can be chemically synthesized with minor batch-to-batch variation, while antibody generation has significant batch-to-batch variation;^{6,7} and (5) aptamers are chemically stable even in harsh conditions (such as high temperature), while antibodies are sensitive to temperature, pH, and ion concentration, and are thus susceptible to degradation, aggregation, and inactivation.^{8,9} Accordingly, a number of published studies have described the use of aptamers in sensors to detect various analytes.^{10,11}

2.1.1. Aptamer-based optical biosensors

Fluorescence and colorimetry are two standard optical techniques for detecting small-molecule targets.¹² Stojanovic et al. developed fluorescent sensors to detect cocaine and adenosine ribonucleotide triphosphate (rATP) using self-assembled aptamer units labeled with a fluorophore-quencher pair (**Figure 2-1A**).¹³ Specifically, the three-way-junction-structured cocaine-binding aptamer and the stem-loop-structured rATP-binding aptamer were each split into two single-stranded aptamer subunits through the complementary stem-loop region. A fluorescein label was added onto the 5'-end of one strand, and a universal dabcyI quencher was added onto the 3'-end of the other complementary strand. The target binding process triggered the assembly of the two aptamer subunits and thereby induced fluorophore quenching, such that the reduction of fluorescence corresponded to the target concentration. This assay achieved specific, and accurate detection of cocaine and rATP, with LOD of 10 μ M for both targets.¹³ However, such sensors require sophisticated instruments for fluorescence detection and carry a high cost due to the need for aptamer labeling.

Stojanovic et al. subsequently investigated a colorimetric dye-displacement assay to detect cocaine (**Figure 2-1B**).¹⁴ They found that diethylthiatricarbocyanine iodide (Cy7), a cyanine dye, can non-covalently bind to the cocaine-binding aptamer MNS-4.1 as a monomer with an absorbance peak at 760 nm. The cocaine target in turn displaces these dye molecules upon binding to the aptamer, and the released dye molecules form dimers in solution with an absorbance peak of 670 nm. With the addition of cocaine, the 760-nm peak was reduced, and the extent of absorbance reduction corresponded to the concentration of cocaine. The authors achieved improved sensitivity compared to the previous fluorescence sensor (LOD = 10 μ M), with a LOD of 0.5 μ M cocaine.¹⁴ After 12 hours of incubation, a light-blue solution with blue precipitate could readily be observed in cocaine-containing samples by the naked eye, while control and other samples remained clear blue. However, it is challenging to find a universal dye molecule that is suitable for every single small-molecule-binding aptamer. For example, Stojanovic et al. tested 35 dyes and only found one that worked for aptamer MNS-4.1.¹⁴ Additionally, the 12 hours required to obtain the color change response is too long to be suitable for real-world, onsite applications.

Liu et al. developed generalizable colorimetric sensors for detecting adenosine and cocaine (**Figure 2-1C**).¹⁵ Their system employs gold nanoparticles, two short oligomers, and a long single-stranded sequence. They attached two short oligomers to the surface of two individual gold nanoparticles through their 3'-end and 5'-end, respectively. The long single-stranded oligonucleotide consisted of a small-molecule-binding region, and two complementary sequences that can hybridize with the oligomers modified onto the gold nanoparticles. In the absence of analyte, the three oligomers were assembled via

hybridization, resulting in aggregation of the gold nanoparticles and producing a purple color. In contrast, in the presence of the target, target binding triggered a conformational change in the aptamer and the subsequent release of the 5'-end gold nanoparticle-modified oligomer. This disassembly caused the separation of the gold nanoparticles, resulting in a color change from purple to red. The authors detected adenosine and cocaine in the concentration range of 0.3-2 mM and 50-500 μ M, respectively.¹⁵ This assay can be utilized to detect other analytes by integrating the relevant aptamer sequence into the long single-stranded fragment. The detection is rapid (within 10 seconds) and can be observed by the naked eye, but this approach is limited by its poor sensitivity (a LOD of 0.1 mM for adenosine detection and a LOD of 0.025 mM for cocaine detection).

2.1.2. Aptamer-based field-effect transistor (FET)

Field-effect transistor (FET)-based sensors have been utilized to analyze many targets due to their ultra-high sensitivity (nMs or pMs).^{16,17} These sensors utilize a semiconducting transistor that is sensitive to surface charge changes. When the target binds to the surface-modified bioreceptors such as aptamers, it triggers different electronic signals corresponding to the target concentrations. For example, Zayats et al. fabricated a FET sensor for the specific and sensitive detection of adenosine (**Figure 2-1D**).¹⁸ Specifically, an adenosine -binding aptamer was modified onto the gate surface and hybridized with a short complementary sequence; after adding the target, the target bound to the aptamer and released the short sequence, producing a voltage change that corresponded to the target concentration. The sensor achieved ultra-sensitive detection of adenosine with a LOD of 500 nM,¹⁸ which is significantly higher than the colorimetric sensors (LOD =25 μ M).

However, since FET sensors are based on measuring changes in charge, they are likely to have low efficiency for uncharged targets.

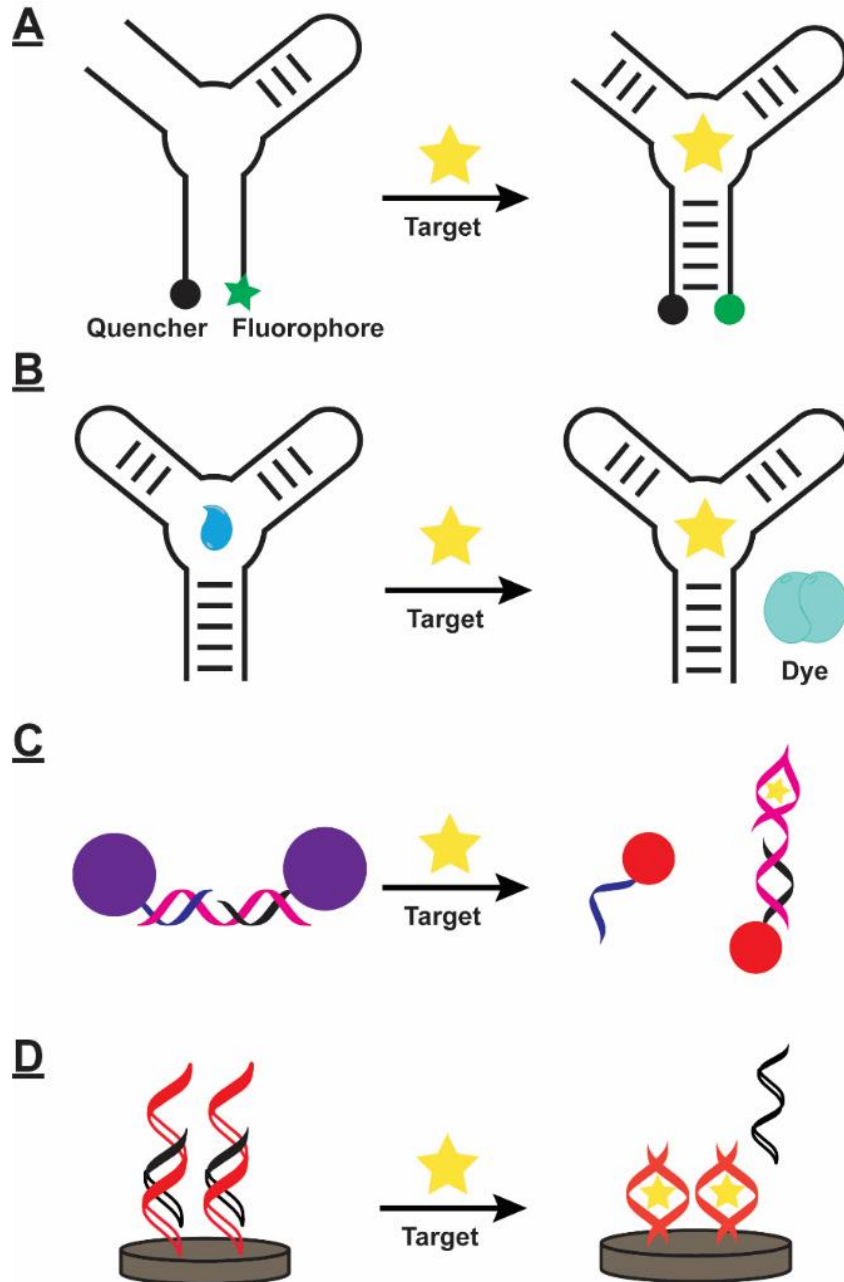


Figure 2-1. Aptamer-based sensors for small-molecule target detection. (A) Split aptamer-based fluorescent sensor, (B) colorimetric dye-displacement assay, (C) nanoparticle-based colorimetric sensor, and (D) field-effect transistor sensor.

2.1.3. Electrochemical aptamer-based (E-AB) sensors

E-AB sensors achieve the sensitive and specific detection of analytes by measuring signals generated by electron transfer between aptamer-conjugated redox molecules and a gold electrode surface in response to target-binding-induced aptamer conformational changes (**Figure 2-2A**).^{19,20} Generally, the aptamer is labeled with a 5' thiol and a 3' redox tag (*e.g.*, methylene blue) and then conjugated onto the surface of a gold electrode by thiol-gold chemistry. In the absence of target, the modified aptamer is unfolded and flexible in the detection matrix, producing minimal current. Upon binding to its target, the aptamer undergoes a major conformational change that brings the redox tag close to the electrode surface, which generates a large current increase. The fabrication of E-AB sensors entails two steps: incubating the smooth and clean electrode with an aptamer solution for the immobilization process, and then immersing the aptamer-modified electrodes into a backfill solution such as 6-mercapto-1-hexanol (MCH) to displace non-specifically bound aptamers and reduce opportunities for adsorption of interferents (**Figure 2-2B**).²¹

E-AB sensors are well-suited for small-molecule detection for a few reasons.²² First, E-AB sensors are able to detect small molecules in complex and impure samples because the target-induced conformational change is a specific signal generation process. Second, the readout of E-AB sensors is based on changes in current, which are easy to measure and interpret. However, these sensors are also limited by poor sensitivity, with LODs for small molecules that are typically in the lower micromolar range.²⁰ This is highly problematic because many small-molecule analytes require a much lower LOD—for example, the concentrations of many illicit drugs are typically in the nanomolar range in biofluids.²³

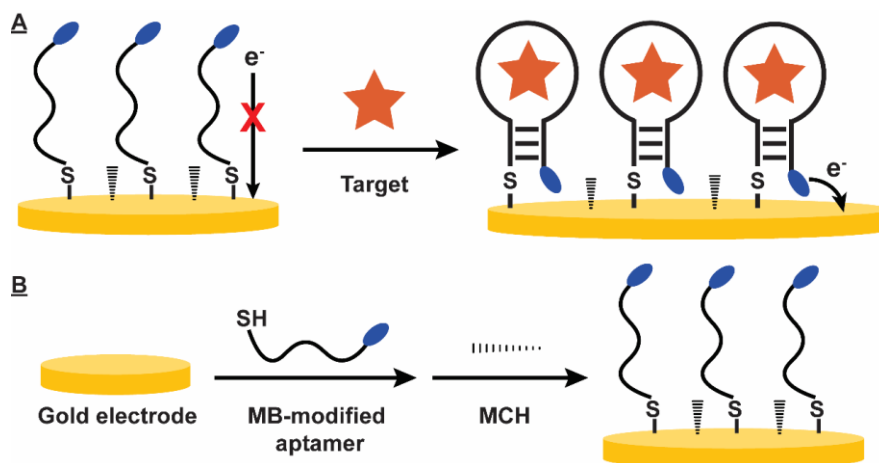


Figure 2-2. Overview of E-AB sensor design and fabrication. (A) Working principle of E-AB sensors. Aptamers are initially unfolded in the absence of target (left), situating the redox tag far from the electrode and producing minimal current. Target binding causes the aptamers to fold, resulting in enhanced electron transfer and increased current (right). (B) E-AB sensor fabrication process. Aptamers are immobilized onto the electrode surface, followed by backfilling with MCH.

2.2. Advanced strategies to enhance E-AB sensor performance

Recently, several methods have been developed to improve the performance of E-AB sensors. These include probe-related approaches as well as novel sensing strategies that can reduce background noise, enhance SNR, or amplify the signal. Other groups have made strides in optimizing measurement parameters and conditions and investigating surface properties that could enhance sensor performance.

2.2.1. Improving sensitivity via sensor probe design

2.2.1.1. Aptamer truncation to enhance sensor performance

Aptamers isolated via SELEX predominantly exist in a folded state without any structure-switching functionality, and thus cannot be directly incorporated into an E-AB sensor. Aptamer truncation offers one strategy for introducing a target-specific conformation change response while maintaining excellent binding affinity.

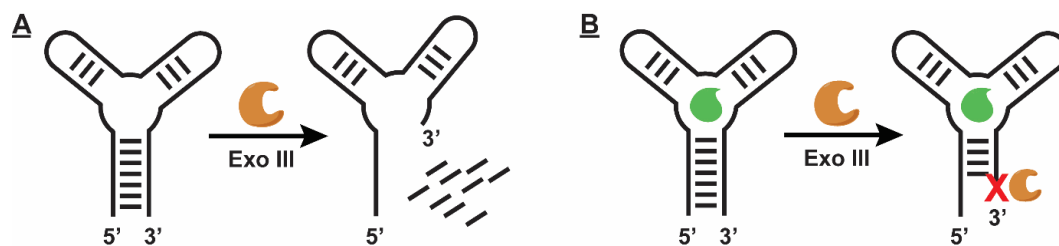


Figure 2-3. Overview of exonuclease-based assay for generating structure-switching aptamers.

For example, one E-AB sensor for the specific detection of cocaine in complex samples was fabricated by testing large numbers of different truncated cocaine-binding aptamers.²⁰ The optimal sensor successfully detected cocaine with a LOD of 10 μM in buffer, with detectable signals in both biofluids (LODs of 500 μM in both fetal calf serum and human saliva) and adulterated samples.²⁰ However, this trial-and-error truncation mutant screening method is laborious, time-consuming, and costly. Our group recently developed an alternative exonuclease-based method for identifying structure-switching aptamers for E-AB sensing via one-step enzyme digestion.²⁴ Specifically, exonuclease III (Exo III), a sequence-independent endonuclease that digests double-stranded oligonucleotides in a 3'-to-5' direction, was utilized to digest the cocaine-binding aptamer. Without target, the aptamer was digested down to a short oligonucleotide (**Figure 2-3A**), but in the presence of cocaine, Exo III digestion was halted four bases prior to the target-binding domain (**Figure 2-3B**), yielding a major digestion product that retained strong cocaine affinity but also exhibited structure-switching functionality. The E-AB sensor fabricated by this digestion product achieved sensitive and specific detection of cocaine with a LOD of 1 μM in buffer.²⁴ This method is a straightforward and generalizable

mechanism for introducing structure-switching functionality into small-molecule-binding aptamers and readying them for use in E-AB sensors.

2.2.1.2. Tuning sensor performance via multiprobe modification

Each E-AB sensor is usually modified with a single probe type. But more recently, multiple probes have been simultaneously modified onto sensors to achieve better performance, including higher sensitivity, broader dynamic range, and even multi-analyte detection capability.^{25,26} For example, Schoukroun-Barnes et al. fabricated E-AB sensors with a mixture of two aptamers with varying binding affinities for the same target.²⁵ The fabricated sensors' linear dynamic range and sensitivity could be predicted and controlled by tuning the ratio between the high-affinity and the low-affinity aptamers, where the tunability was related to the difference in the binding affinities between the two aptamers.²⁵

In the analytical field, it is more efficient to perform detection of multiple structurally-related analytes simultaneously than to determine the signals of each analyte separately. However, finding a bioreceptor that can recognize multiple related analytes while exhibiting minimal response towards non-target interferents is challenging. To solve this problem, we utilized a mixture of two aptamers with distinct binding profiles to fabricate E-AB sensors to broadly detect synthetic cathinones, a large family of dangerous designer drugs.²⁶ One of the two aptamers has high cross-reactivity towards targets and low specificity against interferents, while the other aptamer shows the opposite binding properties. An E-AB sensor fabricated with an optimal 1:1 ratio of the two aptamers achieved accurate and sensitive detection of 12 synthetic cathinones and minimal response

towards 17 interferents.²⁶ It is worth noting that this performance could not be replicated with E-AB sensors incorporating either aptamer alone.

2.2.2. Improving sensitivity via new sensing strategies

Traditional E-AB sensing platforms encounter sensitivity problems when detecting small-molecule targets because of the high background current generated by blank samples. New sensing strategies have subsequently been developed that can reduce this background. For example, Zuo et al. split a cocaine-binding aptamer into two fragments to fabricate an E-AB sensor with significantly enhanced sensitivity and reduced background (**Figure 2-4A**).²⁷ The 5'-hexane-thio-modified fragment is coupled to the electrode surface, while the flexible 3'-methylene blue-modified fragment was added separately. These two fragments were initially destabilized and dissociated, producing a low faradic current. After the addition of the target, the two fragments assembled via target-aptamer binding, resulting in the accumulation of methylene blue-modified fragments at the electrode surface and a 10-fold increase in the faradic current with 4 mM cocaine. This method achieved a LOD of 1 μM ²⁷, whereas a similar E-AB incorporating the unsplit cocaine-binding aptamer-based E-AB sensor could only achieve a LOD of 10 μM ²⁰. This method was also applied towards adenosine triphosphate detection, with a LOD of 1 μM .²⁷ However, this strategy requires careful design of the fragments and optimization of the methylene blue-modified fragments in order to maintain the aptamer's binding affinity while also minimizing the background.

Endonuclease-assisted E-AB sensors eliminate background signal by actively removing the signal probe from the electrode surface when no analyte is present (**Figure**

2-4B).²⁸ Zhang et al.²⁸ designed a 5'-thiol- and 3'-ferrocene-modified stem-loop-structured adenosine-binding aptamer with an EcoRI recognition sequence within the stem region. The aptamer formed a cleavable hairpin structure in the absence of a target, and after EcoRI cleavage, the cleaved ferrocene fragment was rinsed from the electrode surface by buffer solution, resulting in near-zero background current. Target binding induced a conformational change in the aptamer, forming a folded structure without the enzyme recognition site, which cannot be cleaved by EcoRI. This results in a prominent current peak generated by the ferrocene tag in response to target binding. This sensor achieved ultra-sensitive detection of adenosine with a LOD of 0.1 nM, 10,000-fold lower than other previously described E-AB sensors. However, the inefficient process of enzyme cleavage, which took 2 hours at 37 °C, greatly limits this system's utility in seconds detection scenarios.

Complementary DNA (cDNA) displacement is another strategy to improve the signal gain of E-AB sensors. Here, the cDNA forms a duplex with the surface-confined aptamers and lifts the redox tag away from the electrode surface, eliminating the background current. Target binding triggers the release of cDNA and forces the redox tag close to the surface, generating an increase in current (**Figure 2-4C**).²⁸ In one example of such a system, Zuo et al.²⁸ immobilized a 3'-thiol- and 5'-ferrocene-modified ATP-binding aptamer onto a gold electrode surface and hybridized it with a cDNA sequence. They observed almost no electron transfer to the electrode when it was hybridized to the cDNA, but the addition of ATP destabilized the duplex and formed an ATP-aptamer complex that situated the ferrocene tag close to the electrode surface, generating a strong signal and achieving a low LOD of 10 nM.²⁸

Signal amplification via enzyme-assisted target recycling is another approach for enhancing the performance of E-AB sensors. This strategy was first applied to DNA detection,²⁸ but the Wang group subsequently utilized a similar method for ATP detection (**Figure 2-4D**).²⁹ They used a 5'-methylene blue-labeled, hairpin-structured aptamer that changed its conformation to assume a different hairpin structure with a 5'-overhang when bound to ATP. This 5'-overhang was designed to hybridize with a cDNA anchored on the electrode surface, and the reduced distance between the methylene blue and the electrode surface generated a measurable increase in electrochemical signal. The subsequent addition of Exo III, which digests blunt-ended, double-stranded duplexes in a 3'-to-5' direction, resulted in the degradation of this electrode-bound oligonucleotide, releasing the ATP into solution. These released ATP molecules were thus free to bind other aptamer molecules, thereby amplifying the signal. As a result, the authors achieved remarkably sensitive detection of ATP, with a LOD of 34 pM.²⁹

2.2.3. Effect of surface monolayer on sensing performance

The surface of the E-AB electrode comprises a monolayer that is a composite of anchored aptamers and passivating alkanethiol backfills. The backfills can be self-assembled on the electrode surface to displace weakly-adsorbed aptamers, adjust the aptamer probe density, prevent non-specific adsorption of interferents, and lift the aptamers into highly ordered orientations.^{30,31} E-AB sensors typically utilize MCH as a backfill. Josephs et al. found that the sequence of aptamer modification and MCH monolayer formation affected the surface aptamer distribution and the self-assembled monolayer (SAM) stability.³² When they coupled the aptamers to electrodes after the MCH monolayer

was preformed—instead of the typical, reverse order—the modified aptamers exhibited a more uniform distribution instead of forming clusters, yielding SAMs with improved stability with 2-fold less degradation.³²

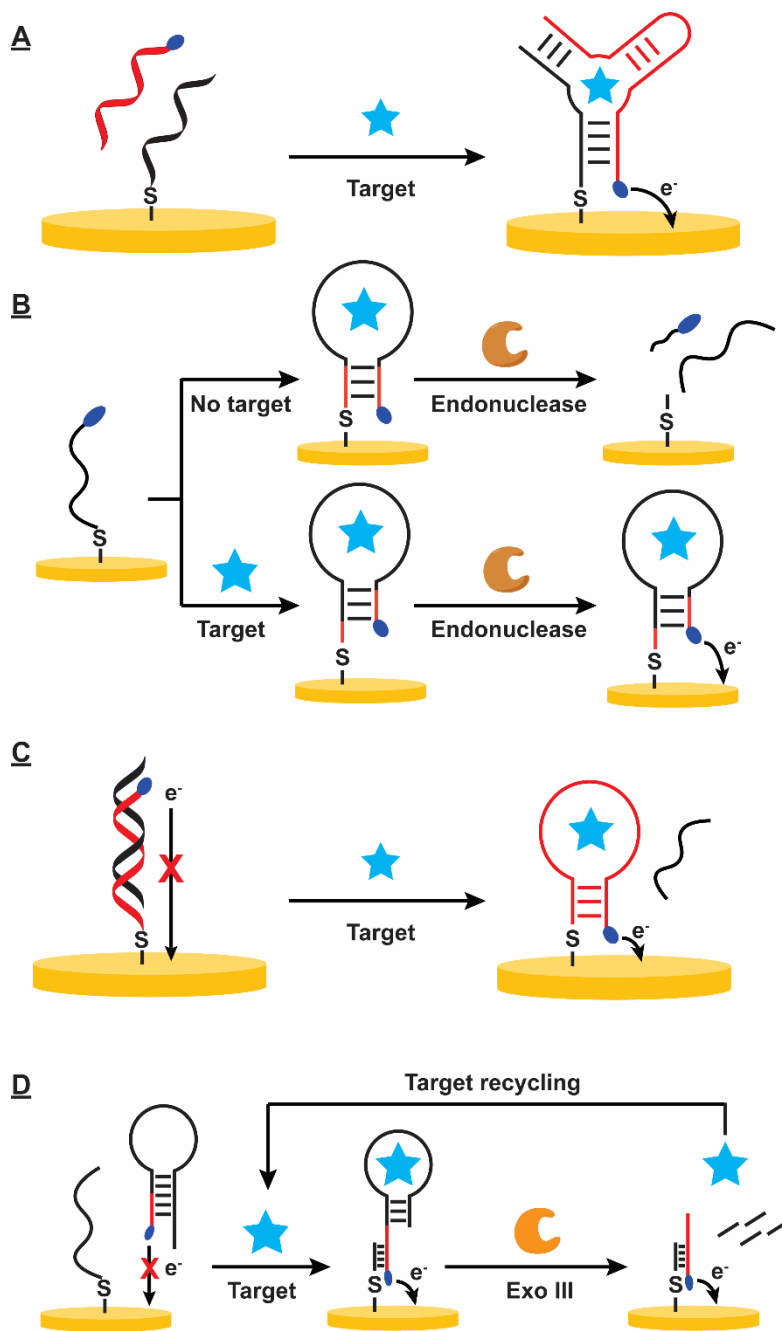


Figure 2-4. Probe-based strategies for improving the sensitivity of E-AB sensors. (A) Split aptamers and (B) endonuclease-assisted E-AB sensors, and (C) cDNA displacement are all

designed to enhance SNR by reducing background, while **(D)** enzyme-assisted target recycling enables amplification of the signal generated by target molecules.

The length of the alkane chain also affects the stability of the SAM. SAMs formed from 11-carbon alkanethiol have much higher stability (10-fold less current decay) than 6-carbon ones due to the tighter packing of longer alkane chains on the gold surface.³³ After 1 week of storage in buffer, a SAM based on 11-carbon thiol exhibited < 7% current decay, whereas one composed of a 6-carbon thiol had a >60% current decrease.³³ However, the increased length of alkanethiol may also compromise the sensor performance because the thick monolayer reduces the electron-transfer rate,³⁴ resulting in reduced faradic currents and bad SNR. Hence, it is critical to select a proper length of alkane chains that leverages both SAM stability and sensor performance. The terminal group of the alkanethiol also affects monolayer stability and sensor performance. Compared to hydrophilic hydroxyl-terminated SAMs based on MCH, hydrophobic methyl-terminated backfills such as 1-hexanethiol—which has the same alkane chain length as MCH—exhibited higher stability (stable at 37 °C for several days) in both physiological buffers and whole blood samples, although such SAMs were unable to prevent fouling in the latter samples.³⁵ An E-AB sensor that used a mixture of hydroxyl- and methyl-terminated backfill molecules at an optimal ratio demonstrated greatly improved stability—from less than 12 hours to 2 days—due to the suppressed desorption of the SAM from the electrode surface over time.³⁵

Baseline drift is another critical issue in performing detection in complex samples such as undiluted blood. Researchers usually use a membrane as a physical barrier to block cells or proteins from approaching the electrode surface to solve this problem.³⁶ However, membrane utilization also reduces the target diffusion efficiency and results in a slow

sensor response time (few seconds to minutes). Li et al. investigated the use of a zwitterionic phosphatidylcholine-terminated monolayer to eliminate biofouling effects during continuous detection in undiluted flowing blood samples over the course of several hours.³⁷ After 12 hours of *in vivo* operation in live animals, the phosphatidylcholine-based E-AB sensor had < 5% drift despite the absence of a membrane.³⁷ An MCH-based sensor, in contrast, exhibited severe baseline drift, resulting in at least 50% signal loss after performing detection in whole blood for 3 hours.³⁷ As an alternative, polyethylene glycol (PEG) has also been reported to exhibit an excellent ability to resist non-specific adsorption of protein in biological samples.³⁸ For instance, Wang et al. fabricated an E-AB sensor for ATP detection that achieved higher sensitivity with a LOD of 0.1 pM and greatly reduced biofouling (2-fold less nonspecific adsorption in 10% human plasma) by immobilizing a mixture of PEG and ATP aptamers onto the electrode surface, followed by MCH backfilling.³⁹ In addition, Wu et al. demonstrated the superiority of utilizing monolayers comprising a combination of α,ω -alkanedithiol dithiothreitol (DTT) and MCH, wherein they simultaneously immobilized the DNA probes and DTT on the electrode surface followed by MCH backfilling.⁴⁰ This resulted in greatly improved SNRs and achieved a LOD of 10 pM for DNA detection. On the other hand, the sensors can only reach a LOD of 1 nM when backfilled with MCH alone.⁴⁰

RNA aptamers usually exhibit high affinity and reasonable specificity for small-molecule targets,⁴¹ but the hydrolysis and degradation of RNA aptamers in complex matrices has drastically hindered their application in E-AB sensors.⁴² Santos-Cancel and White coated a ribonuclease inhibitor onto a collagen membrane, which they overlaid onto an RNA aptamer-based E-AB sensor.⁴³ The membrane prevented large ribonuclease

enzymes from approaching the electrode surface, while the inhibitor inactivated those enzymes. Using this design, the authors successfully achieved long-term and stable detection of tobramycin in undiluted serum with < 3% signal loss over the course of at least six hours.⁴³ In contrast, without protection from the collagen membrane, the signal dramatically degraded within 10 min.⁴³

Moreover, aptamers immobilized on the electrode need sufficient space for target binding, folding, and signal transduction. These aptamers should also be sized properly; otherwise, the sensors would have a reduced SNR due to insufficient space for the probes to be fully active or too few probes to generate signals. Hence, it is necessary to control aptamer quantity and spatial arrangement on the electrode surface to obtain optimal E-AB sensor performance. The simplest way to control the aptamer density is by altering the aptamer concentration during the immobilization. One study has shown that by optimizing aptamer density via concentration, the authors could boost the maximum signal gain of a cocaine E-AB sensor from 60% to 200%.⁴⁴ However, the spatial arrangement of aptamers on the electrode surface was not tuned simultaneously in this work. The Fan group connected one fragment of a split cocaine-binding aptamer to DNA tetrahedrons conjugated on an electrode surface.⁴⁵ These nanostructured tetrahedrons optimized the aptamer orientation while also ensuring homogeneous distribution on the electrode surface. Adequate spacing between adjacent aptamers in this design allowed the efficient assembly of split aptamers induced by target binding process, and the resulting sensors achieved sensitive detection of cocaine with a LOD of 33 nM.⁴⁵

Recently, our group developed a target-assisted immobilization strategy to control the microgeometry of aptamers on the electrode surface.⁴⁶ Unlike traditional approaches, in which the unfolded aptamer is immobilized on its own, we utilized aptamer-target complex with a fully-folded secondary structure solutions during sensor fabrication. When we subsequently removed the target, all the aptamers were uniformly distributed on the surface, with sufficient space for target-induced conformational change and signal transduction.⁴⁶

2.2.4. Effect of measurement parameters on sensing performance

There are multiple different strategies available for measuring electrochemical response in an E-AB system. Cyclic voltammetry (CV) is often used to measure the essential electrochemical properties of the analytes or explore reaction mechanisms.^{47,48} In CV experiments, the potential ramps up and goes back down at a constant scan rate within a set potential range.⁴⁹ Differential pulse voltammetry (DPV) is a more sensitive alternative (DPV can detect as low as nanomole concentrations while CV can only measure micromole concentrations), entail the application of a series of increased potential pulses at fixed increments.⁵⁰ Current is measured before and after each pulse, and the differences are recorded. This process minimizes the capacitive current and reduces the background, resulting in enhanced sensitivity.⁵¹

Alternating current voltammetry (ACV) is another technique for E-AB sensors. In ACV, the sequential sinusoidal waveform potential is superimposed onto the base potential, and the current is measured at a specific frequency.⁵² After conjugating with a lock-in amplifier, the ACV signals are capable to detect even in an extremely noisy environment,

and the sensitivity of ACV is enhanced.⁵³ Tuning the ACV frequency can also improve the signal gain of E-AB sensors.⁴⁴

Square-wave voltammetry (SWV) is another popular technique applied to E-AB sensors due to its excellent sensitivity (detectable concentrations as low as picomoles) and fast detection capability.⁵⁴ SWV entails recording the current difference between the forward pulse and the reverse pulse within a series of staircase pulses, removing the non-faradic current to reduce the background and thereby enhancing the SNR.⁵⁵ Most importantly, changing the SWV frequency and amplitude of the potential pulses alters the electron-transfer kinetics between the bound and unbound states. SWV can be performed under a fast scan rate, making the detection process fast (within seconds), and simultaneously optimizing the frequency and amplitude can improve signal gains by more than two-fold.⁵⁶

Truncation can potentially enhance an aptamer's structure-switching functionality, but this engineering process also destabilizes the aptamer and reduces its binding affinity, influencing the sensor performance. Ideally, the engineered aptamer should undergo a large target-induced conformational change while maintaining high binding affinity. Zhao's group found that the binding affinity of truncated aptamers can be greatly improved at 4 °C compared to room temperature.⁵⁷ They showed that a truncated aflatoxin B1-binding aptamer with a 2-bp stem showed a K_D of 16 nM at 4 °C versus 498 nM at room temperature, and that E-AB sensors fabricated from this aptamer likewise exhibited higher sensitivity at 4 °C, with a low LOD of 6 pM, compared with 25 nM at room temperature.⁵⁷

2.2.5. Effect of redox reporters on sensor performance

Methylene blue and ferrocene are the most commonly-used redox reporters for E-AB sensors. Ferrocene-based E-AB sensors usually exhibit 20% higher signal gains than those based on methylene blue.⁵⁸ However, ferrocene-conjugated E-AB sensors also have several drawbacks. First, ferrocene-based E-AB sensors exhibit reduced signals in terms of detections in complex biologic matrices such as serum and blood.⁵⁹ During detection, ferrocene loses one electron and forms a ferrocenium ion under oxidative conditions,⁶⁰ and these oxidation peaks at varying analyte concentrations are then recorded to calculate the signal gain. However, the ferrocenium ion is also extremely prone to react with oxygen in the sample, which in turn contributes to sensor instability.^{61,62} Furthermore, the oxidation potential of ferrocene is 0.22 V, which is outside the optimal potential window (-0.4 V to -0.2 V for Ag/AgCl reference electrodes)⁶³ of E-AB sensors. In contrast, methylene blue-based sensors are more stable and show less current reduction and only minor signal degradation after multiple scans over the course of a few hours in both buffer and blood serum.^{58,63} Methylene blue transfers two electrons to the gold electrode surface and forms leucomethylene blue during this reaction,⁶⁴ with a reduction peak potential of -0.26 V, which is within the optimal potential window for E-AB sensors. Methylene blue-based E-AB sensors also exhibit good stability during long-term storage, with 4-fold less signal degradation in the regeneration process, high reproducibility, and minor sensor-to-sensor variation.⁵⁸ Collectively, these advantages make methylene blue-based E-AB sensors a better choice compared to ferrocene-based E-AB sensors, especially in complex biological matrices such as undiluted blood.

The position of the methylene blue modification also strongly affects sensor performance. In a typical E-AB sensor, the aptamer is attached to the surface of the gold electrode via a 5' thiol modification, with the methylene blue reporter modified onto the 3'-end of the aptamer. E-AB sensors in which the positions of the thiol group and methylene blue are switched (5'-methylene blue, 3'-thiol) showed similar aptamer binding affinities to conventional sensors, but with shifted optimal detection frequencies and 4-fold reduced signal gains.⁶⁵ This has been observed in three well-established E-AB sensors against cocaine, doxorubicin, and vancomycin.⁶⁵

2.2.6 Effects of electrode morphology on sensor performance

Traditional E-AB sensors employ 2-3 mm diameter gold rod electrodes with a flat and smooth surface. The electrode surface must be cleaned carefully before aptamer immobilization. Recently, researchers have found that a rough or nanostructured electrodes can improve the SNR and the maximum signal gain due to increased surface area.⁶⁶ For example, the Kelley group electrodeposited an Au-Pd alloy onto the surface of a microelectrode with a unique spike-like nanostructure (20–50 nm) to enhance the sensitivity and extend the linear dynamic range for nucleic acid detection.⁶⁷ They then further investigated the applications of these spike-like electrodes for the sensitive detection of small molecules.⁶⁸ They first coated a Si₃N₄ passivation layer onto a SiO₂-coated silicon substrate, and then made a 5- μ m aperture on the passivation layer via photolithography. Gold was then electrodeposited onto the silicon substrate surface through the aperture, followed by electrochemical coating of a Pd layer onto the gold. The spike-like Au/Pd nanostructure was formed by controlling the applied potential and the

types and concentrations of electrolytes. Small-molecule-binding aptamers were then modified onto the surface of the spike-like electrodes. A single-stranded, partially-complementary, lysine-conjugated peptide nucleic acid was used to neutralize the negative charge of the aptamers, notably reducing the charge on the electrode surface. Target addition triggered the displacement of this neutralizing strand, and the resulting enhancement of the surface charge of the electrode was measured electrochemically. This method was successfully used to develop sensors for the sensitive detection of cocaine and ATP with a LOD of 1 μM for both analytes.⁶⁸

The gold wire electrodes typically used for real-time *in vivo* detection are extremely small: typically 75–200 μm in diameter and 3–6 mm in length.⁶⁹ As such, only limited numbers of aptamers can be modified onto their surface, resulting in nanoampere faradaic current and a bad SNR. It is therefore critical to enhance the surface area to increase the number of aptamers that can be modified onto such small electrodes. Several strategies have been developed for such purposes, including a pulsed electrochemical method for fabricating gold wire with rough dendrite-like surfaces.^{36,70} In this example, gold wires with a 5–8 mm working length were immersed in 0.5 M H_2SO_4 , followed by back-and-forth scans with alternating 2 ms pulses at 0.0 V or 2.0 V for 100,000 cycles. During each pulse, the gold was dissolved at 2.0 V and then randomly deposited back onto the electrode surface at 0.0 V. To further enhance the surface area of the electrodes, the pulse duration was increased to 10 ms with a total of 16,000 pulses.⁷¹ After treatment, the electrodes had a 2-fold enhancement in surface area versus untreated gold electrodes.⁷¹ E-AB sensors fabricated with these rough electrodes showed better performance for detecting tobramycin in living animals, with the absolute current improved by 2-fold and 2-fold higher SNR.⁷¹

In other work, a sponge-like nanoporous electrode was developed via a metal alloying-and-dealloying process to further increase the surface area of small-sized electrodes.⁶⁹ A gold wire electrode with a diameter of 200 μm and an exposed 3 mm-long working area was placed in a 115 $^{\circ}\text{C}$ ZnCl_2 solution (dissolved in ethylene glycol) and subjected to ten CV scans from 0.8 to 1.8 V at a scan-rate of 0.01 V s^{-1} . As a result, zinc was deposited onto the electrode surface, forming a layer of Au-Zn alloy. To remove the zinc, the Au-Zn alloy electrodes were first immersed in 5 M HCl for 15 min, and then transferred to a 50 mM H_2SO_4 solution for 5–10 more CV scans between 0 to 1.8 V at a scan-rate of 0.1 V s^{-1} to completely strip off the residual zinc. The resulting sponge-like electrodes achieved a 75–100-fold surface area increase, while the dendrite-like electrodes only had a 2–4-fold increase compared to the smooth electrodes.⁶⁹ The sponge-like electrodes also had 25-fold greater signal currents and 15-fold reduced levels of noise. In this way, working gold electrodes could be miniaturized to a diameter of 75–200 μm and a length of 0.5–3 mm. E-AB sensors fabricated with these miniaturized electrodes successfully detected vancomycin in the jugular of a live rat with similar signal response as seen with larger electrodes.⁶⁹

Another group developed ‘shrink electrodes’ with increased active surface area to improve SNR and sensitivity. These shrink electrodes were fabricated by heating gold-coated polyolefin film at 125 $^{\circ}\text{C}$, causing it to shrink by 95%.⁷² Compared to planar electrodes, these electrodes showed a 6.47-fold enhanced active surface area, and electrochemical sensors based on these sensors demonstrated higher sensitivity for 2-(dibutylamino)-ethanol detection, with a 50% lower LOD (1.7 μM) than the planar electrodes.⁷² In principle, these shrink electrodes can offer an up to 20-fold increase in active surface area. However, the shrinking process tends to trap the air, preventing the

sample solution from approaching the surface and diminishing the available active surface area.⁷³ The Heikenfeld group found that an extra coating of polyvinyl pyrrolidone (PVP) layer on top of the Au/polyolefin film further enhanced the active surface area by 1.9-fold compared to without PVP coating—equivalent to a 12.7-fold enhancement over the planar electrode.⁷⁴ The PVP replaced the air and formed a hydrophilic layer outside the shrink electrode, allowing the aqueous solution to reach the maximum active surface area. When incorporated into an E-AB sensor for kanamycin detection, these PVP-coated shrink electrodes achieved a maximum signal gain of 330%, which was two-fold higher than that of a planar electrode.⁷⁴

2.3. Other electrode types developed for *in vitro* applications

Gold rod electrodes are well-established and commercially available for the fabrication of highly stable E-AB sensors that can handle hundreds of repeated detections in complex samples and have fewer batch-to-batch variations. However, their large size, mechanical rigidity, and high cost (\$90 per electrode) mean that the gold rod electrodes are impractical for portable, flexible, and commercially scalable applications, and are primarily suited for lab use instead.

Screen printing is an alternative method for fabricating electrodes that can replace gold rod electrode in real-life applications. This method is based on the deposition of ink materials onto a designed area of a substrate such as paper or plastic.⁷⁵ However, these inks can easily form aggregates during the fabrication process,⁷⁶ because the ink dispersions typically contain conductive components such as metal-based or carbon-based

nanomaterials with high surface energies⁷⁷. Without adequate stabilization, these nanomaterials will quickly agglomerate in solution.

Paper-based electrodes have attracted much recent attention due to their low cost, versatility, and ready compatibility with portable devices for on-site detection.^{78,79} Our group developed a strategy for fabricating aptamer-modified PEDs via ambient vacuum filtration.⁸⁰ We first deposit single-walled carbon nanotubes onto a designated section of filter paper via vacuum filtration to produce a nanoporous conductive network. Gold nanoparticles are then deposited on top of the single-walled carbon nanotube layer via vacuum filtration in patterns that establish the working or counter electrodes and electric circuits. Finally, silver nanoparticles are vacuum filtered through a mask designed to form the pseudo-reference electrodes. It should be noted that the type, shape, and size of the materials employed for electrode fabrication with this approach is easily customizable. E-AB sensors fabricated onto such PEDs achieved sensitive and specific detection of cocaine and MDPV, with performance similar to E-AB sensors fabricated onto commercial gold rod electrodes. We subsequently constructed a multiplexed aptamer-modified PED with three working electrodes using the ambient vacuum filtration method.⁸⁰ After immobilizing acetyl fentanyl-, adenosine-, and MDPV-binding aptamers onto the three working electrodes, we were able to achieve sensitive, accurate, and simultaneous detection of acetyl fentanyl, adenosine, and MDPV in a single sample within seconds. By incorporating a polydimethylsiloxane (PDMS) chamber on top of this PED, we were able to achieve detection from samples with a small volume of just 200 μL .⁸⁰ Our aptamer-based PED sensors are sensitive, stable, accurate, environmentally-friendly, suitable for large-scale

production, and sufficiently portable for on-site applications such as drug screening or environmental monitoring.

2.4. E-AB sensors for *in vivo* detection

For many clinically-oriented biosensor applications, it would be ideal to achieve real-time detection in living bodies—for instance, accurate real-time detection of drugs within narrow therapeutic windows in order to achieve precise drug dose control for effective and safe therapy.⁸¹ E-AB sensors have the potential to satisfy this need because they: (1) have high specificity, with only specific targets triggering aptamer conformational changes;¹⁹ (2) can achieve sensitive detection of analytes;⁸² (3) can detect analytes across broad dynamic ranges;²⁶ (4) can enable stable and accurate detection in biofluids under physiological conditions;⁸³ and (5) can provide the time-resolution required for subsecond detection and continuous monitoring.^{84,85} But *in vivo* detection with E-AB sensors also faces many challenges. For example, the SNR, sensitivity, and signal gain of E-AB sensors are reduced over extended periods in biofluids due to biofouling.⁸⁶ Baseline drift and signal decay also become substantial issues for E-AB sensors in extended-duration detection.⁸³ Moreover, SAMs tend to become desorbed from the electrode surface over time, and nuclease enzymes circulating in the biofluid are prone to digest aptamers.^{87,88}

Many strategies have been developed to overcome these challenges. Swensen et al. fabricated a micro-scale E-AB sensor device for the continuous detection of cocaine in undiluted flowing serum.⁸³ Their sensor, in which 3'-methylene blue-modified cocaine aptamers were covalently attached to the gold electrode surface, was conjugated to a microfluidic chip and confined within a 750 nL chamber. Undiluted serum containing

various concentrations of cocaine was pumped into the microfluidic chip at a constant speed, and the cocaine concentrations were measured. Ferguson et al. subsequently developed a microfluidic device that can detect small molecules in whole human blood or from the circulatory system of live rats.⁸⁹ The device consisted of two layers: blood was pumped through the lower layer, exiting into a waste container, while the top layer generated a buffer flow in direct contact with the fabricated E-AB sensor. In between, a diffusion filter served as a physical barrier to prevent large interferents from reaching the sensor, whereas small-molecule targets in the blood can approach the E-AB sensor and thereby produce a signal. The authors also developed a strategy termed ‘kinetic differential measurement’ (KDM) for reducing the baseline drift during long-term continuous detection.⁸⁹ Using this system, they achieved continuous, specific, and accurate detection of doxorubicin and kanamycin in flowing human blood flow and in the circulation of live rats with only minor signal drift for 4 hours.⁸⁹ However, despite the remarkable *in vivo* demonstration in this work, it is still inadequate for real-world long-term applications, which typically entail continuous detection for days or even weeks. Additionally, the blood must be pumped outside the body for detection, and cannot be recycled into the body afterward because of possible contamination from the buffers.

Arroyo-Currás et al. developed E-AB sensors with conjugated micro-scale electrodes to detect multiple small-molecule targets in awake animals.³⁶ The electrodes were inserted into the external jugular vein of rats via catheter, and directly measured the aptamer targets in the circulating blood. A polysulfone membrane with 0.2- μm micropores covered the aptamer-modified working area of the gold wire electrode to prevent biofouling. Only the small-molecule targets could pass through this membrane, while other components such as

blood cells, which may cause biofouling during continuous detection, were filtered out. Their sensor also applied KDM to reduce signal drift during real-time detection. With the protective membrane and KDM-mediated drift correction, they were able to achieve accurate and stable real-time detection of multiple analytes over a few hours in awake, moving rats.³⁶

Li et al. developed an alternative baseline correction method to KDM using two redox tags.⁹⁰ They modified aptamers with methylene blue at their 3'-end and another redox tag anthraquinone, at the 5'-end, which was also covalently attached to the electrode. The fixed anthraquinone end generated a minor response to target binding. The redox peak of anthraquinone (-0.42 V) does not overlap with that of methylene blue (-0.26 V), and both anthraquinone and methylene blue had constant baseline drift during continuous detection in whole flowing blood. Hence, subtracting the normalized currents generated by anthraquinone from those generated by methylene blue could correct the baseline drift. The authors first tested cocaine detection in continuous blood flow for 15 hours, and were able to reduce the drift from 50% to < 2% after using this correction method. They then generalized this strategy and tested a kanamycin sensor, which showed a drift reduction from 20% to < 2% during a 20-hour period. One drawback of this method is that the signal gains were reduced by this correction process. Furthermore, certain small-molecule targets such as doxorubicin have redox reactivity at the same potential as anthraquinone,⁹¹ which affects the accuracy of this reference reporter.

With the ability to monitor targets in real-time *in vivo*, E-AB sensors have been successfully demonstrated for potential therapeutic applications. For instance, a

vancomycin-binding aptamer-modified wire electrode was placed into a rat vein for continuous measurement of blood vancomycin with high precision ($\pm 20\%$) for 6 hours.⁹² Such monitoring is beneficial because the clinical blood concentration of the antibiotic vancomycin should be maintained at 6–35 μM to ensure therapeutic effect while minimizing side effects.⁹³ In addition, the Plaxco group fabricated E-AB sensors for the real-time monitoring of irinotecan, a cancer chemotherapy drug. Their E-AB sensors demonstrated precise detection of irinotecan in the blood of live rats over the course of 300 repeated measurements in 1 hour with $< 20\%$ error, enabling in-time adjustment of the drug dose during therapy.⁹⁴ Later, the Plaxco group developed E-AB sensors to detect phenylalanine in real-time, which they used to investigate the disposition kinetics of plasma phenylalanine in live rats—an important consideration for the monitoring and treatment of metabolic disorders.⁹⁵

Researchers have also recently started to detect protein targets in urine for disease diagnostics. Plaxco's group fabricated an E-AB sensor on microelectrodes to detect neutrophil gelatinase-associated lipocalin (NGAL), a protein biomarker that indicates acute kidney injury.⁹⁶ Concentrations of NGAL were monitored in real-time in continuously NGAL-titrated artificial urine over several hours with a 2 nM LOD. This concentration was in the range of 2–32 nM,⁹⁷ which is physiologically appropriate for the diagnosis of kidney injury.

2.5. Small-molecule targets used in this work

2.5.1. Synthetic cathinones

Synthetic cathinones, commonly sold as "bath salts", are a group of psychoactive substances that have recently risen in popularity. These compounds are highly dangerous and have severe side effects that include paranoia, hallucinations, extreme anxiety, and even death.⁹⁸ Synthetic cathinones are stimulants, and most of them are classified as Schedule I drugs under the Federal Controlled Substances Act. The drugs in the synthetic cathinones family share the same beta-keto phenethylamine core structure with various substituents.⁹⁹ So far, hundreds of synthetic cathinones have been synthesized and sold on the market.¹⁰⁰ Among them, twelve popular synthetic cathinones including MDPV, ethylone, butylone, pentylone, naphyrone, methylone, methcathinone, α -pyrrolidinopentiophenone (α -PVP), 3-fluoromethcathinone (3-FMC), cathinone, 4-fluoromethcathinone (4-FMC), and 4-methylmethcathinone (4-MMC) (**Figure 2-5**), were picked as targets in this work.

2.5.2. Cocaine

Cocaine (**Figure 2-6A**), an addictive stimulant drug derived from the leaves of the coca plant. Cocaine is a Schedule II drug with high potential for abuse, but which can be used as a medicine under certain conditions. Cocaine was the third most frequently used drug in 2020.¹⁰¹ 1.9% of people aged 12 or older have been reported as cocaine users, and 0.5% of people suffer from cocaine use disorder.¹⁰² The number of overdoses identified by the National Institute on Drug Abuse has risen dramatically, reaching 19,447 in 2020—

four-fold higher than the number in 2014.¹⁰³ Cocaine overdose is associated with anxiety, depression, tremors, paranoia, and even death.¹⁰⁴

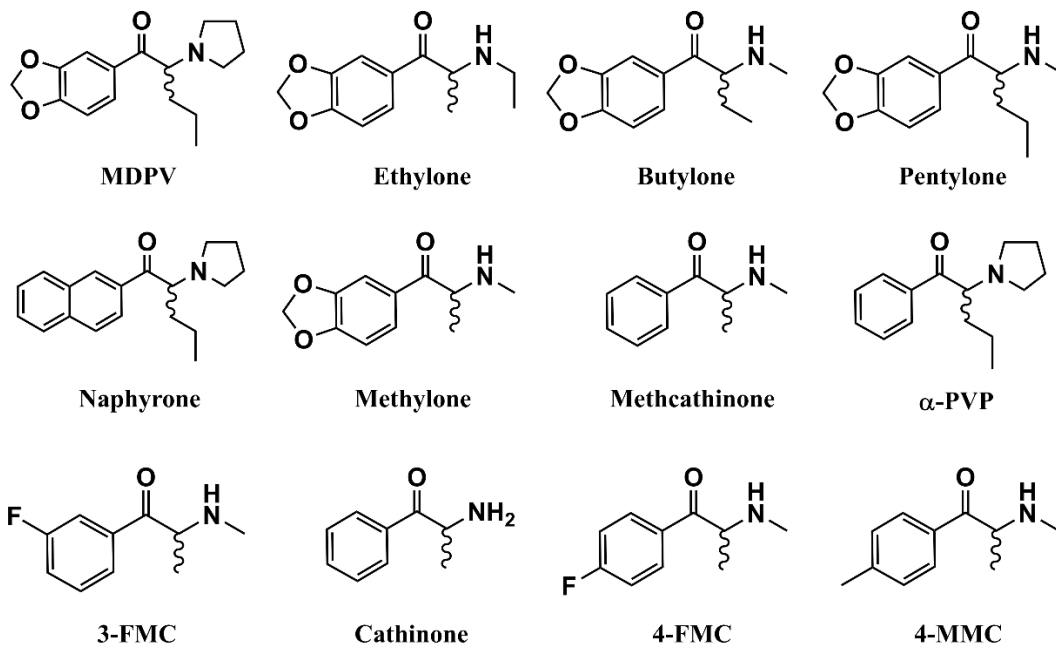


Figure 2-5. Chemical structures of different synthetic cathinones used in this work.

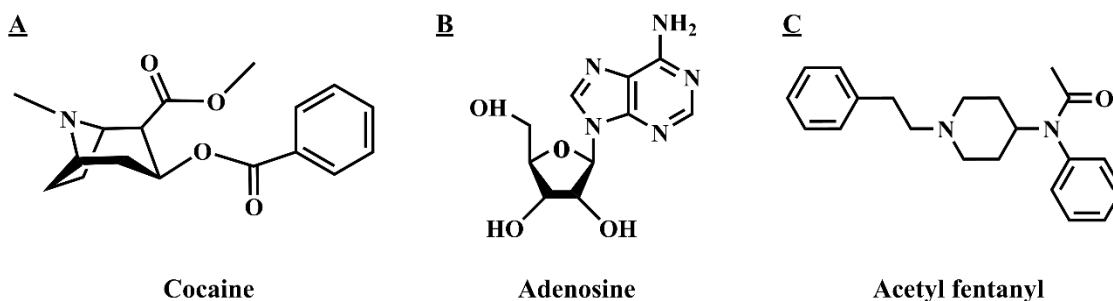


Figure 2-6. Chemical structure of small molecule targets. (A) Cocaine, (B) adenosine, and (C) acetyl fentanyl.

2.5.3. Adenosine

Adenosine (**Figure 2-6B**) is an endogenous small molecule that can regulate extracellular signaling to ensure regular heart rhythms.^{105,106} Adenosine also can regulate

innate immunity.¹⁰⁷ Adenosine concentrations increase dramatically from a resting concentration of ~300 nM to 600–1200 nM when the cell is in an inflammatory state or subject to tissue damage.¹⁰⁸

2.5.4. Acetyl fentanyl

Acetyl fentanyl (**Figure 2-6C**) is a synthetic opioid and an analog of fentanyl. Acetyl fentanyl exhibits very similar properties to heroin and morphine, but its activity is 15.7 times more potent than those drugs.^{109,110} Acetyl fentanyl is a Schedule I drug with high potential for abuse and no medical utility. Misuse or overdose of acetyl fentanyl leads to side effects similar to other opioids, such as drowsiness, dizziness, nausea, vomiting, unconsciousness, and respiratory depression.¹¹¹ Recently, acetyl fentanyl and its fentanyl analogs have become the primary drugs responsible for overdose death in the United States.¹¹²

3.1. Introduction

The detection of structurally-related small molecules such as toxins, antibiotics, and illicit drugs is important for analytical applications in which determining the presence of any member of a designated molecular family – rather than any individual representative of that family – is the priority.^{113–115} Currently, this is typically achieved using immunoassays based on polyclonal antibodies, which comprise of a mixture of antibodies produced by target-immunized animals.¹¹⁶ Polyclonal antibodies are well-suited for such applications, because the combination of multiple antibodies binding to different epitopes greatly expands the target spectrum.¹¹⁷ However, the *in vivo* nature of the antibody generation process provides no control over the binding properties or composition of the resulting reagent mixture.¹¹⁸ This can result in false negatives, since it is impossible to guarantee that polyclonal antibodies will bind to all members of a designated target family with similar binding affinities—or at all.^{116,119} On the other hand, polyclonal antibodies can also be too promiscuous, producing false positives due to recognition of structurally similar non-target compounds.¹¹⁷ The binding profiles of polyclonal antibodies can also greatly vary from batch to batch, as they are generated from different animals.¹¹⁷ One can potentially overcome these limitations by mixing multiple monoclonal antibodies with differing binding spectra at an optimized ratio, but the costly and time-consuming process of monoclonal antibody development discourages such efforts.¹²⁰

Aptamers offer an excellent alternative. These nucleic acid-based biorecognition elements are isolated *in vitro* via systematic evolution of ligands by exponential enrichment

(SELEX)⁴ from randomized oligonucleotide libraries to recognize various targets, and can be chemically synthesized at low cost with no batch-to-batch variation.⁶ Importantly, the binding profile of an aptamer can be precisely controlled by designing the selection process to favor candidates that bind to either a specific target or a family of structurally-related targets.^{121–123} Moreover, the analytical performance of aptamer-based assays can be tailored for specific applications. For example, the sensitivity and dynamic range of assays can be altered by using a mixture of different aptamers¹²⁴ or an aptamer and its truncated or mutated derivatives that bind the same target but with different affinities.^{25,125} Nevertheless, little effort has been made to control the cross-reactivity of aptamer-based assays towards a set of ligands, both targets and interfering compounds.

In this work, we for the first time have demonstrated that the cross-reactivity of aptamer-based sensors can be manipulated to achieve near-ideal sensing performance with unprecedented control by mixing multiple aptamers with differing ligand specificity. This has not yet been achieved with conventional aptamer engineering techniques. As a test bed, we targeted the synthetic cathinones, a large family of designer drugs whose members share the beta-keto phenethylamine core structure but have divergent side chain substituents.¹²⁶ Our goal was to develop a sensor that can give a yes-or-no response for the presence of drugs in this family while yielding no response to interferent molecules relevant to illicit drug detections. Thus, assay cross-reactivity at a specific cut-off (e.g. ligand concentration) is a more appropriate metric to evaluate the analytical performance of our sensors. We have recently isolated two synthetic cathinone-binding DNA aptamers, SCA1.1 and SCA2.1¹²³, via SELEX. SCA1.1 shows high cross-reactivity to synthetic cathinones but responds to several compounds not in this family (hereon specified as

‘interferents’), while SCA2.1 is highly specific to the target family but has lower cross-reactivity to some members. As a result, neither aptamer is ideal for the broad and specific detection of synthetic cathinones. However, by employing an optimized mixture of the two, we were able to maintain advantageous features of both aptamers while minimizing their disadvantages, simultaneously achieving high cross-reactivity to 12 synthetic cathinones and excellent specificity against 17 interferents. Our concept was first demonstrated using SCA1.1 and SCA2.1 in a dye-displacement assay. We found that the target-binding profile of aptamer mixtures at any given molar ratio could be precisely predicted using a mathematical model, which allows for fine tuning of the sensor’s responsiveness. We subsequently utilized the same concept to develop a dual-aptamer-modified electrochemical aptamer-based (E-AB) sensor. Once again, the sensor demonstrated equally impressive performance as the dye-displacement assay and enabled specific detection of analytes in interferent-ridden binary mixtures. Unlike conventional aptamer engineering approaches, such as sequence mutation and truncation, ours is a generalizable strategy that enables precise control of the cross reactivity of aptamer-based sensors towards both targets and interferents and should enable development of near-ideal biosensors for a diversity of targets.

3.2. Experimental section

3.2.1. Materials

Unmodified oligonucleotides were synthesized by Integrated DNA Technologies with HPLC purification and dissolved in PCR-grade water. Thiolated methylene-blue-modified oligonucleotides were purchased from LGC Biosearch Technologies with HPLC

purification and dissolved in 10 mM Tris-HCl (pH 8.0) with 1 mM EDTA. All DNA sequences used in this work are listed in **Table 3-1**.

Table 3-1. Sequence ID and DNA sequences used in Chapter 3.

Sequence ID	Sequence (5' – 3')
SCA2.1	CTTACGACCTTAAGTGGGGTTCGGGTGGAGTTTATGGG GTCGTAAG
SCA2.1-40	CTTACGACCTTAAGTGGGGTTCGGGTGGAGTTTATGGGGT
SCA2.1-34	ACCTTAAGTGGGGTTCGGGTGGAGTTTATGGGGT
SCA1.1	CTTACGACTGAGAAGTGTGATTCAGTATGTTTTCCGAAGT CGTAAG
SCA1.1-40	CTTACGACTGAGAAGTGTGATTCAGTATGTTTTCCGAAGT
SCA1.1-34	ACTGAGAAGTGTGATTCAGTATGTTTTCCGAAGT
SCA-2.1-34-MB	SH-C6-ACCTTAAGTGGGGTTCGGGTGGAGTTTATGGGGT- MB
SCA-1.1-34-MB	SH-C6-ACTGAGAAGTGTGATTCAGTATGTTTTCCGAAGT- MB

SH = thiol modification; MB = methylene blue modification; C6 = (CH₂)₆ linker

Synthetic cathinone standards (all hydrochloride salts and racemic unless specified), including 3,4-methylenedioxypropylvalerone (MDPV), 3-fluoromethcathinone (3-FMC), 4-fluoromethcathinone (4-FMC), 4-methylmethcathinone (4-MMC), alpha-pyrrolidinopentiophenone (α -PVP), butylone, cathinone, ethylone, methcathinone, methylone, naphyrone, pentylone, and pure enantiomers (-)-MDPV and (+)-MDPV were purchased from Cayman Chemicals. (\pm)-Amphetamine hemisulfate, benzocaine, caffeine, cocaine HCl, diethylthiatricarbocyanine iodide (Cy7), (-)-ephedrine HCl, heroin HCl, ketamine HCl, lidocaine HCl, D-lactose monohydrate, (\pm)-3,4-methylenedioxymethamphetamine HCl (MDMA), D-mannitol, paracetamol, phenacetin, procaine HCl, (+)-pseudoephedrine HCl ((+)-PSE), quinine hemisulfate monohydrate, tris(2-carboxyethyl)phosphine HCl, 6-mercapto-1-hexanol (MCH), and all other chemicals were purchased from Sigma-

Aldrich unless otherwise noted. Levamisole HCl was purchased from MP Biomedical. Sucrose was purchased from Amresco. Exonuclease III (*E. coli*) and exonuclease I (*E. coli*) were purchased from New England Biolabs. SYBR Gold was purchased from Thermo Fisher Scientific. Deionized water (resistivity of 18.2 M Ω cm) was produced using a Milli-Q Direct 8 Water Purification System.

3.2.2. Cy7 dye-displacement assay

The Cy7-displacement assay was performed as previously reported.¹²³ Briefly, a 70 μ L mixture of SCA1.1 and SCA2.1 (final total aptamer concentration = 3 μ M) was first mixed with 2 μ L Cy7 (final concentration 2 μ M) in reaction buffer (final concentration 10 mM Tris-HCl, 0.5 mM MgCl₂, 20 mM NaCl, 0.01% Tween 20, 1% DMSO, pH 7.4) to form Cy7-aptamer complex. The molar ratio of SCA2.1 varied from 0 (i.e., SCA1.1 only) to 1 (i.e., SCA2.1 only) in different experiments. An 8 μ L volume of synthetic cathinones (final concentration 10 μ M) or interferent compounds (final concentration 100 μ M) were mixed with the freshly prepared Cy7-aptamer complexes, and 75 μ L of the mixture was loaded into a transparent flat-bottomed 384-well plate. The absorbance at 670 nm and 775 nm was immediately measured using a Tecan M1000 plate reader, and the absorbance ratio A_{670}/A_{775} was calculated for each sample. Signal gain was calculated as $(R-R_0)/R_0$, where R_0 and R are A_{670}/A_{775} values in the absence and presence of the analyte, respectively. Cross-reactivity was calculated based on signal gain, where the signal gain of 10 μ M MDPV was defined as 100% cross-reactivity for each condition. For the synthetic cathinone mixture experiments, a 72 μ L solution containing 1.5 μ M SCA2.1, 1.5 μ M SCA1.1, and 2 μ M Cy7 (final concentrations) in reaction buffer was mixed with 8 μ L of a synthetic cathinone mixture (either MDPV and methylone or 4-FMC and cathinone) with

molar ratios of 0:10, 2:8, 4:6, 8:2, 10:0 with a total ligand concentration of 10 μM . A 75 μL quantity of the mixture was loaded into a transparent flat-bottomed 384-well plate and the absorbance at 670 and 775 nm was determined as mentioned above.

3.2.3. Exonuclease digestion of aptamers

Briefly, 1 μL of 50 μM aptamer was added into a PCR tube and diluted with 4.5 μL of 100 mM Tris-HCl buffer (pH 7.4) and 29.05 μL of deionized water. The mixture was heated at 95°C for 10 minutes and cooled down in ice immediately to disrupt aptamer secondary structure. Next, 5 μL of a 200 mM NaCl/5 mM MgCl₂ solution was added into the PCR tube, followed by 0.45 μL of 10 mg/mL BSA. The solution was incubated in the presence or absence of 5 μL 2.5 mM MDPV at room temperature for 1 hour. Then, 5 μL of 0.1 U/ μL Exo III alone, 0.5 U/ μL Exo I alone, or a mixture of 0.1 U/ μL Exo III and 0.5 U/ μL Exo I was added to initiate the digestion. 5 μL of each sample was collected at different reaction times and mixed with 10 μL of loading buffer (71.25% formamide, 10% glycerol, 0.125% SDS, 25 mM EDTA, and 0.15% (w/v) bromophenol blue and xylene cyanol) to stop the digestion. The sample was analyzed by 15% denaturing polyacrylamide gel electrophoresis (PAGE), stained with 1 \times SYBR Gold dye, and imaged using a ChemiDoc MP imaging system.

The length and concentration of digestion products were characterized using a home-made DNA ladder comprising either SCA2.1 or SCA1.1 and truncated derivatives measuring 43-, 41-, 40-, 39-, 35-, 32- and 29-nt, where the ladder was matched to the aptamer being analyzed.

3.2.4. Circular dichroism (CD)

Experiments were performed in reaction buffer (10 mM Tris-HCl, 20 mM NaCl, 0.5 mM MgCl₂, pH 7.4). Before each experiment, the reaction buffer was degassed for 15 minutes using an ultrasonic cleaner (Fisher Scientific FS60D). SCA1.1-40 or SCA2.1-40 (final concentration 1 μM) dissolved in this degassed buffer was heated at 95 °C for 10 minutes and immediately cooled down on ice. MgCl₂ and NaCl (final concentration of 0.5 mM and 20 mM, respectively) and MDPV (racemic, final concentration 100 μM) were added to the aptamer solution and incubated overnight at room temperature. 300 μL of each sample was added into a quartz cuvette (Hellma Analytics) and the CD spectra were recorded from 220–300 nm using a spectropolarimeter (JASCO J-815) with the following parameters: 5 mdeg sensitivity, 0.2 nm data pitch, 50 nm/minute scanning speed, 1 nm bandwidth, and 8 seconds response time. Each sample was scanned four times, and the data were averaged. Spectra of the reaction buffer, reaction buffer containing 100 μM MDPV, and reaction buffer containing 1 μM aptamer were also obtained. All CD spectra were corrected by subtracting the spectra of the buffer with and without MDPV.

3.2.5. Isothermal titration calorimetry (ITC) experiments

All ITC experiments were carried out at 23 °C using a MicroCal iTC200 Instrument (Malvern). For each experiment, 300 μL of an aptamer solution containing 20 μM of SCA1.1, SCA1.1-40 or SCA2.1-40 in reaction buffer (10 mM Tris-HCl, 20 mM NaCl, 0.5 mM MgCl₂, pH 7.4) were heated at 95 °C for 10 minutes and immediately cooled down on ice before loading into the sample cell. The syringe was then loaded with (–)-MDPV, (+)-MDPV, MDMA, (+)-PSE, procaine, levamisole, or quinine prepared in the same buffer.

Since MDPV is a chiral compound, ITC experiments for the binding affinity of MDPV towards the aptamers was performed with each enantiomer individually. Concentrations of aptamers and ligands are listed in **Table 3-2**. Each experiment consisted of an initial purge injection of 0.4 μL and 19 successive injections of 2 μL , with a spacing of 180 sec between adjacent injections. For (+)-PSE, procaine, and levamisole, 20 more injections were performed following these 20 injections, with an initial purge injection of 0.4 μL and 19 successive injections of 2 μL . The obtained raw data were first corrected with dilution heat obtained from ligand-to-buffer titrations and then analyzed using the MicroCal analysis kit integrated into Origin 7 software, with a single-site binding model to calculate dissociation constants (K_{DS}).

Table 3-2. Aptamer, ligand, and ligand concentration used for ITC experiments and determined K_{DS} .

Aptamer	Ligand	Ligand concentration (μM)	Dissociation constant (μM)
SCA1.1	(-)-MDPV	350	0.23 ± 0.02
SCA1.1	(+)-MDPV	1,000	30.4 ± 1.0
SCA1.1-40	(-)-MDPV	400	1.05 ± 0.05
SCA1.1-40	(+)-MDPV	2,000	181 ± 2
SCA1.1-34	(-)-MDPV	400	1.46 ± 0.03
SCA1.1-34	(+)-MDPV	2,000	185 ± 3
SCA2.1	(-)-MDPV	225	0.047 ± 0.0075
SCA2.1	(+)-MDPV	400	3.61 ± 0.12
SCA2.1-40	(-)-MDPV	400	0.65 ± 0.03
SCA2.1-40	(+)-MDPV	2,000	292 ± 14
SCA2.1-34	(-)-MDPV	400	0.30 ± 0.04
SCA2.1-34	(+)-MDPV	2,000	96 ± 4.0

3.2.6. Electrochemical aptamer-based sensor fabrication and detection

Aptamer-modified electrodes were prepared as previously reported.²¹ Briefly, 2-mm gold disk electrodes (CHI) were polished consecutively by 1 μm diamond suspension and 0.05 μm Gamma Alumina suspension (BASi), followed by electrochemical cleaning. 5'-thiolated and 3'-methylene blue-modified aptamers were incubated with 100 mM Tris(2-carboxyethyl)phosphine in PBS buffer (10 mM phosphate, 1 M NaCl, 1 mM MgCl_2 , pH 7.1) for 2 hours at room temperature to reduce disulfide bonds. The cleaned electrodes were immediately immersed into aptamer solutions containing either SCA2.1-34-MB, SCA1.1-34-MB, or both aptamers at various concentrations (10 – 30 nM) overnight at room temperature. The aptamer-modified electrodes were then incubated with 3 mM 6-mercapto-1-hexanol solution for 2 hours at room temperature to backfill vacant surfaces on the gold electrodes. Finally, the electrodes were washed with deionized water and stored in 10 mM Tris-HCl (pH 7.4) before use. Chronocoulometry was applied to measure surface coverage using the method reported by Tarlov et al.¹²⁷ Detection was performed using a CHI 670D Electrochemical Station with square-wave voltammetry and a three-electrode system, including a platinum counter electrode, an Ag/AgCl reference electrode, and the aptamer-modified working electrode. The peak currents in the absence (I_0) and presence of analyte (I) were measured for 12 synthetic cathinones (10 μM), 17 interferents (100 μM), and binary mixtures including 10 μM MDPV with 100 μM of individual interferents. Signal gain was calculated using the equation: $(I-I_0)/I_0 \times 100\%$. The cross-reactivity of each analyte was calculated by its signal gain, where a cross-reactivity of 100% was defined based on the signal gain achieved with 10 μM MDPV. Each experiment was repeated three times using independently modified electrodes.

3.2.7. Mathematical prediction of signal gain using a mixture of two aptamers

A ligand binding to an aptamer with 1:1 stoichiometry follows the Langmuir equation:

$$\theta = \frac{K \cdot L}{K \cdot L + 1} \quad (\text{Eq. 1})$$

where θ is the fraction occupancy of the aptamer, L is the concentration of the free ligand, and K is the association constant of the aptamer. For the sensor platforms presented in this work, the signal gain is proportional to the aptamer occupancy, therefore:

$$S = \frac{K \cdot L}{K \cdot L + 1} \cdot S_M \quad (\text{Eq. 2})$$

where S is the signal gain produced by the aptamer with a given ligand concentration, and S_M is the maximum signal gain achieved when the aptamer is completely saturated by the ligand. When a mixture of two aptamers is used in a single biosensor, both of which bind the ligand independently, the binding curve can be expressed by the following equation:

$$\theta_{app} = \alpha \cdot \left(\frac{K_1 \cdot L}{K_1 \cdot L + 1} \right) + (1 - \alpha) \cdot \left(\frac{K_2 \cdot L}{K_2 \cdot L + 1} \right) \quad (\text{Eq. 3})$$

where θ_{app} is the global fraction occupancy of the aptamer mixture, K_1 and K_2 are the association constants of aptamer 1 and aptamer 2, respectively, and α is the molar fraction of aptamer 1 in the mixture. Therefore, the signal gain at a given ligand concentration can be calculated as:

$$S_{app} = \alpha \cdot S_{M1} \cdot \left(\frac{K_1 \cdot L}{K_1 \cdot L + 1} \right) + (1 - \alpha) \cdot S_{M2} \cdot \left(\frac{K_2 \cdot L}{K_2 \cdot L + 1} \right) \quad (\text{Eq. 4})$$

where S_{app} is the signal gain produced by the aptamer mixture, and S_{M1} and S_{M2} are the maximum signal gain respectively achieved by aptamer 1 and aptamer 2 when each aptamer is completely saturated by the ligand. Another expression of the equation is:

$$S_{app} = - \left[\left(\frac{K_1 \cdot L}{K_1 \cdot L + 1} \right) \cdot S_1 + \left(\frac{K_2 \cdot L}{K_2 \cdot L + 1} \right) \cdot S_2 \right] \cdot \alpha + S_2 \cdot \left(\frac{K_2 \cdot L}{K_2 \cdot L + 1} \right) \quad (\text{Eq. 5})$$

Thus, for a given ligand concentration and a fixed total concentration of aptamers, the signal gain is linearly related to the molar fraction of aptamer 1.

3.3. Result and discussion

3.3.1. Determination the binding profiles of SCA1.1 and SCA2.1 using the Cy7 dye-displacement assay

We have recently employed a parallel-and-serial selection strategy to isolate two synthetic cathinone-binding DNA aptamers, SCA1.1 and SCA2.1, via library-immobilized SELEX.¹²³ To determine the target-binding profile of these aptamers, we performed a label-free dye-displacement assay that utilizes the dye diethylthiatricarbocyanine (Cy7) as a signal reporter (**Figure 3-1A**). Cy7 exists as both a monomer and dimer in aqueous solution, and these forms exhibit absorption maxima of 775 nm and 670 nm, respectively.¹²⁸ In the absence of target, Cy7 monomers bind to the aptamer (**Figure 3-1A, left**), resulting in enhanced absorbance at 775 nm. Target binding to the aptamer displaces Cy7 monomers, which rapidly dimerize in solution (**Figure 3-1A, right**), causing decreased absorbance at 775 nm and increased absorbance at 670 nm (**Figure 3-2**).¹²³ The absorbance ratio A_{670}/A_{775} can thus be used to measure target binding for these aptamers. We first employed this assay to examine the cross-reactivity of these two aptamers towards 12 synthetic cathinones and their specificity against 17 interferents (**Figure 3-4**), some of which are structurally related to the synthetic cathinone targets. Since both SCA1.1 ($K_D = 0.23 \pm 0.02 \mu\text{M}$ for (-)-MDPV and $K_D = 30.4 \pm 1.0 \mu\text{M}$ for (+)-MDPV) (**Figure 3-3**) and SCA2.1¹²³ bind to methylenedioxyprovalerone (MDPV)

strongly with sub-micromolar binding affinity, we used the signal produced by this analyte as a benchmark to calculate cross-reactivity.

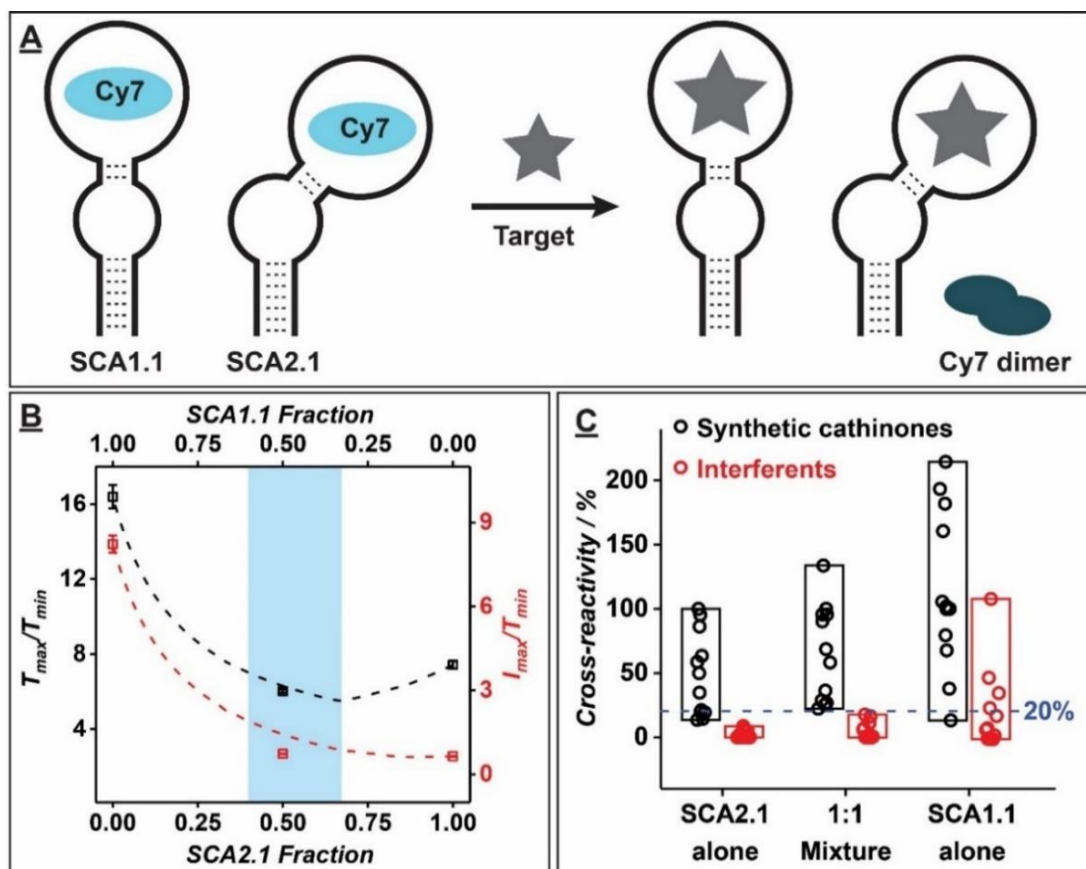


Figure 3-1. Target-binding spectra of SCA1.1, SCA2.1, and their mixtures in a Cy7-displacement assay. **(A)** Schematic of the dual-aptamer Cy7-displacement assay. **(B)** Target cross-reactivity (T_{max}/T_{min}) and specificity (I_{max}/T_{min}) for mixtures of SCA1.1 and SCA2.1 at various molar ratios with a fixed total aptamer concentration of 3 μ M. Predicted values (dashed lines) were obtained from simulated binding spectra generated from results in **Figure 3-5**. Experimental values (scattered points) were calculated based on the results from **Figure 3-6**. Error bars show standard deviation from three measurements. The optimal aptamer ratio achieving both high target cross-reactivity (low T_{max}/T_{min}) and specificity (low I_{max}/T_{min}) is shaded blue. **(C)** Binding profiles of SCA1.1, SCA2.1, and a 1:1 mixture of the two aptamers. Each point corresponds to cross-reactivity towards 12 synthetic cathinones (10 μ M; black) or 17 interferents (100 μ M; red) relative to 10 μ M MDPV. The cut-off for 20% cross-reactivity is marked in blue.

We observed that the aptamers had different binding profiles in the Cy7-displacement assay. SCA2.1 displayed >20% cross-reactivity to eight synthetic cathinones at a

concentration of 10 μM , and minimal response to all interferents at concentrations of 100 μM , with cross-reactivity $< 8.6\%$. However, this aptamer exhibited poor binding ($< 20\%$ cross-reactivity) to methcathione, 3-fluoromethcathinone (3-FMC), cathinone, and 4-fluoromethcathinone (4-FMC) (Figure 3-5A).

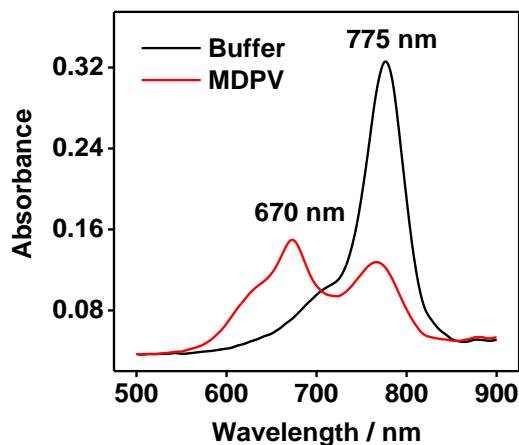


Figure 3-2. Cy7-displacement assay for MDPV detection. Absorbance spectra of 2 μM Cy7 and 3 μM SCA2.1 in the absence (black) or presence (red) of 10 μM MDPV.

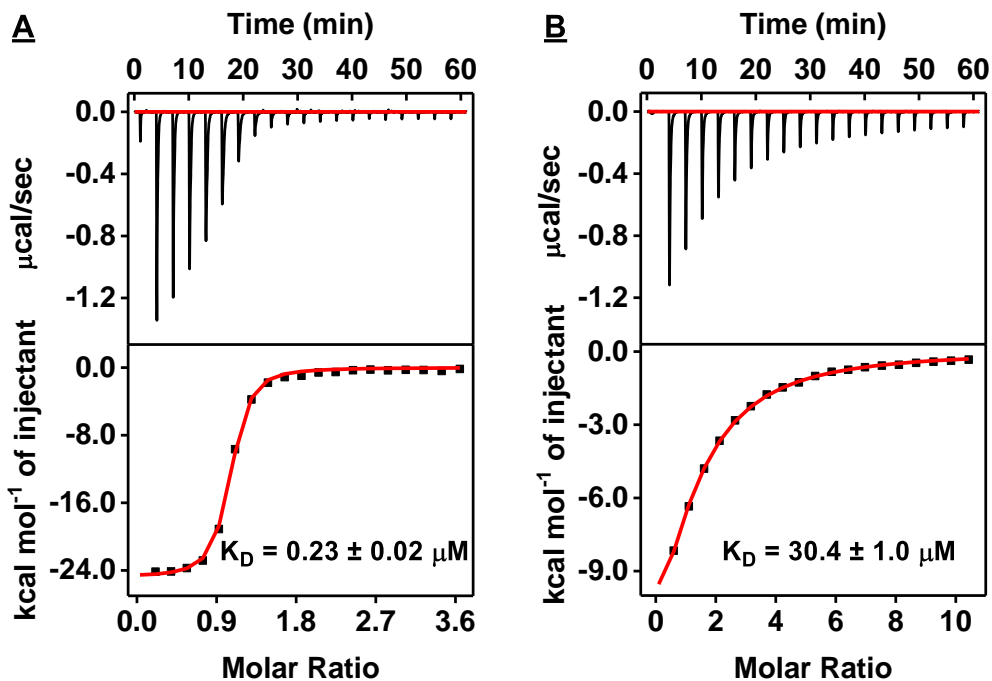


Figure 3-3. Characterization of the target-binding affinity of SCA1.1 using ITC. Top panels present raw data showing the heat generated from each titration of (A) (-)-MDPV

and **(B)** (+)-MDPV into SCA1.1. Bottom panels show the integrated heat of each titration after correcting for dilution heat of the titrant. ITC data were fitted using a single-site model.

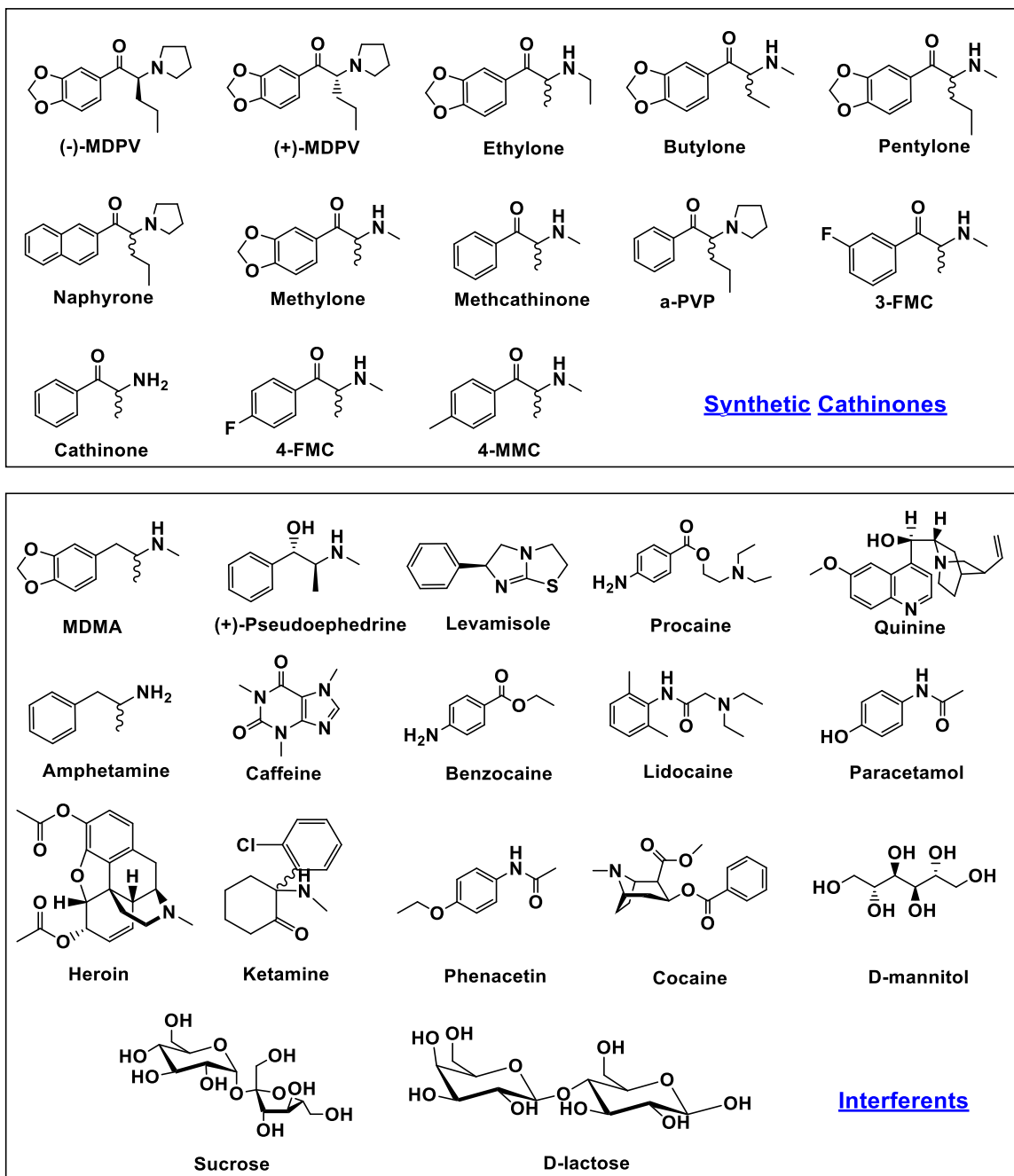


Figure 3-4. Chemical structures of different synthetic cathinones and interferents used in this work.

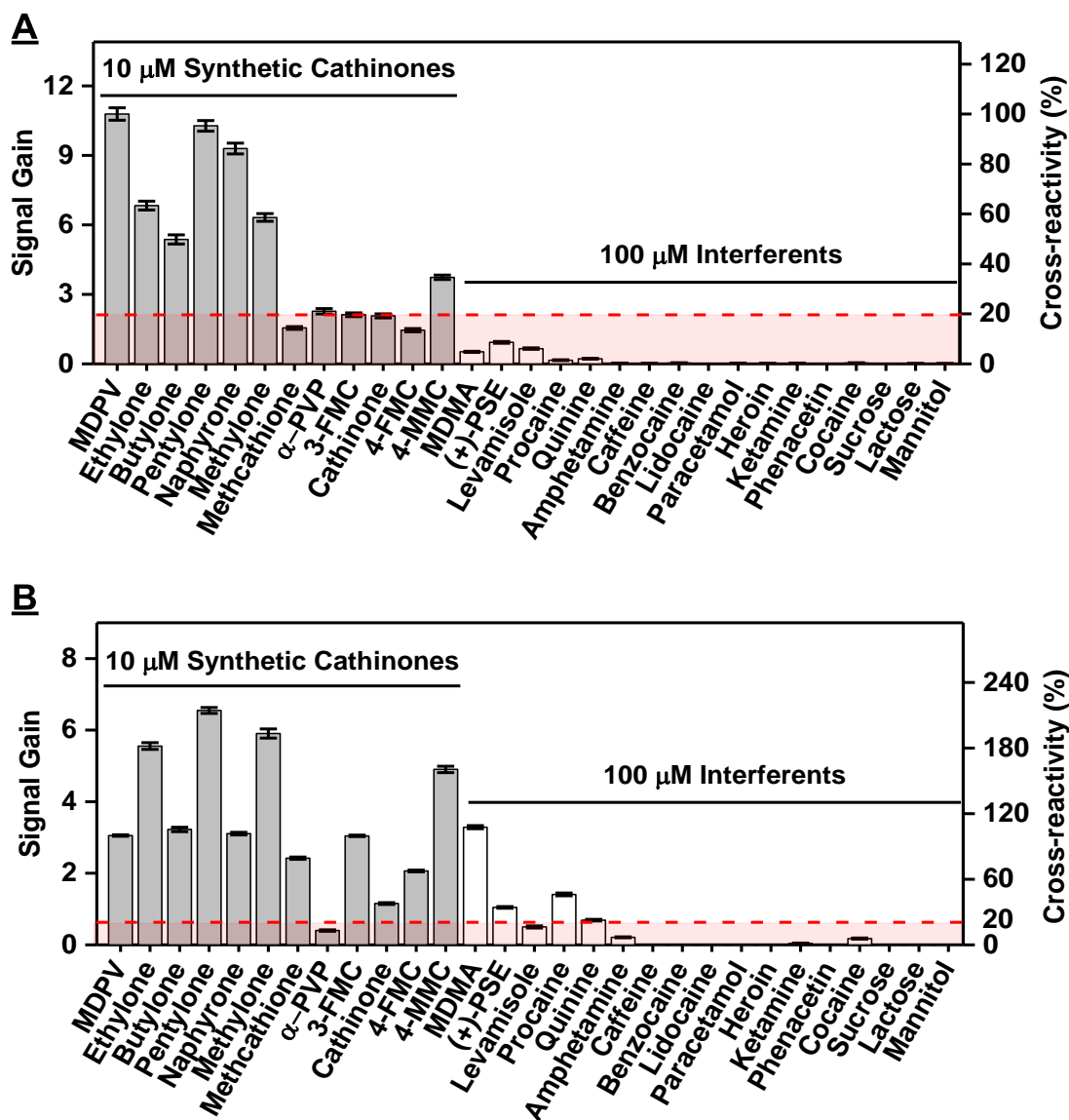


Figure 3-5. Results of Cy7-displacement assays performed with SCA2.1 or SCA1.1 alone. Signal gain and cross-reactivity from colorimetric Cy7-displacement assays performed with (A) SCA2.1 or (B) SCA1.1 against 12 synthetic cathinones (gray) at a concentration of 10 μ M and 17 interferents (white) at a concentration of 100 μ M. The cut-off for 20% cross-reactivity is marked in red. Final concentrations of aptamer and Cy7 in each experiment were 3 μ M and 2 μ M, respectively. Error bars represent the standard deviation of three measurements.

In contrast, SCA1.1 showed >20% cross-reactivity for eleven synthetic cathinones, including those that SCA2.1 was poorly cross-reactive to, and only exhibited low cross-reactivity (13%) to α -pyrrolidinopentiophenone (α -PVP). However, SCA1.1 was much

less specific, with cross-reactivities towards interferents as high as 108% (**Figure 3-5B**). Thus, SCA2.1 boasts excellent specificity against interferents at the expense of limited cross-reactivity towards the synthetic cathinone targets, while the opposite is true for SCA1.1.

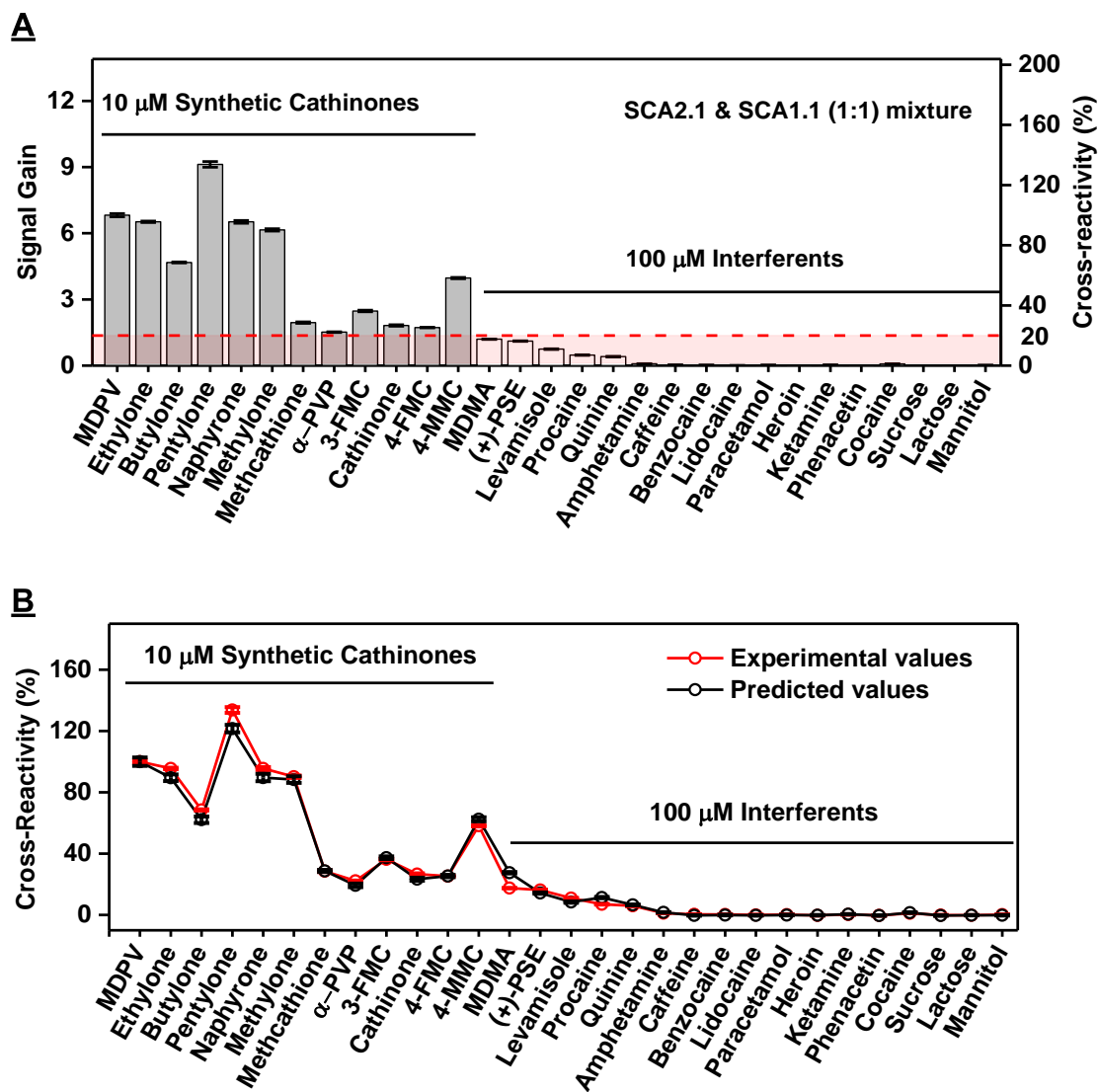


Figure 3-6. Target cross-reactivity and specificity of the Cy7-displacement dual-aptamer assay. (A) High target cross-reactivity and specificity were achieved when these aptamers were present at a 1:1 ratio (total aptamer concentration was 3 μM). (B) The predicted cross-reactivity (black) values for this 1:1 mixture, which we calculated from the signal gain achieved from SCA2.1 alone and SCA1.1 alone, is similar to that obtained experimentally

(red) for both targets and interferents. Cross-reactivity was calculated relative to the signal gain produced by MDPV.

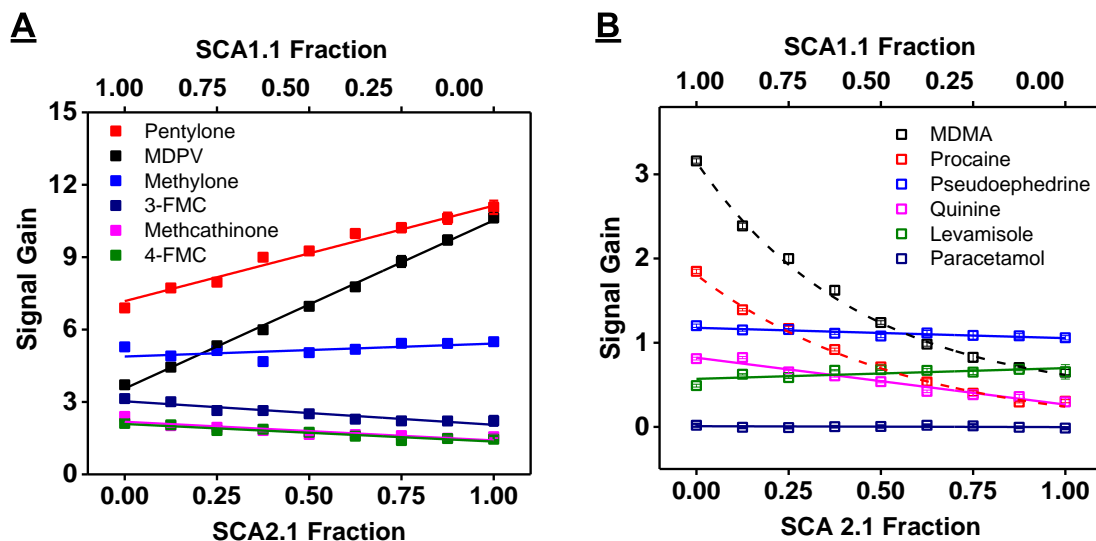


Figure 3-7. Relationship between fraction of aptamer and signal gain for the Cy7-displacement assay. The relationship between the fraction of SCA2.1/SCA1.1 in the aptamer mixture and signal gain obtained for various (A) synthetic cathinones or (B) interferents in the Cy7-displacement dual-aptamer assay. The total aptamer concentration was 3 μ M for each experiment. Error bars represent the standard deviation of three measurements.

3.3.2. Employing defined mixtures of aptamers to control the cross-reactivity of biosensors

We hypothesized that the strengths of both aptamers could be leveraged, and their weaknesses likewise mitigated, by using a mixture of the two. Since target binding to each aptamer is independent, we anticipated that the global response of the aptamer mixture can be mathematically predicted if the target binding profile and molar fraction of each aptamer are known (see **Experimental section** for mathematical model). When the total concentration of a binary aptamer mixture is fixed, there should be a linear relationship between the signal gain and the molar fraction of either aptamer. To verify this, we mixed SCA2.1 and SCA1.1 at various molar ratios with a fixed total aptamer concentration and

tested their response to six synthetic cathinones (pentylone, MDPV, methylone, 3-FMC, methcathinone, and 4-FMC) and six interferents (MDMA, procaine, pseudoephedrine, quinine, levamisole, and paracetamol) in the Cy7-displacement assay. The results confirmed our hypothesis, as almost all analytes showed a linear relationship (**Figure 3-7**). MDMA and procaine displayed a nonlinear trend, but since the response was monotonic, the signal response could be estimated.

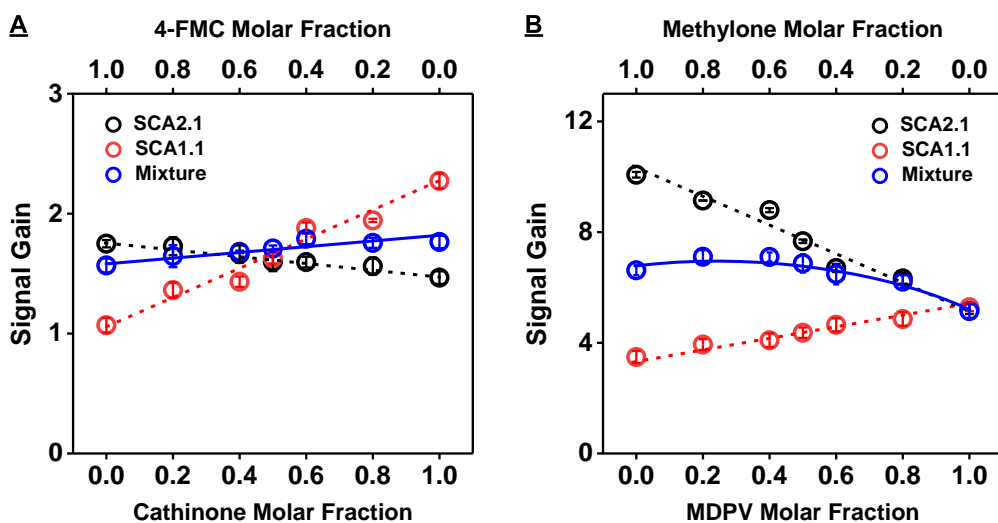


Figure 3-8. Cy7-based displacement assays using SCA2.1, SCA1.1, and a mixture of both aptamers to detect different mixtures of synthetic cathinones. Signal gain is shown at different molar fractions of **(A)** 4-FMC + cathinone and **(B)** methylone + MDPV. The total target concentration for each mixture is 10 μM . Black, red, and blue represent the results from SCA2.1, SCA1.1, and an equimolar mixture of both, respectively. Error bars represent the standard deviation of measurements from two different sets of experiments. For single aptamer experiments, 3 μM aptamer and 2 μM Cy7 were used. For aptamer mixture experiments, 1.5 μM of each aptamer was used along with 2 μM Cy7.

An ideal cross-reactive sensor should respond similarly to all targets, such that the ratio of signal gain between the targets with the highest and lowest response ($T_{\text{max}}/T_{\text{min}}$) is minimal. In addition, the sensor should have minimal response to all interferents, such that the ratio of the signal gain between the interferent with the highest response and the target with the lowest response ($I_{\text{max}}/T_{\text{min}}$) is minimal. We mathematically predicted that the

optimum SCA2.1:SCA1.1 ratio is approximately 1:1 (**Figure 3-1B**). We confirmed this prediction by mixing these aptamers at different ratios and determining their binding profile with the aforementioned targets and interferents. As expected, the equimolar 1:1 ratio demonstrated the best cross-reactivity and specificity (**Figure 3-1C**). Notably, in contrast with either aptamer alone, this 1:1 mixture exhibited >20% cross-reactivity to all synthetic cathinone targets at a 10 μM concentration (**Figure 3-1C** and **Figure 3-6A**). Thus, this combination approach overcame SCA2.1's poor cross-reactivity towards methcathione, cathinone, 3-FMC, and 4-FMC, and SCA1.1's poor response to α -PVP. Meanwhile, the assay also demonstrated excellent specificity, with cross-reactivities <17% for all interferents at a concentration of 100 μM . Additionally, the experimentally determined cross-reactivity profile of the 1:1 aptamer mixture correlated well with the mathematical prediction calculated from the signal gain obtained with either aptamer alone (**Figure 3-6B**). The predicted cross-reactivity is calculated by using the average of the signal gain from each aptamer towards a ligand, where the average signal gain produced by 10 μM MDPV was defined as 100% cross-reactivity. It should be noted that the experimental values for MDMA and procaine were slightly lower than the predicted values due to their nonlinear target responses. This demonstrates that the response profile of an aptamer assay in terms of both $T_{\text{max}}/T_{\text{min}}$ and $I_{\text{max}}/T_{\text{min}}$ can be precisely controlled by using multiple aptamers with differing binding profiles at specific molar fractions.

We then determined the response of the Cy7-displacement assay to mixtures of synthetic cathinones with varying amounts of each constituent. As a demonstration, we prepared two pairs of target mixtures (4-FMC + cathinone and methylone + MDPV) at various molar ratios at a fixed total drug concentration of 10 μM and tested their response

at a constant aptamer concentration. We found that the response of the assays based on SCA1.1 or SCA2.1 alone were sensitive to the molar fraction of constituents for both synthetic cathinone mixtures. However, the aptamer mixture was relatively insensitive to this parameter (**Figure 3-8**), because the mixture has a similar cross-reactivity to both targets. The signal gains obtained for the target mixture are not necessarily an arithmetic mean. This may be due to the aptamer having differing binding affinities for the enantiomers of these drugs, and/or the fact that each aptamer has a different affinity and binding stoichiometry for Cy7.

3.3.3. Identification of structure-switching aptamers for the E-AB sensors

We next explored whether the same multi-aptamer strategy can be generally applied to different sensing platforms such as E-AB sensors. E-AB sensors have been successfully employed for sensitive and specific detection of small molecules in complex samples such as soil, foodstuffs, urine, and whole blood.^{20,129,130} This sensing platform utilizes redox-tag-labeled structure-switching aptamers, which undergo a target-induced conformational change to produce an electrochemical signal that indicates the presence and quantity of the target.^{19,20} SCA1.1 and SCA2.1 are both 46-nt fully-folded stem-loop-structured aptamers that lack structure-switching functionality. We therefore used our previously-developed exonuclease III (Exo III)-based assay²⁴ to introduce this functionality into these two aptamers. Exo III is a 3'-to-5' exonuclease that digests aptamers with duplexed ends into short single-stranded products in the absence of target. For target-bound aptamers, this digestion is halted a few bases prior to the target-binding domain, resulting in truncated aptamers with structure-switching functionality. We found that after 6 hours of Exo III

digestion, both aptamers were digested into 40-nt major products in the presence of target (Figure 3-9). In the absence of target, Exo III generated shortened products, but digestion was incomplete—possibly due to the low activity of this enzyme on single-stranded DNA (Figure 3-11, Exo III and Figure 3-9). To remedy this problem, we combined Exo III with exonuclease I (Exo I), a single-strand 3'-to-5' exonuclease,¹³¹ to perform aptamer digestion. Using this mixture, both aptamers were completely digested in the absence of target, whereas 40-nt major products were retained in the presence of target (Figure 3-11, Exo M and Figure 3-10).

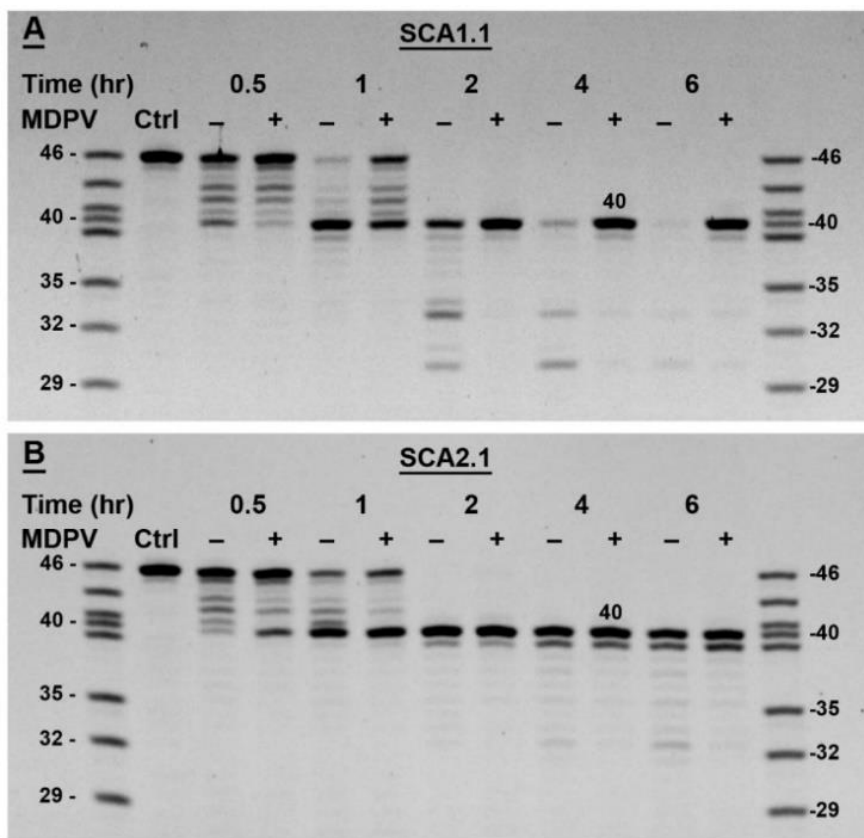


Figure 3-9. PAGE analysis of Exo III digestion of SCA1.1 and SCA2.1. PAGE analysis of time-course digestion of (A) SCA1.1 and (B) SCA2.1 incubated with Exo III over 6 hours in the absence (-) and presence (+) of 250 μ M MDPV. Ctrl (control) contains the same concentration of aptamer with no enzyme added.

To confirm that the truncated aptamers had structure-switching functionality, we synthesized the 40-nt products (SCA1.1-40 and SCA2.1-40) and digested them with Exo I.¹³¹ Both aptamers were completely digested within 2 hours in the absence of target, indicating that they are single-stranded (**Figure 3-12**). In contrast, 89% and 92% of SCA1.1-40 and SCA2.1-40, respectively, remained intact in the presence of target due to the formation of a folded target-aptamer complex that resisted Exo I digestion. The structure-switching functionality of these two truncated aptamers was further confirmed by the dramatic change of their circular dichroism spectra¹³² upon the addition of MDPV (**Figure 3-13**).

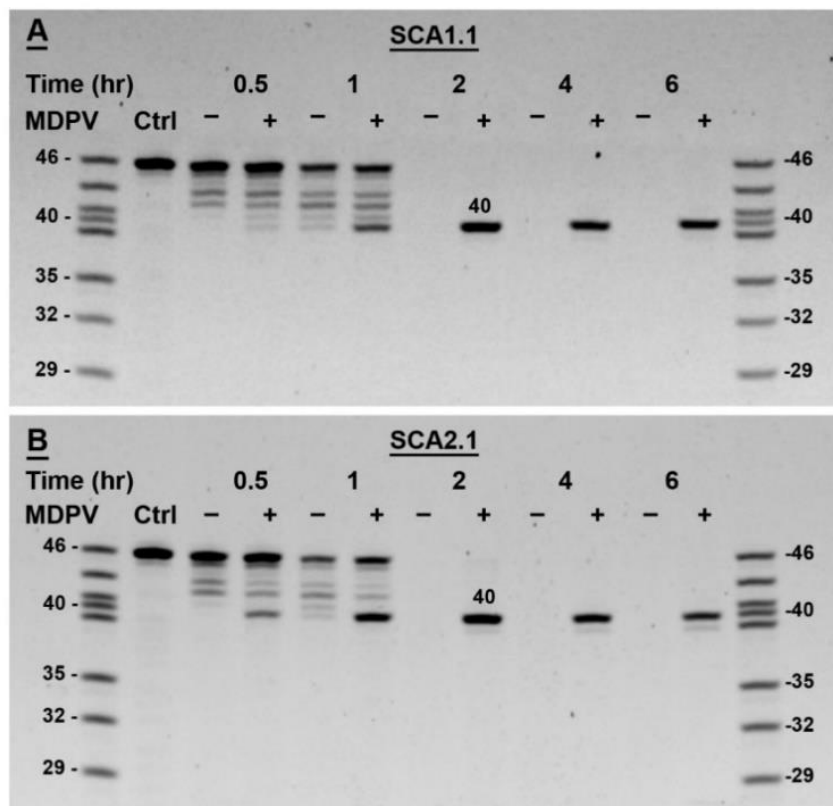


Figure 3-10. PAGE analysis of SCA1.1 and SCA2.1 digestion with a mixture of Exo III and Exo I. PAGE analysis of time-course digestion of (A) SCA1.1 and (B) SCA2.1 incubated with a mixture of Exo III and Exo I over 6 hours in the absence (-) and presence (+) of 250 μ M MDPV. Ctrl (control) contains the same concentration of aptamer with no enzyme added.

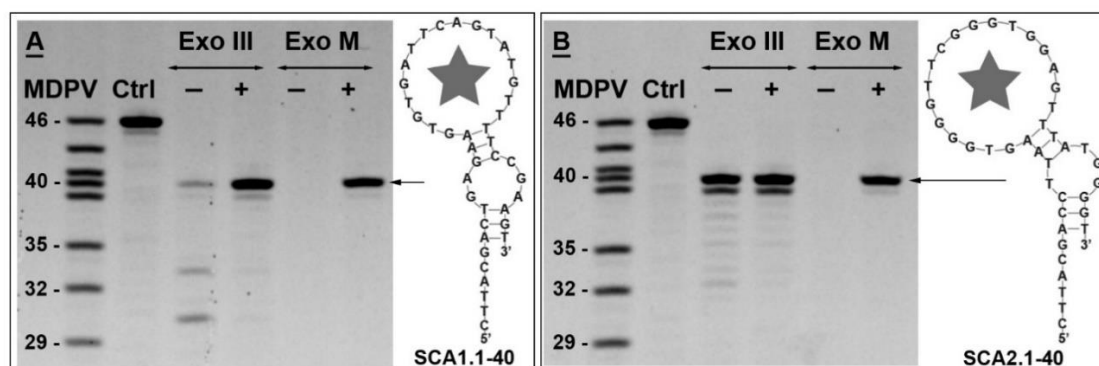


Figure 3-11. PAGE analysis of exonuclease digestions and the structures of the digestion products. PAGE analysis of (A) SCA1.1 and (B) SCA2.1 digested by Exo III or Exo M (the mixture of Exo III and Exo I) after 4 hours in the absence (-) or presence (+) of MDPV. Structures (based on mfold¹³³) and sequences for major digestion products are shown at right of each gel.

Isothermal titration calorimetry experiments were then performed to determine the affinity of the truncated aptamers for both enantiomers of MDPV, (+)-MDPV and (-)-MDPV, as synthetic cathinones are chiral molecules. SCA2.1-40 binds to (-)-MDPV and (+)-MDPV with equilibrium dissociation constants (K_D) of $0.65 \pm 0.03 \mu\text{M}$ and $292 \pm 14 \mu\text{M}$, respectively (**Figure 3-14**). SCA1.1-40 exhibits a similar pattern of binding preferentially to (-)-MDPV, with a K_D of $1.05 \pm 0.05 \mu\text{M}$ versus $181 \pm 2 \mu\text{M}$ for (+)-MDPV (**Figure 3-15**). This weaker affinity for (+)-MDPV should not be of concern for analytical purposes, as synthetic cathinones always exist as racemic mixtures.¹³⁴ We therefore concluded that SCA2.1-40 and SCA1.1-40 retain strong binding to synthetic cathinones and are suitable for fabricating E-AB sensors due to their structure-switching functionality. To achieve efficient electron transfer rates¹³⁵, we further removed the 6-nt overhangs at the 5' terminus of SCA2.1-40 and SCA1.1-40 to generate SCA2.1-34 ($K_D = 0.30 \pm 0.04 \mu\text{M}$ for (-)-MDPV and $K_D = 96 \pm 4.0 \mu\text{M}$ for (+)-MDPV) (**Figure 3-16**) and SCA1.1-34 ($K_D = 1.46 \pm 0.03 \mu\text{M}$ for (-)-MDPV and $K_D = 185 \pm 3.0 \mu\text{M}$ for (+)-MDPV) (**Figure 3-17**) and

tested whether such truncation influenced target binding in a Cy7-displacement assay. The truncated aptamers alone as well as the aptamer mixture yielded lower signal gains relative to the parent aptamer mixture (**Figure 3-18 and 3-19**), indicating that Cy7 and the analytes bind more weakly to the truncated aptamers. Nonetheless, the cross-reactivity profile of the truncated aptamer mixture for both targets and interferents remained unchanged relative to the original aptamers (**Figure 3-20**).

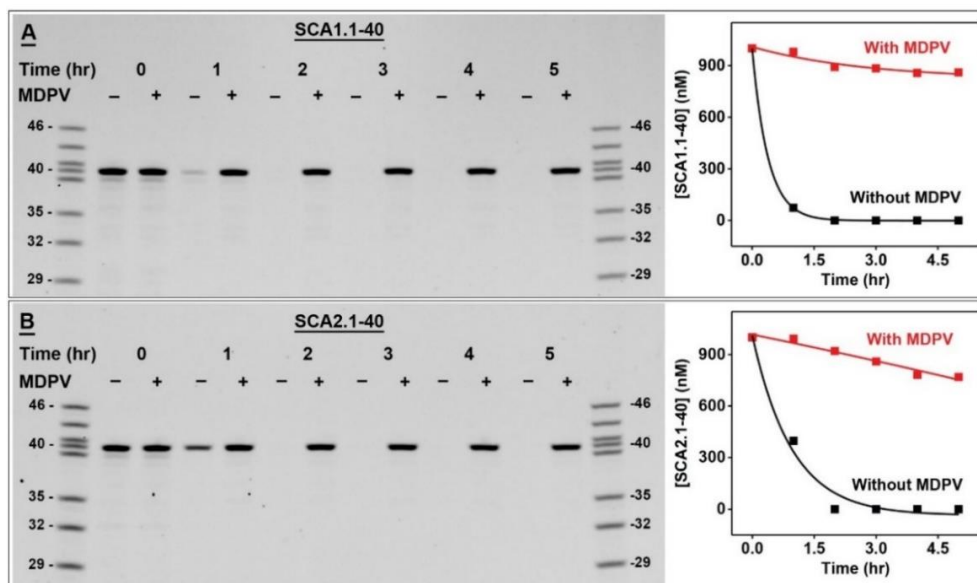


Figure 3-12. PAGE analysis of SCA1.1-40 and SCA2.1-40 digestion with Exo I. PAGE analysis of time-course digestion of (A) SCA1.1-40 and (B) SCA2.1-40 by Exo I over 5 hours in the absence (-) and presence (+) of 250 μ M MDPV. Plots at right show changes in the concentration of intact 40-nt aptamer relative to the 40-nt ladder band over time.

3.3.4. Fabrication of dual-aptamer-based electrochemical sensors

We then fabricated E-AB sensors using each individual aptamer modified with 5' thiol and 3' methylene blue (MB) (SCA2.1-34-MB and SCA1.1-34-MB). Both sensors produced increasing current with increasing concentrations of target, with linear ranges of 0-1,000 nM and limits of detection of 100 nM for MDPV (**Figures 3-21A, B and 3-22A, B**). We then challenged the sensors with 12 synthetic cathinones at a concentration of 10

μM and 17 interferents at $100 \mu\text{M}$. Both sensors had similar target-binding profiles to those seen with the Cy7-displacement assay. Specifically, the SCA2.1-based sensor showed cross-reactivity $>20\%$ for the 12 targets and strong discrimination against all interferents ($\leq 20\%$ cross-reactivity) (**Figure 3-21C**). However, the response to each target was quite variable, and cross-reactivity towards methcathinone, cathinone, and 4-FMC were low.

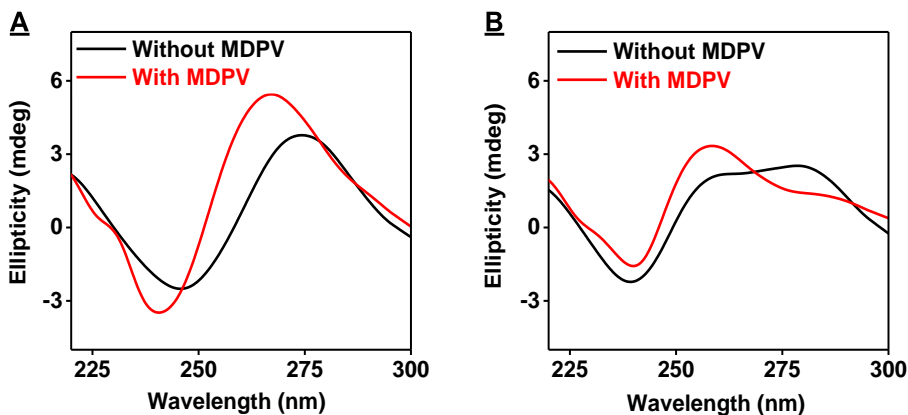


Figure 3-13. Circular dichroism (CD) spectra of SCA1.1-40 and SCA2.1-40. CD spectra of (A) SCA1.1-40 and (B) SCA2.1-40 in the absence (black) and presence (red) of $100 \mu\text{M}$ MDPV after subtracting spectra of reaction buffer without or with MDPV.

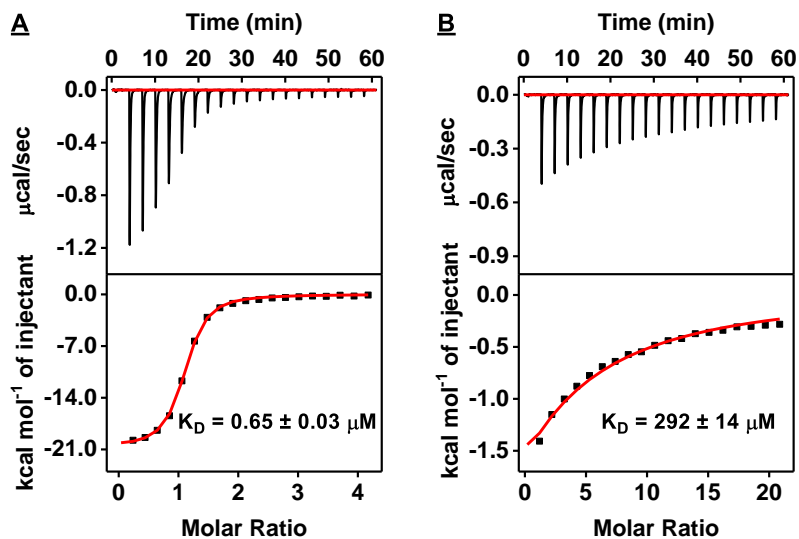


Figure 3-14. Characterization of the target-binding affinity of SCA2.1-40 using ITC. Top panels present raw data showing the heat generated from each titration of (A) (-)-MDPV and (B) (+)-MDPV to SCA2.1-40, while bottom panels show the integrated heat of each

titration after correcting for dilution heat of the titrant. ITC data were fitted using a single-site model.

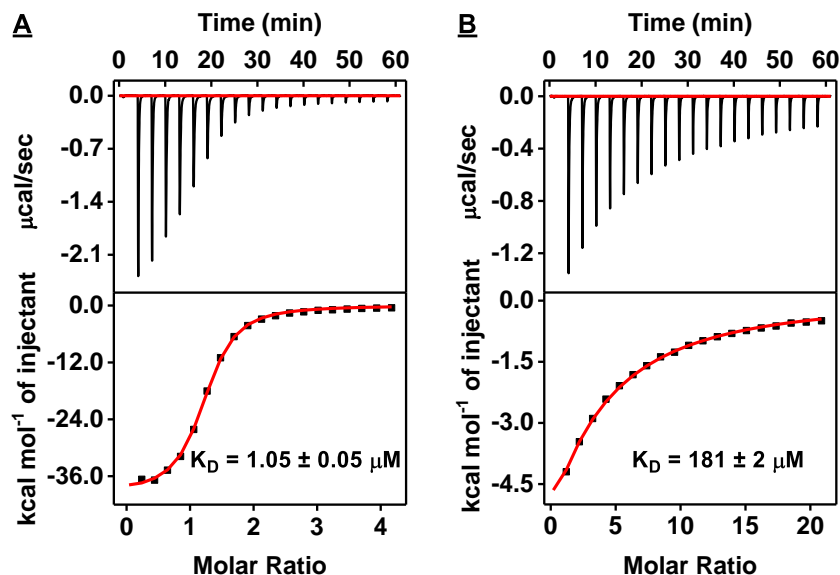


Figure 3-15. Characterization of the target-binding affinity of SCA1.1-40 using ITC. Top panels present raw data showing the heat generated from each titration of (A) (-)-MDPV and (B) (+)-MDPV to SCA1.1-40, while bottom panels show the integrated heat of each titration after correcting for dilution heat of the titrant. ITC data were fitted using a single-site model.

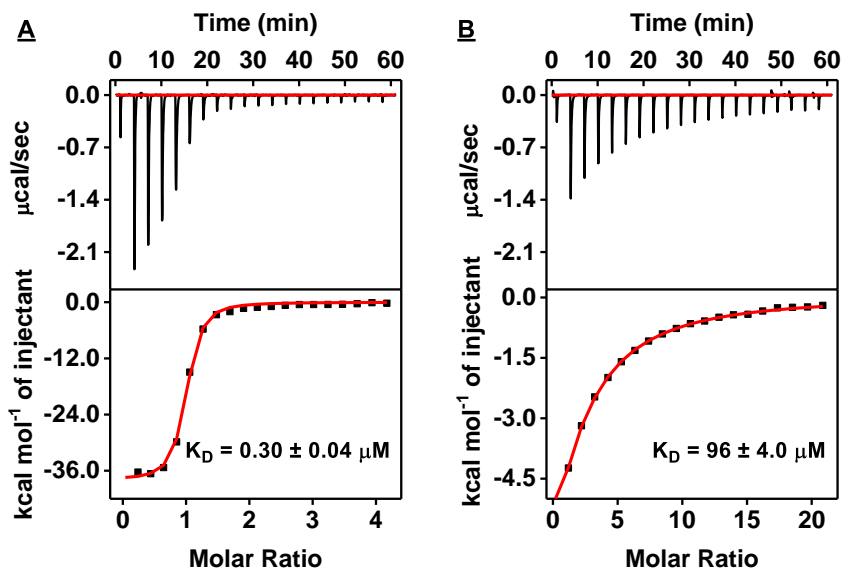


Figure 3-16. Characterization of the target-binding affinity of SCA2.1-34 using ITC. Top panels present raw data showing the heat generated from each titration of (A) (-)-MDPV and (B) (+)-MDPV to SCA2.1-34, while bottom panels show the integrated heat of each

titration after correcting for dilution heat of the titrant. ITC data were fitted using a single-site model.

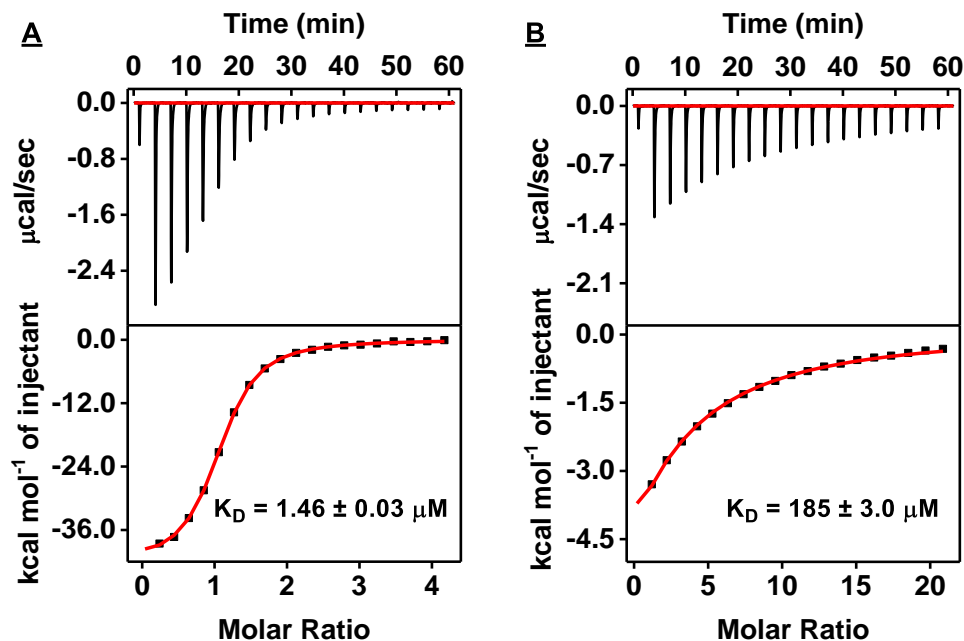


Figure 3-17. Characterization of the target-binding affinity of SCA1.1-34 using ITC. Top panels present raw data showing the heat generated from each titration of (A) (-)-MDPV and (B) (+)-MDPV to SCA1.1-34, while bottom panels show the integrated heat of each titration after correcting for dilution heat of the titrant. ITC data were fitted using a single-site model.

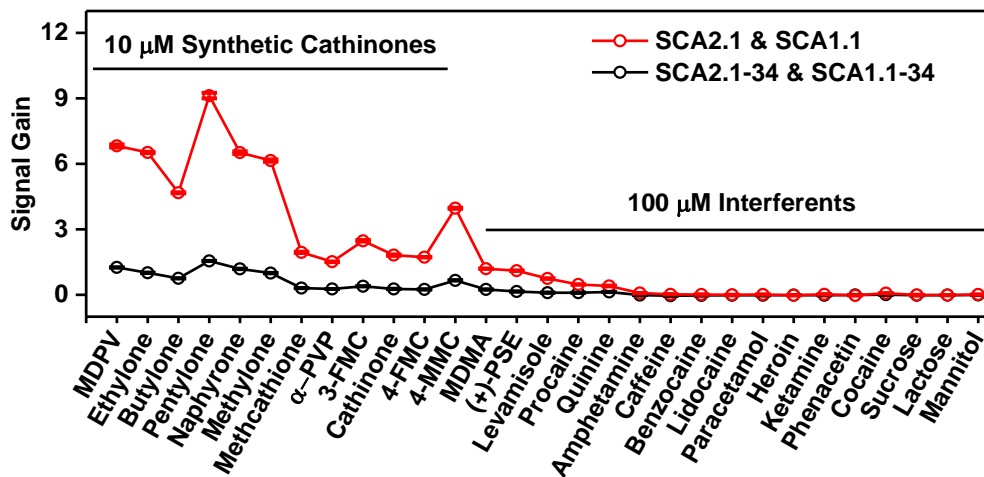


Figure 3-18. SCA2.1/1.1 and SCA2.1-34/1.1-34 mixture performance in the Cy7-displacement assay. Signal gain of the 1:1 aptamer mixtures SCA2.1 & SCA1.1 (red) and SCA2.1-34 & SCA1.1-34 (black) as determined by the Cy7-displacement assay towards 12 synthetic cathinones and 17 interferents at concentrations of 10 μM and 100 μM, respectively. Error bars represent the standard deviation of three individual experiments.

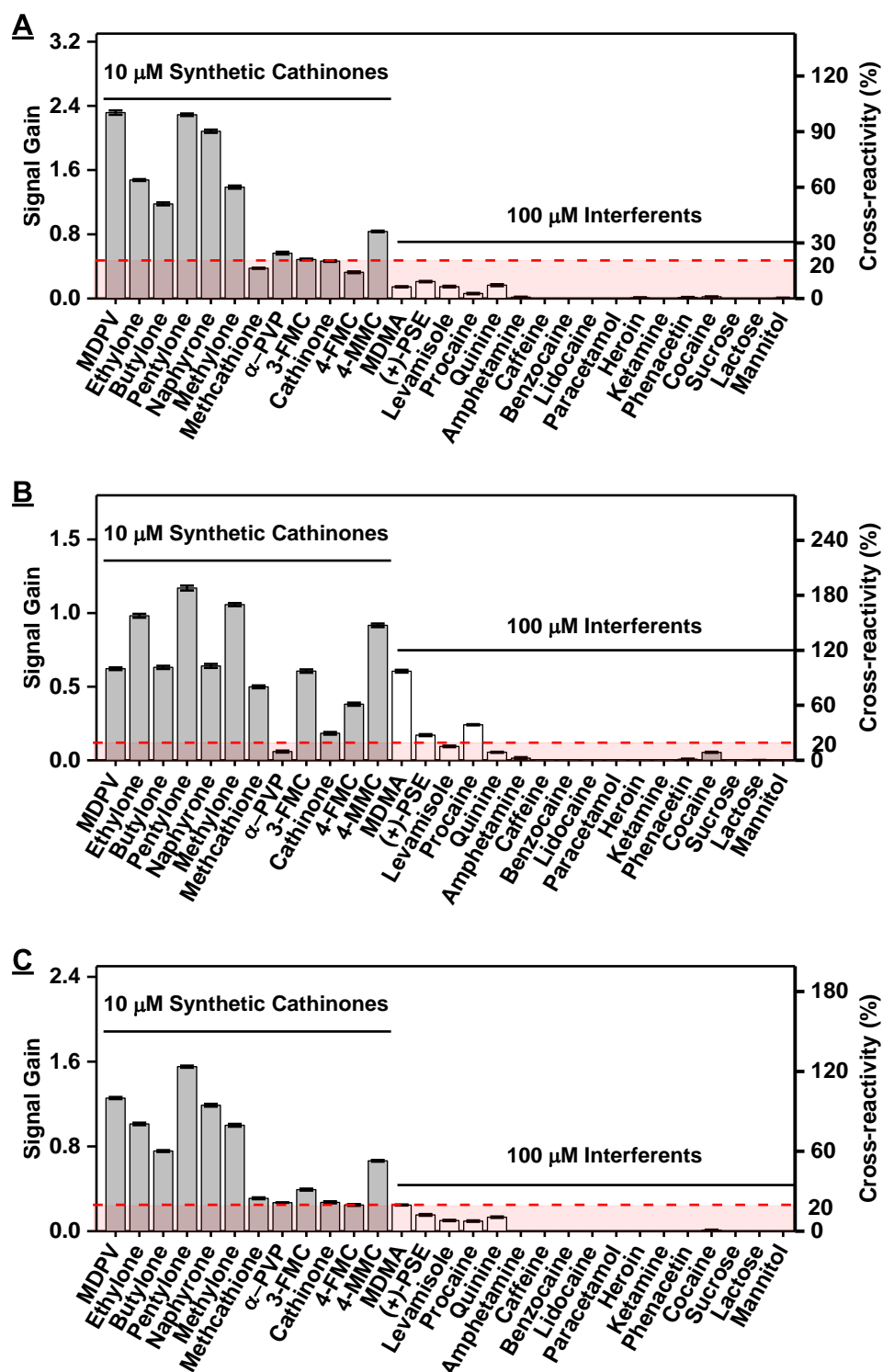


Figure 3-19. Results of Cy7-displacement assays performed with SCA2.1-34, SCA1.1-34 or the mixture of both aptamers. Signal gain and cross-reactivity from colorimetric Cy7-

displacement assays performed with (A) SCA2.1-34 alone (B) SCA1.1-34 alone or (C) the mixture of SCA2.1-34 + SCA1.1-34 against 12 synthetic cathinones (gray) at a concentration of 10 μM and 17 interferents (white) at a concentration of 100 μM . The cut-off for 20% cross-reactivity is marked in red. Error bars represent the standard deviation of three measurements.

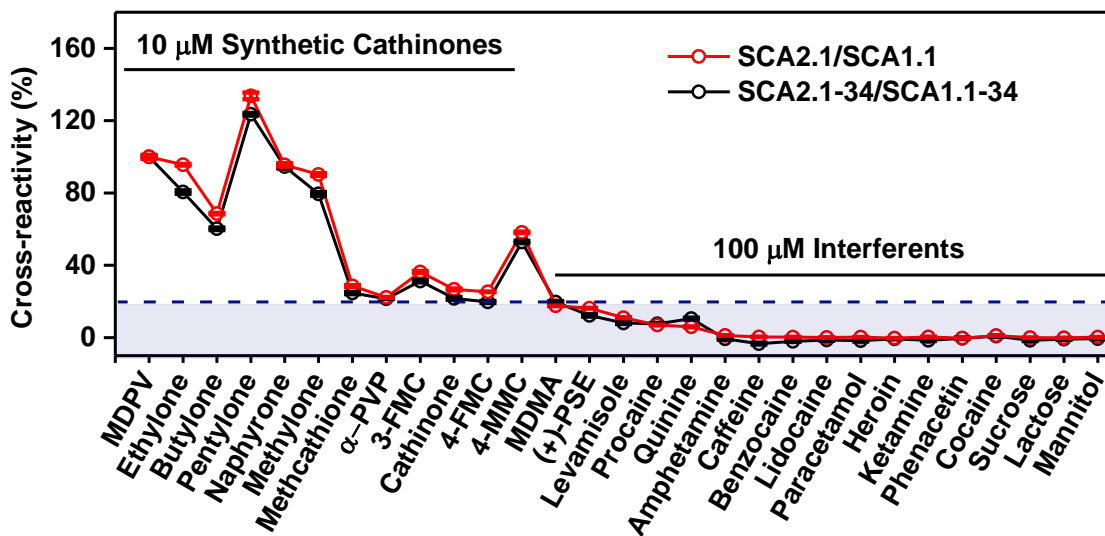


Figure 3-20. Cross-reactivity of SCA2.1/1.1 and SCA2.1-34/1.1-34 mixture performance in the Cy7-displacement assay. Cross-reactivity of SCA2.1 & SCA1.1 (red) and SCA2.1-34 & SCA1.1-34 (black) mixtures in Cy7-displacement assays with 12 synthetic cathinones and 17 interferents at concentrations of 10 μM and 100 μM , respectively. The cut-off for 20% cross-reactivity is marked in blue. Error bars represent the standard deviation of three individual experiments.

The SCA1.1-based sensor responded to all synthetic cathinones with cross-reactivity $>20\%$, but exhibited poor specificity towards some interferents, particularly MDMA, (+)-pseudoephedrine, levamisole, procaine, and quinine, with cross-reactivity ranging from 36–79% (**Figure 3-22C**). ITC confirmed that SCA1.1 binds to these interferents weakly (**Figure 3-23**). Clearly, neither aptamer alone could achieve optimal detection of synthetic cathinones.

We therefore fabricated an E-AB sensor with a 1:1 mixture of SCA1.1-34-MB and SCA2.1-34-MB (**Figure 3-25A**). Given that the electrode surface-modification efficiency

of SCA1.1-34-MB was slightly higher than that of SCA2.1-34-MB (**Figure 3-24**), we used an aptamer ratio of 5:6 (SCA1.1-34-MB:SCA2.1-34-MB) to achieve an approximate surface density ratio of 1:1 during the electrode modification step.

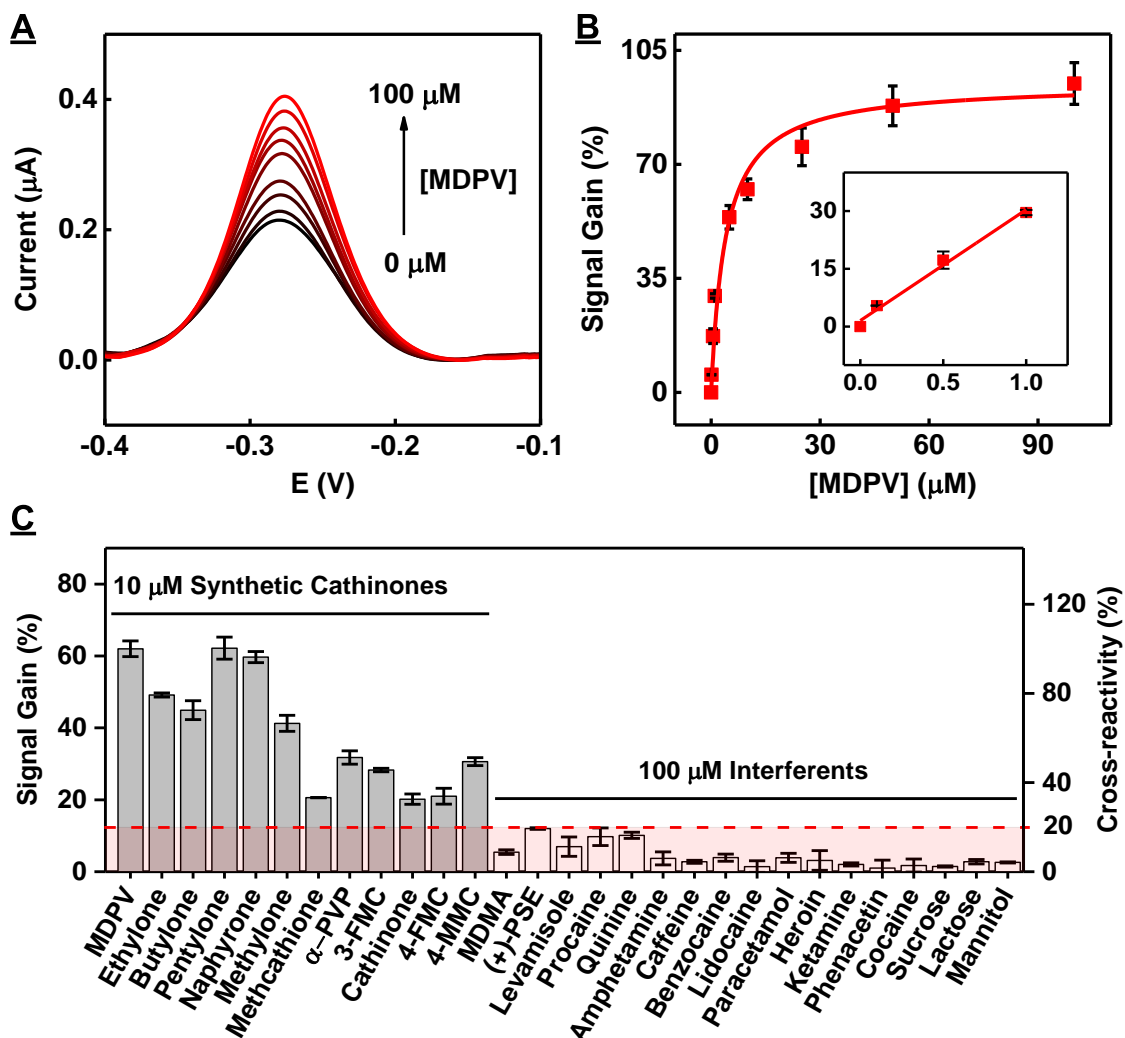


Figure 3-21. Performance of an E-AB sensor modified with SCA2.1-34-MB alone. (A) Square-wave voltammetry spectra collected at various concentrations of MDPV. (B) Calibration curve derived from square-wave voltammetry spectra. (C) Sensor cross-reactivity for 12 synthetic cathinones (gray) at a concentration of 10 μM and 17 interferents (white) at a concentration of 100 μM . Cross-reactivity is calculated relative to the signal gain produced by 10 μM MDPV. The cut-off for 20% cross-reactivity is marked in red. Error bars represent the standard deviation of measurements from three different E-AB sensors.

The dual-aptamer-modified E-AB sensor had a limit of detection of 50 nM for MDPV, with a linear range of 50-500 nM (Figure 3-25B), slightly better than the E-AB sensors fabricated with either aptamer alone. As expected, this sensor exhibited high cross-reactivity (>50%) to all synthetic cathinones at a concentration of 10 μ M while having excellent specificity (\leq 20% cross-reactivity) against all tested interferents at 100 μ M (Figure 3-25C and Figures 3-27 and 3-28).

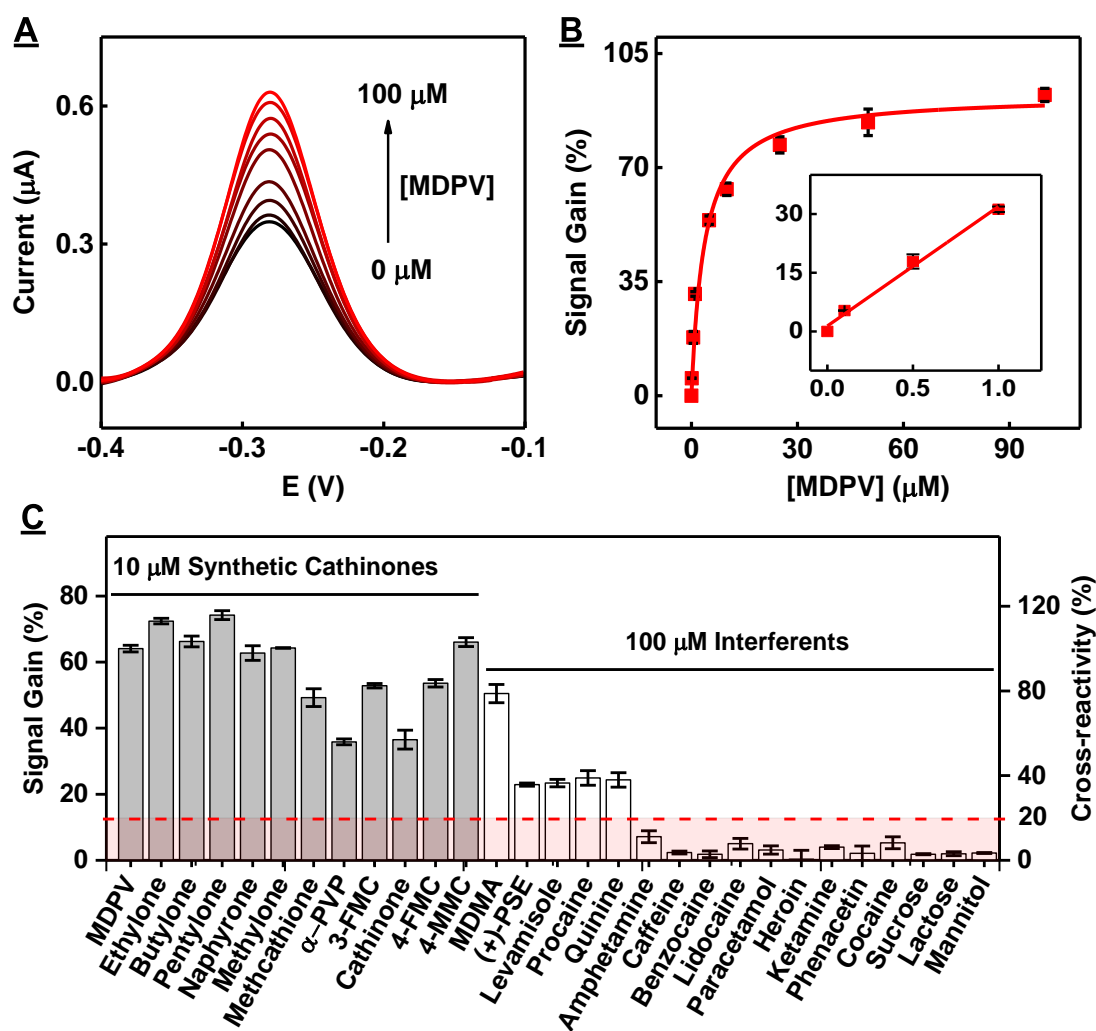


Figure 3-22. Performance of an E-AB sensor modified with SCA1.1-34-MB alone. (A) Square-wave voltammetry spectra collected at various concentrations of MDPV. (B) Calibration curve derived from square-wave voltammetry spectra. (C) Sensor cross-reactivity for 12 synthetic cathinones (gray) at a concentration of 10 μ M and 17 interferents

(white) at a concentration of 100 μM . Cross-reactivity is calculated relative to the signal gain produced by 10 μM MDPV. The cut-off for 20% cross-reactivity is marked in red. Error bars represent the standard deviation of measurements from three different E-AB sensors.

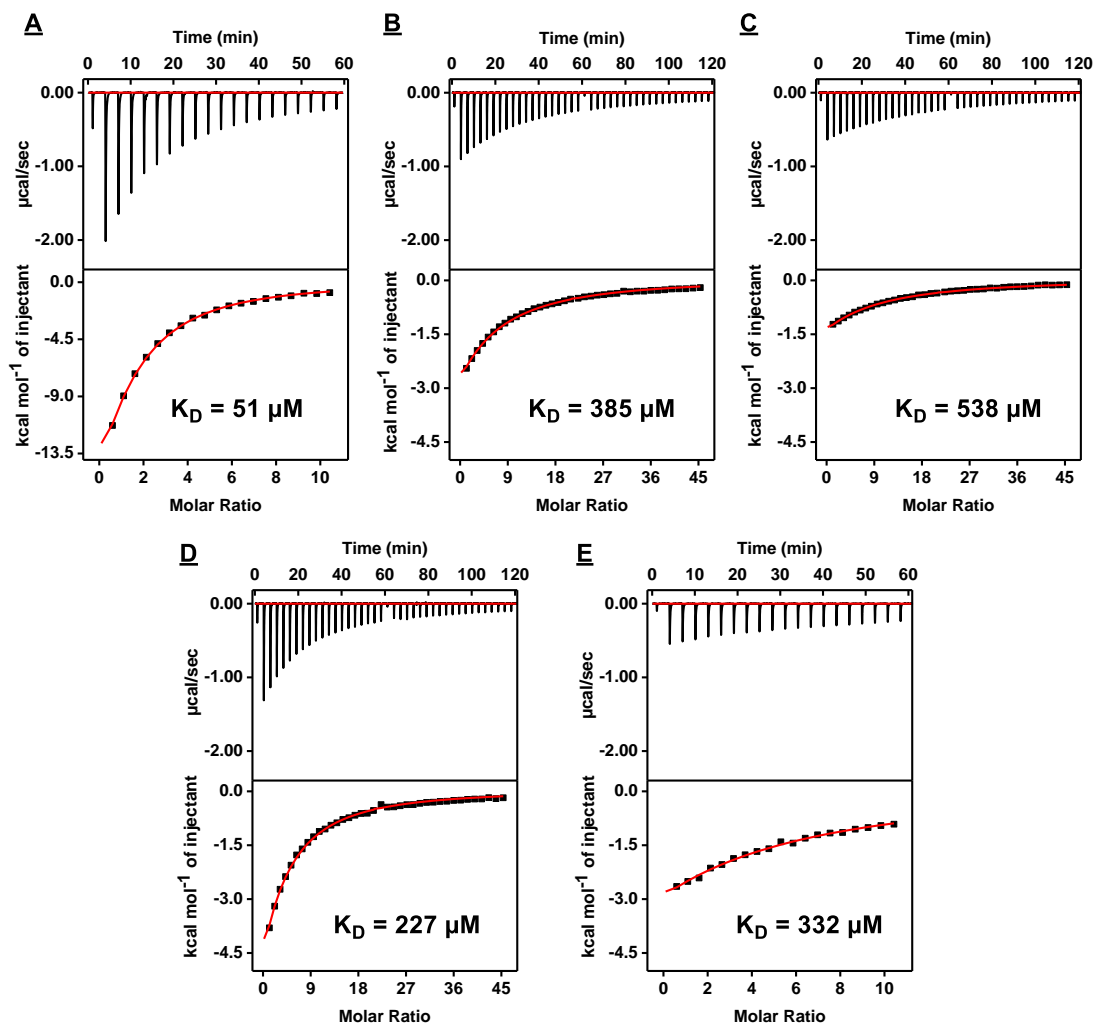


Figure 3-23. Characterization of the interferent-binding affinity of SCA1.1-34 using ITC. Top panels present raw data showing the heat generated from each titration of (A) MDMA, (B) (+)-pseudoephedrine, (C) levamisole, (D) procaine, and (E) quinine to SCA1.1, while bottom panels show the integrated heat of each titration after correcting for dilution heat of the titrant. ITC data were fitted using a single-site model.

We observed similar predicted and experimental cross-reactivity (**Figure 3-26**). These results confirm that the dual-aptamer-modified E-AB sensor is amenable for synthetic cathinone detection in interferent-ridden samples. To demonstrate this, we challenged the

sensor with 17 binary mixtures of 10 μM MDPV with 100 μM interferent. We found that the sensor yielded similar responses to all binary mixtures relative to MDPV alone, except for the mixture containing quinine, which exhibited low levels of signal suppression (**Figures 3-29** and **3-30**). This may occur because quinine has been reported to inhibit electron transfer from methylene blue to electrode surfaces.¹³⁶

The cross-reactivity profile of the Cy7-displacement assay using the truncated aptamer mixture is practically the same as that of the E-AB sensor (**Figure 3-31**). However, the E-AB sensor is generally more cross-reactive to synthetic cathinones as well as interferents like MDMA, procaine, and quinine. There are several potential reasons for this discrepancy including the different signal transduction mechanism between two biosensors as well as different physicochemical conditions (*e.g.* salt concentrations) or the surface-immobilized aptamers have different binding affinities than free aptamers or surface co-immobilization of different aptamers may affect their binding behavior.

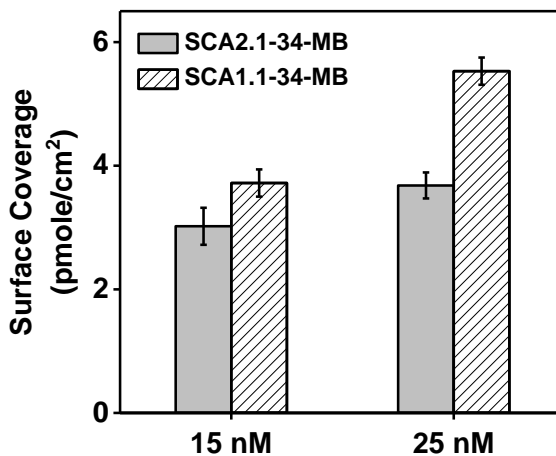


Figure 3-24. Comparison of surface coverages of aptamer-modified electrodes. Comparison of surface coverages of electrodes modified with SCA2.1-34-MB or SCA1.1-34-MB alone at concentrations of 15 nM and 25 nM aptamer. Error bars represent the standard deviation of measurements from three different E-AB sensors.

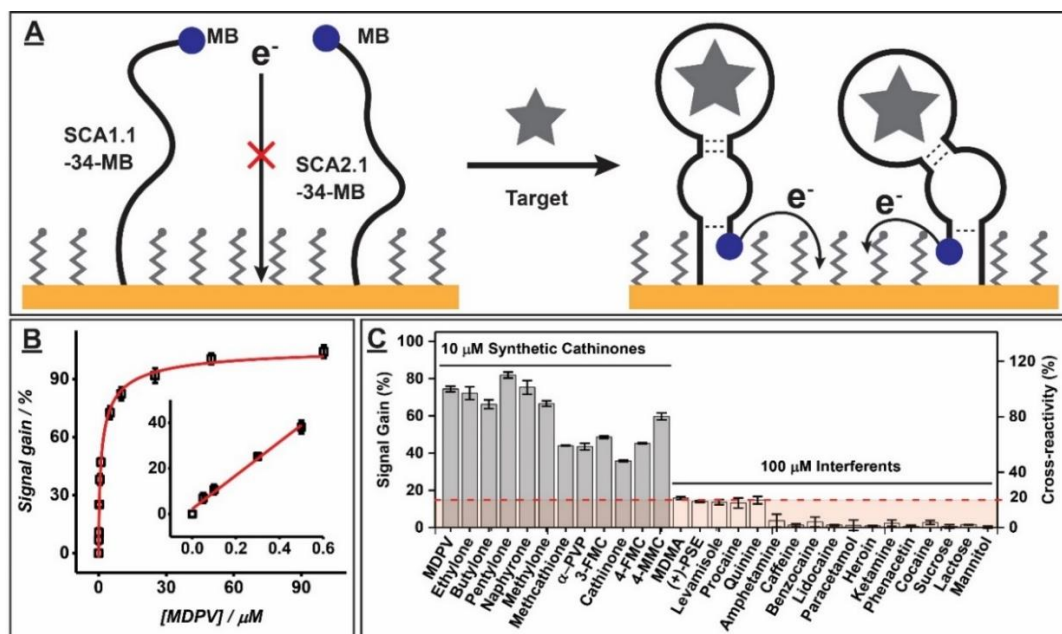


Figure 3-25. Dual-apptamer-based E-AB sensor. (A) Schematic of the assay. Aptamers are initially unfolded in the absence of target (left), situating the MB tag far from the electrode and producing minimal current. Target binding causes the aptamers to fold, resulting in enhanced electron transfer and an increase in current. (B) Calibration curve of MDPV on our 1:1 SCA1.1-34-MB and SCA2.1-34-MB E-AB sensor, obtained via square-wave voltammetry. Inset shows the linear range. (C) The 1:1 dual-apptamer sensor shows high cross-reactivity for 12 synthetic cathinones at a concentration of 10 μM and low cross-reactivity for 17 interferents at a concentration of 100 μM . The dashed red line and box indicate a threshold value of 20% cross-reactivity. Error bars represent the standard deviation of measurements with three different electrodes.

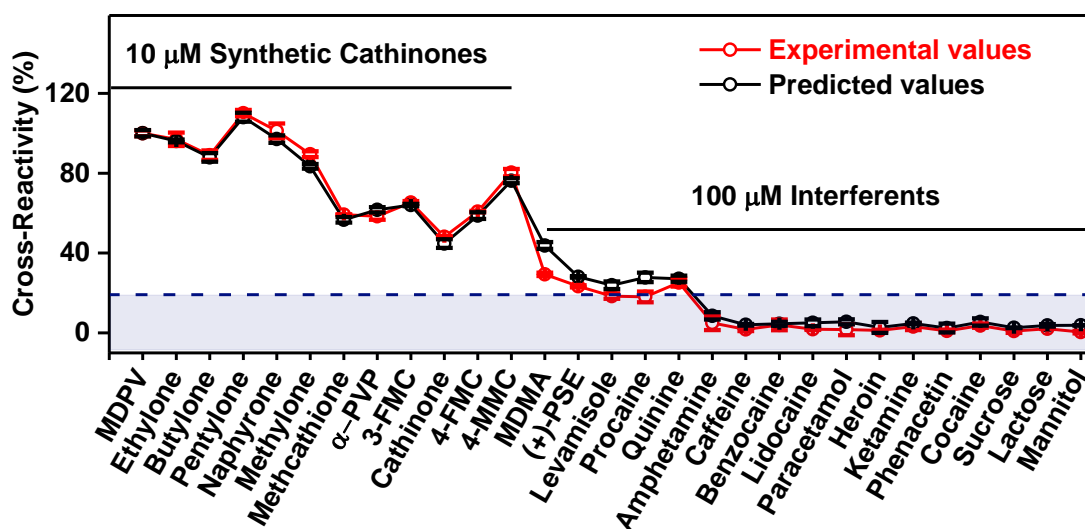


Figure 3-26. Experimental and predicted cross-reactivity of E-AB sensor fabricated with aptamer mixture for synthetic cathinones and interferents. Experimental (red) and predicted

(black) cross-reactivity of SCA2.1-34 and SCA1.1-34 mixtures using E-AB sensors with 12 synthetic cathinones and 17 interferents at concentrations of 10 μM and 100 μM , respectively. The cut-off for 20% cross-reactivity is marked in blue. Error bars represent the standard deviation of three individual experiments.

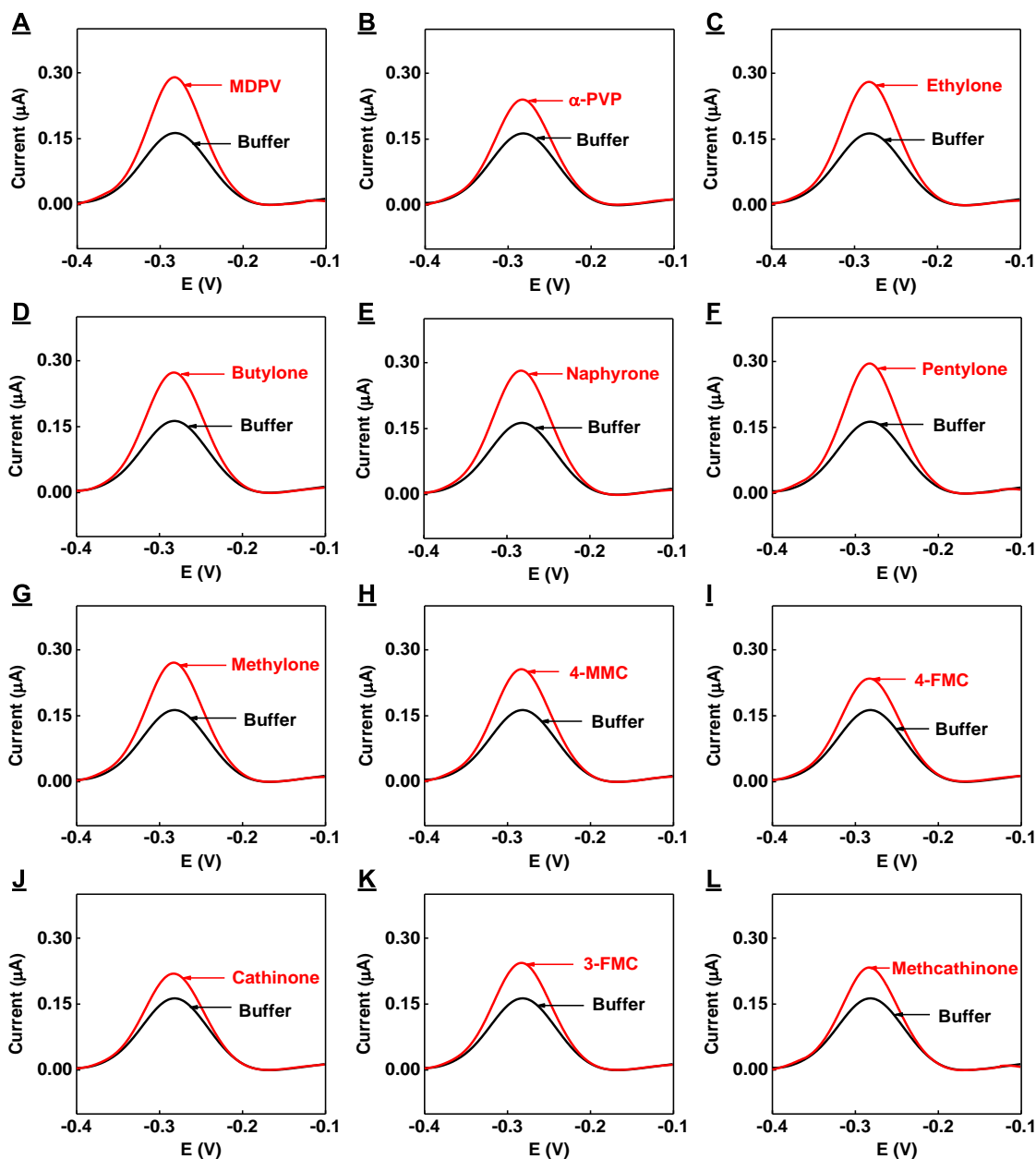


Figure 3-27. Square-wave voltammograms produced by various synthetic cathinones. Square-wave voltammetry spectra collected in the absence (black) and presence (red) of 12 synthetic cathinones at a concentration of 10 μM using the dual-aptamer-modified E-AB sensor.

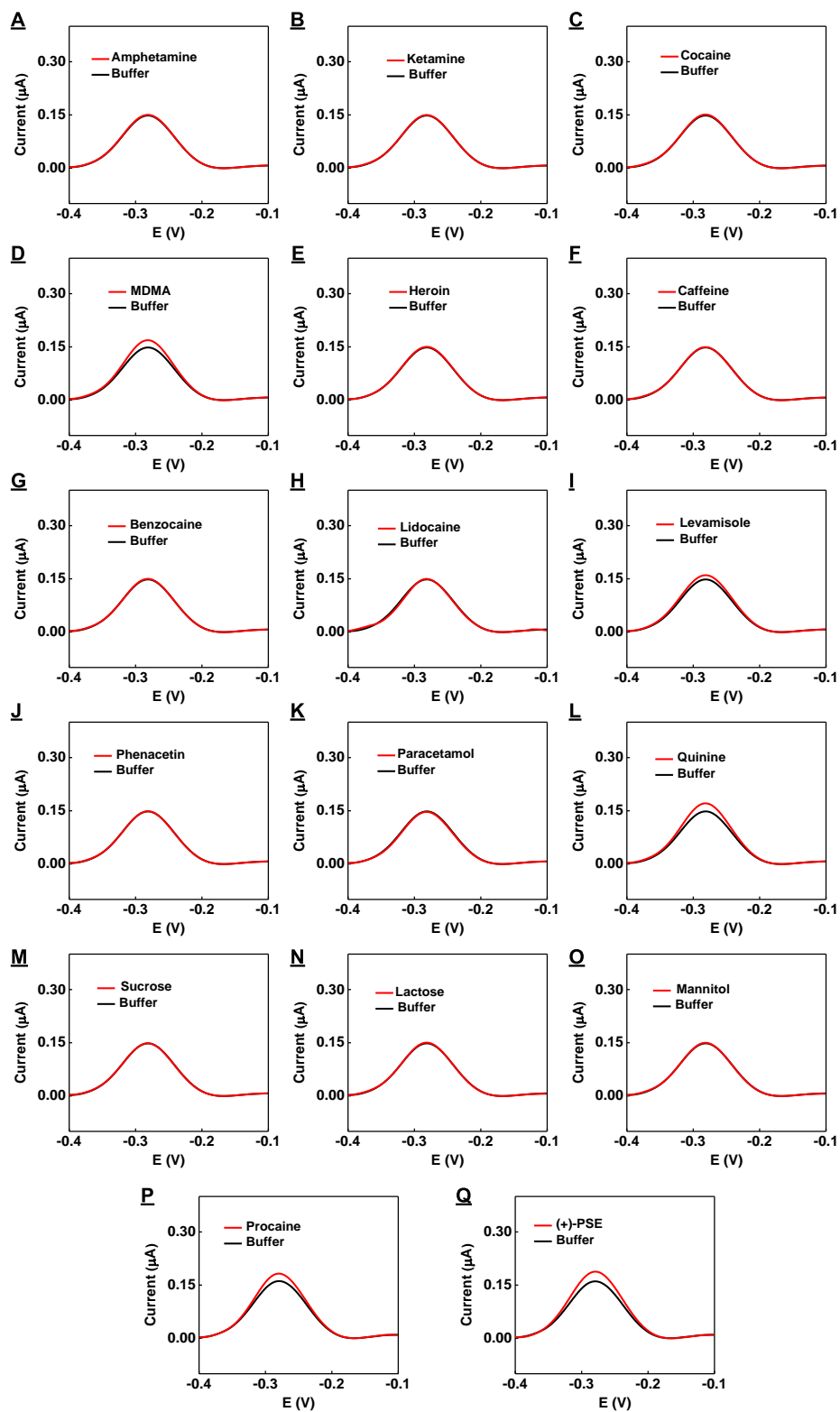


Figure 3-28. Square-wave voltammograms produced by various interferents. Square-wave voltammetry spectra collected in the absence (black) and presence (red) of 17 interferents at a concentration of 100 μM using the dual-aptamer-modified E-AB sensor.

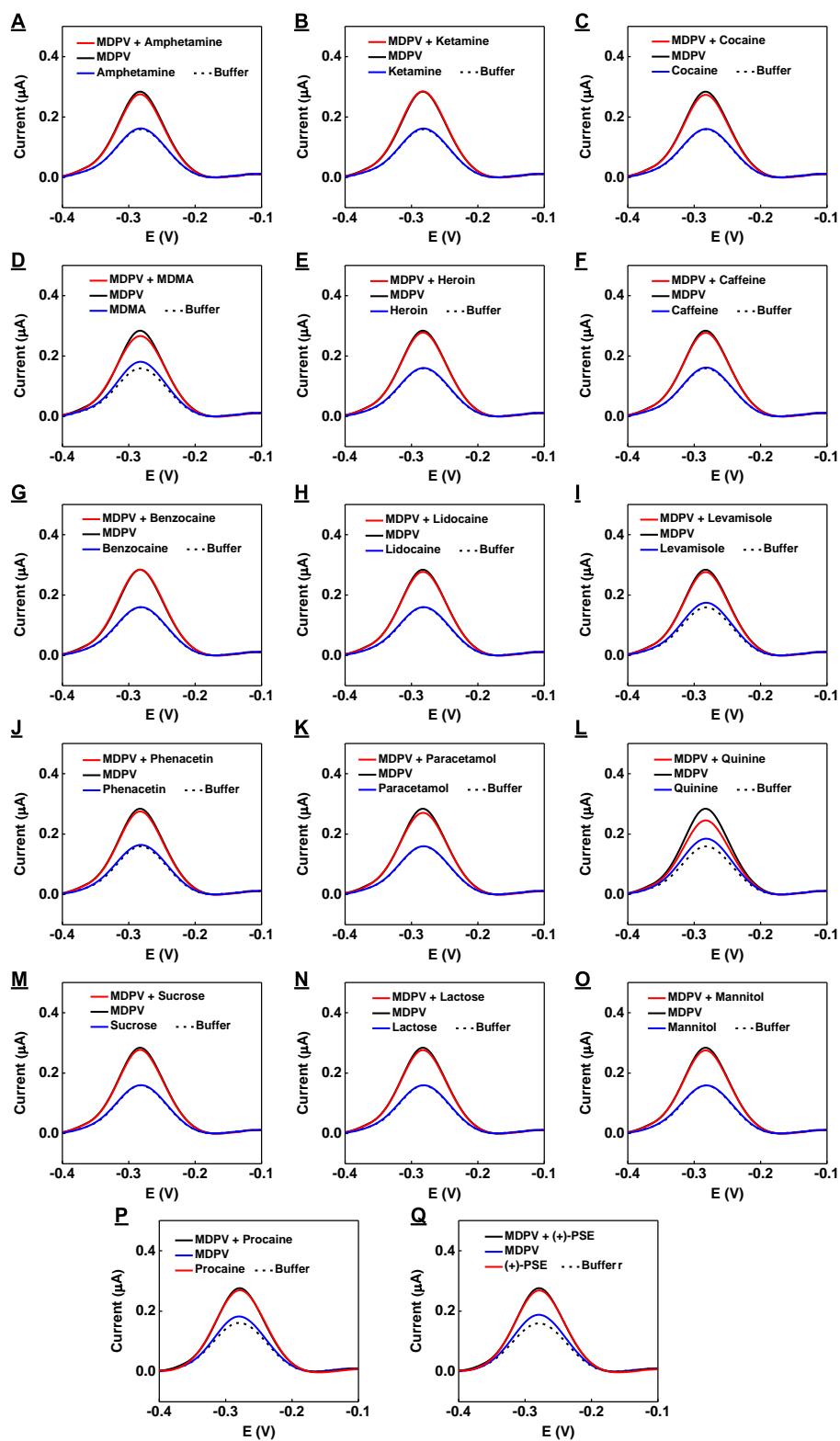


Figure 3-29. Square-wave voltammetry spectra for binary mixtures. Square-wave voltammetry spectra collected in buffer (dashed), with 100 μM of 17 different interferents

(blue), 10 μM MDPV (black), or a binary mixture of 10 μM MDPV and 100 μM of the various interferents (red) using a dual-aptamer-modified E-AB sensor.

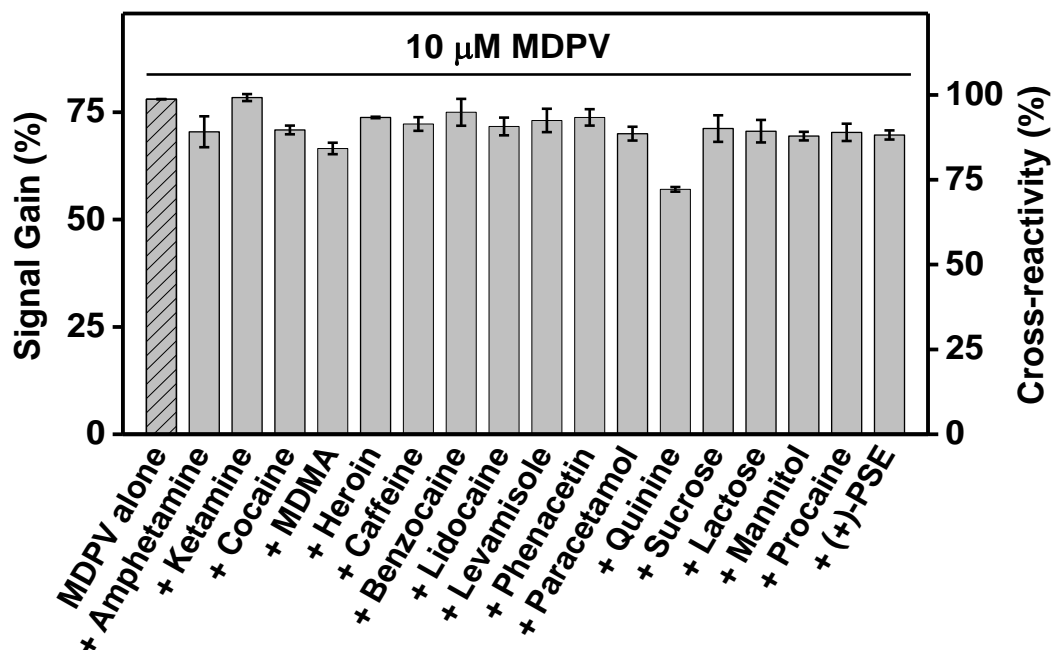


Figure 3-30. Signal gain and cross-reactivity for binary mixtures. Signal gain and cross-reactivity from binary mixtures of 10 μM MDPV and 17 different interferents at a concentration of 100 μM using the dual-aptamer-modified E-AB sensor.

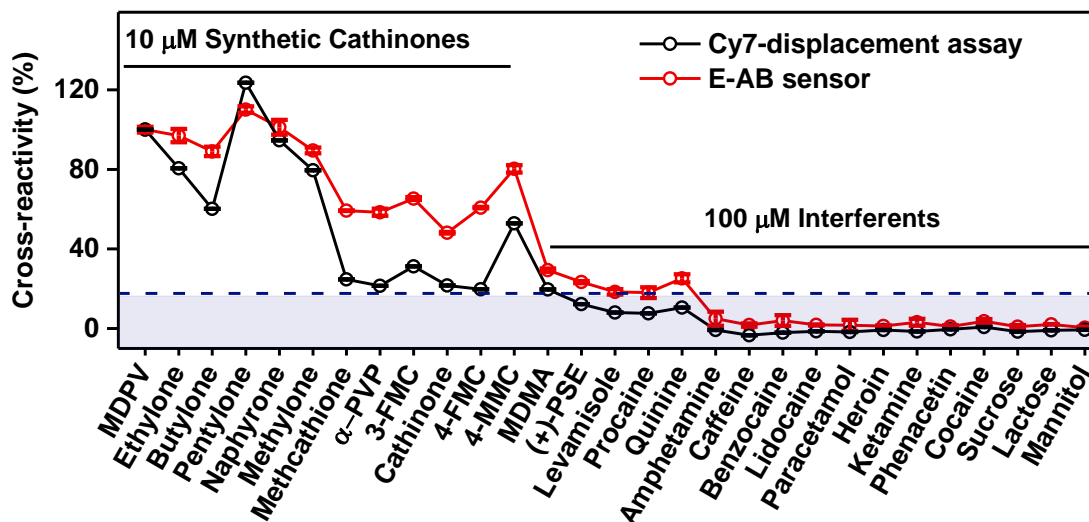


Figure 3-31. Cross-reactivity of aptamer mixture of SCA2.1-34 and SCA1.1-34 in the Cy7-displacement assay and an E-AB sensor. Cross-reactivity of the truncated mixture of SCA2.1-34 and SCA1.1-34 in the Cy7-displacement assay and an E-AB sensor with 12 synthetic cathinones and 17 interferents at concentrations of 10 μM and 100 μM ,

respectively. The cut-off for 20% cross-reactivity is marked in blue. Error bars represent the standard deviation of three individual experiments.

Since our E-AB sensor exhibits strong cross-reactivity to all of the tested synthetic cathinones, our sensor can be used as a general screening assay to sensitively determine the concentration of these drugs in a sample regardless of whether there is a mixture. In this context, it is not necessary for our E-AB sensor to differentiate among different SCs, as almost all members of this family are considered drugs of abuse. As such, a semi-quantitative ‘yes-or-no’ answer is sufficient for on-site drug testing. Likewise, in a medical context, the identity of the synthetic cathinone(s) does not need to be known, as drugs in this family have similar toxicological effects and are treated in the same fashion.

3.4. Conclusion

The detection of a group of structurally related compounds requires a sensor that yields maximal response to its intended targets and minimal response to interferents. To this end, much work has been dedicated to developing biorecognition elements with these ideal binding properties, with limited success to date. We have identified an alternative approach. Rather than searching for one ‘perfect’ bioreceptor, in this work we have employed a mixture of aptamers, each with their own favorable and unfavorable binding properties, that can be used together to develop high-performance sensors that enable broad and specific detection of a molecular family. We first used a Cy7-displacement assay to illustrate the divergent binding profiles of two different synthetic cathinone-binding aptamers. One aptamer (SCA1.1) displays excellent target cross-reactivity but poor specificity, while the other (SCA2.1) has lower target cross-reactivity but higher specificity.

We demonstrated that the strengths of both aptamers could be leveraged by mixing them at an optimized ratio. As a result, up to 12 synthetic cathinones with diverse substituents could be detected with high cross-reactivity with minimal response to 17 interferents, which was not possible using either aptamer alone. The generality of this approach was demonstrated by converting these two aptamers into structure-switching aptamers that possess the same binding profile as their parent aptamers, and then incorporating these into an E-AB sensor at an optimized ratio. As with the Cy7-displacement assay, this dual-aptamer sensor demonstrated high cross-reactivity and specificity, achieving interference-free target detection in binary mixtures containing 90% interferent.

Our results demonstrate for the first time that the cross-reactivity of biosensors can be precisely fine-tuned with the right combination of aptamers. This is extremely valuable, as it can be challenging to identify individual bioreceptors that enable optimal sensor performance. For our purposes, two aptamers were sufficient to enable detection of the current most common synthetic cathinones. However, in future applications, as many aptamers as needed should be employed to provide target coverage that is sufficient for the application at hand. Increasing the number of aptamers greatens target coverage and sensor flexibility. The multi-receptor approach is particularly well-suited for aptamers, especially considering that high-throughput sequencing technologies can easily identify multiple aptamers for a given target or class of targets with varying binding characteristics.¹³⁷ The aptamers need not have similar target-binding affinities – although they should not vary by more than 10-fold – and, of course, should have minimal binding towards any relevant interferents. For scenarios where families of compounds need to be detected, such as with

antibiotics, environmental toxins, explosives, or illicit drugs to name a few, we believe our multi-aptamer method will be a viable option to enable such goal.

CHAPTER 4: Immobilization Strategies for Enhancing Sensitivity of Electrochemical Aptamer-Based Sensors

4.1. Introduction

Electrochemical biosensors that utilize bioreceptors such as enzymes and antibodies can achieve rapid, sensitive, and selective detection of targets via specific molecular recognition.^{138,139} For example, personal glucose meters utilize the enzyme glucose oxidase to quantify glucose concentrations directly in whole blood.¹³⁹ However, the appeal of such sensors is diminished by the lack of enzymes available for detecting a broad range of analytes¹³⁹ and the generally short shelf-life and high cost of protein-based bioreceptors.¹ Aptamers offer a promising alternative in this context; these are single-stranded DNA or RNA oligonucleotides that can be isolated from randomized libraries via an *in vitro* process to bind to virtually any target of interest.^{3,4} Aptamers can be isolated relatively quickly, have high chemical stability and long shelf-lives, and can be synthesized at low cost with minimal batch-to-batch variation.⁶ Electrochemical aptamer-based (E-AB) sensors have great potential for diagnostic, research, and therapeutic applications because they enable rapid detection of specific analytes directly in complex samples such as soil, foodstuffs, urine, and whole blood.^{19,20,22,96,130,140} E-AB sensors are fabricated by immobilizing aptamers that have been modified with a terminal thiol and a redox label (usually methylene blue) onto a gold electrode via thiol-gold chemistry. This step is typically followed by backfilling with alkanethiol diluents to mitigate the adsorption of oligonucleotide probes and interferents onto the electrode surface.²¹ The aptamers employed in E-AB sensors have structure-switching functionality, meaning that they are

unfolded in their unbound state and undergo a conformational change when binding to the target. This structural change alters the distance between the redox label and the electrode surface, leading to a change in current that is proportional to the concentration of the analyte.

E-AB sensors have greatly evolved in the past decade, transitioning from macroscale sensors that can only perform *in vitro* detection to miniaturized devices that can detect analytes directly *in vivo* in real time.^{36,83,89} Despite these advances, many E-AB sensors reported to date are incapable of detecting analytes at relevant levels for specific applications in complex samples due to their poor sensitivity and low signal-to-noise ratios (SNRs).^{20,83,141} For instance, a previously reported cocaine-detecting E-AB sensor has a limit of detection (LOD) of 10 μM in blood,²⁰ which is well outside the range of medically- and forensically-relevant blood concentrations of cocaine (0.1–1 μM).¹⁴² This can be primarily attributed to the biofouling that occurs when detection is performed in biological matrices and the low target affinity of structure-switching aptamers. The biofouling problem has been remedied through the development of new monolayer chemistries and membranes that mitigate protein and cell adsorption.¹⁴³ For example, the Plaxco group has used biomimetic zwitterionic phospholipid-based thiols as backfillers³⁷ and polysulfone membranes as a physical barrier³⁶ to enable continuous detection of analytes directly in the circulating blood of live animals using E-AB sensors. However, the affinity issue has only been partially resolved. Although advances in aptamer selection protocols have facilitated the isolation of high-affinity aptamers,^{123,144} most aptamers still experience considerable reduction in binding affinity upon being engineered with structure-switching functionality

via strategies such as aptamer truncation¹⁴⁵ or splitting,¹³ due to thermodynamic destabilization.

Previous reports have suggested that spacing of oligonucleotide probes on the electrode surface profoundly affects sensor performance.^{32,45} For example, the Fan group fabricated an E-AB sensor for cocaine by immobilizing a split cocaine-binding aptamer incorporated into a DNA tetrahedron construct tethered to the electrode surface.⁴⁵ They hypothesized that the tetrahedron would provide the aptamer sufficient spacing to facilitate aptamer-target assembly, thereby augmenting sensor responsiveness. Indeed, they observed significant improvements in sensitivity compared to previous E-AB sensors for cocaine.²⁰ Here, we described a new method to improve the sensitivity and SNR of E-AB sensors based on the spatial distribution of aptamers on the electrode surface. Although the average spacing between aptamers can be tuned by adjusting the quantity of aptamer⁴⁴ or buffer ionic strength¹⁴⁶ employed during the immobilization step, these strategies do not allow control over the inter-oligonucleotide distance of probes at the microscopic level to favor optimal target binding and signal transduction. Here, we discovered two aspects of the electrode modification step that could optimize spacing of surface-bound aptamer probes. First, we determined that immobilizing the aptamer in its folded, target-bound state rather than its unfolded state—as is done conventionally^{19,21}—improves both SNR and LOD, which is probably due to optimized spacing granted by the complex at the microscopic level. Next, we observed that the use of low ionic strength buffers during the aptamer immobilization process likewise greatly enhances E-AB sensing performance. This improvement in performance can likely be attributed to mitigation of the clustering of surface-bound aptamers, which commonly occurs when high ionic strength buffers are

utilized in conventional protocols.³² These two changes to the immobilization process proved beneficial for E-AB sensing regardless of the aptamer sequence or structure, as we demonstrated in experiments with three different small-molecule-binding aptamers. We therefore believe that our enhanced immobilization protocols are generalizable, and will be highly valuable for the fabrication of E-AB sensors with greater sensitivity.

4.2. Experimental section

4.2.1. Materials

Potassium chloride, magnesium chloride, sodium chloride, monosodium hydrogen phosphate, sodium dihydrogen phosphate, Trizma pre-set crystals (Tris buffer, pH 7.4), tris(2-carboxyethyl) phosphine chloride, 6-mercapto-1-hexanol, cocaine hydrochloride, adenosine, sodium hydroxide, sulfuric acid (95-98%), and calf serum were purchased from Sigma-Aldrich. 3,4-methylenedioxypropylvalerone chloride (MDPV) was purchased from Cayman Chemicals. All solutions were prepared using Milli-Q (Millipore) water with resistivity of $18.2 \text{ M}\Omega \times \text{cm}$ unless specified otherwise. Thiolated methylene blue-modified aptamers were synthesized by Biosearch Technologies and purified with HPLC. All other unmodified oligonucleotides were purchased from Integrated DNA Technologies with HPLC purification and dissolved in PCR-grade water. Oligonucleotides concentrations were measured using a NanoDrop 2000 spectrophotometer. The names and sequences of DNA oligonucleotides used are as follows:

ADE-25: 5'-CCTGGTGGAGTATTGCGGGGAAGG-3'

COC-32: 5'-AGACAAGGAAAATCCTTCAATGAAGTGGGTCT-3'

SC-34: 5'-ACCTTAAGTGGGGTTCGGGTGGAGTTTATGGGGT-3'

ADE-25-MB: 5'-SH-C6-CCTGGTGGAGTATTGCGGGGGAAGG-MB-3'

COC-32-MB: 5'-SH-C6-AGACAAGGAAAATCCTTCAATGAAGTGGGTCT-MB-3'

SC-34-MB: 5'-SH-C6-ACCTTAAGTGGGGTTCGGGTGGAGTTTATGGGGT-MB-3'

(SH = thiol group, MB = methylene blue)

Buffers employed were as follows:

High-salt PBS: 1.6 mM NaH₂PO₄, 8.4 mM Na₂HPO₄, 1 M NaCl, 1 mM MgCl₂, pH 7.2

Low-salt PBS: 1.9 mM NaH₂PO₄, 8.1 mM Na₂HPO₄, 1.9 mM NaCl, 0.5 mM MgCl₂, pH 7.4

Low-salt Tris buffer: 10 mM Tris buffer, 20 mM NaCl, 0.5 mM MgCl₂, pH 7.4

High-salt Tris buffer: 10 mM Tris buffer, 1 M NaCl, 1 mM MgCl₂, pH 7.4

4.2.2. Fabrication of E-AB sensors.

Gold disk electrodes (2 mm diameter) were purchased from CH Instruments and cleaned as previously reported.²¹ First, the electrode was polished on microcloth (Buehler) with 1- μ m diamond suspension (BASi) and 0.05- μ m gamma alumina suspension (Buehler). Each polishing step was followed by sonication in ethanol and distilled water for 5 min. Then, the electrode was electrochemically cleaned with a series of voltammetric scans performed in 0.5 M sodium hydroxide, 0.5 M sulfuric acid, and 0.1 M sulfuric acid solutions. To prepare the aptamers for electrode modification, the disulfide groups on the 5'-end of the thiolated, methylene blue-modified aptamers were reduced by incubation in 100 mM tris(2-carboxyethyl) phosphine chloride for 2 h in the dark at room temperature. The aptamers were then diluted to various concentrations (15–200 nM) in high-salt PBS, low-salt PBS with different pH values (pH = 6.0, 7.0, 7.4, or 8.0), or low-salt Tris buffer with or without their respective target. The cleaned electrodes were rinsed with distilled

water, dried with nitrogen, and immediately incubated in a solution of either aptamer or aptamer-target complexes for 13 h in the dark at room temperature. The electrodes were then backfilled with 1 mM 6-mercapto-1-hexanol solution containing the same concentration of respective target used in the previous step for 2 h at room temperature. Finally, the aptamer-modified electrodes were thoroughly washed with deionized water and then stored in 10 mM Tris (pH 7.4) at room temperature before performing electrochemical measurements.

4.2.3. Electrochemical measurements

All electrochemical measurements were carried out using a CHI760D electrochemical workstation (CH Instruments). We used a three-electrode system, including an Ag/AgCl reference electrode, platinum counter electrode, and aptamer-modified gold working electrode. The aptamer surface densities of the modified electrodes were measured via chronocoulometry using the method reported by Tarlov *et al.*¹²⁷ Square wave voltammetry (SWV) was performed in the low-salt Tris buffer for the adenosine, cocaine, and MDPV E-AB sensors. Signal gain was calculated using the equation $((I_T - I_0) / I_0) \times 100\%$, where (I_0) and (I_T) are the SWV peak currents in the absence and presence of target, respectively.

4.2.4. Aptamer affinity measurement via isothermal titration calorimetry (ITC)

All ITC experiments were performed with a MicroCal ITC200 instrument (Malvern) at 23 °C. A summary of the experimental conditions employed for each experiment is shown in **Table 4-1**. In each experiment, the sample cell was loaded with an aptamer solution (final concentrations: 20 μM or 80 μM for COC-32, 20 μM for ADE-25, 20 μM

for SC-34) and the syringe was loaded with the respective target (final concentrations: 800 μM or 4,000 μM cocaine, 2,500 μM adenosine, 200 or 400 μM (-)-MDPV).

Table 4-1. ITC parameters and conditions used in this work and the calculated K_{D} s. pH of the buffer is 7.4 unless stated otherwise.

Cell content	Syringe content	Buffer	K_{D} (μM)
20 μM SC-34	400 μM (-)-MDPV	Low-salt Tris	0.33 ± 0.04
20 μM SC-34	400 μM (-)-MDPV	Low-salt PBS	0.38 ± 0.03
20 μM SC-34	350 μM (-)-MDPV	Low-salt PBS (pH 6.0)	0.23 ± 0.02
20 μM SC-34	350 μM (-)-MDPV	Low-salt PBS (pH 7.0)	0.38 ± 0.02
20 μM SC-34	350 μM (-)-MDPV	Low-salt PBS (pH 7.4)	0.56 ± 0.03
20 μM SC-34	350 μM (-)-MDPV	Low-salt PBS (pH 8.0)	0.69 ± 0.03
20 μM SC-34	300 μM (-)-MDPV	High-salt Tris	1.80 ± 0.05
20 μM SC-34	200 μM (-)-MDPV (2 \times , back-to-back)	High-salt PBS	1.50 ± 0.04
20 μM COC-32	800 μM cocaine	Low-salt Tris	5.8 ± 0.3
20 μM COC-32	800 μM cocaine	Low-salt PBS	5.9 ± 0.3
80 μM COC-32	4,000 μM cocaine	High-salt PBS	70.4 ± 0.8
			$K_{\text{D1}} = 7.4 \pm 0.1$
20 μM ADE-25	1,200 μM adenosine (2 \times , back-to-back)	Low-salt Tris	$K_{\text{D2}} = 103 \pm 0.5$
			$K_{1/2} = 27.6 \pm 0.2$
			$K_{\text{D1}} = 36.7 \pm 2.4$
20 μM ADE-25	2500 μM Adenosine	High-salt PBS	$K_{\text{D2}} = 14.5 \pm 0.6$
			$K_{1/2} = 23.1 \pm 0.80$

Titration involving COC-32 and SC-34 consisted of an initial purge injection of 0.4 μL followed by 19 successive injections of 2 μL , with a spacing of either 120 s or 180 s

between each injection. Titrations involving ADE-25 consisted of an initial 0.4 μL purge injection followed by 38 successive 1 μL injections with a spacing of 120 s between each injection. For all experiments, if saturation was not reached after one series of injections, a second set of injections was performed in the same fashion after reloading the syringe with the target. The raw data were first corrected based on the dilution heat of each target and then analyzed with the MicroCal analysis kit integrated into Origin 7 software, with a single-site binding model for COC-32 and SC-34 or a two-site sequential binding model for ADE-25.

4.3. Results and discussion

4.3.1. Rationale for enhancing E-AB sensor performance by controlling microscale probe spacing

E-AB sensors utilize structure-switching aptamers, which undergo conformational changes when binding to a target. The termini of these aptamers are labeled with a thiol group for immobilization onto a gold electrode surface via thiol-gold bonding and an electroactive redox molecule such as methylene blue for electrochemical reporting. Most E-AB sensors are fabricated using a previously reported protocol²¹ that entails aptamer immobilization in high ionic strength phosphate-buffered saline (pH 7.2) containing 1 M NaCl and 1 mM MgCl_2 (high-salt PBS). High ionic strength buffers allow for high loading efficiencies of oligonucleotides on gold surfaces, because the negatively-charged phosphate groups of the aptamers are shielded from each other by the relatively high concentration of cations. As a consequence, however, the aptamers are highly flexible with low persistence lengths,¹⁴⁷ and immobilize onto the electrode surface as both individual

probes with low inter-oligonucleotide proximities as well as clusters of probes.¹⁴⁸ Theoretically, limited spacing between aptamer probes imposes restrictions on target recognition and folding that can thus affect signal transduction. The average spacing between aptamers on the electrode surface can be tuned at the macroscopic level by simply altering the quantity of aptamer used for immobilization.⁴⁴ However, it is not possible to control local aptamer spacing at the microscale in order to maximize the number of active probes with optimal spacing for target binding and signaling and avoid the formation of dense clusters of inactive probes. Altering average surface densities alone also cannot overcome probe bundling, which occurs at high ionic strengths. To address this problem, we assessed two hypotheses to improve the robustness and sensitivity of E-AB sensors: 1) inter-oligonucleotide spacing can be optimized by immobilizing aptamer-target complexes rather than the aptamer alone, and 2) bundling effects can be minimized by performing aptamer immobilization in low rather than high ionic strength conditions.

4.3.2. Effects of target-assisted aptamer immobilization on E-AB sensor performance

To test our first hypothesis, we fabricated E-AB sensors from ADE-25, an engineered structure-switching adenosine-binding DNA aptamer¹⁴⁹ derived from an ATP-binding aptamer reported by Huizenga and Szostak.¹⁵⁰ ADE-25 specifically binds to adenosine with micromolar binding affinity ($K_{1/2} = 27.6 \pm 0.2 \mu\text{M}$) (**Figure 4-1A**) in low-salt Tris buffer (10 mM Tris-HCl, 20 mM NaCl, 0.5 mM MgCl₂, pH 7.4) but has no affinity for phosphorylated nucleotide analogs such as ATP, ADP, and AMP.¹⁴⁹ We first prepared E-AB sensors using thiolated, methylene blue-modified ADE-25 (ADE-25-MB) alone, and optimized aptamer surface coverage to tune average inter-oligonucleotide spacing by modifying electrodes with different concentrations of aptamer in high-salt PBS. Increases

in aptamer concentration in the range of 15–75 nM resulted in monotonic increases in aptamer surface density (**Figure 4-2A**). We then evaluated the sensing performance of these E-AB sensors by performing detection in solutions containing various concentrations of adenosine (0–1,000 μM), and found that the current increased with increasing target concentrations (**Figure 4-2B**).

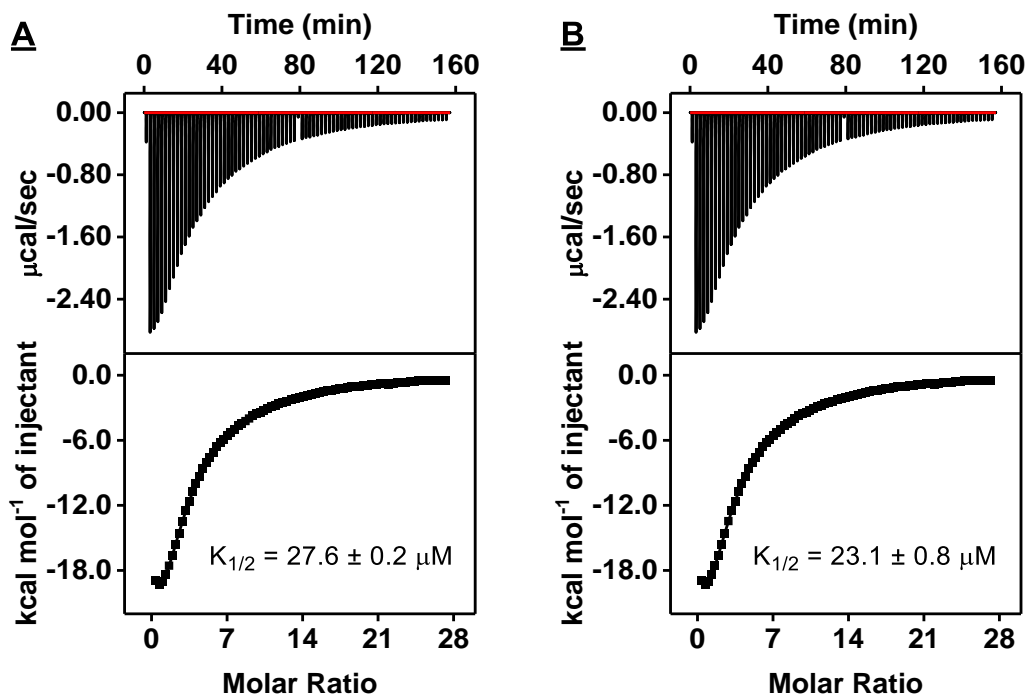


Figure 4-1. Characterization of the affinity of ADE-25 for adenosine using isothermal titration calorimetry (ITC). Top panels present raw data showing the heat generated from each titration of adenosine to ADE-25 in (A) low-salt Tris buffer (10 mM Tris-HCl, 20 mM NaCl, 0.5 mM MgCl_2 , pH 7.4) or (B) high-salt PBS (1.6 mM NaH_2PO_4 , 8.4 mM Na_2HPO_4 , 1 M NaCl, 1 mM MgCl_2 , pH 7.4), while bottom panels show the integrated heat of each titration after correcting for dilution heat of the titrant. ITC data were fitted with a two-site sequential binding model. $K_{1/2} = (K_{D1} \times K_{D2})^{1/2}$

As expected, low signal gain was observed for sensors with very low or very high surface coverage due to insufficient probe loading or probe overcrowding, respectively. Signal gains at all target concentrations increased as surface density increased from 1.89 to 3.77 picomoles/ cm^2 , but a further increase to 11.1 picomoles/ cm^2 resulted in decreased

signal gains (**Figure 4-2C**). The impairment of aptamer functioning at higher surface densities is possibly due to lower inter-oligonucleotide spacing, which has been reported recently using high-resolution atomic force microscopy of oligonucleotide-modified gold surfaces.¹⁴⁸ We predicted that by immobilizing the aptamer in its target-bound folded state, we could produce a self-assembled aptamer monolayer with optimal microscale spacing for target recognition and signaling relative to unbound flexible aptamers, which are arbitrarily spaced on the surface in a non-optimized fashion.

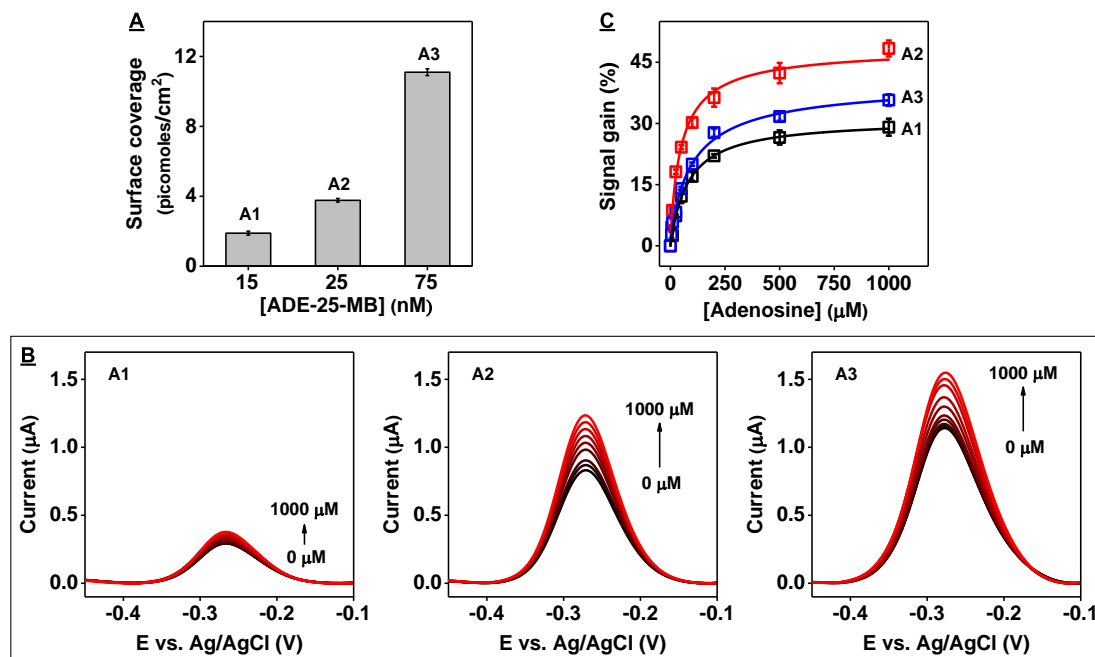


Figure 4-2. Adenosine detection with electrodes modified with ADE-25-MB using the conventional immobilization approach. **(A)** Aptamer surface coverage of electrodes fabricated using 15 nM (A1), 25 nM (A2), or 75 nM (A3) ADE-25-MB in the absence of target. **(B)** Square wave voltammograms (SWV) and **(C)** calibration curves for adenosine detection produced by the different E-AB sensors with 0 – 1,000 μM adenosine. Error bars represent the standard deviation of measurements from three independently fabricated electrodes.

To test this, we modified an electrode using a solution of aptamer-target complexes at the optimal surface coverage determined above. Prior to aptamer immobilization, we first

determined whether ADE-25 retains the ability to bind adenosine in high-salt PBS using isothermal titration calorimetry (ITC). The ITC results showed that ADE-25 binds adenosine with an affinity ($K_{1/2}$) of $23.1 \pm 0.8 \mu\text{M}$ under these conditions (**Figure 4-1B**).

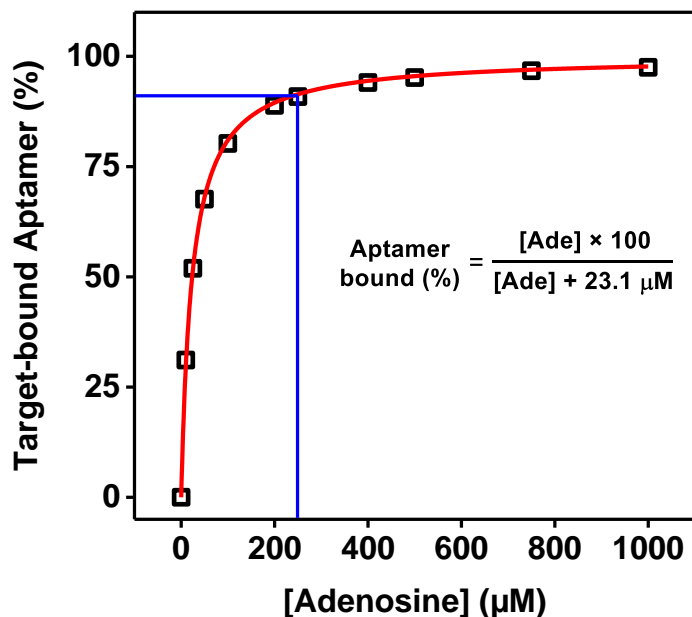


Figure 4-3. Simulated binding curve for ADE-25 based on its affinity for adenosine in high-salt PBS ($K_{1/2} = 23.1 \mu\text{M}$). Blue lines indicate that $\sim 91\%$ of the aptamer is bound in the presence of $250 \mu\text{M}$ adenosine.

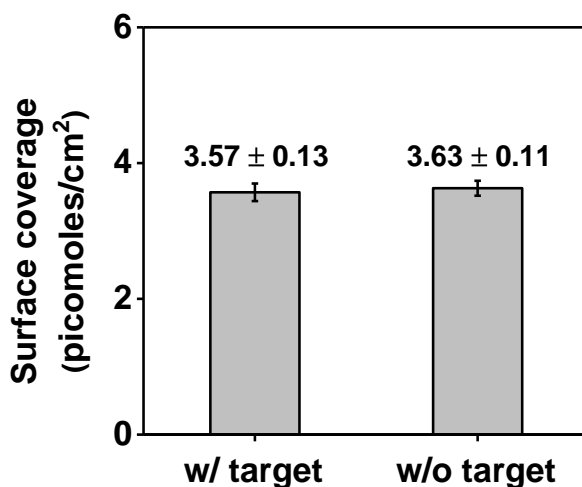


Figure 4-4. Surface coverage of electrodes fabricated with ADE-25-MB via different methods. Aptamer surface coverages of electrodes fabricated by immobilizing the aptamer

in the presence or absence of 250 μM adenosine. Error bars represent the standard deviation of measurements from three independently fabricated electrodes.

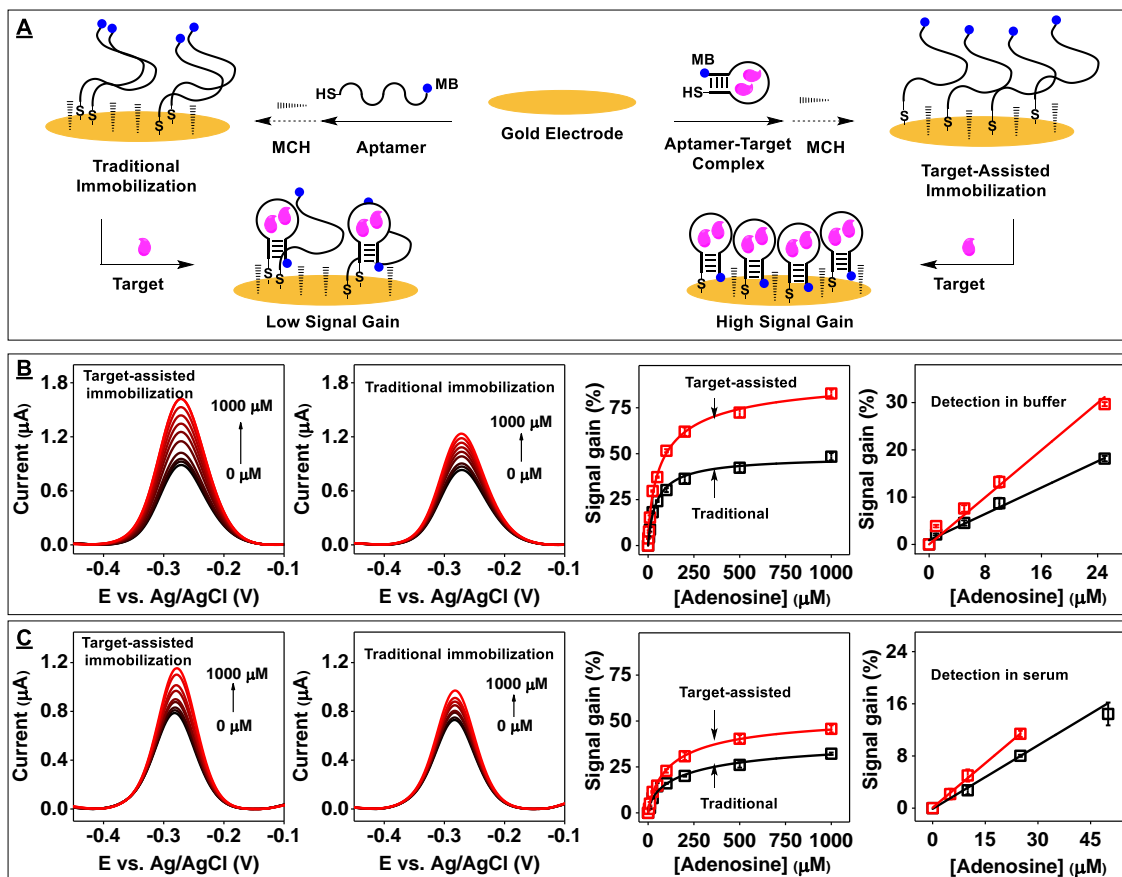


Figure 4-5. E-AB sensor performance using electrodes modified with ADE-25-MB either alone or bound to adenosine. (A) Modification of a gold electrode using either the traditional immobilization protocol (left) or our target-assisted immobilization strategy (right). Square-wave voltammetry (SWV) spectra of electrodes modified with the aptamer-target complex (left) or aptamer alone (middle) in (B) buffer or (C) 50% serum and corresponding calibration curves and linear ranges (right) collected using electrode prepared with target-assisted aptamer immobilization approach (red) or the traditional method (black). Error bars represent the standard deviation for three working electrodes from each measurement.

Based on this affinity measurement, we estimated that $\sim 91\%$ of the aptamer is bound to the target in the presence of 250 μM adenosine (Figure 4-3). For electrode fabrication, we first prepared a solution containing 25 nM freshly-reduced ADE-25-MB in high-salt PBS with 250 μM adenosine and then submerged the electrodes in the aptamer-target

complex solution (**Figure 4-5A, right**). Afterwards, the electrodes were cleaned thoroughly with buffer to remove any residual adenosine. As a control, we prepared another set of gold electrodes modified with 25 nM ADE-25-MB alone using a traditional immobilization approach²¹ (**Figure 4-5A, left**). Both sets of electrodes had virtually the same average surface density (**Figure 4-4**). However, we observed that electrodes modified via target-assisted aptamer immobilization yielded higher SNR and had a lower LOD than electrodes modified with aptamer alone in both buffer (LOD = 1 μ M vs. 5 μ M) and 50% serum (LOD = 5 μ M vs. 10 μ M) (**Figure. 4-5B, C**). Since the total amount of aptamer immobilized on both electrodes was essentially identical, the observed improvement in sensing performance can be most likely be attributed to optimized inter-oligonucleotide spacing.

4.3.3. Confirmation of the generalizability of target-assisted aptamer immobilization

To demonstrate whether target-assisted aptamer immobilization can improve the performance of E-AB sensors regardless of the aptamer sequence and structure, we fabricated sensors with a well-studied three-way-junction-structured cocaine aptamer¹⁵¹ with structure-switching functionality (COC-32).²⁴ We prepared electrodes with the thiolated, methylene-blue labeled version of this aptamer (COC-32-MB) in the absence or presence of cocaine (250 μ M) in high-salt PBS. Once again, although both sets of electrodes displayed similar aptamer surface densities (**Figure 4-6A**), the sensors prepared via target-assisted aptamer immobilization demonstrated greater signal gains at all tested concentrations of cocaine (0–1,000 μ M) (**Figures 4-6B-D**) and improved LODs relative to electrodes modified with aptamer alone (LOD = 1 μ M vs. 2 μ M) (**Figure 4-6E**). This

confirmed that target-assisted aptamer immobilization generally enhances the performance of E-AB sensors.

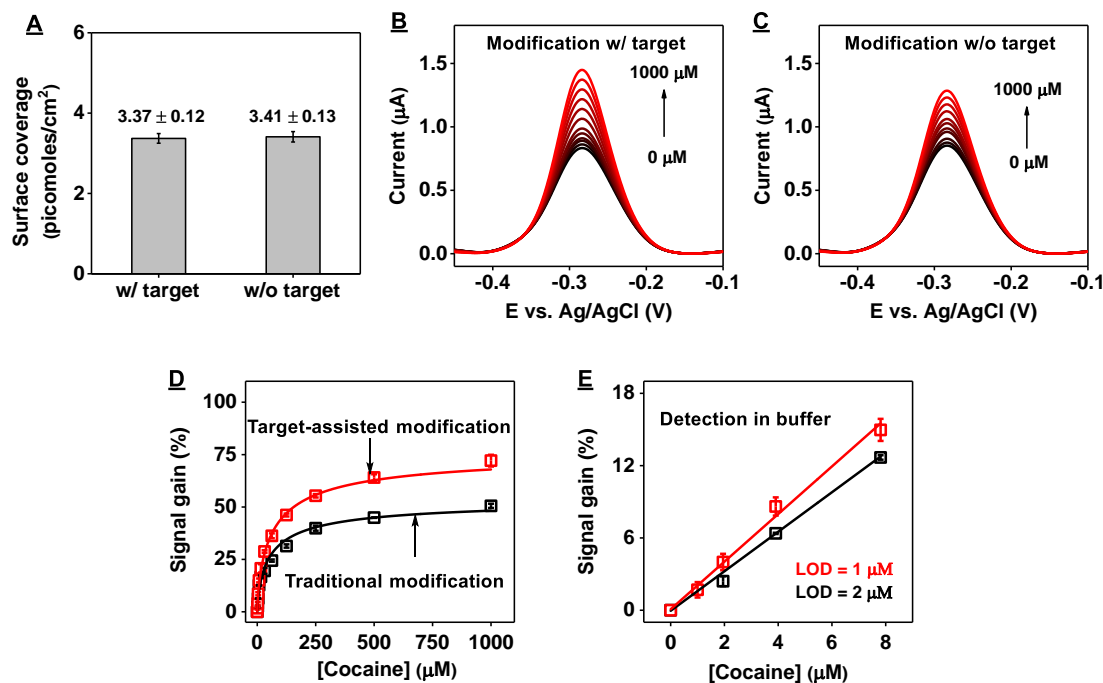


Figure 4-6. Performance of electrodes fabricated with COC-32-MB via target-assisted immobilization or conventional means in high-salt PBS. (A) Surface coverage of electrodes fabricated by immobilizing the aptamer in the presence (w/ target) or absence (w/o target) of 250 μM cocaine. SWV from electrodes fabricated via (B) target-assisted immobilization or (C) traditional means (aptamer only) and challenged with 0–1000 μM cocaine. (D) Calibration curves for detection of cocaine derived from the spectra shown in B (red) and C (black). (E) Sensitivity and LOD of electrodes fabricated using target-assisted immobilization (red) or traditional means (black). Error bars represent the standard deviation of measurements from three independently fabricated electrodes.

4.3.4. Relationship between the concentration of aptamer-target complex used for electrode modification and E-AB sensor performance

It has been reported that the cocaine-binding aptamer has weak affinity for its target at high salt concentrations.¹⁵² We confirmed via ITC that COC-32 binds cocaine with a K_D of $(70.4 \pm 0.8) \mu\text{M}$ in the high-salt PBS buffer commonly used for aptamer immobilization (Figure 4-7A). In these conditions, only ~78% of the aptamer is bound to the target in the

presence of 250 μM cocaine (**Figure 4-9**), such that the resulting monolayer would be predicted to contain both active and inactive, non-optimally-spaced probes. We hypothesized that maximizing the quantity of target-bound aptamer during the aptamer immobilization process would result in the greatest quantity of immobilized active aptamers, thereby yielding the best attainable sensor performance. We therefore fabricated E-AB sensors by immobilizing COC-32-MB in the presence of 2 mM cocaine, where $\sim 96\%$ of the aptamer is in the target-bound state (**Figure 4-9**). Although electrodes prepared in the presence of 250 μM or 2 mM cocaine had the same aptamer surface densities (**Figure 4-8**), the latter sensors yielded higher SNRs at all target concentrations—especially in the range from 100–1,000 μM cocaine, where we saw an 8% improvement in signal gain (**Figure 4-10**). This clearly demonstrates that more active aptamer probes were being immobilized on the electrode surface with immobilization solutions containing a higher proportion of aptamer-target complexes.

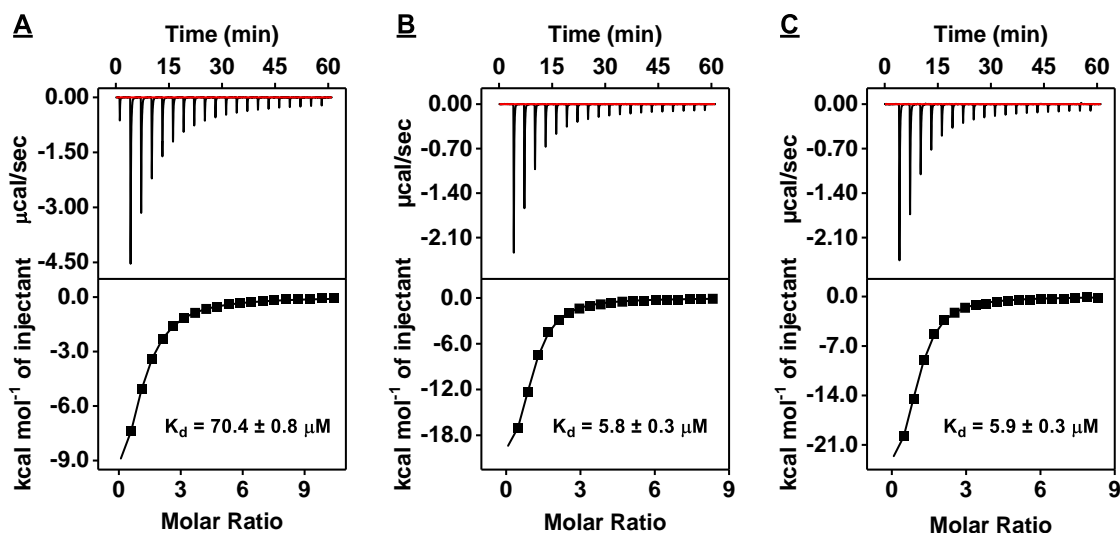


Figure 4-7. Characterization of the affinity of COC-32 for cocaine using ITC. Top panels present raw data showing the heat generated from each titration of cocaine to COC-32 in

(A) high-salt PBS, (B) low-salt PBS, or (C) low-salt Tris buffer, while bottom panels show the integrated heat of each titration after correcting for dilution heat of the titrant. ITC data were fitted with a single-site binding model.

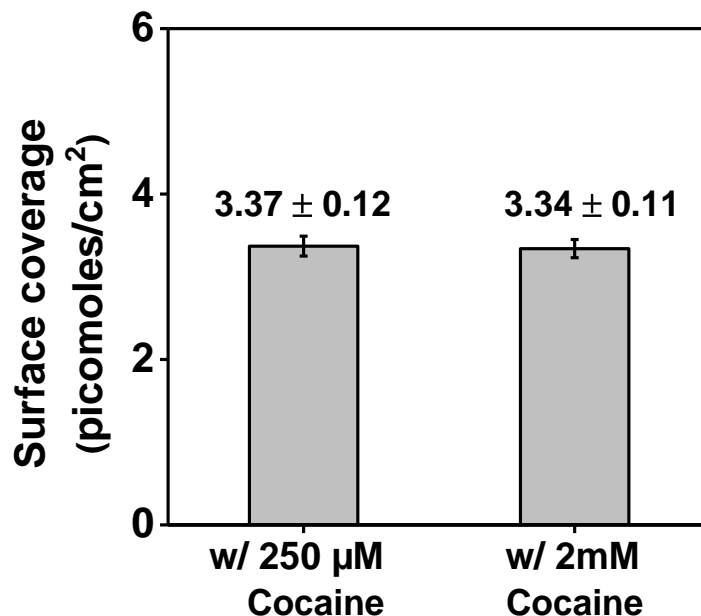


Figure 4-8. Surface coverage of electrodes modified with COC-32-MB and cocaine in high-salt PBS. Surface coverage of electrodes modified with COC-32-MB via target-assisted immobilization in high-salt PBS in the presence of 250 µM or 2 mM cocaine. Error bars represent the standard deviation of measurements from three different electrodes.

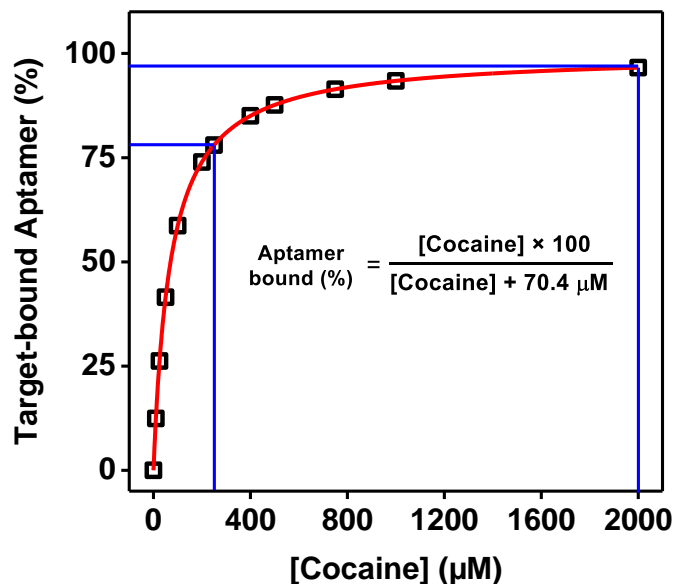


Figure 4-9. Simulated binding curve for COC-32 based on its affinity for cocaine in high-salt PBS ($K_D = 70.4 \mu\text{M}$). The blue lines indicate that ~78% and 96% of the aptamer is bound in the presence of 250 µM and 2 mM cocaine, respectively.

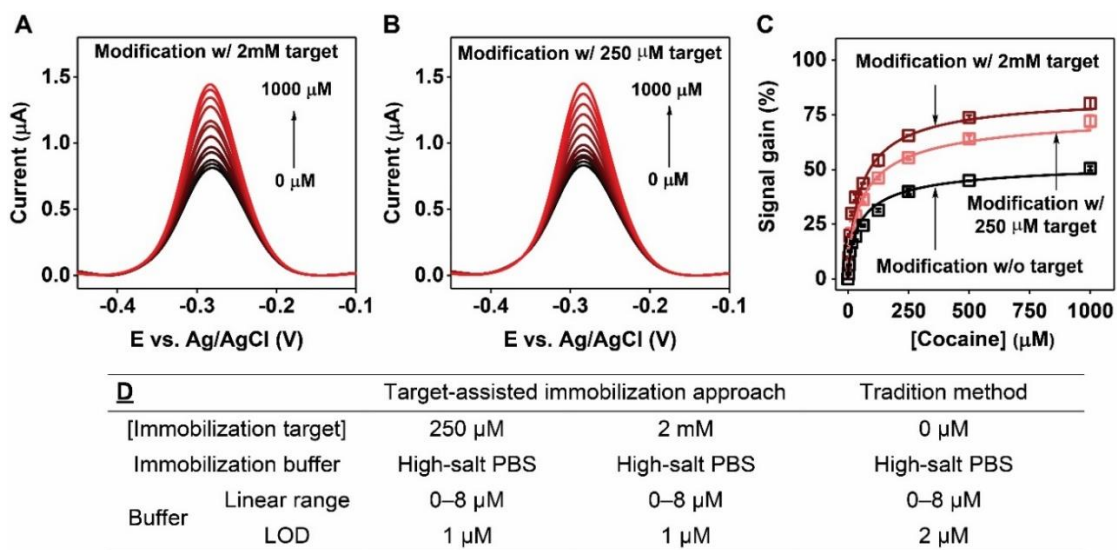


Figure 4-10. E-AB sensor performance using electrodes modified with COC-32-MB via target-assisted immobilization. SWV spectra collected at various concentrations of cocaine using electrodes modified in high-salt PBS with (A) 2 mM or (B) 250 μM cocaine. (C) Calibration curves derived from SWV spectra for electrodes modified with COC-32-MB plus 2 mM (brown) or 250 μM cocaine (pink) and electrodes modified with aptamer alone (black). (D) Linear ranges and LODs of electrodes fabricated via different methods. Error bars represent the standard deviation for three working electrodes from each measurement.

4.3.5. Dependency of E-AB sensor performance on the ionic strength of the immobilization buffer

Having determined that target-assisted aptamer immobilization improves E-AB sensor performance, we next tested our hypothesis on the relationship between the ionic strength of the electrode modification buffer and E-AB sensor performance. It has been reported that local inter-oligonucleotide distances can be increased and probe bundling can be mitigated by decreasing the ionic strength of the buffer used for probe immobilization.¹⁴⁸ To evaluate this, we modified electrodes with COC-32-MB alone in either high-salt PBS or low-salt PBS (10 mM PBS, 1.9 mM NaCl, 0.5 mM MgCl₂, pH 7.4). To ensure that the electrodes had similar surface densities, a greater concentration of aptamer was used for

immobilization in the low ionic strength buffer. Although both electrodes had similar surface densities (**Figure 4-11A**), electrodes prepared in low-salt PBS had improved signal gain in the range of 50–1,000 μM cocaine (**Figures 4-11B-D**). This indicates that the improvement in E-AB performance was most likely due to the mitigation of aptamer bundling and resulting increase in active probes on the electrode surface when lower ionic strength buffer was used.

We then determined whether the addition of target-assisted immobilization would further improve sensor performance. Electrodes were modified with COC-32-MB in low-salt PBS containing 250 μM cocaine as well as in high-salt PBS containing 2 mM cocaine as a control. In both cases, $\sim 96\%$ of the aptamer is bound to cocaine based on the target affinity of the aptamer (high-salt PBS $K_D = 70.4 \pm 0.8 \mu\text{M}$; low-salt PBS $K_D = 5.8 \pm 0.3$;) (**Figures 4-7A and B**) and the target concentration employed (**Figures 4-9 and 4-12**). Despite both sets of electrodes having similar surface coverages (**Figure 4-13**), we observed great improvements in SNR from electrodes immobilized with the aptamer in low ionic strength conditions, with approximately 10% improvement in signal gain in the concentration range of 50–1,000 μM cocaine (**Figures 4-14A-C**).

Given that both experiments demonstrated equivalent surface coverage and similar proportions of aptamer-target complexes for modification ($\sim 96\%$), the improvement in performance can be primarily attributed to the predominance of active aptamers on the electrode surface when the ionic strength of the immobilization buffer was reduced. These results confirm that buffer ionic strength has a significant effect on the performance of E-AB sensors.

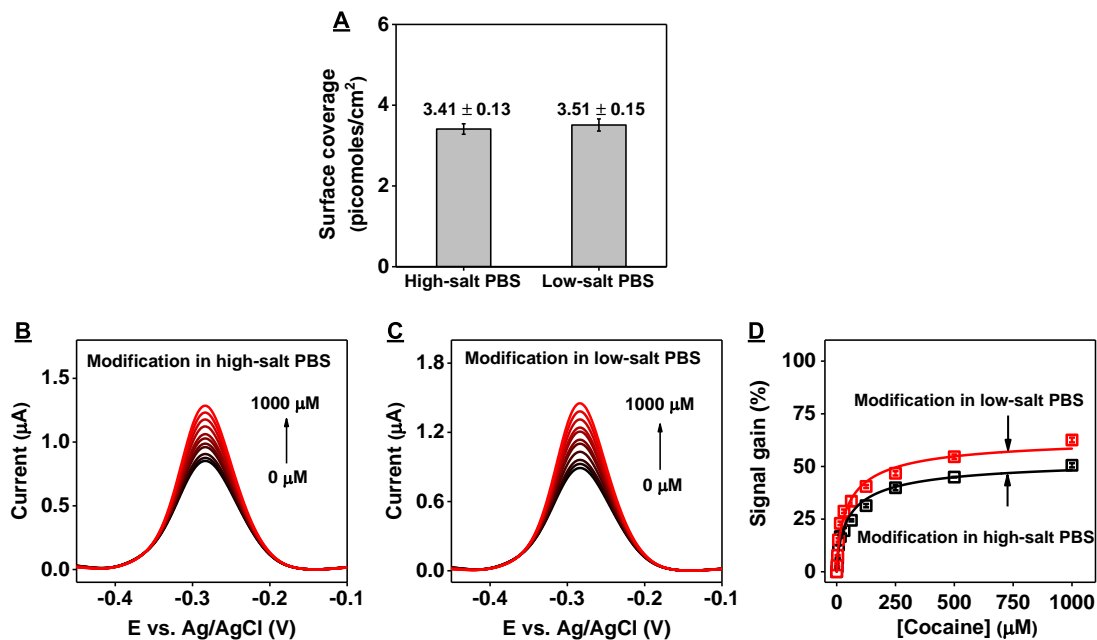


Figure 4-11. Performance of electrodes fabricated with COC-32-MB via conventional means in different buffers. (A) Surface coverage of electrodes fabricated by immobilizing the aptamer in high-salt or low-salt PBS. SWV produced by challenging electrodes fabricated in (B) high-salt or (C) low-salt PBS with 0–1,000 μM cocaine. (D) Calibration curves for detection of cocaine derived from the spectra shown in B (black) and C (red). Error bars represent the standard deviation of measurements from three independently fabricated electrodes.

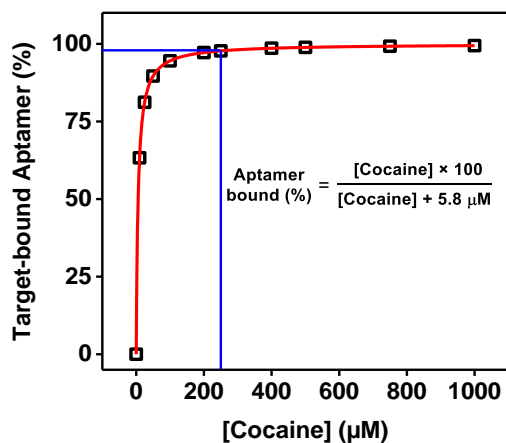


Figure 4-12. Simulated binding curve for COC-32 based on the affinity for cocaine in low-salt PBS ($K_D = 5.8 \mu\text{M}$). The blue lines indicate that 96% of the aptamer is bound in the presence of 250 μM cocaine.

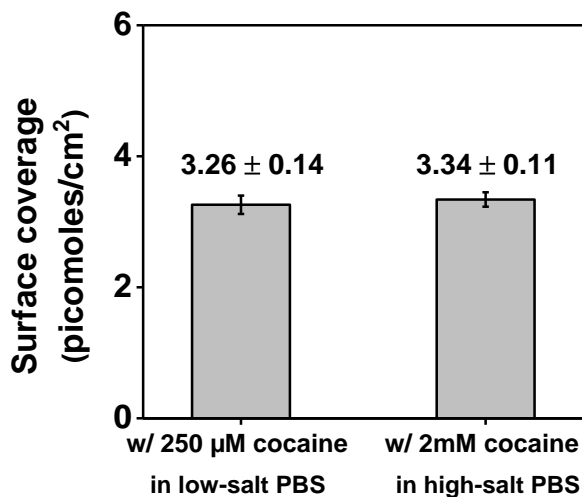


Figure 4-13. Surface coverage of electrodes modified with COC-32-MB with different methods. Surface coverage of electrodes modified with COC-32-MB via target-assisted immobilization in low-salt PBS with 250 µM or in high-salt PBS with 2 mM cocaine. Error bars represent the standard deviation of measurements from three different electrodes.

4.3.6. Effect of the type of buffering system used for aptamer immobilization on E-AB sensor performance

Changing the buffering system used for aptamer immobilization should not affect the performance of the resultant E-AB sensors if the ionic strength and pH remains the same. To confirm this, we modified electrodes with COC-32-MB in the presence of 250 µM cocaine in either low-salt Tris buffer or low-salt PBS with the same ionic strength and pH. As expected, at the same aptamer surface coverage (**Figure 4-15A**), both sensors exhibited similar performance (**Figures 4-15B, C** and **Figure 4-14C**) due to the equivalent binding affinity of COC-32-MB for cocaine in both buffers (**Figures 4-7B** and **C**). Finally, we compared the performance of sensors prepared via target-assisted aptamer immobilization in low-salt Tris buffer versus conventionally prepared electrodes for the detection of cocaine in complex biosamples. We found that electrodes modified using our method

demonstrated higher SNRs and greater sensitivity in 50% saliva relative to conventionally modified electrodes (LOD = 2 μ M vs. 4 μ M) (**Figures 4-14D-G**, and **Figure 4-16**).

4.3.7. Target-assisted immobilization is effective independent of aptamer sequence, structure, and affinity

As a final demonstration of the generalizability of our method, we prepared electrodes using SC-34, a G-rich, high-affinity structure-switching DNA aptamer that binds the synthetic cathinone methylenedioxypropylvalerone (MDPV) with a K_D of 300 nM in low-salt Tris buffer.^{26,123} We modified gold electrodes with the thiolated, methylene blue-modified version of SC-34 (SC-34-MB) in low-salt Tris buffer in the absence or presence of 5, 10 or 50 μ M MDPV, respectively corresponding to 94%, 97%, 99% aptamer-target complex in solution (**Figure 4-17**). Increases in the concentration of MDPV during electrode modification resulted in slightly decreased aptamer surface coverage (**Figure 4-20A**). This is probably because the rigid aptamer-target complex occupies more space than the unbound aptamer, and thus slightly increasing the quantity of the complex results in lower surface coverage. Nevertheless, electrodes modified with aptamer-MDPV complexes consistently yielded higher signal gains at all tested target concentrations compared to electrodes modified with the aptamer alone (**Figure 4-20B** and **Figure 4-18**). However, increasing the MDPV concentration beyond 5 μ M during the modification step yielded no more than a 5% improvement in signal gain (at 100 μ M MDPV), most likely because most aptamers (~94%) are already bound to target at 5 μ M MDPV. Using 50 μ M MDPV for target-assisted aptamer immobilization, we also observed similar improvements in sensitivity for MDPV detection in 50% urine (LOD = 0.5 μ M vs 1 μ M) (**Figure 4-20C** and **Figure 4-19**).

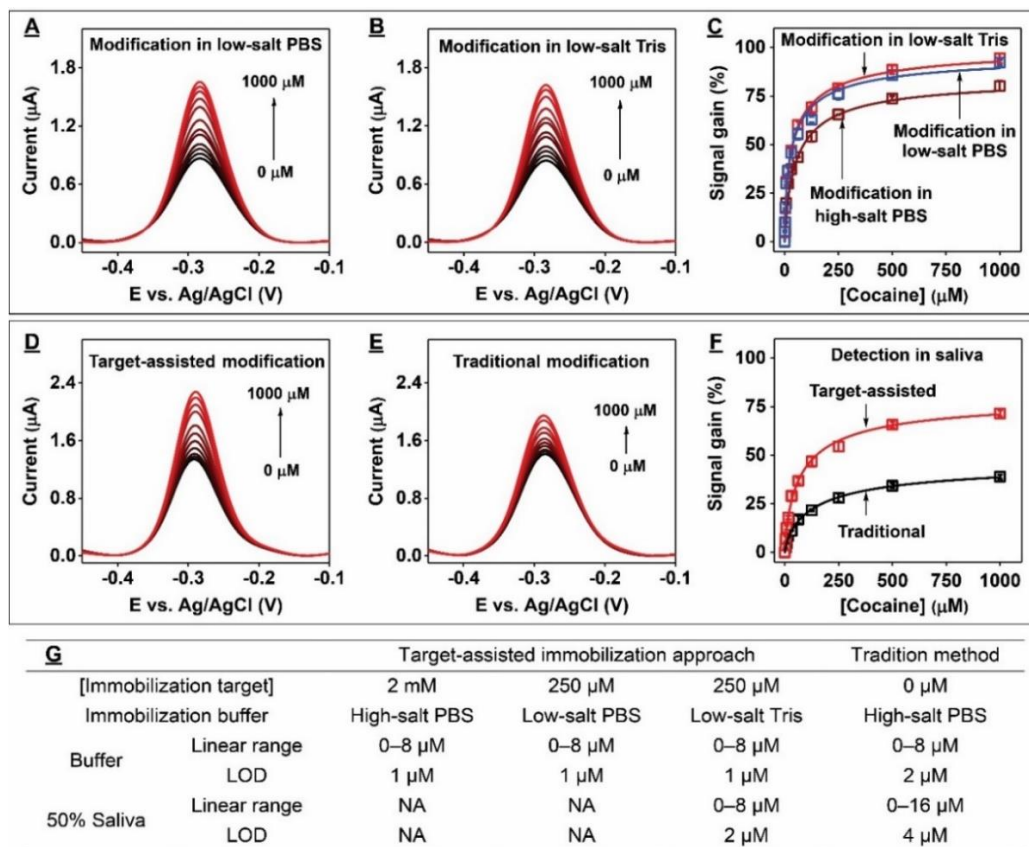


Figure 4-14. E-AB sensor performance using electrodes modified with target-bound COC-32-MB. SWV spectra at various concentrations of cocaine from electrodes modified with COC-32-MB plus cocaine in low-salt (A) PBS or (B) Tris. (C) Calibration curves derived from the SWV spectra shown in A (blue), B (red), or from electrodes modified in cocaine-containing high-salt PBS (brown). Detection of cocaine in 50% saliva using electrodes modified with (D) aptamer-target complexes in low-salt Tris or (E) aptamer alone in high-salt PBS. (F) Calibration curves derived from the SWV spectra shown in D (red) and E (black). (G) Linear ranges and LODs of electrodes fabricated via different methods in buffer or 50% saliva. Error bars represent the standard deviation for three working electrodes from each measurement.

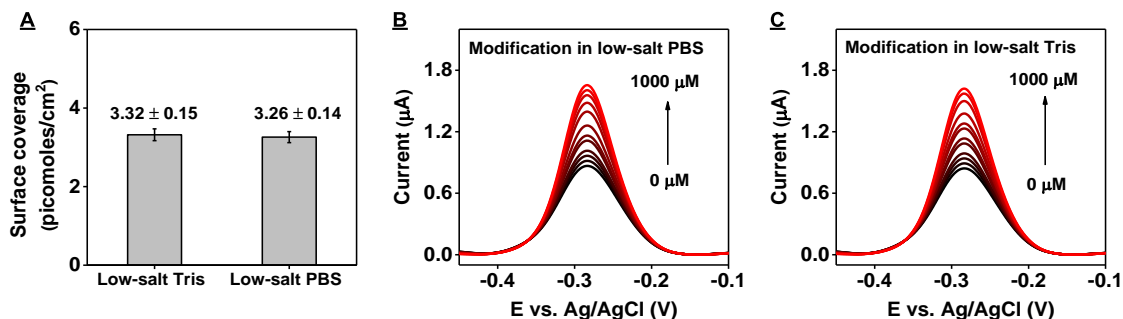


Figure 4-15. Performance of electrodes fabricated with COC-32-MB via target-assisted immobilization in different buffers. (A) Aptamer surface coverages of electrodes fabricated

by immobilizing the aptamer in low-salt Tris buffer or low-salt PBS with 250 μM cocaine. SWV produced by challenging the electrodes fabricated in low-salt (B) PBS or (C) Tris buffer with 0–1,000 μM cocaine. Error bars represent the standard deviation of measurements from three independently fabricated electrodes.

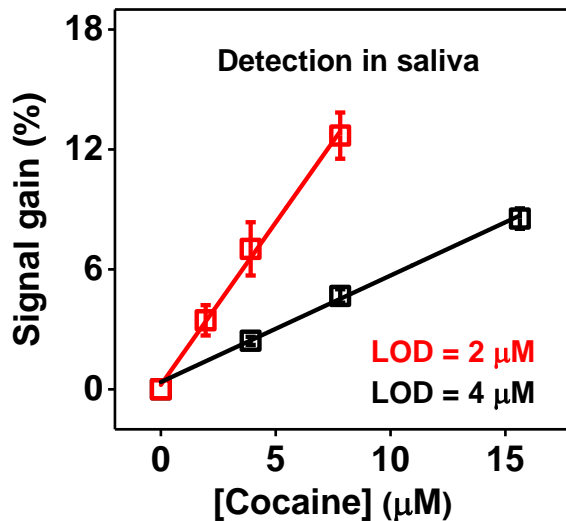


Figure 4-16. Sensitivity and LOD for cocaine detection in 50% saliva with different electrodes. Sensitivity and LOD for cocaine detection in 50% saliva with electrodes fabricated using COC-32-MB via target-assisted immobilization in low-salt Tris buffer with 250 μM cocaine (red) or conventional means in high-salt PBS (black). Error bars represent the standard deviation of measurements from three independently fabricated electrodes.

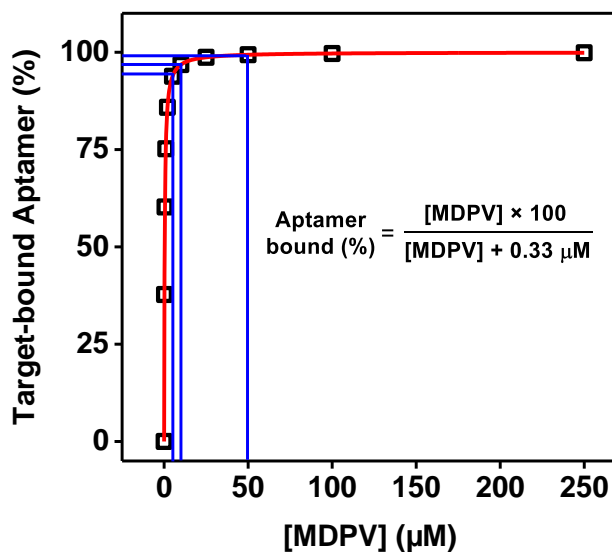


Figure 4-17. Simulated binding curve for SC-34 based on affinity for MDPV in low-salt Tris buffer ($K_D = 0.33 \mu\text{M}$). The blue lines indicate that 94%, 97%, and 99% of the aptamer is bound in the presence of 5, 10, and 50 μM MDPV, respectively.

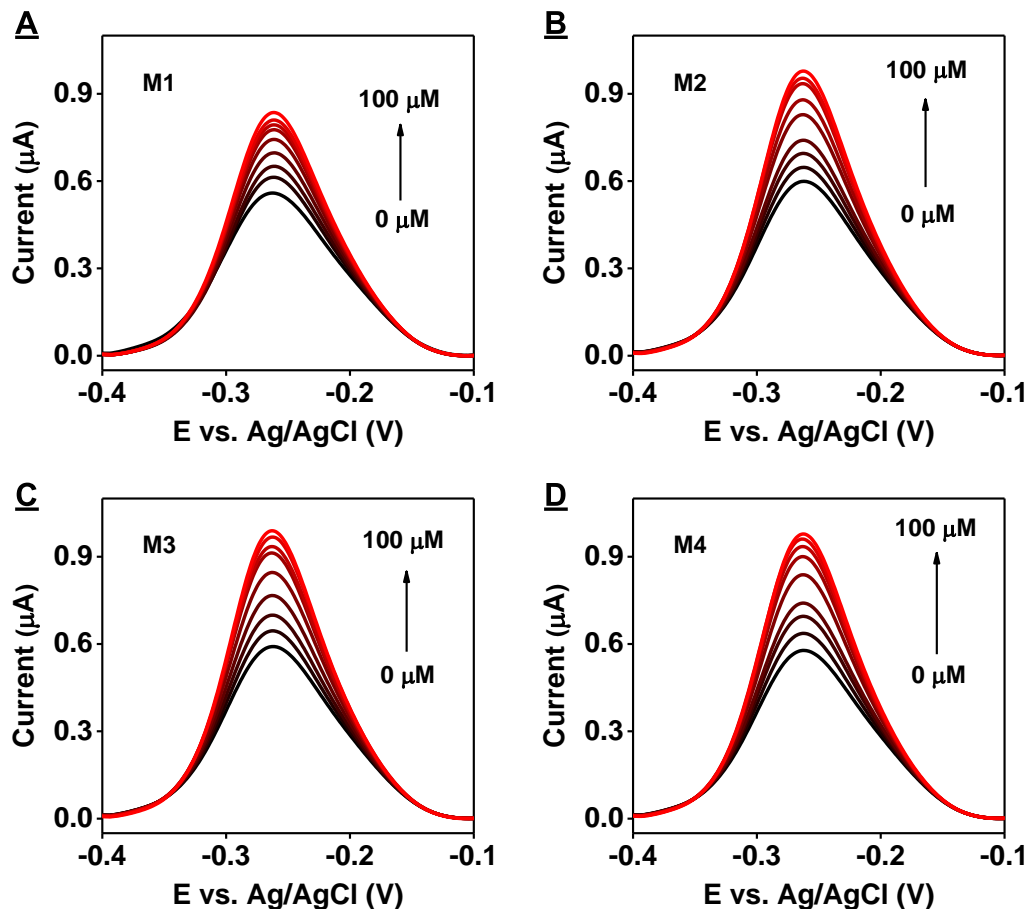


Figure 4-18. Electrodes fabricated using SC-34-MB via target-assisted aptamer immobilization with various concentrations of MDPV. SWV for electrodes modified with SC-34-MB in the presence of (A) 0 μM , (B) 5 μM , (C) 10 μM , and (D) 50 μM MDPV after challenging with 0–100 μM MDPV.

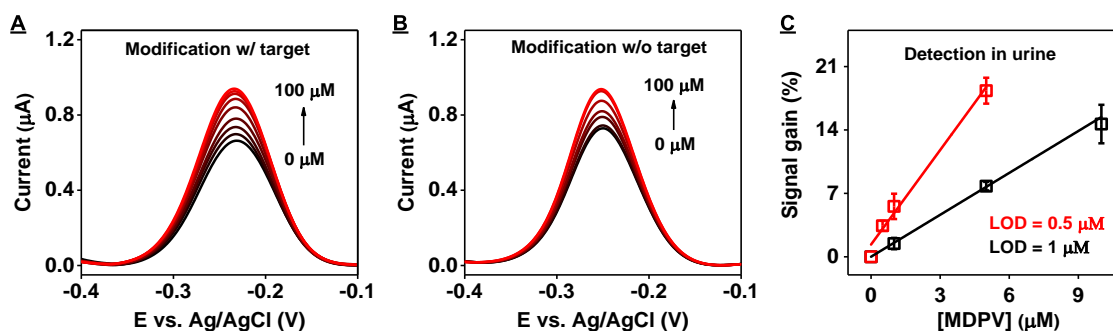


Figure 4-19. Detection of MDPV in 50% urine using electrodes fabricated via different methods. Detection of MDPV in 50% urine using electrodes modified with SC-34-MB via (A) target-assisted immobilization in low-salt Tris buffer with 50 μM MDPV or (B) conventional means in high-salt PBS. (C) Calibration curves derived from spectra shown

in **A** (red) and **B** (black). Error bars represent the standard deviation of measurements from three independently fabricated electrodes.

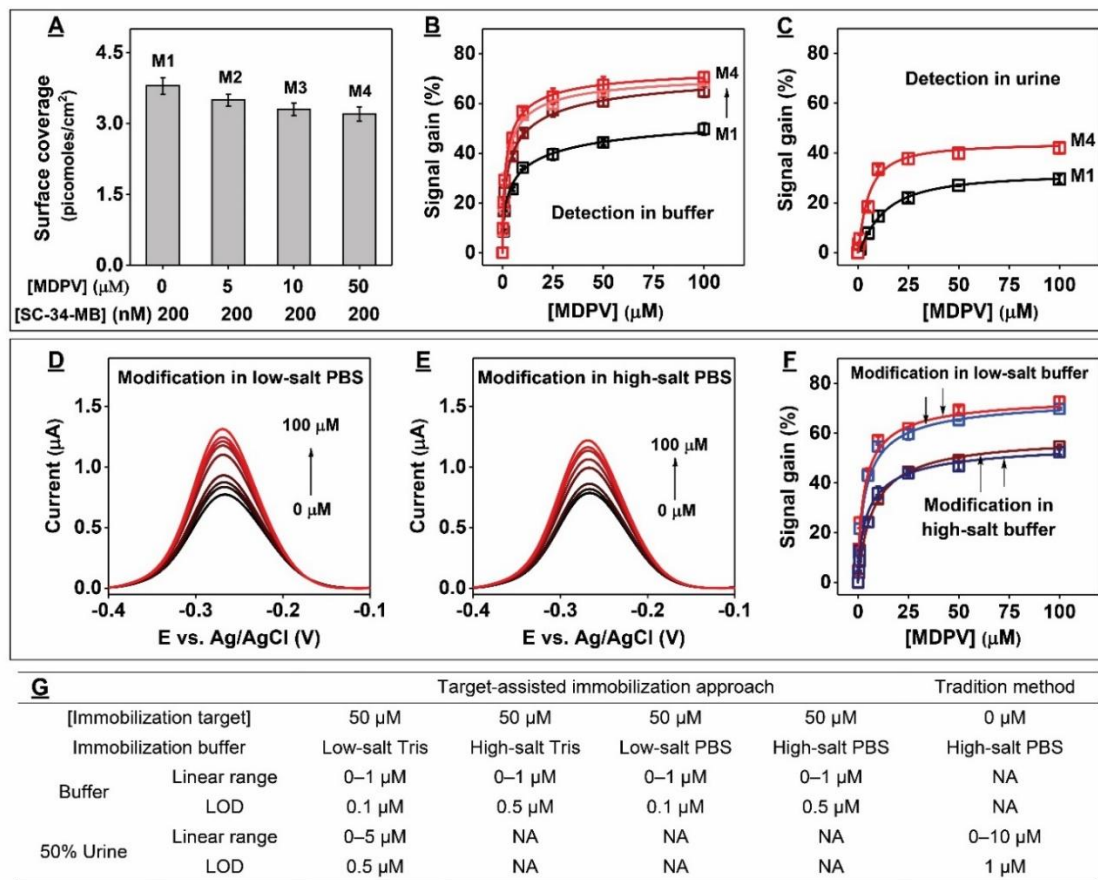


Figure 4-20. E-AB sensor performance using electrodes fabricated with SC-34-MB. **(A)** Effect of MDPV concentration on surface coverage during electrode modification. **(B)** Signal gain for the various electrodes prepared in **A** from various concentrations of MDPV in buffer. **(C)** Detection of MDPV in 50% urine using modified electrodes prepared in low-salt Tris with SC-34-MB alone (M1) or in the presence of 50 μM MDPV (M4). SWV spectra from various concentrations of MDPV using electrodes modified via target-assisted immobilization in either **(D)** low-salt or **(E)** high-salt PBS. **(F)** Calibration curves derived from the SWV spectra shown in **D** (red) and **E** (brown) or from electrodes prepared in low-salt (blue) or high-salt (navy) Tris buffer. **(G)** Linear ranges and LODs of electrodes fabricated via different methods in buffer or 50% urine. Error bars represent the standard deviation for three working electrodes from each measurement.

We then confirmed that the buffer system employed for aptamer immobilization has no effect on sensor performance in low-salt buffer; electrodes modified in either low-salt Tris buffer or PBS had nearly the same response at all tested target concentrations (**Figures**

4-20D and F). This is probably because the aptamer has the same K_D (~ 300 nM) in both buffers, as we confirmed by ITC (Figures 4-21A and B).

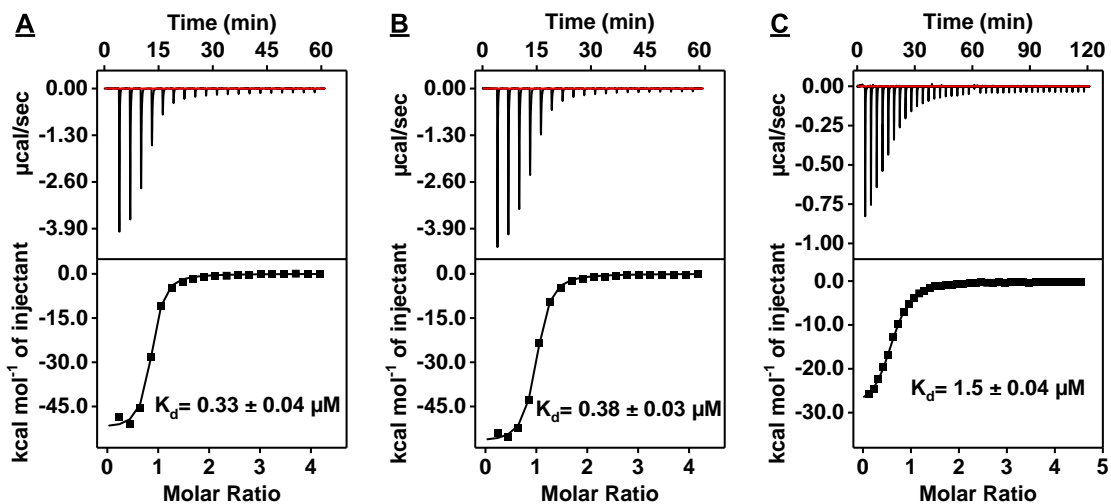


Figure 4-21. Characterization of the affinity of SC-34 for MDPV using ITC. Top panels present raw data showing the heat generated from each titration of MDPV to SC-34 in (A) low-salt Tris buffer, (B) low-salt PBS, or (C) high-salt PBS, while bottom panels show the integrated heat of each titration after correcting for dilution heat of the titrant. ITC data were fitted with a single-site binding model.

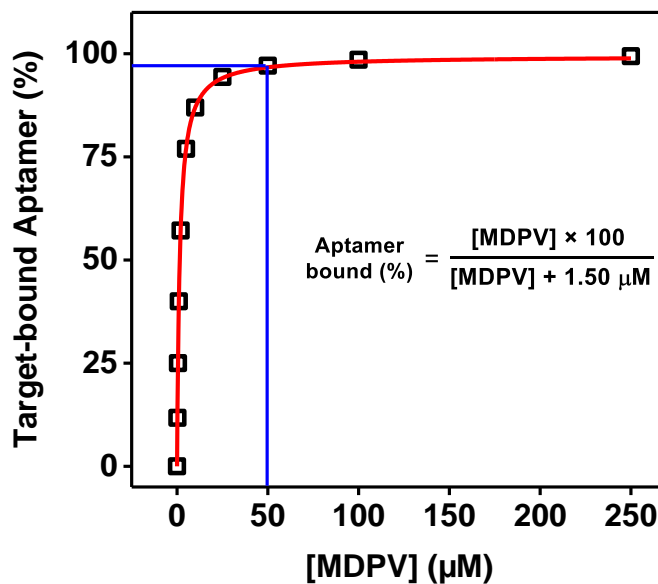


Figure 4-22. Simulated binding curve for SC-34 based on affinity for MDPV in high-salt PBS ($K_D = 1.50$ μM). The blue lines indicate that 97% of the aptamer is bound in the presence of 50 μM MDPV.

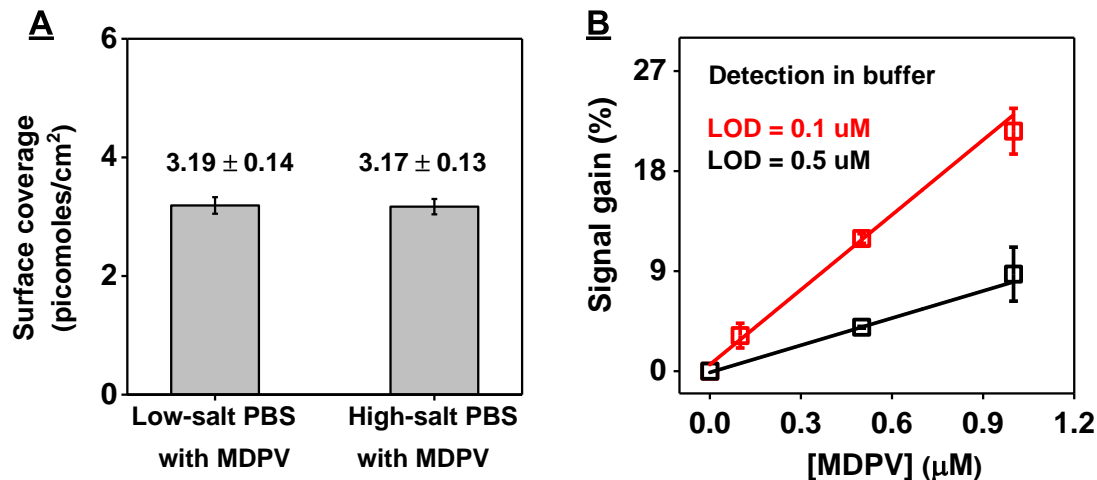


Figure 4-23. Performance of electrodes fabricated with SC-34-MB via target-assisted immobilization in different buffers. (A) Surface coverage of electrodes fabricated by immobilizing the aptamer in low-salt or high-salt PBS with 50 μM MDPV. (B) Calibration curve and LOD for MDPV detection using electrodes modified with SC-34-MB via target-assisted immobilization in low-salt (red) or high-salt PBS (black). Error bars represent the standard deviation of measurements from three independently fabricated electrodes.

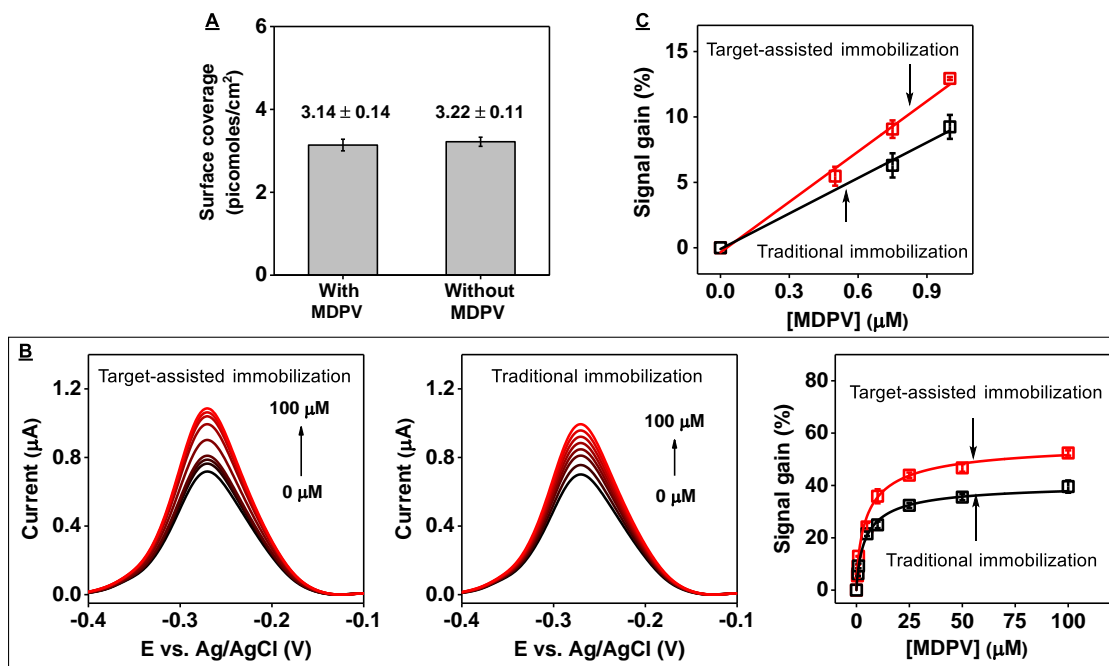


Figure 4-24. Performance of electrodes fabricated with SC-34-MB via different methods. Performance of electrodes fabricated with SC-34-MB in the presence or absence of 50 μM MDPV in high-salt Tris buffer. (A) Aptamer surface coverage of fabricated electrodes. (B) SWV measurements from electrodes fabricated via target-assisted aptamer immobilization approach (left) or traditional aptamer immobilization (middle) in the presence of 0–1,000 μM MDPV. The derived calibration curve is shown at right. (C) Linear ranges from the

curves shown in B. Error bars represent the standard deviation of measurements from three independently fabricated electrodes.

In addition, to confirm that the ionic strength used during target-assisted aptamer immobilization affects E-AB sensing performance, we fabricated electrodes modified with SC-34-MB in either low-salt or high-salt PBS in the presence of 50 μM MDPV. In both buffers, $\geq 97\%$ of the aptamer was bound to MDPV (**Figures 4-17 and 4-22**); based on ITC, the aptamer's K_D in high-salt PBS is $1.50 \pm 0.04 \mu\text{M}$ (**Figure 4-21C**). Although both sets of electrodes had similar surface coverage (**Figure 4-23A**), electrodes modified in low-salt PBS were more sensitive than those modified in high-salt PBS (LOD = 0.1 μM vs. 0.5 μM) (**Figures 4-20E-G, and Figure 4-23B**).

Finally, we confirmed that immobilization buffer type also had no effect on E-AB sensor performance with high-salt condition. Specifically, we modified electrodes with SC-34-MB in high-salt Tris buffer in the absence and presence of 50 μM MDPV and challenged the resulting sensors with 0 – 100 μM MDPV. Although both sets of electrodes had similar surface coverages (**Figure 4-24A**), electrodes modified via target-assisted immobilization yielded higher signal gains (**Figure 4-24B**) and demonstrated lower limits of detection than traditionally-modified electrodes (**Figure 4-24C**). These results further support the conclusion that target-assisted aptamer immobilization results in E-AB sensors with improved sensing performance. Notably, electrodes modified via target-assisted aptamer immobilization in high-salt Tris buffer or PBS exhibited similar performance (**Figure 4-20F**). ITC confirmed that the binding affinity of SC-34 was similar in high-salt PBS (**Figure 4-21C**, $K_D = 1.50 \pm 0.05 \mu\text{M}$) and high-salt Tris buffer (**Figure 4-25**, $K_D = 1.80 \pm 0.04 \mu\text{M}$), demonstrating that the use of different immobilization buffer systems

does not affect sensor performance. These results further support the conclusion that sensor performance was primarily improved due to increased inter-oligonucleotide spacing and minimization of strand ‘bundling’ in the low ionic strength buffer during modification.

4.3.8. Effect of buffer pH used for aptamer immobilization on E-AB sensor performance

We finally tested the effect of altering the immobilization buffer pH on the performance of the resulting E-AB sensors. As a demonstration, we prepared gold electrodes with SC-34-MB in the absence or presence of 50 μM MDPV in low-salt PBS formulations with the same ionic strengths but different pH values (pH = 6.0, 7.0, 7.4, or 8.0). Buffer pH did not significantly affect aptamer surface coverage, although electrodes fabricated via target-assisted immobilization consistently had slightly lower surface coverage (3.28 ± 0.07 pmol/cm²) than those modified via the traditional aptamer immobilization method (3.55 ± 0.06 pmol/cm²) (**Figure 4-27**). We first tested the performance of traditionally-modified electrodes by challenging them with 0–100 μM MDPV. E-AB sensors fabricated at pH 8.0 (**Figure 4-26A** and **Figure 4-28A**) or 7.4 (**Figure 4-26B** and **Figure 4-28B**) produced nearly identical signal gains, while aptamer immobilization at pH 7.0 yielded sensors with only slightly inferior performance (**Figure 4-26C** and **Figure 4-28C**). In contrast, sensors fabricated at pH 6.0 yielded noticeably lower signal gains at all target concentrations (**Figure 4-26D** and **Figure 4-28D**). This may be because the phosphate groups of the aptamers are predominantly singly protonated at this pH, rather than being doubly- protonated as occurs at pH ≥ 7.0 . This would result in less electrostatic repulsion between aptamers, thus increasing the likelihood of bundling during immobilization.

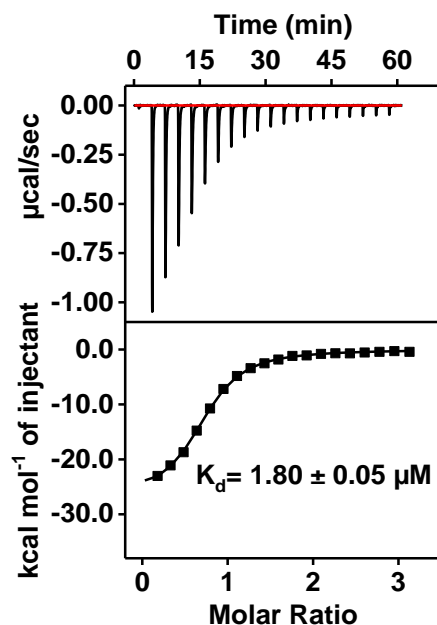


Figure 4-25. ITC characterization of SC-34 affinity for MDPV in high-salt Tris buffer. Top panels present raw data, showing the heat generated from each titration of MDPV to SC-34, while bottom panels show the integrated heat of each titration after correcting for dilution heat of the titrant. ITC data were fitted with a single-site binding model.

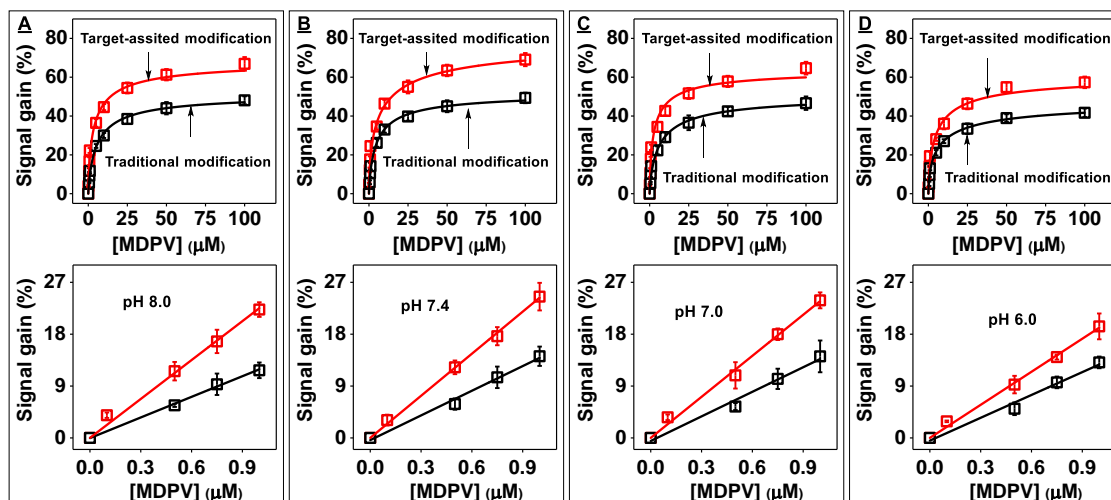


Figure 4-26. E-AB sensor performance in various pH buffers. E-AB sensor performance using electrodes modified with SC-34-MB in the presence (target-assisted immobilization) or absence (traditional immobilization) of 50 μM MDPV in low-salt PBS at pH (A) 8.0, (B) 7.4, (C) 7.0 and (D) 6.0. The top panels show calibration curves for electrodes fabricated via target-assisted aptamer immobilization (red) or traditional modification method (black) produced by challenging with 0–100 μM MDPV, and bottom panels show their respective linear ranges. Error bars represent the standard deviation of measurements from three independently fabricated electrodes.

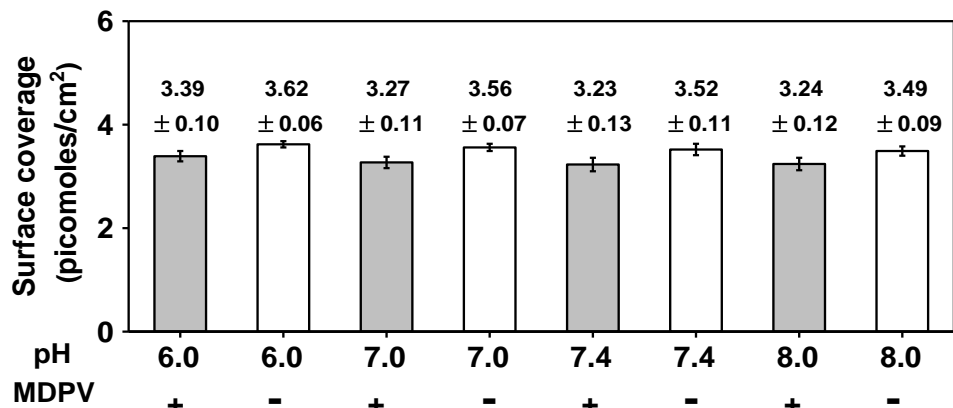


Figure 4-27. Surface coverage of electrodes fabricated with SC-34-MB in various pH buffers. Aptamer surface coverages of electrodes fabricated with SC-34-MB in the absence (white bars) or presence of 50 μM MDPV (gray bars) in low-salt PBS with a pH of 6.0, 7.0, 7.4 or 8.0. Error bars represent the standard deviation of measurements from three independently fabricated electrodes.

We then tested the performance of electrodes modified via target-assisted immobilization. As expected, regardless of immobilization buffer pH, these electrodes consistently yielded higher signal gains and had lower limits of detection compared to traditionally modified electrodes (**Figure 4-26**). Although we observed a similar pattern of pH effects on electrode performance, the magnitude of signal gain was consistently greater after target-assisted immobilization at every pH tested (**Figures 4-26A-D**).

We next used ITC to determine if buffer pH affected sensor performance by affecting the formation and stability of aptamer-target complexes during aptamer immobilization. Specifically, we measured the binding affinity of SC-34 to MDPV in low-salt PBS at pH 6.0, 7.0, 7.4, or 8.0. In all pH conditions, the binding affinity values did not greatly differ (**Figure 4-29**). This meant that in all buffers containing 50 μM MDPV, $\geq 97\%$ of the aptamer was bound to the target, indicating that pH did not affect the extent of aptamer-target complexation. Our results therefore suggest that the use of relatively low-pH buffers

for aptamer immobilization promotes aptamer bundling due to reduced electrostatic repulsion, which in turn negatively impacts sensor performance.

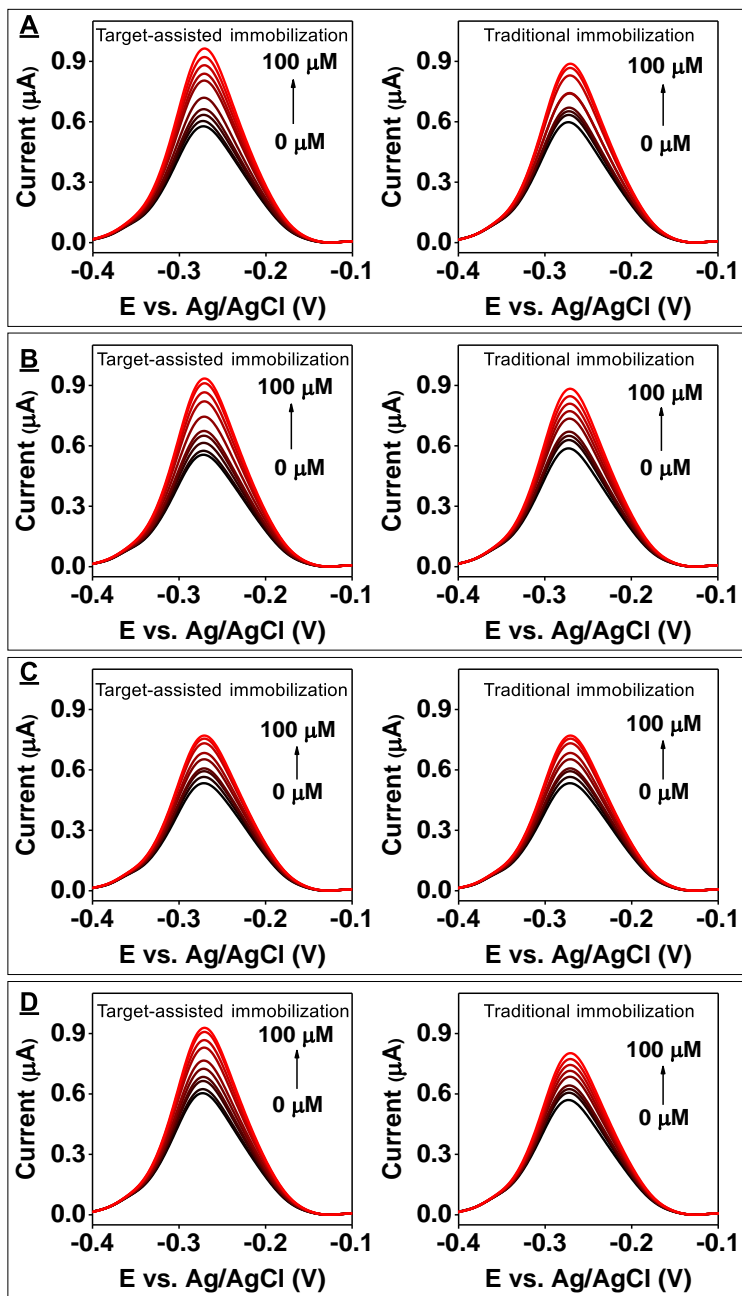


Figure 4-28. Performance of electrodes fabricated with SC-34-MB via different methods. SWV spectra of E-AB sensors modified with SC-34-MB in the presence (target-assisted immobilization) or absence (traditional immobilization) of $50 \mu\text{M}$ MDPV in low-salt PBS at pH (A) 8.0, (B) 7.4, (C) 7.0 and (D) 6.0. SWV spectra for electrodes prepared under these two immobilization conditions and then exposed to 0–100 μM MDPV. Error bars

represent the standard deviation of measurements from three independently fabricated electrodes.

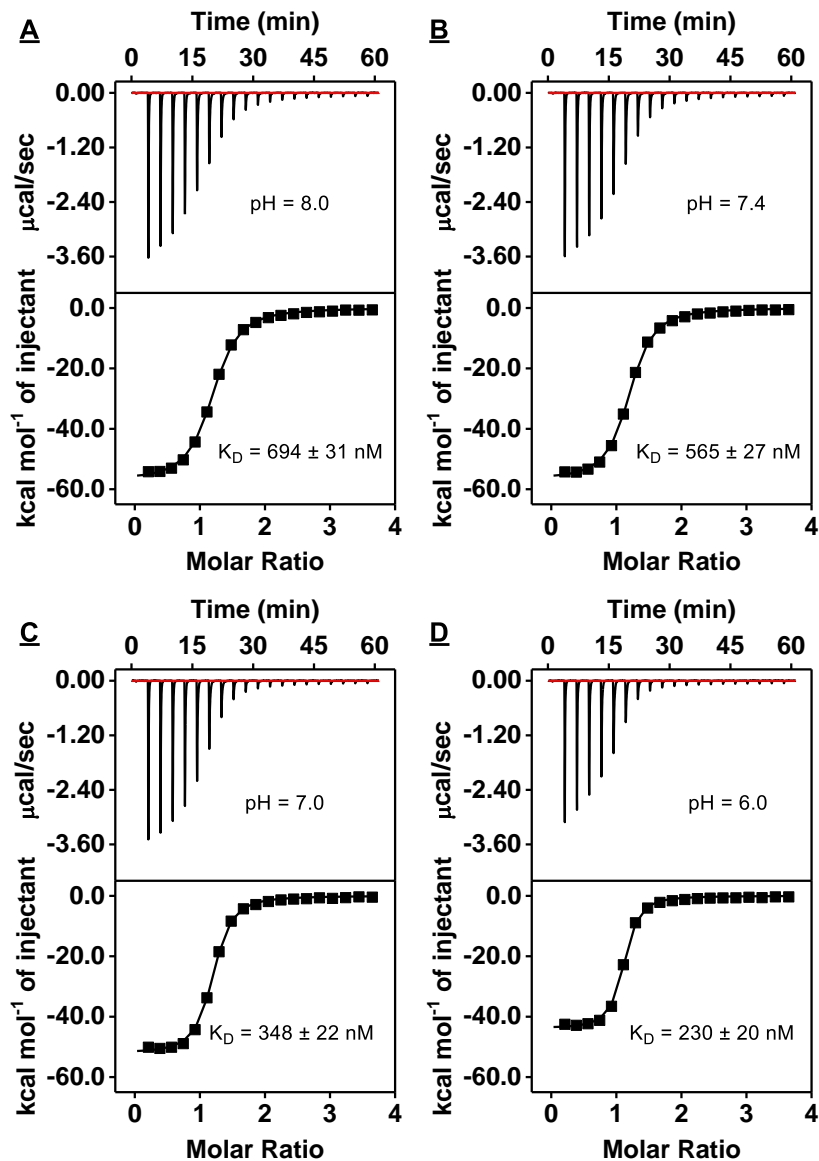


Figure 4-29. Characterization of the pH-dependence of SC-34 affinity for MDPV using ITC. Top panels present raw data showing the heat generated from each titration of MDPV to SC-34 in low-salt PBS at pH (A) 8.0, (B) 7.4, (C) 7.0, or (D) 6.0, while bottom panels show the integrated heat of each titration after correcting for dilution heat of the titrant. ITC data were fitted with a single-site binding model.

4.4. Conclusion

E-AB sensors are a promising class of analytical devices that have the potential for broad adoption in commercial applications due to their high selectivity, robustness, and

ease of use. However, such devices are often hobbled by insufficient sensitivity and low SNRs, primarily due to the low target affinity of structure-switching aptamers and matrix effects. Several strategies have been devised to address these factors, but we have also determined here that an underappreciated factor—the conditions employed in the aptamer immobilization step of the electrode fabrication process—can also profoundly affect sensor performance. We have analyzed the impact of two modifications to this process: immobilizing aptamers in a folded, target-bound state on the electrode rather than an unbound single-stranded state, and lowering buffer ionic strength to reduce aptamer bundling on the surface. Our results confirm that both target-assisted aptamer immobilization and the use of low ionic strength buffers generally improves the SNR and LOD of E-AB sensors relative to those fabricated using conventional immobilization methods. We also determined that the pH of the immobilization buffer can have negatively affect the performance of the resulting E-AB sensors if the pH is below 7. We attribute this to the protonation of the phosphate group of DNA, which reduces electrostatic repulsion and promotes aptamer bundling. Based on our findings, we believe the ideal buffer for aptamer immobilization should have relatively low ionic strength while also supporting aptamer-target binding. We suggest testing target-binding affinity at various ionic strengths, and then using the lowest ionic strength conditions at which >90% of aptamer bound to target can readily be achieved during the immobilization process. Although we do not currently have direct evidence for our proposed mechanisms by which E-AB sensing is altered, the use of surface analysis techniques such as high-resolution atomic force microscopy should allow for a more definitive understanding of these phenomenon.

CHAPTER 5: Aptamer-Integrated Multi-Analyte Detecting Paper Electrochemical Device

5.1. Introduction

The on-site detection of small molecules is important for applications such as environmental monitoring and medical diagnostics.^{153,154} Simultaneous detection of multiple small-molecule analytes can provide detailed information on the chemical composition of samples, which gives end-users a wider range of decision-making options compared to having information on only a single analyte. Multi-analyte detection also makes more efficient use of precious samples that are difficult to procure in large quantities, such as human biofluids. Currently, on-site multi-analyte detection is typically achieved with lateral-flow immunoassays that use a set of antibodies in multiple separate channels¹⁵⁵ as recognition elements for analytes such as illicit drugs¹⁵⁶ and food-borne contaminants¹⁵⁷. However, lateral-flow immunoassays have two shortcomings that generally limit their utility. First, they make use of antibodies, which suffer from high cost and short shelf-life.⁸ Second, these assays generally rely on colorimetric readouts, which are qualitative in nature and therefore subject to interpretation bias. Paper electrochemical devices (PEDs) have recently emerged as an excellent sensing platform for on-site detection applications due to their low cost, portability, ease of use, and capability to provide quantitative digital readouts.¹⁵⁸ Perhaps the most successful example of a PED is the personal glucose meter, which enables the rapid (within seconds) quantification of glucose directly in microliter volumes of unprocessed blood with a digital readout. Unfortunately, the development and broad commercial adoption of PEDs has been stymied by the limited availability of suitable

recognition elements (*e.g.*, enzymes and antibodies) that can be incorporated into such sensors for the detection of specific targets.

Aptamers are oligonucleotide-based receptors^{3,4} that have gained widespread interest as excellent biorecognition elements for molecular sensing due to advantageous properties that include low cost of production, high stability, and long shelf-life.⁶ Through *in vitro* selection protocols, aptamers can be generated for essentially any molecular target with high affinity and specificity.¹⁵⁹ In addition, they can be readily incorporated into electrochemical aptamer-based (E-AB) sensors¹⁹ for the sensitive, rapid, and reproducible detection of various small molecules like antibiotics, illicit drugs, pharmaceuticals, and medical biomarkers directly in complex samples.^{20,36,83,160} However, all E-AB sensors developed to date can only detect one target and there is no architecture or design that can facilitate multi-target detection based on this sensor platform. Although a paper E-AB device was fabricated for detection of a single target,¹⁶¹ there are currently no facile and cost-effective methods that can be employed to fabricate multiple electrodes of different material, size, and shape on the same paper substrate.

In this work, we describe a new method to fabricate aptamer-modified multiplex PEDs (mPEDs) that can robustly detect multiple small molecules in complex samples within seconds. As a demonstration, we fabricated mPEDs featuring a silver reference electrode, a gold counter electrode, and three gold working electrodes. We first determined the reproducibility of the fabrication method by assessing the variability of the electrochemical properties of the three bare gold working electrodes both on individual mPEDs (intra-device precision) and across different mPEDs (inter-device precision). In both comparisons, the working electrodes exhibited < 3% variation in terms of their surface area, roughness,

and electron transfer rate. We then modified four different mPEDs with distinct small-molecule-binding aptamers, and determined that all devices were sensitive and specific to their target and produced highly precise measurements with similar performances to conventional gold disk electrodes. Finally, we demonstrated simultaneous detection of three small molecules – acetyl fentanyl, 3,4-methylenedioxypyrovalerone (MDPV), and adenosine – in saliva and urine with a single mPED modified with three different aptamers. Our results demonstrate that aptamer-modified mPEDs can achieve accurate, rapid, and sensitive detection of small-molecule targets in complex samples without any cross-talk between the working electrodes. With the incorporation of a polydimethylsiloxane (PDMS) chamber, our mPED could detect these analytes in microliter volumes of biological samples. In the future, we believe it will be feasible to create mPEDs with tens of working electrodes for the simultaneous detection of numerous small-molecule analytes in minute volumes of unprocessed sample. This could be an enabling technology for applications such as point-of-care metabolomics in the context of personalized medicine.

5.2. Experimental section

5.2.1. Materials

Potassium chloride, magnesium chloride, sodium chloride, monosodium hydrogen phosphate, sodium dihydrogen phosphate, trisodium citrate dihydrate, L-ascorbic acid, Trizma pre-set crystals (pH 7.4), tris(2-carboxyethyl) phosphine hydrochloride, 6-mercapto-1-hexanol, hexaammineruthenium(III) chloride, potassium hexacyanoferrate (III), adenosine, sulfuric acid (95–98%), nitric acid (70%), hydrochloric acid (36.5–38%), gold (III) chloride trihydrate, silver nitrate, and Triton X-100 were purchased from Sigma-

Aldrich. Acetyl fentanyl hydrochloride, cocaine hydrochloride, and 3,4-methylenedioxypropylvalerone (MDPV) hydrochloride were purchased from Cayman Chemicals. Mixed cellulose ester filter papers (pore size: 100 nm, diameter: 47 mm, thickness: 100 μm) and 0.22- μm syringe filter were purchased from Millipore. Polyethylene terephthalate films (thickness = 76.2 μm) were purchased from AmazonBasics. Pure single-walled carbon nanotube (SWCNT) solutions (0.25 mg/mL) were purchased from NanoIntegris. SYLGARD 184 silicone elastomer curing agent and SYLGARD 184 silicone elastomer base were purchased from Dow Corning. Exonuclease I (*E. coli*) was purchased from New England Biolabs. Bemis parafilm, SYBR Gold, ethylenediaminetetraacetic acid (EDTA), and formamide were purchased from Thermo Fisher Scientific. All solutions were prepared using Milli-Q (Millipore) water with resistivity of 18.2 $\text{M}\Omega \times \text{cm}$ unless specified otherwise. Methylene blue-modified aptamers were synthesized by Biosearch Technologies and dissolved in TE buffer (10 mM Tris-HCl with 1 mM EDTA, pH 8.0). All other unmodified oligonucleotides were purchased from Integrated DNA Technologies and dissolved in PCR-grade water. Oligonucleotide concentrations were measured using a NanoDrop 2000 spectrophotometer (Thermo Fisher Scientific). DNA sequences used are as follows:

COC-32: 5'-SH-C6-AGACAAGGAAAATCCTTCAATGAAGTGGGTCT-MB-3'

AF-32: 5'-SH-C6-CCATGGGTGTTTGC ACTAAGTCCGGTTCTTGG-MB-3'

MDPV-34: 5'-SH-C6-ACCTTAAGTGGGGTTCGGGTGGAGTTTATGGGGT-MB-3'

ADE-25: 5'-SH-C6-CCTGGTGGAGTATTGCGGGGGAAGG-MB-3'

COC-apt: 5'-AGACAAGGAAAATCCTTCAATGAAGTGGGTCT-3'

AF-apt: 5'-CCATGGGTGTTTGC ACTAAGTCCGGTTCTTGG-3'

MDPV-apt: 5'-ACCTTAAGTGGGGTTCGGGTGGAGTTTATGGGGT-3'

ADE-apt: 5'-CCTGGTGGAGTATTGCGGGGAAGG-3'

(SH = thiol, MB = methylene blue)

5.2.2. Synthesis of metal nanoparticles

Gold nanoparticles (AuNPs) (15 nm) were synthesized using a modified version of the Turkevich method.¹⁶² Briefly, 500 μ L of 100 mM gold (III) chloride trihydrate was diluted to 50 mL in distilled water and boiled at 100 °C with a reflux setup. After 2 min, 5 mL of 1% trisodium citrate solution (w/v) was added quickly. The liquid was boiled and vigorously mixed for 30 min. After cooling down to room temperature, the prepared AuNPs were filtered through a 0.22- μ m syringe filter and stored in the dark at 4 °C.

Silver nanoparticles (AgNPs) (32 nm) were prepared according to a previously reported method.¹⁶³ Specifically, 50 μ L of 1.76% L-ascorbic acid (w/v) was added into 47.5 mL boiled distilled water with a reflux setup. Meanwhile, in a 15-mL Falcon tube, 500 μ L of 1% AgNO₃ (w/v) was first mixed with 2.5 mL distilled water. This solution was then slowly added into 2 mL of 1% trisodium citrate solution (w/v) and the mixture was incubated at room temperature for 4 min. Afterwards, the mixture was quickly added into the boiling L-ascorbic acid solution with vigorous stirring. The solution was continued to boil for 1 h and then slowly cooled down to room temperature. Finally, the synthesized AgNPs were filtered through a 0.22- μ m syringe filter and stored in the dark at room temperature.

5.2.3. Isothermal titration calorimetry (ITC)

All ITC experiments were performed with a MicroCal ITC200 instrument (Malvern) in 10 mM Tris buffer (20 mM NaCl, 0.5 mM MgCl₂, pH 7.4) at 23 °C. The sample cell was loaded with a solution containing the aptamer (20 μM for COC-apt and ADE-apt, 40 μM for AF-apt) and the syringe was loaded with the respective target of the aptamer (800 μM cocaine, 1200 μM adenosine, or 550 μM acetyl fentanyl). Each experiment consisted of an initial purge injection of 0.4 μL followed by 19 successive injections of 2 μL, with a spacing of 180 s between each injection. For ADE-apt, an additional 20 injections were performed afterward, consisting of an initial 0.4 μL purge injection followed by 19 successive 2 μL injections. The raw data were first corrected based on the dilution heat of each target and then analyzed with the MicroCal analysis kit integrated into Origin 7 software with a single-site binding model for the COC-apt and AF-apt titrations or a two-site sequential binding model for the ADE-apt titration.

5.2.4. Fabrication of multiplex paper electrochemical devices (mPEDs)

Our mPEDs were prepared using a vacuum filtration protocol developed in our laboratory.¹⁶⁴ Specifically, one layer of Bemis parafilm was thermally laminated (130 °C, ~2 cm/sec) on the rough side of the polyethylene terephthalate film using a thermal laminator machine (AmazonBasics). To prepare the top stencil and bottom mask, the laminated films were cut with pre-designed patterns using a Silhouette Portrait 2 Electronic Cutting Tool. The top stencil is circular, has the same diameter as the filter paper, and contains two mPED patterns. Each mPED consisted of three working electrodes, one counter electrode, and one reference electrode. The bottom mask is also circular and has

the same diameter as the filter paper, but has no engravings within. The top of a mixed cellulose ester filter paper was laminated with the parafilm-laminated side of the top stencil. The laminated paper was first rinsed with a few milliliters of water and then placed in a vacuum filtration system and moisturized with another 10 mL of water. Afterwards, 10 mL of 6 $\mu\text{g/mL}$ SWCNT suspended in 1% Triton X-100 was added to the paper with a flux of 0.29 $\text{mL/cm}^2\cdot\text{min}$, which led to the formation of a thin SWCNT basal layer. Immediately after, the paper was washed five times with 10 mL of distilled water to remove Triton X-100. Any air bubbles present on the top of the filter paper were carefully removed between each wash using a pipette. Subsequently, 10 mL of 0.13 nM 15-nm AuNPs was then added onto the SWCNT-patterned paper with a flux of 0.77 $\text{mL/cm}^2\cdot\text{min}$, which resulted in the formation of a shiny AuNP film that served as the working and counter electrodes as well as the connection circuit. Next, 50 μL of 6.9 nM 32-nm AgNPs was pipetted to the paper area designated for the reference electrode under vacuum. This step was repeated three times to form the AgNP pseudo-reference electrode. After the paper completely dried, the parafilm-laminated side of the bottom mask (a circular PET film with no engravings) was laminated with the bottom side of the paper by heating at 65 $^{\circ}\text{C}$ for 5 min. Two mPEDs were formed on a single piece of paper, and then separated for detection.

5.2.5. Fabrication of aptamer-modified mPEDs

Prior to aptamer modification, the three working electrodes of each mPED underwent electrochemical cleaning using a modified version of our previously published protocol.²¹ Ten cycles of cyclic voltammetry (scan range: 0.2 to 1.5 V, scan rate: 100 mV/s) were performed in 0.05 M sulfuric acid with a standard Ag/AgCl reference electrode. Afterwards,

these electrodes were rinsed with distilled water and dried using nitrogen gas. To reduce the disulfide bonds of the aptamers, the thiolated, methylene blue-modified aptamers (COC-32, AF-32, MDPV-34, and ADE-25) were each mixed with a 100-fold excess of Tris(2-carboxyethyl)phosphine (100 mM) and incubated for 2 h at room temperature. Then, the freshly-reduced aptamers were diluted (final concentration 100 nM for MDPV-34, 200 nM for all other aptamers) with modification buffer, which consisted of 10 mM Tris (pH 7.4), 20 mM NaCl, and 0.5 mM MgCl₂ for AF-32, or 10 mM PBS (pH 7.2), 1 M NaCl, and 1 mM MgCl₂ for all other aptamers. For modification of electrodes with ADE-25, 250 μM of adenosine was included in the modification buffer to facilitate the formation of a target-bound aptamer complex in solution and the immobilization of the folded aptamers on the electrode surface. This immobilization procedure was found to increase the target-induced signal change compared to immobilization in the absence of adenosine. To immobilize aptamers on the gold working electrodes, the clean mPED was placed in a petri dish, and 10 μL of diluted aptamer was immediately added onto the cleaned working electrode surface and incubated for 2 h in the dark at room temperature. To prevent evaporation of the aptamer solution, 10-20 water droplets were placed around the device, and the petri dish was sealed with parafilm. After aptamer modification, the electrodes were backfilled with 10 μL of 1 mM 6-mercapto-1-hexanol for 1 h. The modified mPEDs were washed with distilled water and dried using nitrogen gas before use.

5.2.6. Fabrication of polydimethylsiloxane (PDMS) chamber

PDMS was prepared by mixing curing agent and PDMS base in a 1:10 ratio (w/w). The mixture was stirred for 40 min until homogenous. The prepared mixture was poured into a clean petri dish to form a thin layer and allowed to settle at room temperature for 1

h to remove bubbles, and nitrogen gas was used to assist the degassing process. Afterwards, polymerization was achieved by heating in an oven for 4 h at 65 °C. The solidified PDMS was subsequently cut into 23 × 9 mm rectangles, after which the interior was cut out to produce the frame of a chamber with interior dimensions of 19 × 5 mm. The cut PDMS were cleaned by sonication in 100% ethanol for 2 min and then dried with nitrogen prior to use. Finally, the PDMS chamber was formed by tightly pressing the fabricated PDMS onto the surface of mPED such that all electrodes were confined by the chamber.

5.2.7. Electrochemical measurements

All electrochemical measurements were carried out in a 2 mL electrochemical cell or a 200 µl PDMS chamber using a CHI760D electrochemical workstation (CH Instruments). Electron transfer rates were measured from the mPEDs by performing cyclic voltammetry at various scan-rates in 1 mM $K_3[Fe(CN)_6]$ containing 0.1 M KCl.⁴⁸ Working electrode surface coverage was measured using the method developed by Tarlov *et al.*¹²⁷ Square-wave voltammetry (SWV) was used for the detection of targets spiked into 10 mM Tris buffer (20 mM NaCl, 0.5 mM $MgCl_2$, pH 7.4), 50% saliva, or 50% urine. The signal gain was calculated based on the equation: $(I_T - I_0) / I_0 \times 100\%$, where I_T and I_0 represent the SWV peak currents in the presence and absence of target, respectively. All electrochemical data were collected using three independently fabricated mPEDs.

5.2.8. Aptamer digestion experiments

Aptamer digestion experiments were performed using our previously reported method.^{24,165} Specifically, 1 µM aptamer (final concentration) was incubated with various concentrations of acetyl fentanyl (final concentration 0, 25, or 200 µM), MDPV (final

concentration 0, 10, or 125 μM), or adenosine (final concentration 0, 80, or 500 μM) in 10 mM Tris buffer (20 mM NaCl, 0.5 mM MgCl_2 and 0.1 mg/mL BSA, pH 7.4) at 25 °C for 1 h. Blank controls containing only aptamer were also prepared. Exo I (final concentration: 0.05 U/ μL) was then added to initiate digestion. For all experiments, 5 μL of digestion products were collected at various time points (0 – 120 min) and mixed with 25 μL of 15% formamide, 30 mM EDTA, 1.2 \times SYBR Gold and 12 mM Tris buffer (pH 7.4) to stop digestion. The samples were loaded into a 384-well black plate and fluorescence intensities at 537 nm were recorded using a Tecan microplate reader (Infinite M1000 PRO) with excitation at 495 nm. The resistance value of each sample was used to determine the relative affinity of each ligand for its aptamer, and was calculated using the equation $((\text{AUC}_1 - \text{AUC}_0)/\text{AUC}_0) \times 100\%$, where (AUC_1) and (AUC_0) represent the areas under the curves of the fluorescence digestion time courses in the presence and absence of ligand, respectively.

5.3. Results and discussion

5.3.1. Design and fabrication of the mPED

A single mPED contains three gold working electrodes (WE1–3), one gold counter electrode (CE), one silver pseudo-reference electrode (RE), and a gold circuit network. The footprint of each mPED is 1.8 \times 1.0 cm, and two devices can be fabricated on a single 47-mm diameter circular filter paper substrate (**Figure 5-1**). The device was fabricated by first cutting out a top stencil of the electrode and circuitry patterns on parafilm-laminated polyterephthalate (PET) film (**Figure 5-1A**) using a desktop engraving machine, and then laminating the top stencil onto a filter paper (**Figure 5-1B**). The inclusion of parafilm on

PET film allows for greater adhesion between the top stencil and paper substrate, and increases the overall structural integrity of the device. The laminated area on the paper is impermeable to water and enables the deposition of nanomaterials on confined areas via routine vacuum filtration techniques. A solution of single-walled carbon nanotubes (SWCNTs) was first filtered onto the paper substrate under vacuum to establish a conductive bedding (**Figure 5-1C**). Then, a solution of AuNPs was added to the paper substrate and filtered to selectively form a thin gold film on the SWCNTs (**Figure 5-1D**). AgNPs were then immediately added to a designated area to form the silver pseudo-RE (**Figure 5-1E**). After drying, the bottom of the paper substrate was sealed with a parafilm-laminated PET bottom mask as a rigid foundation. Each filter contains two completed mPEDs (**Figure. 5-1F**).

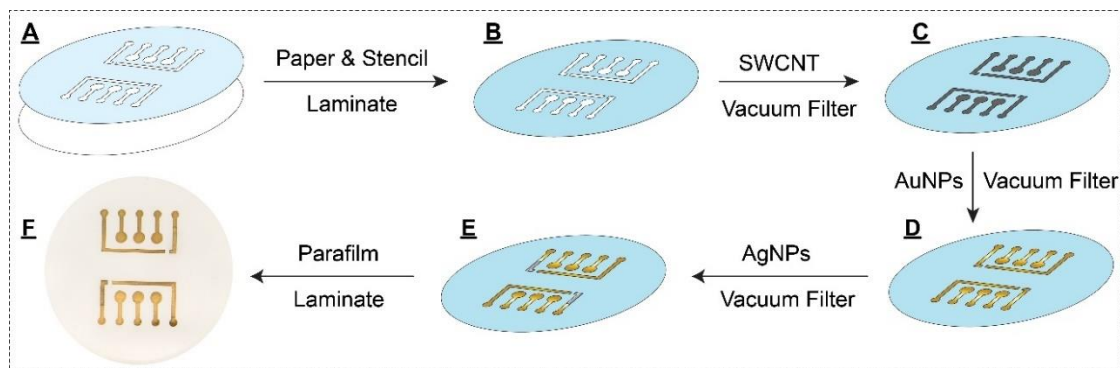


Figure 5-1. Scheme for the fabrication of mPEDs using ambient vacuum filtration. (A) A parafilm-laminated PET stencil (blue) and a piece of mixed cellulose ester filter paper (white) are combined to form (B) a PET-laminated filter paper. (C) A SWCNT solution is added to the paper and filtered under vacuum to form an underlayer pattern. (D) An AuNP solution is then applied under vacuum filtration to form a thin gold film on the paper substrate, followed by (E) the addition of AgNPs onto the designated area to generate the silver pseudo-reference electrode. (F) Lastly, a parafilm-laminated PET bottom mask is laminated onto the bottom of the paper substrate to complete device fabrication.

5.3.2. Evaluation of mPED electrochemical performance

Upon fabrication of the mPEDs, we first tested the variation in the electrochemical performance of WE1, WE2, and WE3 on a single device (**Figure 5-2A**). First, we determined the surface area and roughness of these working electrodes by performing cyclic voltammetry measurements in 0.05 M H₂SO₄ (scan rate 100 mV/s). We observed that the typical oxidation peak of gold and the reduction peak of gold oxide occurred at 1.35 V and 0.83 V, respectively (**Figure 5-2B**). The cyclic voltammograms produced by the three working electrodes overlapped, indicating very similar surface area. We used their reduction peaks to calculate the electrochemically-active surface area, and found that all working electrodes had a greater surface area ($0.18 \pm 0.01 \text{ cm}^2$) than the designed area of the electrode (0.08 cm^2), with an average surface roughness of 2.3, which can be attributed to the rough surface of the porous filter paper. We then characterized the electrochemical performance of the working electrodes by performing cyclic voltammetry scans at a rate of 100 mV/s in 1 mM K₃[Fe(CN)₆] and 0.1 M KCl. All three showed reversible redox behavior with overlapping reduction and oxidation peak potentials ($E_{pc} = 0.107 \text{ V}$ and $E_{pa} = 0.197 \text{ V}$) and a peak-to-peak separation of 90 mV (**Figure 5-2C**). We further performed cyclic voltammetry at different scan-rates and determined the electron transfer rates of the three electrodes using the Nicholson method.⁴⁸ As expected, all three electrodes produced similar electron transfer rates of $(3.3 \pm 0.1) \times 10^{-3} \text{ cm/s}$ (**Figure 5-3**). Finally, we evaluated the reproducibility of the device fabrication process by performing the same series of electrochemical experiments on four newly-fabricated mPEDs. We observed < 4% standard deviation in the tested surface area (**Figure 5-4**) and electron transfer rate (**Figure**

5-2D), demonstrating that our method produces mPEDs with minimal batch-to-batch variation.

5.3.3. Fabrication and testing of aptamer-modified mPEDs for small-molecule detection

We then prepared mPEDs modified with a series of small-molecule binding aptamers. We first modified all three working electrodes on a single mPED with COC-32, an aptamer derived from the cocaine-binding aptamer¹⁵¹ that binds cocaine with a dissociation constant (K_D) of $9.1 \pm 0.9 \mu\text{M}$ per isothermal titration calorimetry (Figure 5-5).

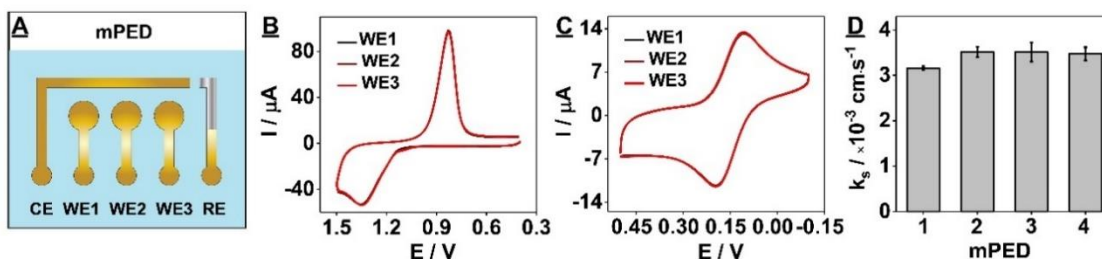


Figure 5-2. Determination of the surface area and electrochemical performance of mPEDs. (A) A diagram of a single mPED, which contains a gold counter electrode (CE), three gold working electrodes (WE1–3), and a silver pseudo-reference electrode (RE). (B) Surface area of the three working electrodes from one mPED determined by cyclic voltammetry in 0.05 M H_2SO_4 . (C) Cyclic voltammograms of the three working electrodes in 1 mM $\text{K}_3[\text{Fe}(\text{CN})_6]$ and 0.1 M KCl . (D) Average electron transfer rates for four mPEDs. Error bars represent the standard deviation for three working electrodes from each device.

Specifically, we used a previously reported protocol²¹ to perform electrochemical cleaning of the surfaces of WE1–3. We then pipetted a freshly-reduced COC-32 onto each working electrode surface and incubated at room temperature. The working electrodes were then rinsed with deionized water, and backfilled with 6-mercapto-hexanol, and finally rinsed once more with water and dried with nitrogen gas prior to use. We then tested the response of the three modified electrodes to various concentrations of cocaine. In the absence of cocaine, the immobilized aptamer is initially unfolded and the methylene blue

tag remains distant from the electrode surface, resulting in a low redox current. In the presence of cocaine, the aptamer undergoes a target-binding induced conformational change that brings methylene blue close to the electrode surface, resulting in an increase in redox current.

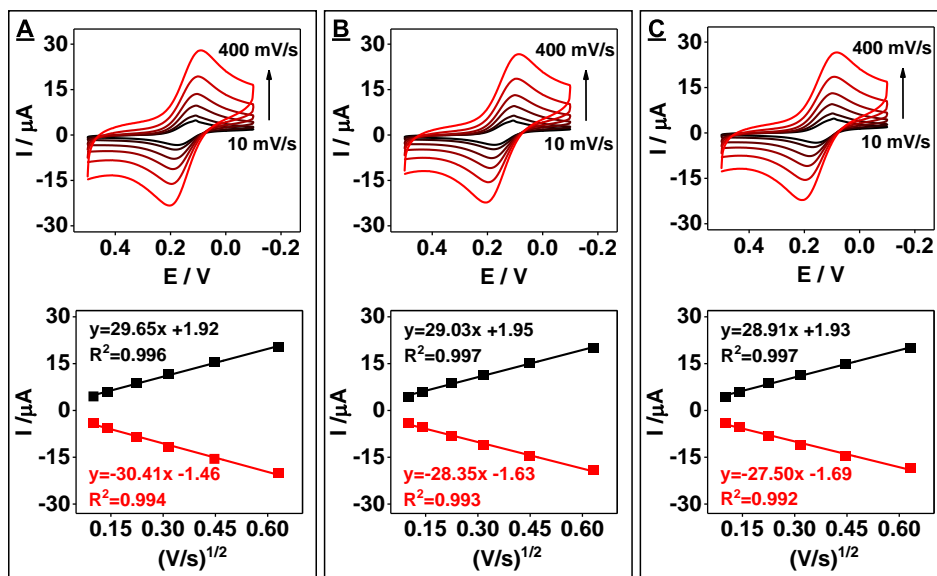


Figure 5-3. Determination of electron transfer rates of different working electrodes. Determination of electron transfer rates of (A) WE1, (B) WE2, and (C) WE3 from a single mPED using cyclic voltammetry. Top panels represent cyclic voltammograms produced in 1 mM $K_3[Fe(CN)_6]$ and 0.1 M KCl at various scan-rates (10 – 400 mV/s, indicated by the black-to-red color gradient) and bottom panels display the peak cathodic (black) and peak anodic currents (red) as a function of the square root of the scan-rate.

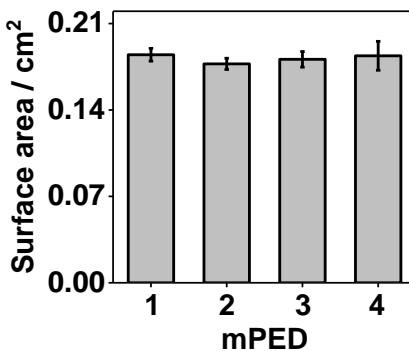


Figure 5-4. Surface area measurements of the working electrodes for four different mPEDs were tested. Standard deviations are for the three working electrodes from each individual device.

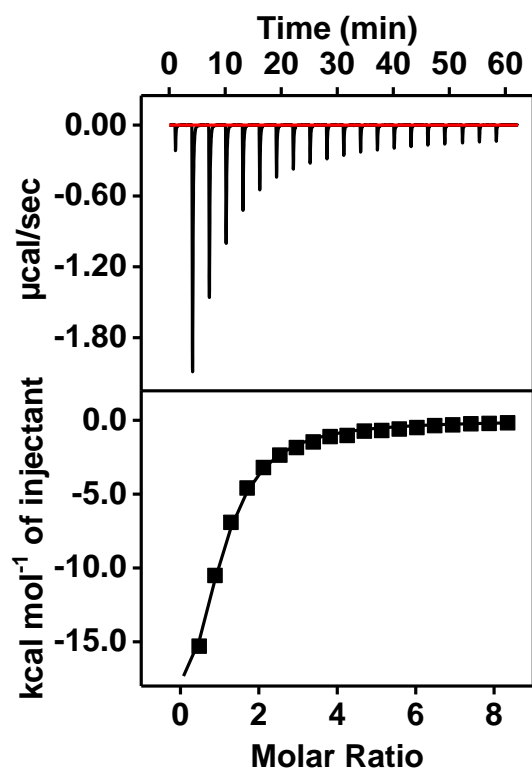


Figure 5-5. Determination of the binding affinity of COC-apt to cocaine using isothermal titration calorimetry (ITC). The top panel presents raw data showing the heat generated from the titration of 800 μM cocaine into 20 μM COC-apt. The bottom panel shows the integrated heat of each titration after correcting for dilution heat of the titrant plotted against the molar ratio of cocaine to COC-apt. ITC data was fitted using a single-site model.

We generated calibration curves for the three electrodes by submerging the COC-32-modified mPED in a 2 mL electrochemical cell containing varying concentrations of cocaine (0–800 μM). All three electrodes produced a target-dependent signal, and yielded similar signal gains at each tested target concentration with standard deviations of < 3% (**Figure 5-6A**). The calibration curves from the device had linear ranges of 1–100 μM , with a limit of detection (LOD) of 1 μM (**Figure 5-6B**), which confirmed the high precision of electrodes on the same device for target detection. Notably, our mPED exhibited similar

performance to a previously reported cocaine-detecting E-AB sensor fabricated on a conventional gold disk electrode.²⁴

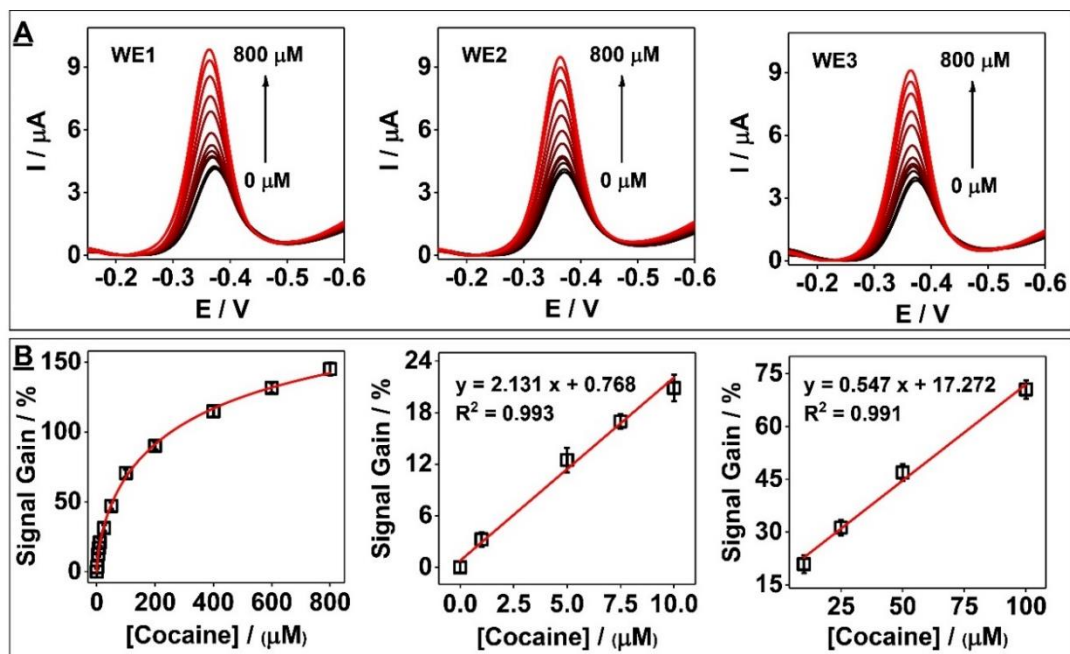


Figure 5-6. Detection of cocaine using a COC-32-modified mPED. (A) Square wave voltammetry (SWV) of the three working electrodes modified with COC-32 in the presence of 0–800 μM cocaine. (B) Corresponding calibration curve (left) and close-ups of the two linear ranges (middle and right). Error bars represent the standard deviation of measurements from the three working electrodes.

To evaluate the generalizability of our aptamer-modified mPED development process, we fabricated mPEDs modified with other small-molecule-binding aptamers with different sequences and secondary structures. Specifically, we chose thiol- and methylene blue-modified versions of aptamers AF-apt (AF-32),¹⁶⁶ MDPV-apt (MDPV-34),²⁶ and ADE-apt (ADE-25),¹⁴⁹ which respectively bind to the synthetic opioid acetyl fentanyl ($K_D = 3.8 \pm 0.2 \mu\text{M}$) (**Figure 5-7A**), the synthetic cathinone methylenedioxypropylvalerone (MDPV; $K_D = 0.3 \pm 0.04 \mu\text{M}$), and adenosine ($K_{D1} = 7.4 \pm 0.1 \mu\text{M}$, $K_{D2} = 103 \pm 0.5 \mu\text{M}$) (**Figure 5-7B**). For each device, the same aptamer was modified onto all three working electrodes to assess their sensing precision with a surface coverage of $(2.93 \pm 0.12) \times 10^{12}$, (2.78 ± 0.14)

$\times 10^{12}$, and $(3.95 \pm 0.74) \times 10^{12}$ molecules/cm² for AF-32, MDPV-34, and ADE-25, respectively. In general, all three electrodes produced similar signal gains when challenged with their respective target at a wide range of concentrations (**Figures 5-8-10**).

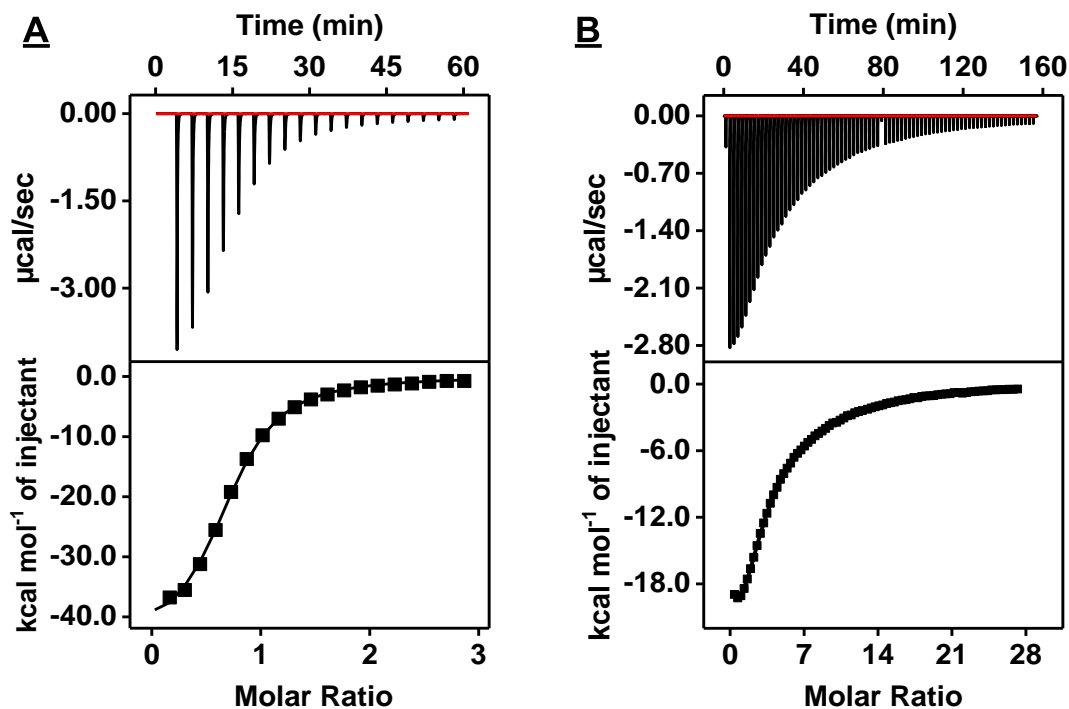


Figure 5-7. Determination of the binding affinity via ITC. Determination of the binding affinity of (A) 550 μM acetyl fentanyl to 40 μM AF-apt or (B) 1200 μM adenosine to 20 μM ADE-apt using ITC. Top panels present raw data showing the heat generated from the titration. Bottom panels show the integrated heat of each titration after correcting for dilution heat of the titrant plotted against the molar ratio of ligand to aptamer. AF-apt titration data was fitted using a single-site model and ADE-apt titration data was fitted using a two-site cooperative binding model.

We also observed low intra- and inter-device variability, with standard deviations < 5%. The AF-32, MDPV-34- and ADE-25-modified mPEDs also proved sensitive, with linear ranges of 0.5–15 μM, 0.1–10 μM, and 1–200 μM and LODs of 0.5 μM, 0.1 μM, 1 μM for acetyl fentanyl, MDPV, and adenosine, respectively (**Figures 5-8-10**). To determine the stability of the aptamer-modified devices, we fabricated five ADE-25-

modified mPEDs and stored them at room temperature in the dark. Every three days over a period of two weeks, one of the devices was challenged with 100 μM adenosine and then discarded. All devices produced reliable and reproducible sensing behavior and similar signal gain values ($58.9 \pm 3.0\%$) (**Figure 5-11**), indicating that the aptamer-modified mPEDs can be stored at room temperature without affecting their sensing performance.

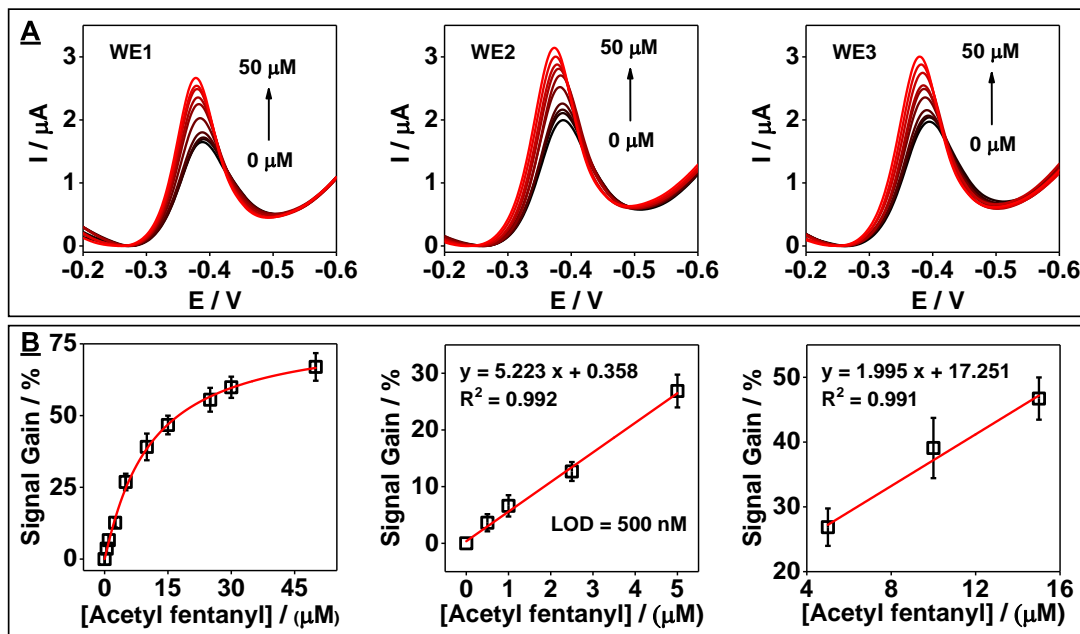


Figure 5-8. Detection of acetyl fentanyl using a mPED modified with AF-32. (A) Square-wave voltammetry (SWV) of the three working electrodes in the presence of various concentrations of acetyl fentanyl (0 – 50 μM). (B) Corresponding calibration curve (left) and close ups of the two linear ranges (middle and right). Error bars represent the standard deviation of the measurements of the three working electrodes of a single mPED.

5.3.4. Multi-target detection in biological samples

We next demonstrated simultaneous detection of three small-molecule targets using a single mPED. First, we performed our recently developed exonuclease-based binding assay¹⁶⁵ to confirm that AF-32, MDPV-34 and ADE-25 would not cross-react to each other's targets. In this assay, unbound aptamers are completely digested by exonuclease I

(Exo I), an enzyme that digests single-strand DNA into mononucleotides. However, ligand binding induces aptamer folding, which greatly reduces the digestion rate of the aptamer, and the magnitude of inhibition closely corresponds to the aptamer's ligand affinity. Thus, comparing the resistance of the aptamer digestion in the presence versus the absence of ligand allows for the determination of relative aptamer-ligand binding strength, and thereby specificity.

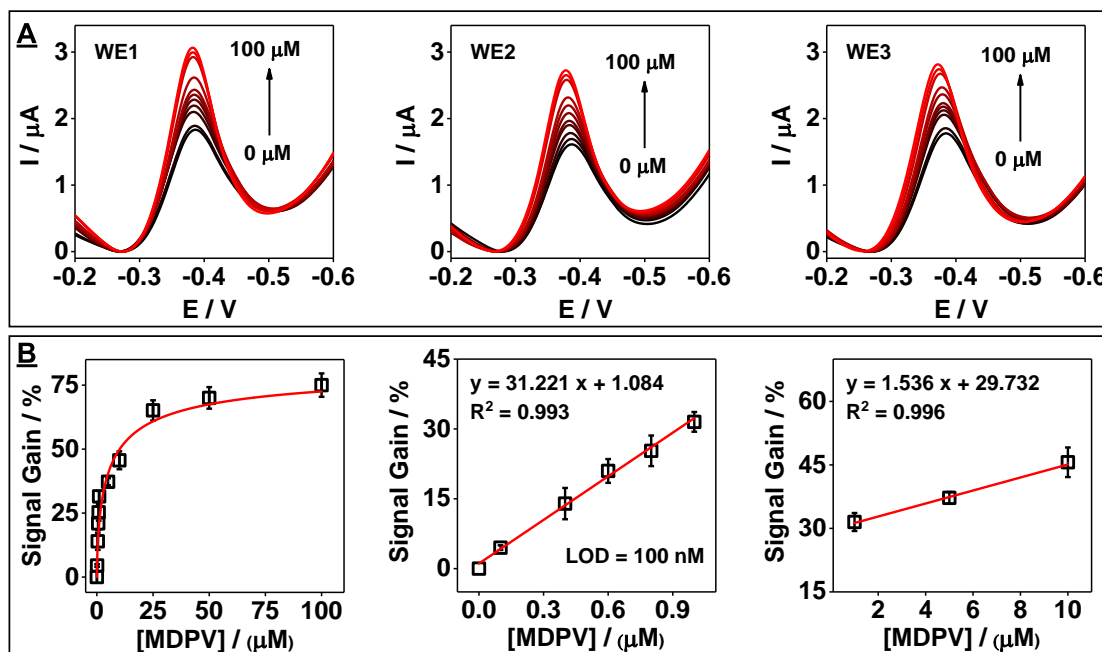


Figure 5-9. Detection of MDPV using a mPED modified with MDPV-34. (A) SWV of the three working electrodes in the presence of various concentrations of MDPV (0 – 100 μM). (B) Corresponding calibration curve (left) and close-ups of the two linear ranges (middle and right). Error bars represent the standard deviation of measurements from the three working electrodes of a single mPED.

We digested AF-apt, MDPV-apt, and ADE-apt in the absence or presence of acetyl fentanyl, MDPV, or adenosine. All aptamers greatly resisted digestion in the presence of their respective target, but were rapidly digested in the presence of non-target ligands (Figure 5-12A-C). Based on the resistance value of each ligand (see **Experimental section**) (Figure 5-12D), we determined that each aptamer only binds to its respective target,

indicating that they could be incorporated into the same mPED without crosstalk among electrodes.

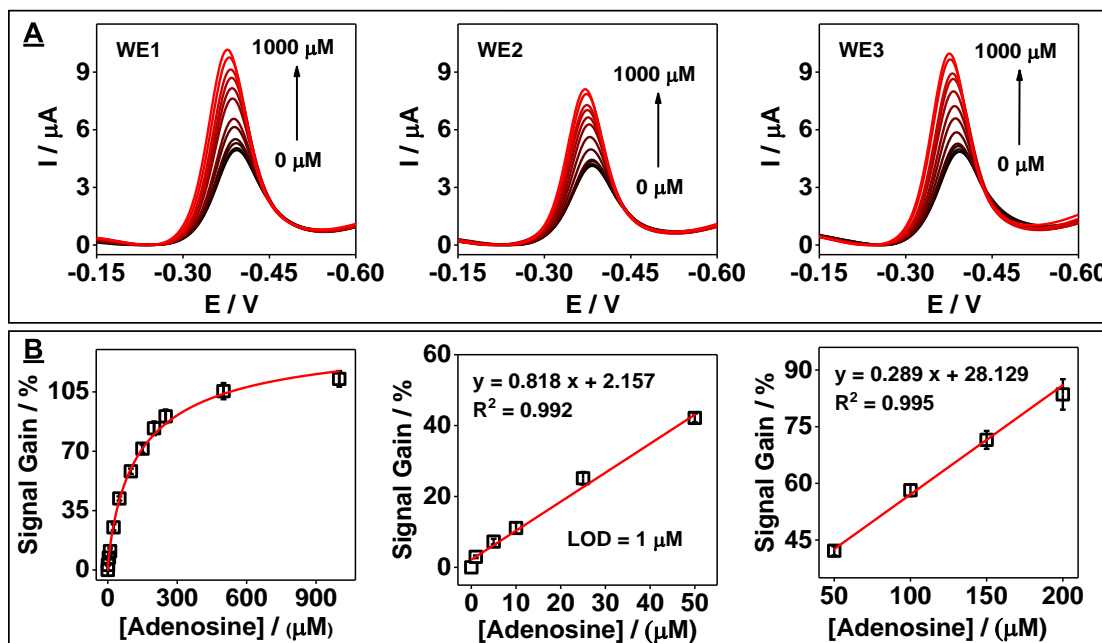


Figure 5-10. Detection of adenosine using a mPED modified with ADE-25. (A) SWV of the three working electrodes in the presence of various concentrations of adenosine (0 – 1,000 μM). (B) Corresponding calibration curve (left) and close ups of the two linear ranges (middle and right). Error bars represent the standard deviation of the measurements of the three working electrodes of a single mPED.

We then prepared a triple-modified mPED by immobilizing AF-32, MDPV-34 and ADE-25 onto WE1, WE2 and WE3, respectively (**Figure 5-15A**). We first tested whether each electrode would only respond to its respective target. We challenged the triple-modified mPED with samples containing different concentrations of each individual target. With acetyl fentanyl, we observed a target-concentration-dependent increase in current at WE1, but not the other two working electrodes (**Figure 5-15B** and **5-13**). Likewise, the MDPV-34-modified WE2 and ADE-25-modified WE3 produced target concentration-dependent signal increases only in the presence of their respective target, with no crosstalk observed from the other electrodes (**Figure 5-13**).

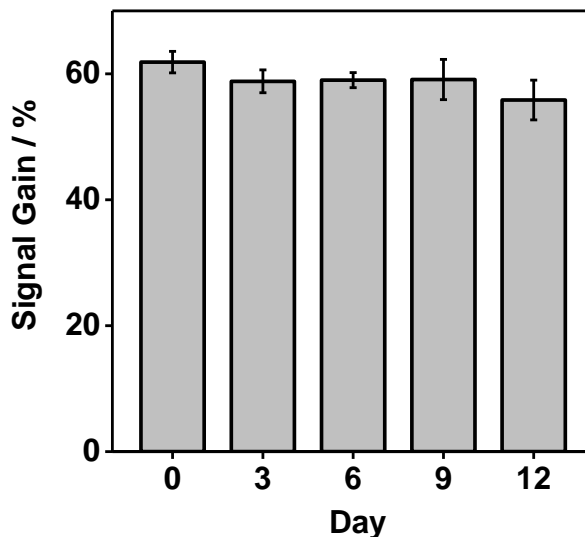


Figure 5-11. Stability of ADE-25 modified mPEDs. Stability of mPEDs modified with ADE-25 as determined by SWV measurements in 100 μ M adenosine immediately after fabrication or 3, 6, 9, or 12 days later. Error bars represent the standard deviation of the measurements of the three aptamer-modified working electrodes of a single mPED.

Notably, the background current of WE3 was higher because the aptamer surface coverage of this electrode ($3.95 \pm 0.74 \times 10^{12}$ molecules/cm²) was greater than for WE1 ($2.93 \pm 0.12 \times 10^{12}$ molecules/cm²) and WE2 ($2.78 \pm 0.14 \times 10^{12}$ molecules/cm²). This is reasonable, as different aptamers have unique surface coverage requirements for optimal sensing performance. We next performed a series of spike-and-recovery experiments with binary and ternary mixtures of the three analytes. For each analyte, we chose two concentrations that fell within the linear range of the respective calibration curves generated with single-aptamer modified mPEDs (**Figures 5-8–10**). As expected, WE1 and WE2 generated a current increase for a binary mixture of acetyl fentanyl and MDPV, with no measurable current change from ADE-25-modified WE3 (**Figure 5-15C**).

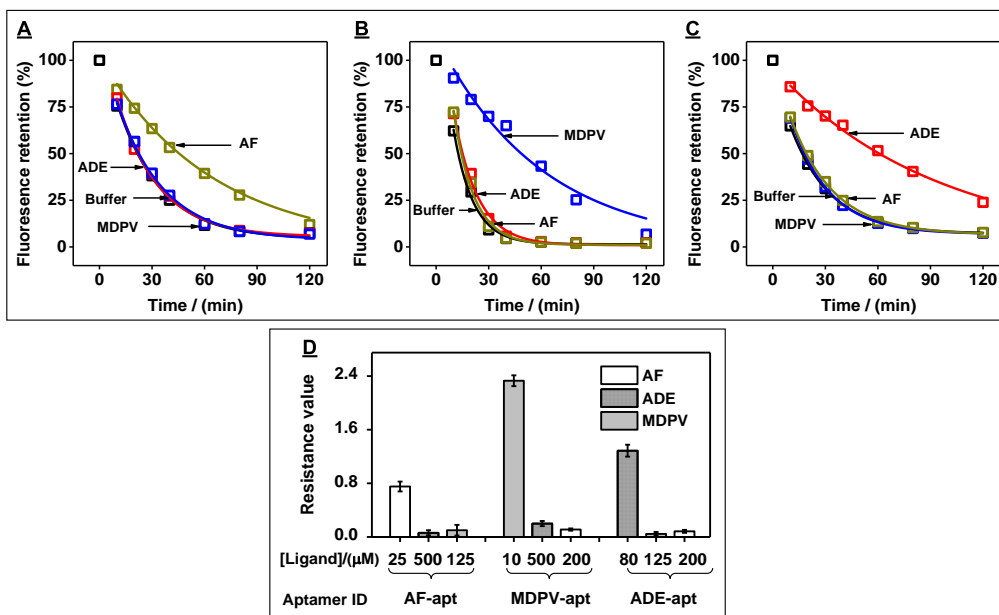


Figure 5-12. Characterization of the specificity of different aptamers using the exonuclease-based binding assay. Characterization of the specificity of AF-apt, MDPV-apt, and ADE-apt using our recently developed exonuclease-based binding assay. Fluorescence time course for Exonuclease I digestion of (A) AF-apt in the absence and presence of 25 μM acetyl fentanyl (AF), 500 μM adenosine (ADE), or 125 μM MDPV, (B) MDPV-apt in the absence and presence of 10 μM MDPV, 500 μM ADE, or 200 μM AF, (C) ADE-apt in the absence and presence of 80 μM ADE, 125 μM MDPV, or 200 μM AF. (D) The resistance value of each aptamer-ligand pair calculated from the plots presented in A-C. Error bars represent the standard deviation of three measurements.

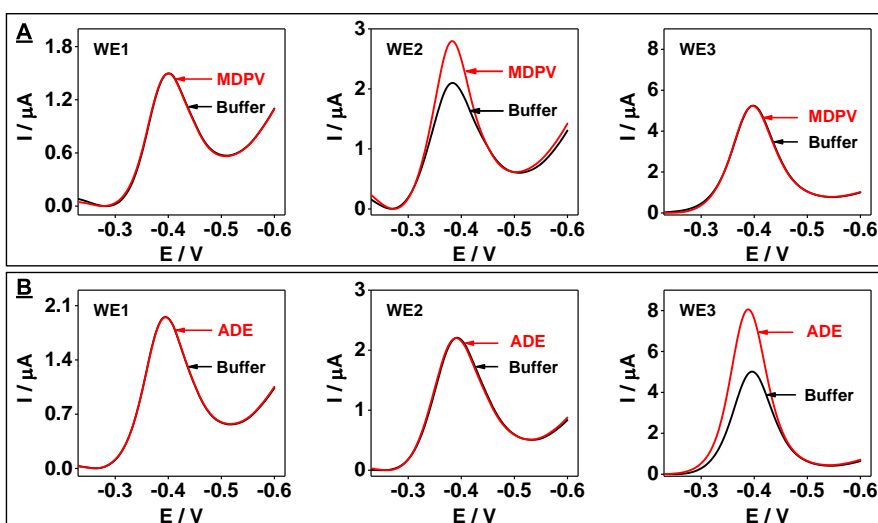


Figure 5-13. Simultaneous detection of multiple small-molecule analytes using triple-modified mPEDs. WE1, WE2, and WE3 were respectively modified with AF-32, MDPV-

34, and ADE-25. Plots show SWV response of each working electrode to (A) 5 μM MDPV or (B) 120 μM adenosine (ADE).

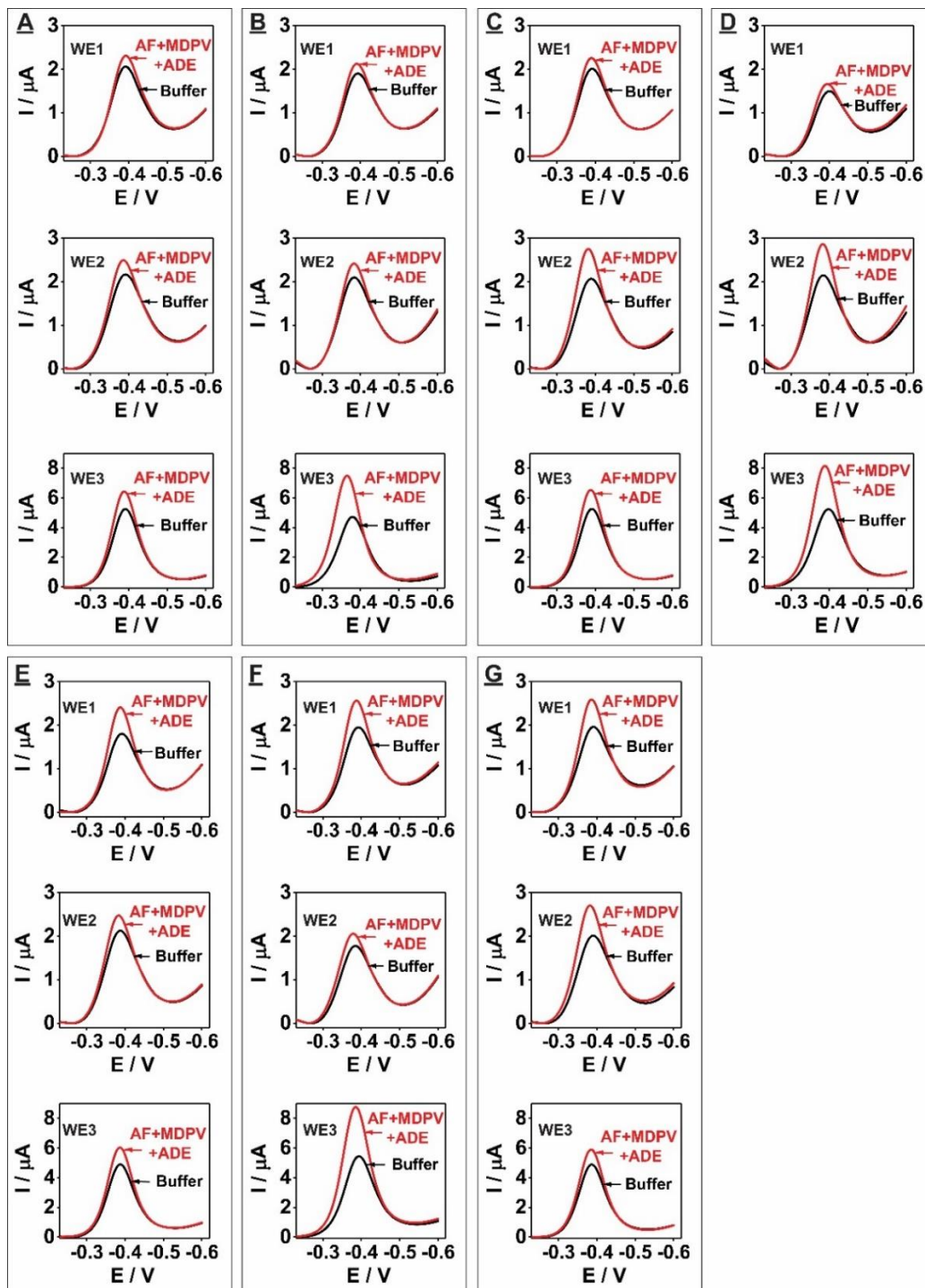


Figure 5-14. SWV response of the triple-modified mPED to ternary mixtures. SWV response of each working electrode of a triple-modified mPED to ternary mixtures of acetyl fentanyl (AF), MDPV, and adenosine (ADE) in buffer. A-G corresponds to sample #s 1-7

listed in **Table 1A**. WE1, WE2, and WE3 were respectively modified with AF-32, MDPV-34, and ADE-25.

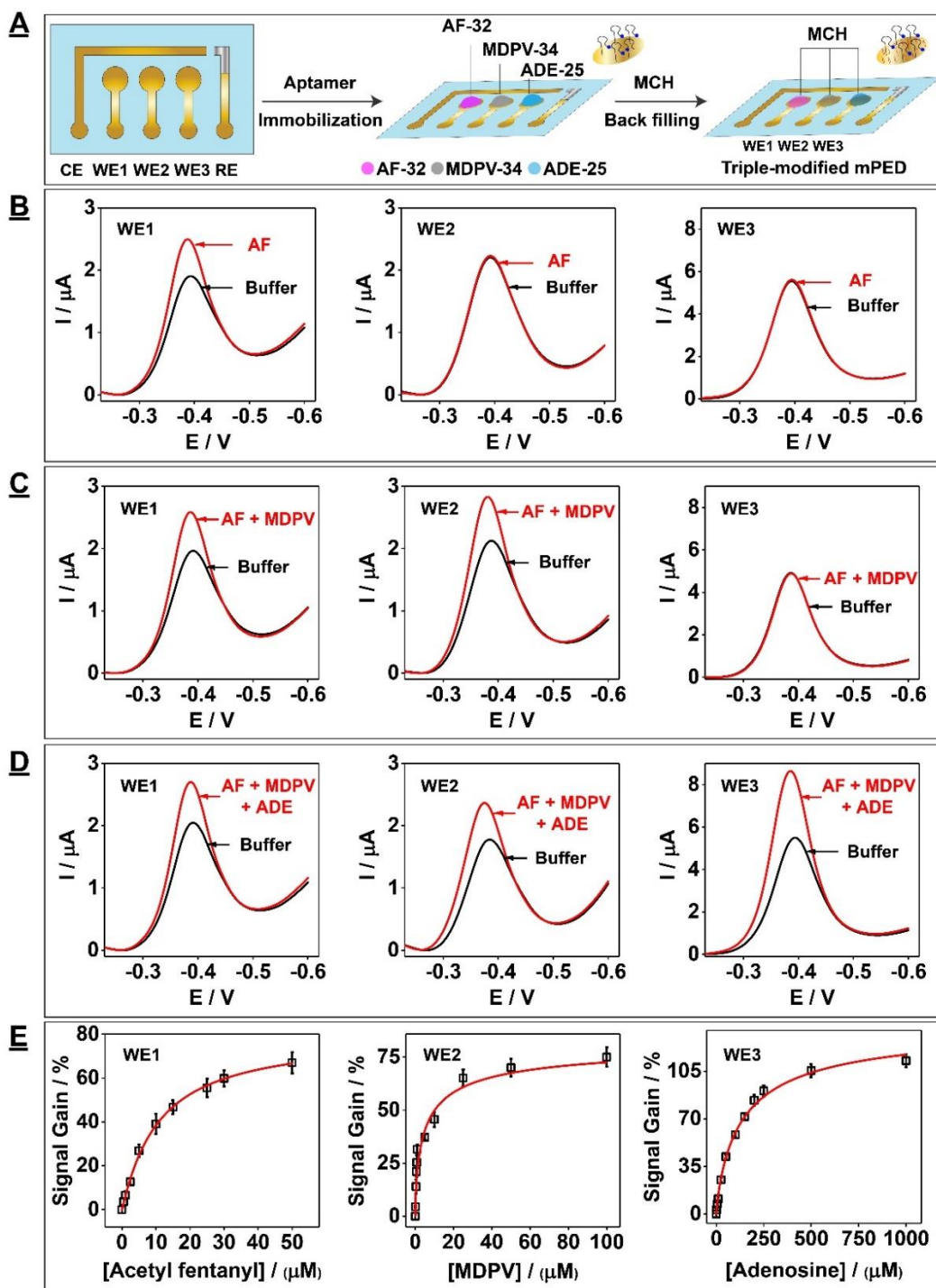


Figure 5-15. Simultaneous detection of multiple small-molecule analytes with triple-modified mPEDs. (A) Schematic for the fabrication of a mPED modified with aptamers AF-32 (WE1), MDPV-34 (WE2), and ADE-25 (WE3). (B–D) SWV response of each

working electrode to (B) 10 μ M acetyl fentanyl (AF), (C) a binary mixture of 10 μ M AF and 5 μ M MDPV, (D) and a ternary mixture of 10 μ M AF, 5 μ M MDPV, and 120 μ M adenosine (ADE). (E) Calibration curve for the three different targets collected from single-aptamer-modified mPEDs. Error bars represent the standard deviation of measurements from the three working electrodes on the same device.

Table 5-1. Recoveries from spike-and-recovery experiments with ternary mixture detection in (A) buffer, (B) 50% urine, and (C) 50% saliva.

A	Sample ID	[Spiked concentration] (μ M)			[Found concentration] (μ M)			Recovery in buffer (%)		
		AF	MDPV	ADE	AF	MDPV	ADE	AF	MDPV	ADE
A1	2.5	0.5	25.0	2.6 \pm 0.1	0.5 \pm 0.0	25.7 \pm 0.8	102.7 \pm 5.2	100.3 \pm 6.6	102.8 \pm 3.3	
A2	2.5	0.5	120.0	2.4 \pm 0.1	0.5 \pm 0.0	121.0 \pm 6.4	97.1 \pm 2.8	101.4 \pm 7.5	100.9 \pm 5.3	
A3	2.5	5.0	25.0	2.5 \pm 0.1	4.9 \pm 0.4	25.1 \pm 1.5	100.9 \pm 5.5	98.2 \pm 7.5	100.5 \pm 6.1	
A4	2.5	5.0	120.0	2.4 \pm 0.1	4.9 \pm 0.4	116.2 \pm 2.2	96.8 \pm 5.6	98.4 \pm 7.3	96.9 \pm 1.9	
A5	10.0	0.5	25.0	10.9 \pm 0.1	0.5 \pm 0.0	26.6 \pm 0.5	109.5 \pm 1.3	103.7 \pm 4.9	106.4 \pm 2.0	
A6	10.0	0.5	120.0	9.7 \pm 0.1	0.5 \pm 0.0	121.9 \pm 5.2	97.2 \pm 1.0	104.3 \pm 2.2	101.6 \pm 4.3	
A7	10.0	5.0	25.0	10.5 \pm 0.4	4.7 \pm 0.1	25.4 \pm 1.2	104.8 \pm 4.4	93.8 \pm 2.3	101.4 \pm 5.0	
A8	10.0	5.0	120.0	10.4 \pm 0.5	5.1 \pm 0.3	117.3 \pm 2.3	104.1 \pm 4.5	102.3 \pm 5.4	97.8 \pm 1.9	
B	Sample ID	[Spiked concentration] (μ M)			[Found concentration] (μ M)			Recovery in 50% urine (%)		
		AF	MDPV	ADE	AF	MDPV	ADE	AF	MDPV	ADE
B1	2.5	2.5	25.0	2.7 \pm 0.0	2.7 \pm 0.1	24.1 \pm 2.2	106.5 \pm 1.0	107.7 \pm 2.0	96.3 \pm 9.0	
B2	2.5	2.5	150.0	2.6 \pm 0.1	2.5 \pm 0.1	152.8 \pm 19.1	102.9 \pm 5.3	101.5 \pm 5.2	101.8 \pm 12.7	
B3	2.5	15.0	25.0	2.7 \pm 0.2	15.1 \pm 1.6	28.0 \pm 0.5	107.0 \pm 8.8	100.8 \pm 10.8	111.8 \pm 2.0	
B4	2.5	15.0	150.0	2.5 \pm 0.1	15.8 \pm 1.3	165.3 \pm 11.4	98.6 \pm 5.0	105.4 \pm 8.6	110.2 \pm 7.6	
B5	10.0	2.5	25.0	9.5 \pm 0.2	2.5 \pm 0.1	27.2 \pm 1.3	94.8 \pm 2.0	100.2 \pm 2.7	108.7 \pm 5.4	
B6	10.0	2.5	150.0	9.7 \pm 1.3	2.5 \pm 0.1	156.7 \pm 17.1	96.7 \pm 12.8	100.9 \pm 5.6	104.5 \pm 11.4	
B7	10.0	15.0	25.0	10.7 \pm 0.9	14.1 \pm 1.2	23.7 \pm 1.1	107.7 \pm 9.4	94.1 \pm 7.8	95.0 \pm 4.3	
B8	10.0	15.0	150.0	10.1 \pm 1.1	14.9 \pm 1.6	160.9 \pm 13.7	101.1 \pm 11.4	99.5 \pm 10.3	107.3 \pm 9.1	
C	Sample ID	[Spiked concentration] (μ M)			[Found concentration] (μ M)			Recovery in 50% saliva (%)		
		AF	MDPV	ADE	AF	MDPV	ADE	AF	MDPV	ADE
C1	2.5	2.5	25.0	2.4 \pm 0.2	2.5 \pm 0.1	24.9 \pm 1.9	97.0 \pm 7.9	99.0 \pm 5.7	99.4 \pm 7.5	
C2	2.5	2.5	150.0	2.5 \pm 0.1	2.5 \pm 0.3	148.0 \pm 8.0	100.4 \pm 3.8	100.4 \pm 9.8	98.7 \pm 5.3	
C3	2.5	15.0	25.0	2.5 \pm 0.2	16.2 \pm 1.3	23.0 \pm 0.5	101.5 \pm 6.4	108.1 \pm 8.6	91.8 \pm 2.1	
C4	2.5	15.0	150.0	2.6 \pm 0.1	16.0 \pm 1.0	153.5 \pm 9.9	105.9 \pm 3.6	106.9 \pm 6.7	102.3 \pm 6.6	
C5	10.0	2.5	25.0	10.5 \pm 0.4	2.6 \pm 0.2	23.6 \pm 0.7	105.2 \pm 4.2	104.1 \pm 7.1	94.5 \pm 2.8	
C6	10.0	2.5	150.0	10.7 \pm 0.4	2.5 \pm 0.1	148.3 \pm 12.1	107.1 \pm 4.4	99.2 \pm 5.5	99.0 \pm 8.0	
C7	10.0	15.0	25.0	10.3 \pm 0.6	15.8 \pm 1.4	25.8 \pm 0.9	103.2 \pm 6.4	105.6 \pm 9.0	103.1 \pm 3.4	
C8	10.0	15.0	150.0	10.7 \pm 1.2	15.9 \pm 1.2	147.5 \pm 23.6	106.7 \pm 11.7	106.1 \pm 8.3	98.4 \pm 15.7	

For the ternary mixture, we observed specific target concentration-dependent increases in current from each electrode (Figure 5-15D and Figure 5-14). The triple-modified mPEDs showed high accuracy and precision, with 94–110% recoveries calculated based on the calibration curves for each analyte (Figure 5-15E), and ~4% average inter-device variability from three different devices (Table 5-1A). These results

indicate that aptamer-modified mPEDs can robustly detect multiple small molecules simultaneously in a single sample.

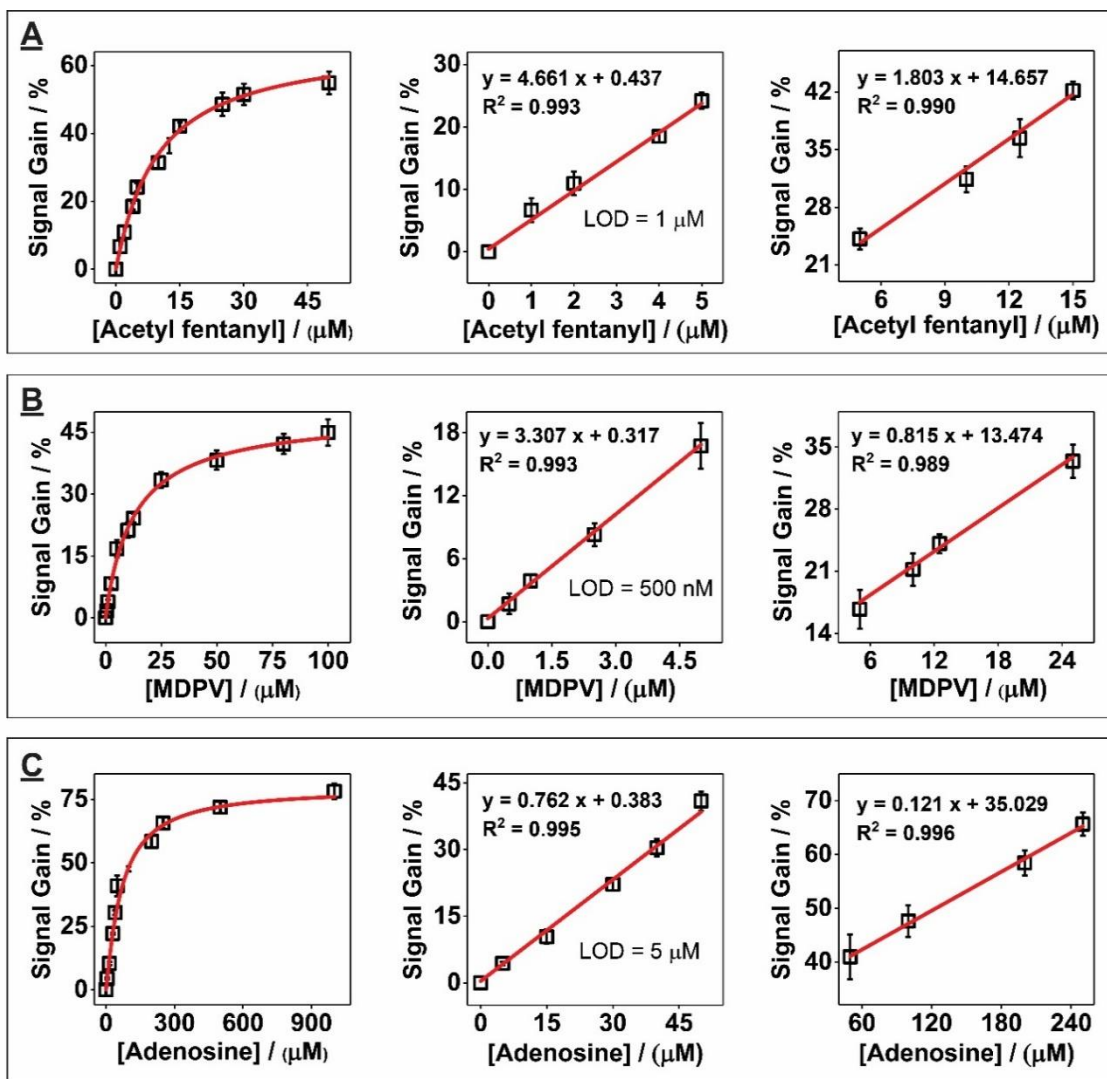


Figure 5-16. Detection of different targets in 50% urine using single-aptamer-modified mPEDs. Detection of acetyl fentanyl, MDPV, or adenosine in 50% urine using single-aptamer-modified mPEDs. The three working electrodes of a mPED modified entirely with either (A) AF-32, (B) MDPV-34, or (C) ADE-25 were incubated with various concentrations of acetyl fentanyl (0 – 50 μM), MDPV (0 – 100 μM), or adenosine (0 – 1000 μM), respectively. Panels show the calibration curves (left) and close ups of the two linear ranges (middle and right). Error bars represent the standard deviation of the measurements of the three working electrodes from the same mPED.

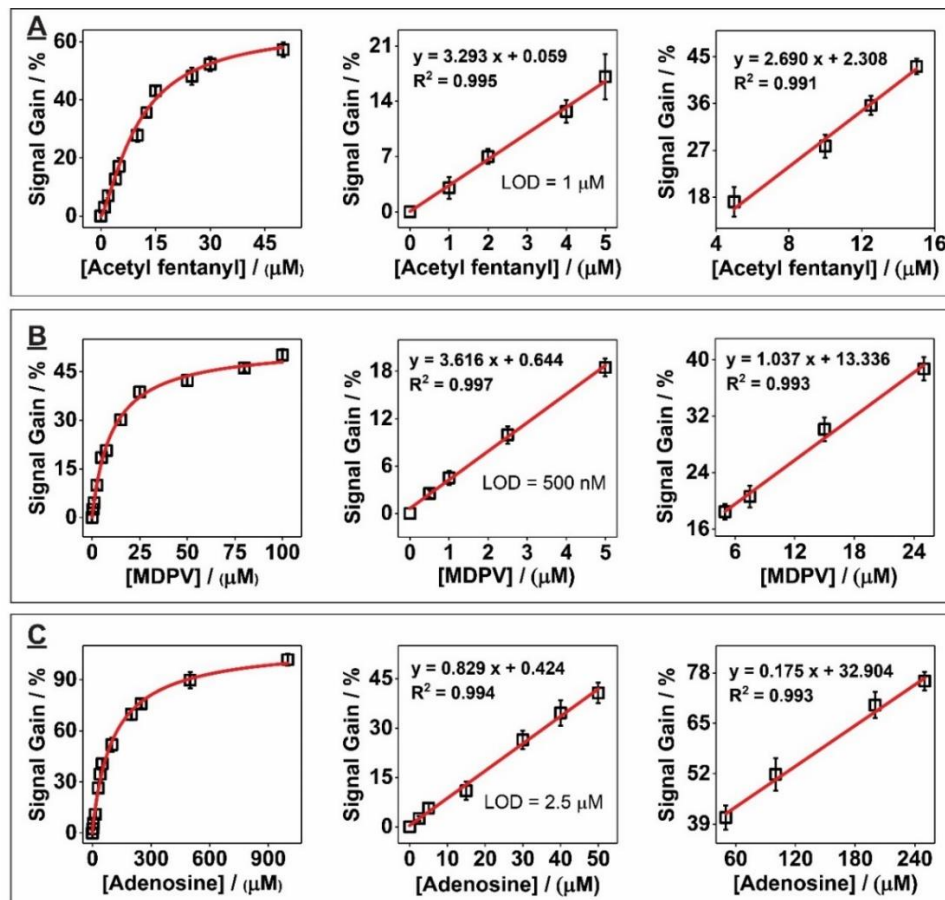


Figure 5-17. Detection of various targets in 50% saliva using a single-aptamer-modified mPEDs. Detection of acetyl fentanyl, MDPV, or adenosine in 50% saliva using a single-aptamer-modified mPEDs. The three working electrodes of a mPED modified entirely with either (A) AF-32, (B) MDPV-34, or (C) ADE-25 were incubated with various concentrations of acetyl fentanyl (0 – 50 μM), MDPV (0 – 100 μM), or adenosine (0 – 1,000 μM), respectively. Panels show the calibration curves (left) and close-ups of the two linear ranges (middle and right). Error bars represent the standard deviation of the measurements of the three working electrodes from the same mPED.

Table 5-2. Recoveries obtained from spike-and-recovery experiments with a ternary mixture in 50% saliva using a PDMS-confined triple-modified mPED.

Sample ID	[Spiked concentration] (μM)			[Found concentration] (μM)			Recovery in saliva (%)		
	AF	MDPV	ADE	AF	MDPV	ADE	AF	MDPV	ADE
1	2.5	2.5	25.0	2.6 ± 0.2	2.5 ± 0.1	24.0 ± 0.5	103.8 ± 8.7	98.4 ± 5.0	96.2 ± 2.1
2	2.5	2.5	150.0	2.5 ± 0.1	2.4 ± 0.1	153.2 ± 13.2	99.2 ± 2.4	96.5 ± 5.1	102.2 ± 8.8
3	2.5	15.0	25.0	2.6 ± 0.1	15.9 ± 0.8	25.9 ± 1.4	103.9 ± 2.7	106.4 ± 5.3	103.9 ± 5.7
4	2.5	15.0	150.0	2.6 ± 0.2	15.2 ± 0.4	159.3 ± 1.9	102.0 ± 6.7	101.3 ± 2.4	106.2 ± 1.2
5	10.0	2.5	25.0	10.7 ± 0.5	2.6 ± 0.1	27.3 ± 0.5	106.5 ± 4.7	97.8 ± 4.5	109.0 ± 2.1
6	10.0	2.5	150.0	10.3 ± 0.7	2.4 ± 0.1	140.0 ± 8.6	103.0 ± 6.8	94.4 ± 4.1	93.4 ± 5.7
7	10.0	15.0	25.0	10.3 ± 0.4	14.6 ± 0.5	24.4 ± 1.1	103.4 ± 3.5	97.4 ± 3.6	97.5 ± 4.2
8	10.0	15.0	150.0	10.3 ± 0.3	14.3 ± 0.9	165.7 ± 2.8	102.7 ± 2.6	95.0 ± 6.5	110.5 ± 1.8

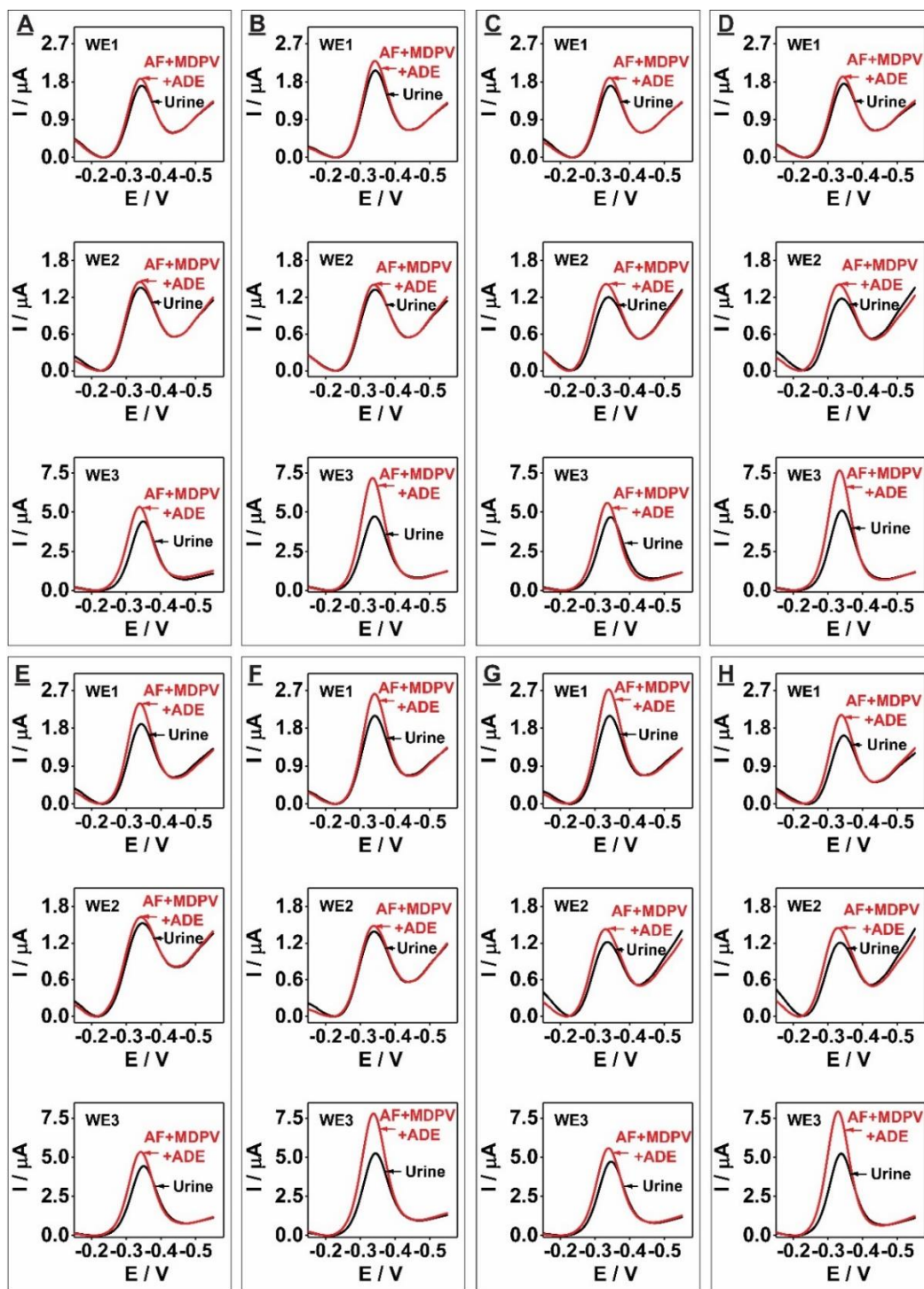


Figure 5-18. SWV response of each working electrode of a triple-modified mPED in 50% urine. SWV response of each working electrode of a triple-modified mPED in the absence (black) and presence (red) of ternary mixtures of acetyl fentanyl (AF), MDPV, and adenosine (ADE) in 50% urine. Plots **A-H** correspond to sample #s 1-8 listed in **Table 5-1B**.

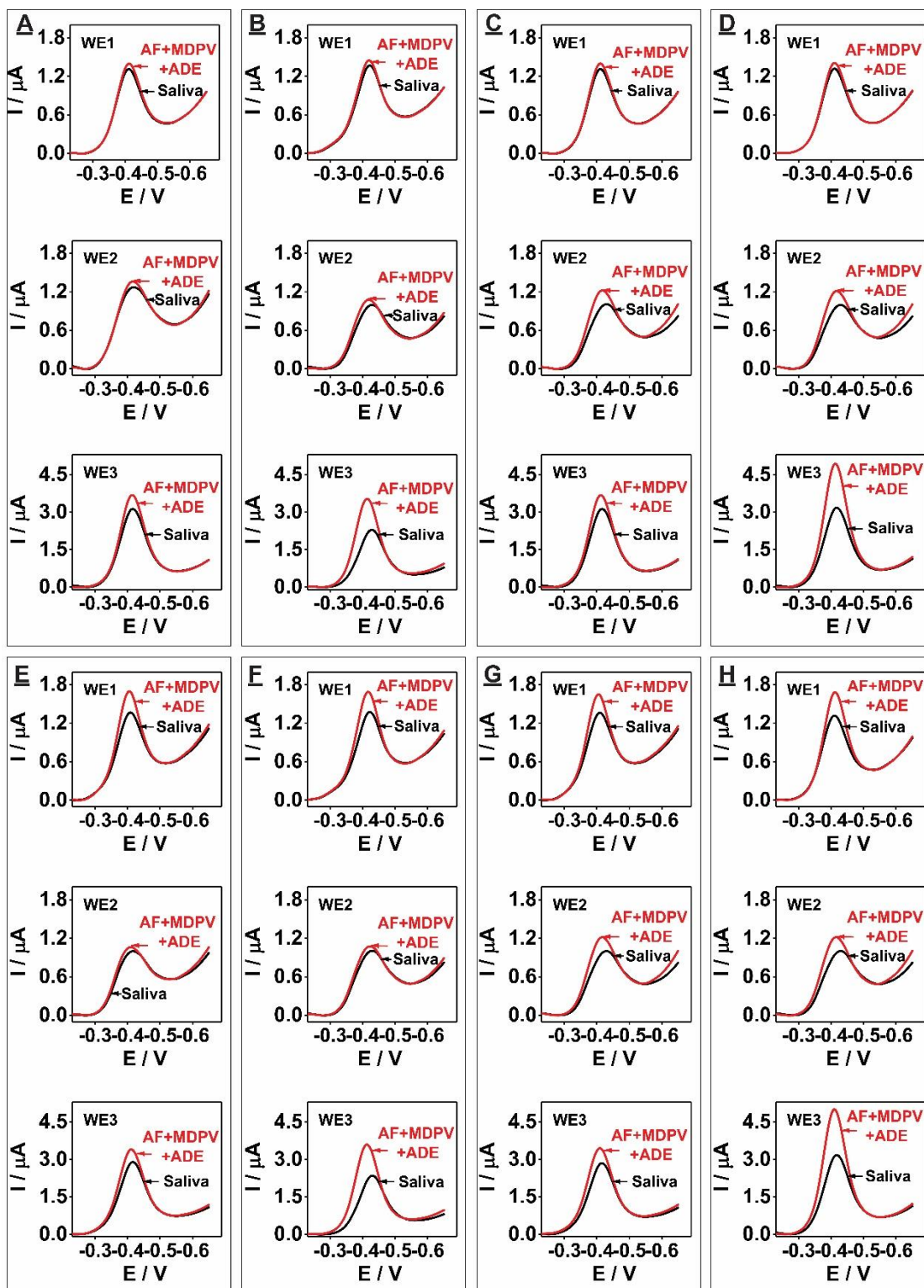


Figure 5-19. SWV response of each working electrode of a triple-modified mPED in 50% saliva. SWV response of each working electrode of a triple-modified mPED in the absence (black) and presence (red) of ternary mixtures of acetyl fentanyl (AF), MDPV, and

adenosine (ADE) in 50% saliva. Plots **A-H** corresponds to the sample #s 1-8 listed in **Table 5-1C**.

We further demonstrated the capability of our triple-modified mPEDs to detect multiple small-molecule targets in biological samples. We first generated calibration curves by challenging single aptamer-modified devices with varying concentrations of their respective target in 50% diluted urine (**Figure 5-16**) or saliva (**Figure 5-17**). The modified mPEDs demonstrated a clear target concentration-dependent signal, with $\leq 5\%$ intra-device variability. However, we did observe that the devices yielded lower signal gains and 2–5-fold lower sensitivities (based on LOD) in these biological samples compared to buffer. This is probably due to surface fouling by macromolecules present in the biosamples.^{19,167}

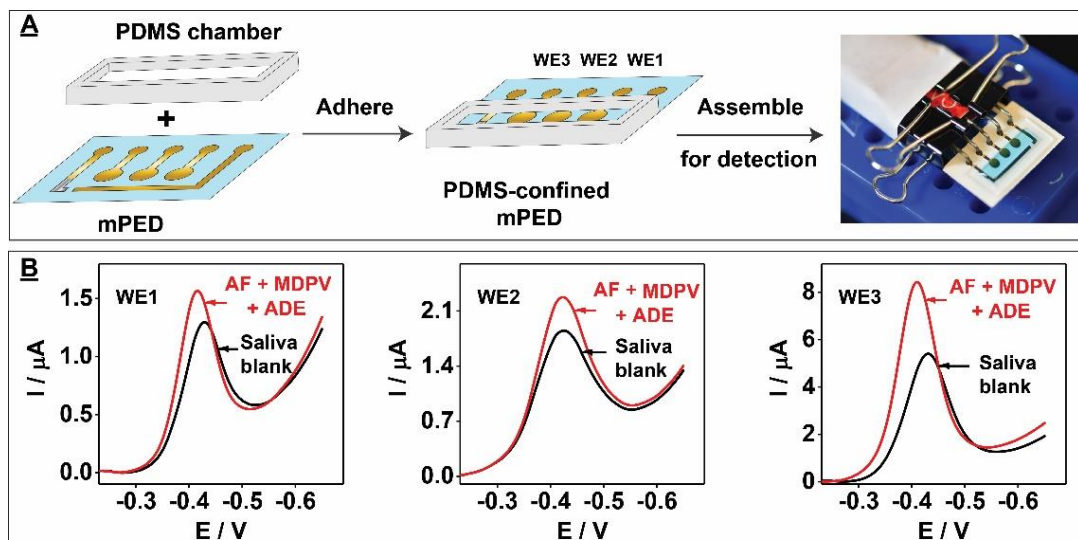


Figure 5-20. Fabrication of an aptamer-modified mPED with a PDMS sample-containment chamber. (A) Schematic for the fabrication of the PDMS-confined mPED, with photograph at right showing a device containing 200 μL of a blue dye for visualization of the chamber. (B) SWV readings from each working electrode of the device measured with 50% saliva containing a ternary mixture of 10 μM acetyl fentanyl (AF), 15 μM MDPV, and 150 μM adenosine (ADE).

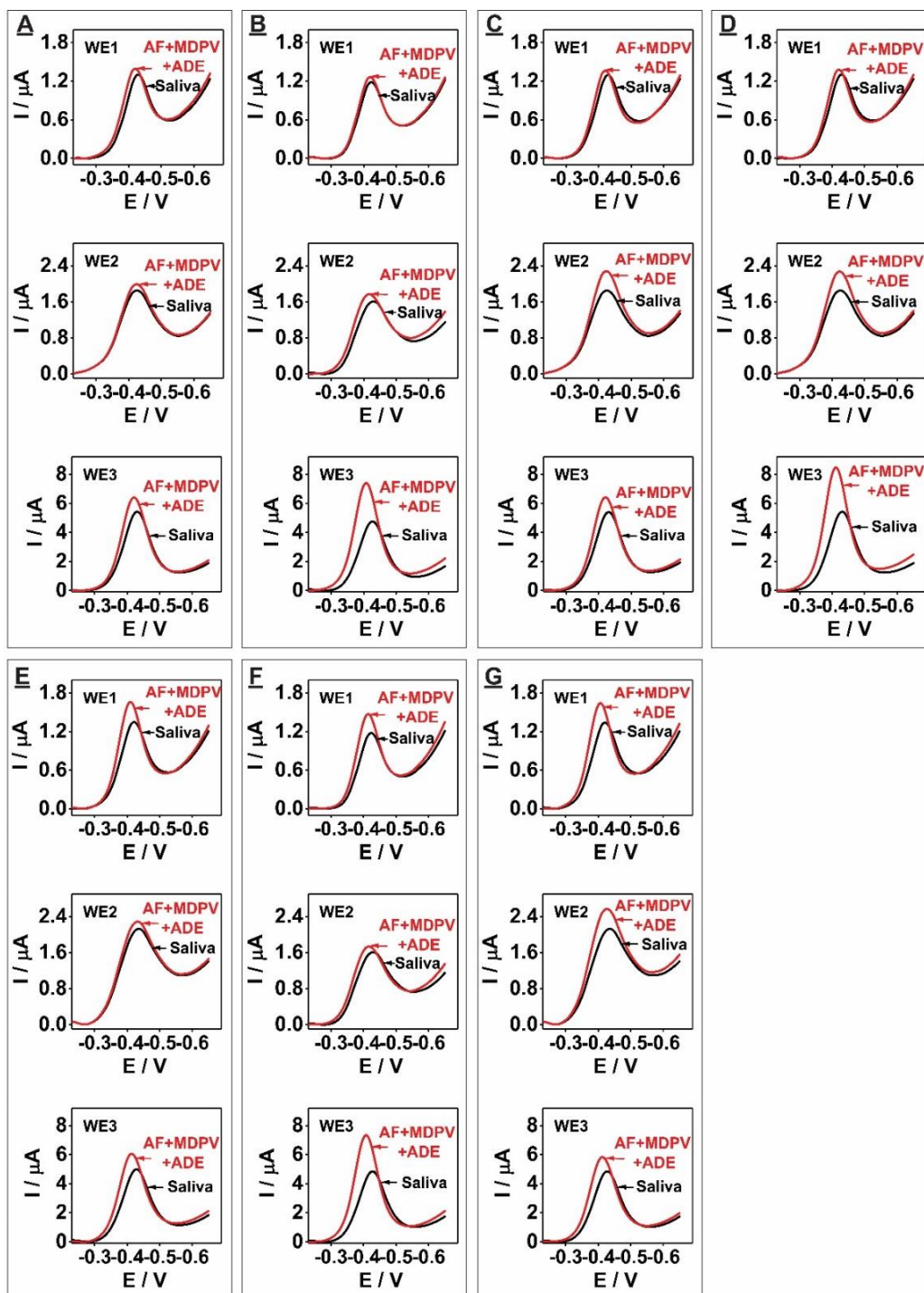


Figure 5-21. SWV response of each working electrode of a PDMS-confined triple-modified mPED in 50% saliva. SWV response of each working electrode of a PDMS-confined triple-modified mPED in the absence (black) and presence (red) of ternary mixtures of acetyl fentanyl (AF), MDPV, and adenosine (ADE) in 50% saliva. Plots A-G correspond to sample #s 1-7 listed in **Table 5-2**.

We then used the triple-modified mPEDs to perform spike-and-recovery experiments in 50% urine or saliva spiked with ternary mixtures of acetyl fentanyl, MDPV, and adenosine. As expected, these devices proved robust for accurate and specific detection of these ternary mixtures, and demonstrated high inter-device precision, with satisfactory recoveries of 94–112% in urine (**Table 5-1B, Figure 5-18**) and 92–108% in saliva (**Table 5-1C, Figure 5-19**). These findings clearly demonstrate that the aptamer-modified mPEDs can achieve sensitive, specific, and robust multi-target detection in complex biomatrices.

5.3.5. Incorporation of a sample confinement zone into a triple-modified mPED

To further enhance the potential of our device for on-site detection, we incorporated a polydimethylsiloxane (PDMS) chamber surrounding all electrodes as a means of confining the samples on the device. The PDMS chamber (outer dimensions: 23×9 mm, inner dimensions: 19×5 mm) readily adheres onto the mPED and creates a hydrophobic barrier that retains microliter samples within the detection zone where electrochemical measurements are performed (**Figure 5-20A**). We validated the performance of PDMS-containing triple-modified device by detecting a ternary mixture of acetyl fentanyl, MDPV, and adenosine spiked into 50% saliva (**Figure 5-20B**). These devices demonstrated comparable performance (94–110% recovery, **Table 5-2** and **Figure 5-21**) as non-confined mPEDs, while enabling analyte detection with a 10-fold smaller sample volume (~ 200 μL). The PDMS chamber design is therefore particularly well suited for precious biosamples that are difficult to procure in large amounts.

5.4. Conclusion

The on-site detection of multiple small molecules could enable more comprehensive chemical profiling of complex samples in the context of analytical applications such as medical diagnostics, food safety, and environmental monitoring. Current lateral-flow immunoassays can detect multiple small-molecule analytes in a single sample, but these assays are limited by high cost, large batch-to-batch variation of antibodies, and the qualitative nature of their colorimetric readouts. As an alternative, PEDs offer low cost, rapid turnaround, portability, and ability to accurately quantify analytes, but it is generally difficult to develop PEDs that can detect multiple analytes in parallel due to the lack of specific bioreceptors that can be incorporated in this electrochemical platform. Here, we have taken advantage of the flexibility and customizability of our fabrication method to prepare mPEDs with multiple gold working electrodes, which can achieve sensitive, accurate, and robust multi-analyte detection with a single device. Our fabrication method is highly reproducible, yielding high-quality devices with nearly identical physical and electrochemical properties and minimal batch-to-batch variation. The mPEDs described in this work can be modified with three different aptamers that bind distinct targets (in this work, acetyl fentanyl, MDPV, and adenosine) in a multiplexed fashion. Our mPEDs achieved accurate and robust analytical performance for sensitive and specific detection of small molecules, comparable in all respects to E-AB sensors developed with conventional gold disk electrodes. Importantly, the triple-modified mPEDs could simultaneously quantify mixtures of small molecules in biological samples such as urine and saliva without any measurable crosstalk among electrodes. In addition, a custom PDMS chamber can be easily attached to our aptamer-modified mPEDs to confine samples on the device, allowing

for multiple analyte detection in microliters of unprocessed biological samples such as saliva within seconds.

Our mPED fabrication process is highly reproducible. To understand why, it is helpful to assess the production process, which can be separated into two phases. In the first phase, metallic thin film electrodes are deposited on the filter paper with the aid of stencils and a vacuum filtration setup. During this phase of production, we were visually able to identify defective devices based on, for example, failure of nanoparticle deposition. Roughly 10% of devices failed this visual inspection. We attribute the high rate of successful device fabrication to the simplicity of the filtration process and the high level of control of material deposition on the paper substrates. In particular, variability in the first phase of fabrication arises from two sources that can be easily and tightly controlled: solution flux during vacuum filtration and the homogeneity and high reproducibility of manufacturing the raw materials (i.e., gold and silver nanoparticles, carbon nanotubes, filter paper). In the second phase, the paper-based electrodes are modified with aptamers via a very well-established protocol.²¹ This entails adding 10 μ L of thiolated methylene blue-modified aptamer onto the working electrode and incubating for 1 h at room temperature. The concentration and amount of aptamer, and therefore the resulting aptamer surface coverage, can be accurately controlled. Of 16 aptamer-modified devices, only one did not function: a success rate of \sim 94%. We observed that the absolute currents produced by each mPED can be slightly different (\sim 10% relative standard deviation), perhaps due to slight differences in surface roughness between each working electrode. However, the target-induced change in signal (measured here as signal gain) is highly precise (3–5% relative standard deviation) among different electrodes of the same device as well as between different devices.

This work demonstrates a generalizable and cost-effective strategy for the manufacture of aptamer-modified mPEDs for the accurate, rapid, and robust detection of multiple analytes in a single complex sample. Although we have demonstrated sensitive detection of three small-molecule analytes here, our vacuum filtration technique allows the flexible fabrication of electrodes of diverse material, thickness, and shape, and we believe that it should be feasible to fabricate up to 16 working electrodes on a stamp-sized single paper device at a cost of less than \$2. And given the rapid development of SELEX and sequencing techniques,¹⁶⁸ it has become increasingly straightforward to isolate aptamers that selectively recognize various targets with different binding properties. These in turn can readily be incorporated into mPEDs, and we envision that with a handheld potentiostat, facile multianalyte detection of virtually any set of analyte or combination of analytes in a drop of sample can be achieved on-site.

CHAPTER 6: Summary and Future Work

6.1. Summary

E-AB sensors have attracted much attention due to their advantages of simple fabrication, ease of use, accuracy, specificity, sensitivity, and the ability to detect analytes in complex sample matrices in real-time. However, applying E-AB sensors in the real world is challenging. This dissertation aims to develop highly sensitive and specific E-AB sensors and paper-based devices for detecting small molecules in real-life applications.

It is more efficient to use a single receptor to detect families of structurally-related analytes than it is to generate many reagents that collectively target these molecules. However, it remains challenging to develop affinity reagents that can recognize all compounds in a given family while also retaining high specificity against interferents. In Chapter 3, we described a novel method to control the specificity and cross-reactivity of aptamer-based sensors by utilizing a mixture of two aptamers that exhibit different binding profiles. As a demonstration, we used two synthetic cathinone-binding aptamers to detect synthetic cathinones, a family of dangerous illicit designer drugs. One aptamer had high cross-reactivity towards 12 commonly-used drugs in the synthetic cathinone family and low specificity against 17 frequently-observed interferents or adulterants, while another aptamer had low cross-reactivity and high specificity. We first performed a Cy7 dye-displacement assay to determine the optimal molar ratio between the two aptamers to maximize their target responsiveness and specificity against interferents. Then we fabricated dual-aptamer-based E-AB sensors that can detect all 12 synthetic cathinones with high cross-reactivity and minimal response to the various interferents tested. Notably,

this sensor performance could not be achieved by E-AB sensors based on either aptamer alone.

In Chapter 4, we described a novel immobilization strategy to improve E-AB sensor sensitivity and SNR for small-molecule detection in biological sample matrices. In conventional methods, the electrodes are first incubated with an aptamer solution and then backfilled with MCH. This can leave the immobilized aptamers with insufficient spacing to fold and transduce their signal efficiently once bound to the target. Surface probe density can be controlled by varying the concentration of aptamer solution, but it is difficult to control the appropriate spatial arrangement of the aptamers on the electrode surface. Here, we developed a target-assisted immobilization strategy that can effectively control the aptamers' spatial arrangement and thereby greatly enhance E-AB sensor performance. Specifically, we incubated electrodes with aptamer-target complexes instead of aptamers alone, such that the aptamers maintain a folded state during immobilization. We also found that modifying at lower ionic strength conditions (20 mM NaCl and 0.5 mM MgCl₂ versus 1 M NaCl and 1 mM MgCl₂) can effectively reduce aptamer bundling on the electrode surface. Using this strategy, we fabricated sensitive E-AB sensors with two-fold lower LODs in biological samples and two-fold higher signal gains than sensors modified by conventional methods. This strategy is generalizable for E-AB sensors fabricated with arbitrary small-molecule-binding aptamers, regardless of their sequence or secondary structure.

In Chapter 5, we fabricated portable aptamer-modified multiplex paper electrochemical devices (mPEDs) for multi-analyte detection in single samples within

seconds. We utilized an ambient vacuum filtration method to deposit the carbon nanotubes and gold or silver nanoparticles in layers onto designed areas of a piece of filter paper. Three specific small-molecule-binding aptamers were immobilized onto three different working electrodes on a single PED device. We achieved sensitive and accurate measurement for three small-molecule analytes—acetyl fentanyl, MDPV, and adenosine—in saliva and urine. By incorporating a PDMS chamber around the detection area of the device as a physical barrier, we were able to reduce the sample volume required for detection to the microliter scale.

6.2. Future work

Electrochemical aptamer-based (E-AB) sensors are excellent sensor platforms for diverse applications such as law enforcement¹⁶⁹, environmental monitoring¹⁷⁰, food safety¹⁷¹, and medical diagnostics¹⁷² because they are label-free, highly sensitive and specific, user friendly, and compatible with biosamples.¹⁷³ However, limited sensitivity for detecting analytes at clinically relevant concentrations and the lack of portable devices for point-of-care applications have greatly hindered the maturation of E-AB sensors from proof-of-concept designs to commercial systems. My dissertation described a novel immobilization strategy to improve E-AB sensor sensitivity by controlling the spatial morphology of aptamers on the surface. There are still multiple opportunities to further enhance the performance of E-AB sensors. For example, the redox reporter methylene blue only transfers two electrons; in the future, we can find new redox reporters with more than two electron transfer numbers to increase the signal generated by detection events. Additionally, sensor performance suffers from the desorption of oligonucleotides from the

sensor surface over time. Usually, aptamers are anchored onto the surface via gold-thiol bond, which is a weak bonding strategy that is unstable over the long term. New strategies such as "click" chemistry,¹⁷⁴ which offer simple means for generating highly stable covalent linkages, can be utilized to improve the stability of surface oligonucleotides during long-term measurements.

In addition, the use of E-AB sensors to detect hydrophobic molecules is still challenging. The conventional backfill chemical is MCH, a polar, hydrophilic molecule. Hydrophobic analytes can easily form aggregates or clusters on the electrode surface due to the hydrophobic effect,¹⁷⁵ but the identification of new hydrophobic backfills could solve this problem. Biofouling is another critical issue hindering the sensitive detection of analytes in biofluids via E-AB sensors. The use of new backfills or mixtures of different backfills to form SAMs could further suppress interferent adsorption during continuous detection over days or even weeks. More effective antifouling may improve sensor sensitivity, reduce baseline drift, and minimize signal decay in order to maintain sensor performance for long-time monitoring.

Importantly, our work has demonstrated the feasibility of using mPEDs for multi-analyte detection in a single sample within seconds. In the future, we aim to achieve simultaneous detection of up to 16 analytes by designing devices with more working electrodes and utilizing a portable, multi-channel potentiostat. Different materials and shapes of nanoparticles with high conductivity could also be used in the electrode to further enhance the sensor performance.

REFERENCES

- (1) Zhou, J.; Rossi, J. Aptamers as Targeted Therapeutics: Current Potential and Challenges. *Nat. Rev. Drug Discovery* **2017**, *16*, 181–202.
- (2) Yu, H.; Alkhamis, O.; Canoura, J.; Liu, Y.; Xiao, Y. Advances and Challenges in Small-Molecule DNA Aptamer Isolation, Characterization, and Sensor Development. *Angew. Chem., Int. Ed.* **2021**, *60*, 16800–16823.
- (3) Ellington, A. D.; Szostak, J. W. In Vitro Selection of RNA Molecules That Bind Specific Ligands. *Nature* **1990**, *346*, 818–822.
- (4) Tuerk, C.; Gold, L. Systematic Evolution of Ligands by Exponential Enrichment: RNA Ligands to Bacteriophage T4 DNA Polymerase. *Science* **1990**, *249*, 505–510.
- (5) Harlow, E.; Lane, D. *Antibodies: A Laboratory Manual*; Cold Spring Harbor Laboratory, New York, 1988.
- (6) Dunn, M. R.; Jimenez, R. M.; Chaput, J. C. Analysis of Aptamer Discovery and Technology. *Nat. Rev. Chem.* **2017**, *1*, 0076.
- (7) Toh, S. Y.; Citartan, M.; Gopinath, S. C. B.; Tang, T.-H. Aptamers as a Replacement for Antibodies in Enzyme-Linked Immunosorbent Assay. *Biosens. Bioelectron.* **2015**, *64*, 392–403.
- (8) Jayasena, S. D. Aptamers: An Emerging Class of Molecules That Rival Antibodies in Diagnostics. *Clin. Chem.* **1999**, *45*, 1628–1650.
- (9) Zhang, Y.; Lai, B. S.; Juhas, M. Recent Advances in Aptamer Discovery and Applications. *Molecules* **2019**, *24*, 941.
- (10) Song, S.; Wang, L.; Li, J.; Zhao, J.; Fan, C. Aptamer-Based Biosensors. *TrAC, Trends Anal. Chem.* **2008**, *27*, 108–117.
- (11) Alkhamis, O.; Canoura, J.; Yu, H.; Liu, Y.; Xiao, Y. Innovative Engineering and Sensing Strategies for Aptamer-Based Small-Molecule Detection. *TrAC, Trends Anal. Chem.* **2019**, *121*, 115699.
- (12) Cho, E. J.; Lee, J.-W.; Ellington, A. D. Applications of Aptamers as Sensors. *Annu. Rev. Anal. Chem.* **2009**, *2*, 241–264.
- (13) Stojanovic, M. N.; de Prada, P.; Landry, D. W. Fluorescent Sensors Based on Aptamer Self-Assembly. *J. Am. Chem. Soc.* **2000**, *122*, 11547–11548.

- (14) Stojanovic, M. N.; Landry, D. W. Aptamer-Based Colorimetric Probe for Cocaine. *J. Am. Chem. Soc.* **2002**, *124*, 9678–9679.
- (15) Liu, J.; Lu, Y. Fast Colorimetric Sensing of Adenosine and Cocaine Based on a General Sensor Design Involving Aptamers and Nanoparticles. *Angew. Chem., Int. Ed.* **2006**, *45*, 90–94.
- (16) Syu, Y.-C.; Hsu, W.-E.; Lin, C.-T. Review—Field-Effect Transistor Biosensing: Devices and Clinical Applications. *ECS J. Solid State Sci. Technol.* **2018**, *7*, Q3196–Q3207.
- (17) Wadhwa, T.; Kakkar, D.; Wadhwa, G.; Raj, B. Recent Advances and Progress in Development of the Field Effect Transistor Biosensor: A Review. *J. Electron. Mater.* **2019**, *48*, 7635–7646.
- (18) Zayats, M.; Huang, Y.; Gill, R.; Ma, C.-A.; Willner, I. Label-Free and Reagentless Aptamer-Based Sensors for Small Molecules. *J. Am. Chem. Soc.* **2006**, *128*, 13666–13667.
- (19) Xiao, Y.; Lubin, A. A.; Heeger, A. J.; Plaxco, K. W. Label-Free Electronic Detection of Thrombin in Blood Serum by Using an Aptamer-Based Sensor. *Angew. Chem., Int. Ed.* **2005**, *44*, 5456–5459.
- (20) Baker, B. R.; Lai, R. Y.; Wood, M. S.; Doctor, E. H.; Heeger, A. J.; Plaxco, K. W. An Electronic, Aptamer-Based Small-Molecule Sensor for the Rapid, Label-Free Detection of Cocaine in Adulterated Samples and Biological Fluids. *J. Am. Chem. Soc.* **2006**, *128*, 3138–3139.
- (21) Xiao, Y.; Lai, R. Y.; Plaxco, K. W. Preparation of Electrode-Immobilized, Redox-Modified Oligonucleotides for Electrochemical DNA and Aptamer-Based Sensing. *Nat. Protoc.* **2007**, *2*, 2875–2880.
- (22) Schoukroun-Barnes, L. R.; Macazo, F. C.; Gutierrez, B.; Lottermoser, J.; Liu, J.; White, R. J. Reagentless, Structure-Switching, Electrochemical Aptamer-Based Sensors. *Annu. Rev. Anal. Chem.* **2016**, *9*, 163–181.
- (23) Gjerde, H.; Langel, K.; Favretto, D.; Verstraete, A. G. Estimation of Equivalent Cutoff Thresholds in Blood and Oral Fluid for Drug Prevalence Studies. *J. Anal. Toxicol.* **2014**, *38*, 92–98.
- (24) Wang, Z.; Yu, H.; Canoura, J.; Liu, Y.; Alkhamis, O.; Fu, F.; Xiao, Y. Introducing Structure-Switching Functionality into Small-Molecule-Binding Aptamers via Nuclease-Directed Truncation. *Nucleic Acids Res.* **2018**, *46*, e81.

- (25) Schoukroun-barnes, L. R.; Glaser, E. P.; White, R. J. Heterogeneous Electrochemical Aptamer-Based Sensor Surfaces for Controlled Sensor Response. *Langmuir* **2015**, *31*, 6563–6569.
- (26) Liu, Y.; Yu, H.; Alkhamis, O.; Moliver, J.; Xiao, Y. Tuning Biosensor Cross-Reactivity Using Aptamer Mixtures. *Anal. Chem.* **2020**, *92*, 5041–5047.
- (27) Zuo, X.; Xiao, Y.; Plaxco, K. W. High Specificity, Electrochemical Sandwich Assays Based on Single Aptamer Sequences and Suitable for the Direct Detection of Small-Molecule Targets in Blood and Other Complex Matrices. *J. Am. Chem. Soc.* **2009**, *131*, 6944–6945.
- (28) Zhang, S.; Hu, R.; Hu, P.; Wu, Z.-S.; Shen, G.-L.; Yu, R.-Q. Blank Peak Current-Suppressed Electrochemical Aptameric Sensing Platform for Highly Sensitive Signal-on Detection of Small Molecule. *Nucleic Acids Res.* **2010**, *38*, e185.
- (29) Bao, T.; Shu, H.; Wen, W.; Zhang, X.; Wang, S. A Sensitive Electrochemical Aptasensor for ATP Detection Based on Exonuclease III-Assisted Signal Amplification Strategy. *Anal. Chim. Acta* **2015**, *862*, 64–69.
- (30) Herne, T. M.; Tarlov, M. J. Characterization of DNA Probes Immobilized on Gold Surfaces. *J. Am. Chem. Soc.* **1997**, *119*, 8916–8920.
- (31) Levicky, R.; Herne, T. M.; Tarlov, M. J.; Satija, S. K. Using Self-Assembly to Control the Structure of DNA Monolayers on Gold: A Neutron Reflectivity Study. *J. Am. Chem. Soc.* **1998**, *120*, 9787–9792.
- (32) Josephs, E. A.; Ye, T. Nanoscale Spatial Distribution of Thiolated DNA on Model Nucleic Acid Sensor Surfaces. *ACS Nano* **2013**, *7*, 3653–3660.
- (33) Lai, R. Y.; Seferos, D. S.; Heeger, A. J.; Bazan, G. C.; Plaxco, K. W. Comparison of the Signaling and Stability of Electrochemical DNA Sensors Fabricated from 6- or 11-Carbon Self-Assembled Monolayers. *Langmuir* **2006**, *22*, 10796–10800.
- (34) Miller, C.; Cuendet, P.; Grätzel, M. Adsorbed ω -Hydroxy Thiol Monolayers on Gold Electrodes: Evidence for Electron Tunneling to Redox Species in Solution. *J. Phys. Chem.* **1991**, *95*, 877–886.
- (35) Shaver, A.; Curtis, S. D.; Arroyo-Currás, N. Alkanethiol Monolayer End Groups Affect the Long-Term Operational Stability and Signaling of Electrochemical, Aptamer-Based Sensors in Biological Fluids. *ACS Appl. Mater. Interfaces* **2020**, *12*, 11214–11223.

- (36) Arroyo-Currás, N.; Philip A. Vieira, J. S.; Ploense, K. L.; Kippin, T. E.; Plaxco, K. W. Real-Time Measurement of Small Molecules Directly in Awake, Ambulatory Animals. *Proc. Natl. Acad. Sci. U. S. A.* **2017**, *114*, 645–650.
- (37) Li, H.; Dauphin-Ducharme, P.; Arroyo-Currás, N.; Tran, C. H.; Vieira, P. A.; Li, S.; Shin, C.; Somerson, J.; Kippin, T. E.; Plaxco, K. W. A Biomimetic Phosphatidylcholine-Terminated Monolayer Greatly Improves the In Vivo Performance of Electrochemical Aptamer-Based Sensors. *Angew. Chem., Int. Ed.* **2017**, *56*, 7492–7495.
- (38) Lowe, S.; O'Brien-Simpson, N. M.; Connal, L. A. Antibiofouling Polymer Interfaces: Poly(Ethylene Glycol) and Other Promising Candidates. *Polym. Chem.* **2015**, *6*, 198–212.
- (39) Wang, G.; Xu, Q.; Liu, L.; Su, X.; Lin, J.; Xu, G.; Luo, X. Mixed Self-Assembly of Polyethylene Glycol and Aptamer on Polydopamine Surface for Highly Sensitive and Low-Fouling Detection of Adenosine Triphosphate in Complex Media. *ACS Appl. Mater. Interfaces* **2017**, *9*, 31153–31160.
- (40) Wu, J.; Campuzano, S.; Halford, C.; Haake, D. A.; Wang, J. Ternary Surface Monolayers for Ultrasensitive (Zeptomole) Amperometric Detection of Nucleic Acid Hybridization without Signal Amplification. *Anal. Chem.* **2010**, *82*, 8830–8837.
- (41) Kang, K.-N.; Lee, Y.-S. RNA Aptamers: A Review of Recent Trends and Applications. In *Future Trends in Biotechnology. Advances in Biochemical Engineering/Biotechnology*. Zhong, J.-J., Ed.; Springer, Berlin, Heidelberg, 2013; pp 153–169.
- (42) Weickmann, J. L.; Olson, E. M.; Glitz, D. G. Immunological Assay of Pancreatic Ribonuclease in Serum as an Indicator of Pancreatic cancer. *Cancer Res.* **1984**, *44*, 1682–1687.
- (43) Santos-Cancel, M.; White, R. J. Collagen Membranes with Ribonuclease Inhibitors for Long-Term Stability of Electrochemical Aptamer-Based Sensors Employing RNA. *Anal. Chem.* **2017**, *89*, 5598–5604.
- (44) White, R. J.; Phares, N.; Lubin, A. A.; Xiao, Y.; Plaxco, K. W. Optimization of Electrochemical Aptamer-Based Sensors via Optimization of Probe Packing Density and Surface Chemistry. *Langmuir* **2008**, *24*, 10513–10518.

- (45) Wen, Y.; Pei, H.; Wan, Y.; Su, Y.; Huang, Q.; Song, S.; Fan, C. DNA Nanostructure-Decorated Surfaces for Enhanced Aptamer-Target Binding and Electrochemical Cocaine Sensors. *Anal. Chem.* **2011**, *83*, 7418–7423.
- (46) Liu, Y.; Canoura, J.; Alkhamis, O.; Xiao, Y. Immobilization Strategies for Enhancing Sensitivity of Electrochemical Aptamer-Based Sensors. *ACS Appl. Mater. Interfaces* **2021**, *13*, 9491–9499.
- (47) Heinze, J. Cyclic Voltammetry—“Electrochemical Spectroscopy”. New Analytical Methods (25). *Angew. Chem., Int. Ed.* **1984**, *23*, 831–847.
- (48) Nicholson, R. S. Theory and Application of Cyclic Voltammetry for Measurement of Electrode Reaction Kinetics. *Anal. Chem.* **1965**, *37*, 1351–1355.
- (49) Kissinger, P. T.; Heineman, W. R. Cyclic Voltammetry. *J. Chem. Educ.* **1983**, *60*, 702–706.
- (50) Osteryoung, J. G.; Schreiner, M. M. Recent Advances in Pulse Voltammetry. *C R C Crit. Rev. Anal. Chem.* **1998**, *19*, S1–S27.
- (51) Venton, B. J.; DiScenza, D. J. Chapter 3 - Voltammetry. In *Electrochemistry for Bioanalysis*; Elsevier, 2020; pp 27–50.
- (52) Westbroek, P. Electrochemical Methods. In *Analytical Electrochemistry in Textiles*; Elsevier: Amsterdam, 2005; pp 37–69.
- (53) Scholz, F. Voltammetric Techniques of Analysis: The Essentials. *ChemTexts* **2015**, *1*, 17.
- (54) Mirceski, V.; Komorsky-Lovric, S.; Lovric, M. *Square-Wave Voltammetry: Theory and Application*; Monographs in Electrochemistry; Springer Berlin Heidelberg: Berlin, Heidelberg, 2007.
- (55) Simões, F. R.; Xavier, M. G. 6 - Electrochemical Sensors. In *Nanoscience and its Applications. Micro and Nano Technologies*; William Andrew Publishing, 2017; pp 155–178.
- (56) Dauphin-Ducharme, P.; Plaxco, K. W. Maximizing the Signal Gain of Electrochemical-DNA Sensors. *Anal. Chem.* **2016**, *88*, 11654–11662.
- (57) Wang, C.; Liu, L.; Zhao, Q. Low Temperature Greatly Enhancing Responses of Aptamer Electrochemical Sensor for Aflatoxin B1 Using Aptamer with Short Stem. *ACS Sens.* **2020**, *5*, 3246–3253.

- (58) Kang, D.; Ricci, F.; White, R. J.; Plaxco, K. W. Survey of Redox-Active Moieties for Application in Multiplexed Electrochemical Biosensors. *Anal. Chem.* **2016**, *88*, 10452–10458.
- (59) Kang, D.; Zuo, X.; Yang, R.; Xia, F.; Plaxco, K. W.; White, R. J. Comparing the Properties of Electrochemical-Based DNA Sensors Employing Different Redox Tags. *Anal. Chem.* **2009**, *81*, 9109–9113.
- (60) Page, J. A.; Wilkinson, G. The Polarographic Chemistry of Ferrocene, Ruthenocene and the Metal Hydrocarbon Ions. *J. Am. Chem. Soc.* **1952**, *74*, 6149–6150.
- (61) Prins, R.; Korswagen, A. R.; Kortbeek, A. G. T. G. Decomposition of the Ferricenium Cation by Nucleophilic Reagents. *J. Organomet. Chem.* **1972**, *39*, 335–344.
- (62) Singh, A.; Chowdhury, D. R.; Paul, A. A Kinetic Study of Ferrocenium Cation Decomposition Utilizing an Integrated Electrochemical Methodology Composed of Cyclic Voltammetry and Amperometry. *Analyst* **2014**, *139*, 5747–5754.
- (63) Leung, K. K.; Downs, A. M.; Ortega, G.; Kurnik, M.; Plaxco, K. W. Elucidating the Mechanisms Underlying the Signal Drift of Electrochemical Aptamer-Based Sensors in Whole Blood. *ACS Sens.* **2021**, *6*, 3340–3347.
- (64) Ju, H.; Zhou, J.; Cai, C.; Chen, H. The Electrochemical Behavior of Methylene Blue at a Microcylinder Carbon Fiber Electrode. *Electroanalysis* **1995**, *7*, 1165–1170.
- (65) Chamorro-Garcia, A.; Ortega, G.; Mariottini, D.; Green, J.; Ricci, F.; Plaxco, K. W. Switching the Aptamer Attachment Geometry Can Dramatically Alter the Signalling and Performance of Electrochemical Aptamer-Based Sensors. *Chem. Commun.* **2021**, *57*, 11693–11696.
- (66) Sage, A. T.; Besant, J. D.; Lam, B.; Sargent, E. H.; Kelley, S. O. Ultrasensitive Electrochemical Biomolecular Detection Using Nanostructured Microelectrodes. *Acc. Chem. Res.* **2014**, *47*, 2417–2425.
- (67) Soleymani, L.; Fang, Z.; Sargent, E. H.; Kelley, S. O. Programming the Detection Limits of Biosensors through Controlled Nanostructuring. *Nat. Nanotechnol.* **2009**, *4*, 844–848.
- (68) Das, J.; Cederquist, K. B.; Zaragoza, A. A.; Lee, P. E.; Sargent, E. H.; Kelley, S. O. An Ultrasensitive Universal Detector Based on Neutralizer Displacement. *Nat. Chem.* **2012**, *4*, 642–648.

- (69) Downs, A. M.; Gerson, J.; Hossain, M. N.; Ploense, K.; Pham, M.; Kraatz, H.-B.; Kippin, T.; Plaxco, K. W. Nanoporous Gold for the Miniaturization of in Vivo Electrochemical Aptamer-Based Sensors. *ACS Sens.* **2021**, *6*, 2299–2306.
- (70) Liu, J.; Wagan, S.; Dávila Morris, M.; Taylor, J.; White, R. J. Achieving Reproducible Performance of Electrochemical, Folding Aptamer-Based Sensors on Microelectrodes: Challenges and Prospects. *Anal. Chem.* **2014**, *86*, 11417–11424.
- (71) Arroyo-Currás, N.; Scida, K.; Ploense, K. L.; Kippin, T. E.; Plaxco, K. W. High Surface Area Electrodes Generated via Electrochemical Roughening Improve the Signaling of Electrochemical Aptamer-Based Biosensors. *Anal. Chem.* **2017**, *89*, 12185–12191.
- (72) Pegan, J. D.; Ho, A. Y.; Bachman, M.; Khine, M. Flexible Shrink-Induced High Surface Area Electrodes for Electrochemiluminescent Sensing. *Lab Chip* **2013**, *13*, 4205–4209.
- (73) Freschauf, L. R.; McLane, J.; Sharma, H.; Khine, M. Shrink-Induced Superhydrophobic and Antibacterial Surfaces in Consumer Plastics. *PLoS One* **2012**, *7*, e40987.
- (74) Hauke, A.; Kumar, L. S. S.; Kim, M. Y.; Pegan, J.; Khine, M.; Li, H.; Plaxco, K. W.; Heikenfeld, J. Superwetting and Aptamer Functionalized Shrink-Induced High Surface Area Electrochemical Sensors. *Biosens. Bioelectron.* **2017**, *94*, 438–442.
- (75) Tudorache, M.; Bala, C. Biosensors Based on Screen-Printing Technology, and Their Applications in Environmental and Food Analysis. *Anal. Bioanal. Chem.* **2007**, *388*, 565–578.
- (76) Antuña-Jiménez, D.; González-García, M. B.; Hernández-Santos, D.; Fanjul-Bolado, P. Screen-Printed Electrodes Modified with Metal Nanoparticles for Small Molecule Sensing. *Biosensors* **2020**, *10*, 9.
- (77) Tso, C.-P.; Zhung, C.-M.; Shih, Y.-H.; Tseng, Y.-M.; Wu, S.-C.; Doong, R.-A. Stability of Metal Oxide Nanoparticles in Aqueous Solutions. *Water Sci. Technol.* **2010**, *61*, 127–133.
- (78) Nery, E. W.; Kubota, L. T. Sensing Approaches on Paper-Based Devices: A Review. *Anal. Bioanal. Chem.* **2013**, *405*, 7573–7595.
- (79) Mahadeva, S. K.; Walus, K.; Stoeber, B. Paper as a Platform for Sensing Applications and Other Devices: A Review. *ACS Appl. Mater. Interfaces* **2015**, *7*, 8345–8362.

- (80) Yu, H.; Chen, Z.; Liu, Y.; Alkhamis, O.; Song, Z.; Xiao, Y. Fabrication of Aptamer-Modified Paper Electrochemical Devices for On-Site Biosensing. *Angew. Chem., Int. Ed.* **2021**, *60*, 2993–3000.
- (81) Arroyo-Currás, N.; Dauphin-Ducharme, P.; Scida, K.; Chávez, J. L. From the Beaker to the Body: Translational Challenges for Electrochemical, Aptamer-Based Sensors. *Anal. Methods* **2020**, *12*, 1288–1310.
- (82) Lai, R. Y.; Plaxco, K. W.; Heeger, A. J. Aptamer-Based Electrochemical Detection of Picomolar Platelet-Derived Growth Factor Directly in Blood Serum. *Anal. Chem.* **2007**, *79*, 229–233.
- (83) Swensen, J. S.; Xiao, Y.; Ferguson, B. S.; Lubin, A. A.; Lai, R. Y.; Heeger, A. J.; Plaxco, K. W.; Soh, H. T. Continuous, Real-Time Monitoring of Cocaine in Undiluted Blood Serum via a Microfluidic, Electrochemical Aptamer-Based Sensor. *J. Am. Chem. Soc.* **2009**, *131*, 4262–4266.
- (84) Downs, A. M.; Gerson, J.; Ploense, K. L.; Plaxco, K. W.; Dauphin-Ducharme, P. Subsecond-Resolved Molecular Measurements Using Electrochemical Phase Interrogation of Aptamer-Based Sensors. *Anal. Chem.* **2020**, *92*, 14063–14068.
- (85) Arroyo-Currás, N.; Dauphin-Ducharme, P.; Ortega, G.; Ploense, K. L.; Kippin, T. E.; Plaxco, K. W. Subsecond-Resolved Molecular Measurements in the Living Body Using Chronoamperometrically Interrogated Aptamer-Based Sensors. *ACS Sens.* **2018**, *3*, 360–366.
- (86) Hanssen, B. L.; Siraj, S.; Wong, D. K. Y. Recent Strategies to Minimise Fouling in Electrochemical Detection Systems. *Rev. Anal. Chem.* **2016**, *35*, 1–28.
- (87) Flynn, N. T.; Tran, T. N. T.; Cima, M. J.; Langer, R. Long-Term Stability of Self-Assembled Monolayers in Biological Media. *Langmuir* **2003**, *19*, 10909–10915.
- (88) Deng, M.; Li, M.; Li, F.; Mao, X.; Li, Q.; Shen, J.; Fan, C.; Zuo, X. Programming Accessibility of DNA Monolayers for Degradation-Free Whole-Blood Biosensors. *ACS Mater. Lett.* **2019**, *1*, 671–676.
- (89) Ferguson, B. S.; Hoggarth, D. A.; Maliniak, D.; Ploense, K.; White, R. J.; Woodward, N.; Hsieh, K.; Bonham, A. J.; Eisenstein, M.; Kippin, T. E.; Plaxco, K. W.; Soh, H. T. Real-Time, Aptamer-Based Tracking of Circulating Therapeutic Agents in Living Animals. *Sci. Transl. Med.* **2013**, *5*, 213ra165.
- (90) Li, H.; Arroyo-Currás, N.; Kang, D.; Ricci, F.; Plaxco, K. W. Dual-Reporter Drift Correction To Enhance the Performance of Electrochemical Aptamer-Based Sensors in Whole Blood. *J. Am. Chem. Soc.* **2016**, *138*, 15809–15812.

- (91) Hahn, Y.; Lee, H. Y. Electrochemical Behavior and Square Wave Voltammetric Determination of Doxorubicin Hydrochloride. *Arch. Pharmacol Res.* **2004**, *27*, 31–34.
- (92) Dauphin-Ducharme, P.; Yang, K.; Arroyo-Currás, N.; Ploense, K. L.; Zhang, Y.; Gerson, J.; Kurnik, M.; Kippin, T. E.; Stojanovic, M. N.; Plaxco, K. W. Electrochemical Aptamer-Based Sensors for Improved Therapeutic Drug Monitoring and High-Precision, Feedback-Controlled Drug Delivery. *ACS Sens.* **2019**, *4*, 2832–2837.
- (93) Rybak, M.; Lomaestro, B.; Rotschafer, J. C.; Moellering, R.; Craig, W.; Billeter, M.; Dalovisio, J. R.; Levine, D. P. Therapeutic Monitoring of Vancomycin in Adult Patients: A Consensus Review of the American Society of Health-System Pharmacists, the Infectious Diseases Society of America, and the Society of Infectious Diseases Pharmacists. *Am. J. Health-Syst. Pharm.* **2009**, *66*, 82–98.
- (94) Idili, A.; Arroyo-Currás, N.; Ploense, K. L.; Csordas, A. T.; Kuwahara, M.; Kippin, T. E.; Plaxco, K. W. Seconds-Resolved Pharmacokinetic Measurements of the Chemotherapeutic Irinotecan in Situ in the Living Body. *Chem. Sci.* **2019**, *10*, 8164–8170.
- (95) Idili, A.; Gerson, J.; Kippin, T.; Plaxco, K. W. Seconds-Resolved, in Situ Measurements of Plasma Phenylalanine Disposition Kinetics in Living Rats. *Anal. Chem.* **2021**, *93*, 4023–4032.
- (96) Parolo, C.; Idili, A.; Ortega, G.; Csordas, A.; Hsu, A.; Arroyo-Currás, N.; Yang, Q.; Ferguson, B. S.; Wang, J.; Plaxco, K. W. Real-Time Monitoring of a Protein Biomarker. *ACS Sens.* **2020**, *5*, 1877–1881.
- (97) Soni, S. S.; Cruz, D.; Bobek, I.; Chionh, C. Y.; Nalesso, F.; Lentini, P.; De Cal, M.; Corradi, V.; Virzi, G.; Ronco, C. NGAL: A Biomarker of Acute Kidney Injury and Other Systemic Conditions. *Int. Urol. Nephrol.* **2010**, *42*, 141–150.
- (98) Prosser, J. M.; Nelson, L. S. The Toxicology of Bath Salts: A Review of Synthetic Cathinones. *J. Med. Toxicol.* **2012**, *8*, 33–42.
- (99) Valente, M. J.; Guedes De Pinho, P.; De Lourdes Bastos, M.; Carvalho, F.; Carvalho, M. Khat and Synthetic Cathinones: A Review. *Arch. Toxicol.* **2014**, *88*, 15–45.
- (100) Glennon, R. A.; Dukat, M. Synthetic Cathinones: A Brief Overview of Overviews with Applications to the Forensic Sciences. *Ann. forensic Res. Anal.* **2017**, *4*, 1040.
- (101) U. S. Department of Justice, U. S. Drug Enforcement Administration. *National Forensic Laboratory Information System: NFLIS-Drug 2021 Midyear Report*; 2021.

- (102) Substance Abuse and Mental Health Services Administration. *Key Substance Use and Mental Health Indicators in the United States: Results from the 2020 National Survey on Drug Use and Health*; Rockville, MD, 2021.
- (103) National Institute on Drug Abuse. Overdose Death Rates. <https://nida.nih.gov/drug-topics/trends-statistics/overdose-death-rates> (accessed May 12, 2022).
- (104) Riezzo, I.; Fiore, C.; De Carlo, D.; Pascale, N.; Neri, M.; Turillazzi, E.; Fineschi, V. Side Effects of Cocaine Abuse: Multiorgan Toxicity and Pathological Consequences. *Curr. Med. Chem.* **2012**, *19*, 5624–5646.
- (105) Snyder, S. H. Adenosine as a Neuromodulator. *Annu. Rev. Neurosci.* **1985**, *8*, 103–124.
- (106) Layland, J.; Carrick, D.; Lee, M.; Oldroyd, K.; Berry, C. Adenosine: Physiology, Pharmacology, and Clinical Applications. *JACC Cardiovasc. Interv.* **2014**, *7*, 581–591.
- (107) Haskó, G.; Cronstein, B. N. Adenosine: An Endogenous Regulator of Innate Immunity. *Trends Immunol.* **2004**, *25*, 33–39.
- (108) Bellezza, I.; Tucci, A.; Minelli, A. 2-Chloroadenosine and Human Prostate Cancer Cells. *Anti-cancer Agents Med. Chem.* **2008**, *8*, 783–789.
- (109) Cunningham, S. M.; Haikal, N. A.; Kraner, J. C. Fatal Intoxication with Acetyl Fentanyl. *J. Forensic Sci.* **2016**, *61*, S276–S280.
- (110) Higashikawa, Y.; Suzuki, S. Studies on 1-(2-Phenethyl)-4-(N-Propionylanilino)Piperidine (Fentanyl) and Its Related Compounds. VI. Structure-Analgesic Activity Relationship for Fentanyl, Methyl-Substituted Fentanyls and Other Analogues. *Forensic Toxicol.* **2008**, *26*, 1–5.
- (111) Kuczyńska, K.; Grzonkowski, P.; Kacprzak, Ł.; Zawilska, J. B. Abuse of Fentanyl: An Emerging Problem to Face. *Forensic Sci. Int.* **2018**, *289*, 207–214.
- (112) Mattson, C. L.; Tanz, L. J.; Quinn, K.; Kariisa, M.; Patel, P.; Davis, N. L. Trends and Geographic Patterns in Drug and Synthetic Opioid Overdose Deaths — United States, 2013–2019. *Morb. Mortal. Wkly. Rep.* **2021**, *70*, 202–207.
- (113) Huet, A.-C.; Fodey, T.; Haughey, S. A.; Weigel, S.; Elliott, C.; Delahaut, P. Advances in Biosensor-Based Analysis for Antimicrobial Residues in Foods. *TrAC - Trends Anal. Chem.* **2010**, *29*, 1281–1294.

- (114) Gandhi, S.; Suman, P.; Kumar, A.; Sharma, P.; Capalash, N.; Suri, C. R. Recent Advances in Immunosensor for Narcotic Drug Detection. *BioImpacts* **2015**, *5*, 207–213.
- (115) Verma, N.; Bhardwaj, A. Biosensor Technology for Pesticides—A Review. *Appl. Biochem. Biotechnol.* **2015**, *175*, 3093–3119.
- (116) Spinks, C. A. Broad-Specificity Immunoassay of Low Molecular Weight Food Contaminants: New Paths to Utopia! *Trends Food Sci. Technol.* **2000**, *11*, 210–217.
- (117) Ascoli, C. A.; Aggeler, B. Overlooked Benefits of Using Polyclonal Antibodies. *BioTechniques* **2018**, *65*, 127–136.
- (118) Leenaars, M.; Hendriksen, C. F. M. Critical Steps in the Production of Polyclonal and Monoclonal Antibodies: Evaluation and Recommendations. *ILAR J.* **2005**, *46*, 269–279.
- (119) Zhang, H.; Wang, S. Review on Enzyme-Linked Immunosorbent Assays for Sulfonamide Residues in Edible Animal Products. *J. Immunol. Methods* **2009**, *350*, 1–13.
- (120) Yokoyama, W. M.; Christensen, M.; Dos Santos, G.; Miller, D.; Ho, J.; Wu, T.; Dziegelewski, M.; Neethling, F. A. Production of Monoclonal Antibodies. *Curr. Protoc. Immunol.* **2013**, *102*, 2.5.1-2.5.29.
- (121) Jenison, R. D.; Gill, S. C.; Pardi, A.; Polisky, B. High-Resolution Molecular Discrimination by RNA. *Science* **1994**, *263*, 1425–1429.
- (122) White, R.; Rusconi, C.; Scardino, E.; Wolberg, A.; Lawson, J.; Hoffman, M.; Sullenger, B. Generation of Species Cross-Reactive Aptamers Using “Toggle” SELEX. *Mol. Ther.* **2001**, *4*, 567–573.
- (123) Yang, W.; Yu, H.; Alkhamis, O.; Liu, Y.; Canoura, J.; Fu, F.; Xiao, Y. In Vitro Isolation of Class-Specific Oligonucleotide-Based Small-Molecule Receptors. *Nucleic Acids Res.* **2019**, *47*, e71.
- (124) Drabovich, A. P.; Okhonin, V.; Berezovski, M.; Krylov, S. N. Smart Aptamers Facilitate Multi-Probe Affinity Analysis of Proteins with Ultra-Wide Dynamic Range of Measured Concentrations. *J. Am. Chem. Soc.* **2007**, *129*, 7260–7261.
- (125) Porchetta, A.; Vallée-Bélisle, A.; Plaxco, K. W.; Ricci, F. Using Distal-Site Mutations and Allosteric Inhibition to Tune, Extend, and Narrow the Useful Dynamic Range of Aptamer-Based Sensors. *J. Am. Chem. Soc.* **2012**, *134*, 20601–20604.

- (126) German, C. L.; Fleckenstein, A. E.; Hanson, G. R. Bath Salts and Synthetic Cathinones: An Emerging Designer Drug Phenomenon. *Life Sci.* **2014**, *97*, 2–8.
- (127) Steel, A. B.; Herne, T. M.; Tarlov, M. J. Electrochemical Quantitation of DNA Immobilized on Gold. *Anal. Chem.* **1998**, *70*, 4670–4677.
- (128) Garoff, R. A.; Litzinger, E. A.; Connor, R. E.; Fishman, I.; Armitage, B. A. Helical Aggregation of Cyanine Dyes on DNA Templates: Effect of Dye Structure on Formation of Homo- and Heteroaggregates. *Langmuir* **2002**, *18*, 6330–6337.
- (129) Somerson, J.; Plaxco, K. W. Electrochemical Aptamer-Based Sensors for Rapid Point-of-Use Monitoring of the Mycotoxin Ochratoxin A Directly in a Food Stream. *Molecules* **2018**, *23*, 912.
- (130) Xiao, Y.; Rowe, A. A.; Plaxco, K. W. Electrochemical Detection of Parts-per-Billion Lead via an Electrode-Bound DNAzyme Assembly. *J. Am. Chem. Soc.* **2007**, *129*, 262–263.
- (131) Lehman, I. R.; Nussbaum, A. L. The Deoxyribonucleases of Escherichia Coli. V. on the Specificity of Exonuclease I (Phosphodiesterase). *J. Biol. Chem.* **1964**, *239*, 2628–2636.
- (132) Kypr, J.; Kejnovská, I.; Renčuk, D.; Vorlíčková, M. Circular Dichroism and Conformational Polymorphism of DNA. *Nucleic Acids Res.* **2009**, *37*, 1713–1725.
- (133) Zuker, M. Mfold Web Server for Nucleic Acid Folding and Hybridization Prediction. *Nucleic Acids Res.* **2003**, *31*, 3406–3415.
- (134) Silva, B.; Fernandes, C.; Tiritan, M. E.; Pinto, M. M. M.; Valente, M. J.; Carvalho, M.; de Pinho, P. G.; Remião, F. Chiral Enantioresolution of Cathinone Derivatives Present in “Legal Highs”, and Enantioselectivity Evaluation on Cytotoxicity of 3,4-Methylenedioxypyrovalerone (MDPV). *Forensic Toxicol.* **2016**, *34*, 372–385.
- (135) White, R. J.; Rowe, A. A.; Plaxco, K. W. Re-Engineering Aptamers to Support Reagentless, Self-Reporting Electrochemical Sensors. *Analyst* **2010**, *135*, 589–594.
- (136) Zhang, Q.; Huang, Y.; Guo, L.; Chen, C.; Guo, D.; Chen, Y.; Fu, Y. DNA-Based Nanocomposite as Electrochemical Chiral Sensing Platform for the Enantioselective Interaction with Quinine and Quinidine. *New J. Chem.* **2014**, *38*, 4600–4606.
- (137) Quang, N. N.; Perret, G.; Ducongé, F. Applications of High-Throughput Sequencing for in Vitro Selection and Characterization of Aptamers. *Pharmaceuticals* **2016**, *9*, 76.

- (138) Privett, B. J.; Shin, J. H.; Schoenfisch, M. H. Electrochemical Sensors. *Anal. Chem.* **2010**, *82*, 4723–4741.
- (139) Labib, M.; Sargent, E. H.; Kelley, S. O. Electrochemical Methods for the Analysis of Clinically Relevant Biomolecules. *Chem. Rev.* **2016**, *116*, 9001–9090.
- (140) Li, H.; Somerson, J.; Xia, F.; Plaxco, K. W. Electrochemical DNA-Based Sensors for Molecular Quality Control: Continuous, Real-Time Melamine Detection in Flowing Whole Milk. *Anal. Chem.* **2018**, *90*, 10641–10645.
- (141) Rowe, A. A.; Miller, E. A.; Plaxco, K. W. Reagentless Measurement of Aminoglycoside Antibiotics in Blood Serum via an Electrochemical , Ribonucleic Acid Aptamer-Based Biosensor. **2010**, *82*, 7090–7095.
- (142) Jones, A. W.; Holmgren, A. Concentrations of Cocaine and Benzoylcegonine in Femoral Blood from Cocaine-Related Deaths Compared with Venous Blood from Impaired Drivers. *J. Anal. Toxicol.* **2014**, *38*, 46–51.
- (143) Jiang, C.; Wang, G.; Hein, R.; Liu, N.; Luo, X.; Davis, J. J. Antifouling Strategies for Selective in Vitro and in Vivo Sensing. *Chem. Rev.* **2020**, *120*, 3852–3889.
- (144) Nakatsuka, N.; Yang, K.-A.; Abendroth, J. M.; Cheung, K. M.; Xu, X.; Yang, H.; Zhao, C.; Zhu, B.; Rim, Y. S.; Yang, Y.; Weiss, P. S.; Stojanović, M. N.; Andrews, A. M. Aptamer–Field-Effect Transistors Overcome Debye Length Limitations for Small-Molecule Sensing. *Science* **2018**, *362*, 319–324.
- (145) Neves, M. A. D.; Reinstein, O.; Johnson, P. E. Defining a Stem Length-Dependent Binding Mechanism for the Cocaine-Binding Aptamer. A Combined NMR and Calorimetry Study. *Biochemistry* **2010**, *49*, 8478–8487.
- (146) Petrovykh, D. Y.; Kimura-Suda, H.; Whitman, L. J.; Tarlov, M. J. Quantitative Analysis and Characterization of DNA Immobilized on Gold. *J. Am. Chem. Soc.* **2003**, *125*, 5219–5226.
- (147) Chen, H.; Meisburger, S. P.; Pabit, S. A.; Sutton, J. L.; Webb, W. W.; Pollack, L. Ionic Strength-Dependent Persistence Lengths of Single-Stranded RNA and DNA. *Proc. Natl. Acad. Sci. U. S. A.* **2012**, *109*, 799–804.
- (148) Gu, Q.; Nanney, W.; Cao, H. H.; Wang, H.; Ye, T. Single Molecule Profiling of Molecular Recognition at a Model Electrochemical Biosensor. *J. Am. Chem. Soc.* **2018**, *140*, 14134–14143.

- (149) Canoura, J.; Yu, H.; Alkhamis, O.; Roncancio, D.; Farhana, R.; Xiao, Y. Accelerating Post-SELEX Aptamer Engineering Using Exonuclease Digestion. *J. Am. Chem. Soc.* **2021**, *143*, 805–816.
- (150) Huizenga, D. E.; Szostak, J. W. A DNA Aptamer That Binds Adenosine and ATP. *Biochemistry* **1995**, *34*, 656–665.
- (151) Stojanovic, M. N.; de Prada, P.; Landry, D. W. Aptamer-Based Folding Fluorescent Sensor for Cocaine. *J. Am. Chem. Soc.* **2001**, *123*, 4928–4931.
- (152) Neves, M. A. D.; Slavkovic, S.; Churcher, Z. R.; Johnson, P. E. Salt-Mediated Two-Site Ligand Binding by the Cocaine-Binding Aptamer. *Nucleic Acids Res.* **2017**, *45*, 1041–1048.
- (153) Song, Y.; Huang, Y.-Y.; Liu, X.; Zhang, X.; Ferrari, M.; Qin, L. Point-of-Care Technologies for Molecular Diagnostics Using a Drop of Blood. *Trends Biotechnol.* **2014**, *32*, 132–139.
- (154) Rodriguez-Mozaz, S.; Lopez de Alda, M. J.; Barceló, D. Biosensors as Useful Tools for Environmental Analysis and Monitoring. *Anal. Bioanal. Chem.* **2006**, *386*, 1025–1041.
- (155) Wu, Y.; Zhou, Y.; Leng, Y.; Lai, W.; Huang, X.; Xiong, Y. Emerging Design Strategies for Constructing Multiplex Lateral Flow Test Strip Sensors. *Biosens. Bioelectron.* **2020**, *157*, 112168.
- (156) Anfossi, L.; Di Nardo, F.; Cavalera, S.; Giovannoli, C.; Baggiani, C. Multiplex Lateral Flow Immunoassay: An Overview of Strategies towards High-Throughput Point-of-Need Testing. *Biosensors* **2019**, *9*, 2.
- (157) Lattanzio, V. M. T.; Nivarlet, N.; Lippolis, V.; Gatta, S. D.; Huet, A.-C.; Delahaut, P.; Granier, B.; Visconti, A. Multiplex Dipstick Immunoassay for Semi-Quantitative Determination of Fusarium Mycotoxins in Cereals. *Anal. Chim. Acta* **2012**, *718*, 99–108.
- (158) Mettakoonpitak, J.; Boehle, K.; Nantaphol, S.; Teengam, P.; Adkins, J. A.; Srisa-Art, M.; Henry, C. S. Electrochemistry on Paper-Based Analytical Devices: A Review. *Electroanalysis* **2016**, *28*, 1420–1436.
- (159) Ruscito, A.; DeRosa, M. C. Small-Molecule Binding Aptamers: Selection Strategies, Characterization, and Applications. *Front. Chem.* **2016**, *4*, 14.

- (160) Santos-Cancel, M.; Simpson, L. W.; Leach, J. B.; White, R. J. Direct, Real-Time Detection of Adenosine Triphosphate Release from Astrocytes in Three-Dimensional Culture Using an Integrated Electrochemical Aptamer-Based Sensor. *ACS Chem. Neurosci.* **2019**, *10*, 2070–2079.
- (161) Cunningham, J. C.; Brenes, N. J.; Crooks, R. M. Paper Electrochemical Device for Detection of DNA and Thrombin by Target-Induced Conformational Switching. *Anal. Chem.* **2014**, *86*, 6166–6170.
- (162) Turkevich, J.; Stevenson, P. C.; Hillier, J. A Study of the Nucleation and Growth Processes in the Synthesis of Colloidal Gold. *Discuss. Faraday Soc.* **1951**, *11*, 55–75.
- (163) Li, H.; Xia, H.; Wang, D.; Tao, X. Simple Synthesis of Monodisperse, Quasi-Spherical, Citrate-Stabilized Silver Nanocrystals in Water. *Langmuir* **2013**, *29*, 5074–5079.
- (164) Guntupalli, B.; Liang, P.; Lee, J.-H.; Yang, Y.; Yu, H.; Canoura, J.; He, J.; Li, W.; Weizmann, Y.; Xiao, Y. Ambient Filtration Method To Rapidly Prepare Highly Conductive, Paper-Based Porous Gold Films for Electrochemical Biosensing. *ACS Appl. Mater. Interfaces* **2015**, *7*, 27049–27058.
- (165) Alkhamis, O.; Yang, W.; Farhana, R.; Yu, H.; Xiao, Y. Label-Free Profiling of DNA Aptamer-Small Molecule Binding Using T5 Exonuclease. *Nucleic Acids Res.* **2020**, *48*, e120.
- (166) Canoura, J.; Liu, Y.; Xiao, Y. Development of Aptamer-Based Sensors for Rapid Detection of Fentanyl Opioids. *To be Submitt. Publ.*
- (167) Campuzano, S.; Pedrero, M.; Yáñez-Sedeño, P.; Pingarrón, J. M. Antifouling (Bio)Materials for Electrochemical (Bio)Sensing. *Int. J. Mol. Sci.* **2019**, *20*, 423.
- (168) Zhuo, Z.; Yu, Y.; Wang, M.; Li, J.; Zhang, Z.; Liu, J.; Wu, X.; Lu, A.; Zhang, G.; Zhang, B. Recent Advances in SELEX Technology and Aptamer Applications in Biomedicine. *Int. J. Mol. Sci.* **2017**, *18*, 2142.
- (169) Mokhtarzadeh, A.; Dolatabadi, J. E. N.; Abnous, K.; de la Guardia, M.; Ramezani, M. Nanomaterial-Based Cocaine Aptasensors. *Biosens. Bioelectron.* **2015**, *68*, 95–106.
- (170) Hayat, A.; Marty, J.L. Aptamer Based Electrochemical Sensors for Emerging Environmental Pollutants. *Front. Chem.* **2014**, *2*, 41.
- (171) Li, F.; Yu, Z.; Han, X.; Lai, R.Y. Electrochemical Aptamer-Based Sensors for Food and Water Analysis: A Review. *Anal. Chim. Acta* **2019**, *1051*, 1–23.

- (172) Jarczewska, M.; Górski, Ł.; Malinowska, E. Electrochemical Aptamer-Based Biosensors as Potential Tools for Clinical Diagnostics. *Anal. Methods* **2016**, *8*, 3861–3877.
- (173) E Ferapontova, E.; V Gothelf, K. Recent Advances in Electrochemical Aptamer-Based Sensors. *Curr. Org. Chem.* **2011**, *15*, 498–505.
- (174) Moses, J. E.; Moorhouse, A. D. The Growing Applications of Click Chemistry. *Chem. Soc. Rev.* **2007**, *36*, 1249–1262.
- (175) Hummer, G.; Garde, S.; García, A. E.; Paulaitis, M. E.; Pratt, L. R. Hydrophobic Effects on a Molecular Scale. *J. Phys. Chem. B* **1998**, *102*, 10469–10482.

VITA

YINGZHU LIU
Born, Wuhan, China

EDUCATION

- 2007–2011 B.S., Chemical Engineering
Jingchu University of Technology
Jingmen, China
- 2012–2015 M.S., Chemical Engineering
Wuhan University of Science and Technology
Wuhan, China
- 2016–2018 Teaching Assistant
Florida International University
Miami, FL
- 2018–2022 Research Assistant
Florida International University
Miami, FL

SELECTED PUBLICATIONS AND PRESENTATIONS

Liu, Y.; Alkhamis, O.; Liu, X.; Yu, H.; Canoura, J.; Xiao, Y. Aptamer-Integrated Multianalyte-Detecting Paper Electrochemical Device. *ACS Appl. Mater. Interfaces* 2021, *13*, 17330–17339.

Liu, Y.; Canoura, J.; Alkhamis, O.; Xiao, Y. Immobilization Strategies for Enhancing Sensitivity of Electrochemical Aptamer-Based Sensors. *ACS Appl. Mater. Interfaces* 2021, *13*, 9491–9499.

Yu, H.; Chen, Z.; Liu, Y.; Alkhamis, O.; Song, Z.; Xiao, Y. Fabrication of Aptamer-Modified Paper Electrochemical Devices for On-Site Biosensing. *Angew. Chem. Int. Ed.* 2021, *60*, 2993–3000.

Yu, H.; Alkhamis, O.; Canoura, J.; Liu, Y.; Xiao, Y. Advances and Challenges in Small-Molecule DNA Aptamer Isolation, Characterization, and Sensor Development. *Angew. Chem. Int. Ed.* 2021, *60*, 2–26.

Paudyal, J.; Wang, P.; Zhou, F.; Liu, Y.; Cai, Y.; Xiao, Y. Platinum-Nanoparticle-Modified Single-Walled Carbon Nanotube-Laden Paper Electrodes for Electrocatalytic Oxidation of Methanol. *ACS Appl. Nano Mater.* 2021, 4, 13798–13806.

Liu, Y.; Yu, H.; Alkhamis, O.; Moliver, J.; Xiao, Y. Tuning Biosensor Cross-Reactivity Using Aptamer Mixtures. *Anal. Chem.* 2020, 92, 5041–5047.

Luo, Y.; Yu, H.; Alkhamis, O.; Liu, Y.; Lou, X.; Yu, B.; Xiao, Y. Label-Free, Visual Detection of Small Molecules Using Highly Target-Responsive Multimodule Split Aptamer Constructs. *Anal. Chem.* 2019, 91, 7199–7207.

Alkhamis, O.; Canoura, J.; Yu, H.; Liu, Y.; Xiao, Y. Innovative Engineering and Sensing Strategies for Aptamer-Based Small-Molecule Detection. *TrAC, Trends Anal. Chem.* 2019, 121, 115699.

Yang, W.; Yu, H.; Alkhamis, O.; Liu, Y.; Canoura, J.; Fu, F.; Xiao, Y. *In Vitro* Isolation of Class-Specific Oligonucleotide-Based Small-Molecule Receptors. *Nucleic Acids Res.* 2019, 47, e71.

Wang, Z.; Yu, H.; Canoura, J.; Liu, Y.; Alkhamis, O.; Fu, F.; Xiao, Y. Introducing Structure-Switching Functionality into Small-Molecule-Binding Aptamers via Nuclease-Directed Truncation. *Nucleic Acids Res.* 2018, 46, e81.

Liu, Y.; Yu, H.; Alkhamis, O.; Moliver, J.; Xiao, Y. (2020) Achieving Near-ideal Binding Spectra using Subideal Bioreceptors. *Oral & Poster presentations*, PITTCON 2020, Chicago, Illinois, USA, March 1-5.

Liu, Y.; Alkhamis, O.; Yu, H.; Luo, Y.; Xiao, Y. (2019) Development of Electrochemical Aptamer-Based Sensor for On-site Synthetic Cathinone Detection. *Oral presentation*, PITTCON 2019, Philadelphia, Pennsylvania, USA, March 17-21.

Liu, Y.; Moliver, J.; Canoura, J.; Xiao, Y. (2018) Utilizing Exonucleases to Engineer a Structure-Switching MDPV-Binding Aptamer for the Electrochemical Detection of Synthetic Cathinones. *Oral presentation*, PITTCON 2018, Orlando, Florida, USA, February 27- March 1.

Liu, Y.; Wang Z.; Yu H.; Canoura J.; Alkhamis O.; Fu F.; Xiao Y. (2018) Introducing structure-switching functionality into small-molecule-binding aptamers via nuclease-directed truncation. Oral presentation, FIU's annual Scholarly Forum during Graduate Student Appreciation Week (GSAW), Florida International University, Miami, FL, March 19–23.